PERFORMANCE OF BEAM-COLUMN JOINTS IN CONCRETE FILLED STEEL TUBULAR FRAMES

A thesis

submitted in fulfilment of the requirement for the Award of Degree of

DOCTOR OF PHILOSOPHY

in

CIVIL ENGINEERING

Submitted By

Beena Kumari
Reg. No. 951102002

Supervisor (s)

Dr. Naveen Kwatra
Professor

Dr. Shruti Sharma
Associate Professor

THAPAR INSTITUTE
OF ENGINEERING & TECHNOLOGY
(Deemed to be University)

DEPARTMENT OF CIVIL ENGINEERING
Patiala- 147004

AUGUST- 2018

DECLARATION

I, Beena Kumari hereby declare that the thesis entitled, **"Performance Of Beam-Column Joints in Concrete Filled Steel Tubular Frames"** submitted to the Thapar Institute of Engineering and Technology in fulfilment of the requirement for the award of the Degree of Doctor of Philosophy in Civil Engineering is a record of original and independent research work done by me during the period 2013-2017, under the supervision and guidance of **Dr. Naveen Kwatra,** Professor, Department of Civil Engineering, Thapar Institute of Engineering and Technology, Patiala and **Dr. Shruti Sharma,** Associate Professor, Department of Civil Engineering, Thapar Institute of Engineering and Technology, Patiala. The work contained in this thesis has not been previously submitted to meet the requirements for a degree or diploma at this or any other higher education institution.

(Beena Kumari)
Registration No: 951102002

CERTIFICATE

This is to certify that the work presented in this thesis titled **"Performance of Beam-Column Joints in Concrete Filled Steel Tubular Frames"** being submitted by **Beena Kumari (Regd. No. 951102002)** in fulfillment of requirements for the award of degree of **'Doctor of Philosophy'** submitted in the **Civil Engineering Department, Thapar Institute of Engineering and Technology, Patiala,** is an authentic record of the research work carried out by her under our supervision and guidance. The matter embodied in this report has not been submitted in part or full to any other Institute or University for the award of any degree.

(Dr. Naveen Kwatra)
Professor
Department of Civil Engineering
(Supervisor)

(Dr. Shruti Sharma)
Associate Professor
Department of Civil Engineering
(Supervisor)

ACKNOWLEDGEMENTS

A very special debt of gratitude is owned to my thesis supervisors, **Dr. Naveen Kwatra,** Professor & Head and **Dr. Shruti Sharma**, Associate Professor of Department of Civil Engineering, Thapar Institute of Engineering & Technology, for their gracious efforts and keen pursuit, which has remained as a valuable asset for the successful completion of my thesis report. Apart from the invaluable guidance, constant encouragement and support throughout the course of work is gratefully acknowledged. Their diligent enthusiasm has been highly helpful in keeping my spirit high. The flawless and forthright suggestions blended with an essential intelligent application have completed my task with success.

I am profoundly thankful to the members of the doctoral committee. I express my sincere thanks to Dr. Shweta Goyal, Associate Professor, Department of Civil Engineering, for her moral support. I would also like to offer my sincere thanks to all faculty members and non-teaching staff of Civil Engineering Department (CED), TIET, Patiala for their assistance. I sincerely acknowledge the help extended by Mr. Varinder Kumar Sharma and Mr. Simran for performing the experiments.

No project is ever the product of one person's efforts, and certainly this one was no different. The process of forming this thesis report is a collaborative experience involving direct or indirect efforts of many people. I convey my special words of thanks to my very special students/ friends Ar. Amy Arora and Ar. Pappal Suneja for their respective contribution. I am also thankful to all my colleagues at Department of Architecture, Guru Nanak Dev University, Amritsar for their support.

My special words of thanks are for Ms. Narinder Kaur and Ms. Renu Nagar, Mess managers of PG hostel and I-hostel respectively for their support during my stay at Thapar University.

My friend, Dr. Swapna Mishra, Director, Textile Sector Skill Council, deserves a very special word of thanks as she is the only one who planted the seed of Ph.D. in my mind and

constantly nurtured the same with her all-time motivation. I would like to thank Madhu Sharma, Assistant Professor, JNE Sunder Nagar for her help extended during the work.

I would like to give special word of thanks to my family specially my husband Rajesh Ji and my loving son Anshuman, for their immense patience and constant moral support during the entire course of my work. I would also like to thank my parents for their sheer belief in me and unending blessings.

Thanks to all who have helped me directly or indirectly in completion of my thesis project.

Finally, I am thankful to the Almighty for making this day possible in my life.

BEENA KUMARI

ABSTRACT

The use of concrete filled steel tubes (CFST) in building construction has seen renaissance in recent years due to their numerous advantages, apart from their superior structural performance. Their practice as columns in high-rise buildings, as beams in low-rise industrial buildings and as arch bridges, has become widespread in countries like China in past two decades. But unfortunately, their usage in India is a new concept and has hardly seen the light of the day. The focus of this research is to explore the bounties of CFST sections to investigate potential usage in the building industry; mainly considering the structural behaviour.

It is widely recognized that innovative use of two or more different materials in a structure usually lead to more efficient system for resisting seismic forces. The CFST structures make an efficient structural system with the advantage of both steel and reinforced concrete frame. It has numerous advantages in terms of structural performance and construction sequence. The concrete in-fill delays inherent buckling problem of thin-walled steel tubes and confinement effect exerted by the steel tube improves their performance. The steel at the outer perimeter performs most effectively in tension and bending enhancing its structural performance. CFST system has all the merits which bring it into the category of sustainable construction system as it reduces the cost of construction in many ways and this helps to save resources.

Main focus of the present study is to investigate the behaviour of beam-column joints in CFST frames. Various parameters influencing the behaviour of these columns have been studied. Numerical study of short columns has been carried out by using the experimental data available in literature and the model has been validated by comparison. From the comparison of the experimental results with the results obtained from finite element (FE) model it can be concluded that the proposed FE model is capable of predicting the column behaviour very accurately. It is observed from the experimental and the numerical investigations that the capacity of the columns is significantly affected by various factors viz; slenderness ratio, thickness, cross section of steel tube, strength of concrete core and the grade of steel.

The focus of the study is to explore the prospective of CFST beam-column joints as part of CFST frame structures. For this purpose, two types of connections using extended end plate and seat angle, are proposed to investigate the static performance and failure modes of the proposed connections. An experimental program has been conducted involving exterior beam-to-column joints subjected to monotonic loading applied at the free end of beam. The performance is evaluated in terms of load deformation behaviour, moment-rotation curves and failure modes. The test parameters chosen for comparison are the length, diameter and type of bolts. It can be concluded from the experimental investigations that extended end plate connections exhibit higher strength over seat angle connections. Variation in size of end plate, diameter, length and grade of bolts significantly affect the capacity of the joints. The experimental results indicate that the proposed connections perform in a semi-rigid and partial strength mode as per EC3 specification, and their rotational capacity satisfies the ductility requirements.

To validate the experimental behaviour of the proposed connections in CFST beam-column joints, finite element analysis (FEA) has been carried out under the static load using software ATENA-3D. Results of the proposed model are compared with the experimental results. The proposed FE model of CFST beam-column connections is found capable of predicting the behaviour of beam-column joints. Subsequently, the behaviour of the composite frame comprising CFST columns and beams using end plate connections has been studied under a lateral monotonically increasing load.

The environmental durability of CFST structures is a major issue in context with their performance. The susceptibility of CFST sections to corrosion can severely reduce the strength and durability of these structures. Interfacial debonding caused by corrosion weakens the confinement effect of steel tube and results in the loss of load-carrying capacity. Unfortunately, such damage cannot be visually identified. Hence, it is necessary to develop a non-intrusive technique for early detection of damages in the form of cracks, debonds and corrosion in CFST members. In this study, ultrasonic guided waves are used for monitoring two type of defects i.e. notches and delamination simulating loss of area and debond due to corrosion. Specific guided wave modes are used for investigating varying extents of notches and simulated delamination defects. It is concluded that Pulse Transmission (PT) signatures can relate to the percentage

notch and delamination very efficiently. The method is further applied to CFST sections undergoing accelerated corrosion. It can successfully relate to the state of steel tube undergoing chloride induced corrosion and can be applied to real time corrosion monitoring of CFST sections.

LIST OF PUBLICATIONS

[1] Kumari, B., Sharma, S., Sharma, S. and Kwatra, N., "Monitoring degradation of CFST sections using guided waves" Smart Structures and Systems, Vol. 19, No. 4 (2017) 371-382.

[2] Kumari, B., Kwatra, N. and Sharma, S., "Behaviour of bolted connections in concrete-filled steel tubular beam-column joints" Steel and Composite Structures, Vol. 25, No. 4 (2017) 443-456.

[3] Kumari, B., Kwatra, N. Sharma, S., "Experimental and numerical investigation of bolted beam-column connections in concrete-filled steel tubular frames" Iranian Journal of Science and Technology, Transactions of Civil Engineering. (Accepted).

CONTENTS

LIST OF FIGURES

LIST OF TABLES

NOTATION AND SYMBOLS	
CFST	Concrete filled steel tube
B	Width of square steel tube
H	Depth of square steel tube
L	Column length of test specimen
t	Thickness of steel tube
f_y	Yield strength of steel
f_u	Ultimate strength of steel
E_s	Young's modulus for steel
f_{cu}	Compressive cube strength of concrete
f_c'	Equivalent cylinder strength of concrete
f_{cc}	Compressive strength of confined concrete
E_C	Young's modulus for concrete
ε_c	Strain in concrete
ε_{cc}	Strain in confined concrete
K_{tt}	initial elastic shear (tangential) stiffness
K_{nn}	initial elastic normal stiffness
σ	Normal stress
τ	Shear stress
P_u	Ultimate axial force/ maximum test load on the beam tip
A_c	Area of core concrete
A_s	Area of steel tube

EI_b	Flexural rigidity for the beam
t_p	Thickness of end plate
Δ	Displacement
M	Connection moment
M_u	Ultimate moment of the test joint
θ_r	Connection rotation
θ_b	Beam rotation
$\theta_{r,u}$	Connection rotation corresponding to the ultimate moment of the connection
m	Dimensionless connection moment.
θ	Dimensionless connection rotation
$S_{j, ini}$	Initial stiffness of connection

GREEK SYMBOLS	
β	Beta
$\sum$	Sigma
σ	Sigma
Δ	Delta
θ	Theta
$\surd$	Under root
ε	Epsilon

CHAPTER-1

INTRODUCTION

1.1 GENERAL

The use of concrete filled steel tubular (CFST) sections in building construction has seen renaissance in recent years due to their numerous advantages, apart from its superior structural performance making a typical composite frame structure. Their usage as columns in high-rise and multi-story buildings, as beams in low-rise industrial buildings and as arch bridges, has been used extensively all over the world in past decades with abundant examples. As far as their usage in India is concerned, it is a new concept.

CFST sections comprise of a steel hollow section of circular or rectangular shape filled with plain or reinforced concrete. Typical CFST composite columns are represented in Figure 1.1.

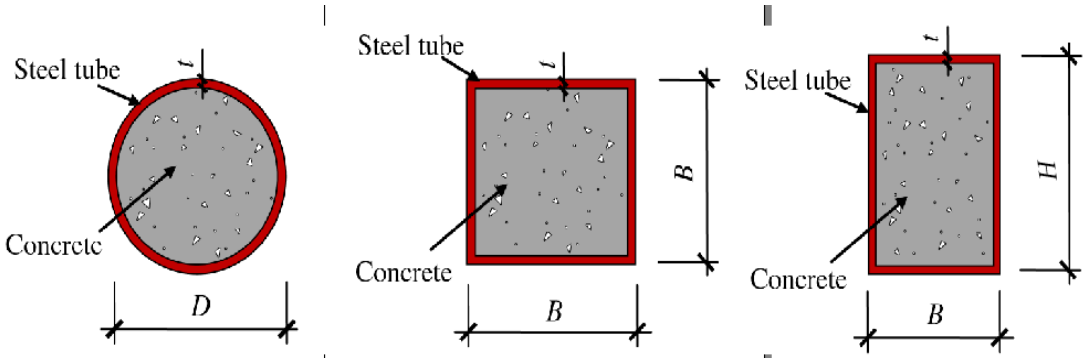

Figure 1.1 Typical Forms of CFST Members

The CFST structures make an efficient structural system with the advantage of both steel and reinforced concrete frame. It has numerous advantages in terms of structural performance and construction sequence. The concrete in-fill delays inherent buckling problem related to thin-walled steel tubes and improves the performance due to confinement effect exerted by the steel shell. The steel at the outer perimeter performs most effectively in tension and bending enhancing its efficiency in term of its structural performance. It offers the maximum stiffness as the material lies furthest from the centroid providing the maximum contribution to the moment of inertia. The concrete

core contributes significantly to axial compression resistance. Amongst other advantages are: elimination of form work, low construction cost, quick curing, fast erection, saving in manpower, improved fire resistance performance and seismic behavior. CFST system leads to slender columns and thus reduces the size of foundations, maintenance cost and cost of applied finishes. The cost of transportation and assembly of columns is reduced as they are built by erecting the hollow steel tube first, then pouring concrete into it.

CFST system has all the merits which bring it into the category of sustainable construction system as it reduces the cost of construction in many ways, helps to save resources. The environmental burden can be reduced by omitting the formwork. Above all steel which is a major constituent material of CFST frame, itself being almost totally recycled material, is a green material. All these merits make CFST sections a wonderful structural component.

1.2 BACKGROUND OF THE STUDY

1.2.1 CFST as Frames

This has been well established that the compressive strength of concrete filled steel tubular columns subjected to concentric compression is enhanced because of concrete confinement and the yield strength of steel tube [Shams and Saadeghvaziri (1997), Shanmugam and Lakshmi (2001), and Nishiyama et al. (2002)]. Further buckling resistance is also improved due to infilled concrete [Uy (2001b)]. Subsequently, it is also found that CFST have shown enhanced flexural strength as well [Zhang and Brahmachari (1994), Zhao (2002), Han (2004) and Kang et al. (2007)]. The flexural behaviour and ultimate moment capacity of concrete-filled rectangular hollow sections is enhanced by infilled concrete. It further improves load-deflection response, moment-strain behaviour, ductility, stiffness degradation and energy absorption of concrete-filled rectangular hollow section (RHS) beams.

The usefulness of CFST sections as columns is well recognized for their excellent performance and its application as flexural members has also been recognized approved by various researchers. But their efficacy as part of composite frames is still

unexplored. Many earlier studies are available for CFST composite frames in which CFST columns and steel beams are part the frame but very few studies are available in the literature where CFST members are used as columns and beams.

Hence, the present study has been undertaken to explore the potential usage of theses incredibly useful sections as part of CFST frame. Beam-column joints being the most crucial part of any type of frame and are designed more conservatively than individual members. Moreover, due to their connection components, they are more complex to analyze than individual members and the deviation between analysis and actual behavior is large. Hence, there is need to investigate the behaviour of CFST beam-column joints. Subsequently, these joints are to become a part of CFST frame, so their performance as part of frame is required to be investigated.

It is also a well-known fact that the experimental investigations are highly expensive and time-consuming specially in case of CFST frames due to the large scale. Further, there are several parameters which influence the behaviour of beam-column connections, make the experimental study difficult even though it provides dependable results. Hence, there is need to develop a Finite Element (FE) model to study the behaviour of CFST joints as well as frame.

1.2.2 Durability of CFST Sections

The environmental durability of CFST section is a major issue. One major flaw of structures made of CFST sections is their vulnerability to corrosion caused by environmental degradation which can severely reduce the strength and life of these structures. Corrosion of steel is one of the major durability problems to maintain aging CFST structures. Interfacial debonding caused by it weakens the confinement effect of steel tube on the concrete core resulting into the loss of load-carrying capacity. Unfortunately, such debonding damage cannot be visually identified but such damages are most unfavorable. Therefore, it is necessary to develop a non-intrusive technique for early detection of damages in the form of cracks, debonds and corrosion in steel tubes in CFST members. Guided waves have been exploited by researchers for monitoring various types of damages. The research in the last two decades has shown the capability of ultrasonic guided waves for monitoring various kinds of damages in RC structures. Very few research works have been reported on corrosion monitoring of

CFST members. Bolts being necessary elements of the joints used in these types of structures, chances of ingression of water inside the members are there resulting propagation of corrosion. Hence to explore the suitability of Ultrasonic Guided Waves for actual corrosion monitoring in CFST sections and a more elaborate and detailed investigation of various kinds of damages in CFST sections, it is required to develop a complete damage monitoring methodology.

1.3 GAPS IN THE RESEARCH AREA

From the literature survey following notable observations/gaps have been observed:

1. The behaviour of CFST column connected to CFST beams has not been studied extensively.
2. Numerical modeling is the most effective way to study the behaviour of CFST structures because the experimental method is highly expensive and time-consuming. There is need to develop numerical technique to model CFST beam-column joint and frames.
3. CFST sections are susceptible to environmental degradation like corrosion and non-destructive techniques need to develop to monitor the same.

1.4 OBJECTIVES OF WORK

Following objectives have been specifically laid down for the research:

1. To study the behaviour of different types of CFST beam-column joints experimentally to propose a model to be used in CFST frame.
2. To develop finite element models of various CFST beam-column joints used in experimental studies for analyzing their load-deformation behaviour.
3. To apply the developed FE model to study the non-linear behaviour of CFST frames with proposed model of CFST beam-column joint using finite element analysis.
4. To carry out corrosion-monitoring of CFST sections/joints using guided waves to study the degradation of these sections due to corrosion.

1.5 ORGANIZATION OF THESIS

The content of the thesis is divided in seven chapters.

CHAPTER 1: Introduction

CHAPTER 2: In this chapter, a relevant literature review is presented in two parts. The first segment presents an account of state-of-the-art of the field of CFST structures covering CFST columns, CFST beam-column joints, CFST frames and nonlinear studies of CFST members. The second segment the studies carried by various researchers on detection of degradation using ultrasonic waves.

CHAPTER 3: Experimental as well as numerical investigations of CFST columns have been presented in this chapter. The investigation has been elaborated by parametric study.

CHAPTER 4: The prospective of CFST sections as exterior beam-column joints of CFST frame structures has been explored in this chapter. An experimental program has been conducted involving two types of connections using extended end plate and seat angle. The performance is evaluated in terms of their load deformation behaviour and failure modes considering various test parameters. Finite element analysis has been carried out and results have been validated with the experimental results.

CHAPTER 5: This chapter presents the nonlinear analysis of the composite frame using CFST columns and beams, subjected to a lateral monotonic load.

CHAPTER 6: This chapter discusses a non-destructive degradation monitoring technique for early detection of corrosion and various defects caused by it in steel tubes in CFST members using guided waves.

CHAPTER 7: This chapter contains the important conclusions drawn from the various studies undertaken. Recommendations for further research in this field are also suggested.

At the end of the report references have been given in alphabetical manner.

CHAPTER 2

LITERATURE REVIEW

2.1 GENERAL

The present work aims to study performance of beam-column joints in concrete filled steel tubular frames. The performance of such structures can be assessed through their load deformation behavior and at the same time the assessment of their degradation due to many reasons amongst which corrosion is the primary one. Hence, the present study comprises of two different studies which have been carried out on CFST members i.e., investigation of beam-column joints in CFST frames and health monitoring of degradation of CFST sections mainly due to corrosion, notching and debonding. Hence, the literature study has been divided in two parts. A review of relevant literature to highlight the works related to CFST beams and columns is briefly discussed. Further, works related to CFST beam column joints have been discussed in detail. Finally, the studies related to degradation due to corrosion have been discussed in brief.

2.2 REVIEW OF WORKS DONE ON CFST STRUCTURES

The research work on concrete-filled steel tubular structures includes the research dealing with its component members i.e. columns and beams, connections/ joints and structural systems. The proposed study is related to CFST beam column joints in frames. Hence, the literature study of CFST systems has been further divided in following sub parts covering various aspects, including the static performance and the construction and durability issues. The results aim to provide insight to explore the applications of this composite structures in real civil engineering projects.

- CFST columns
- CFST beams
- CFST beam - column joints
- CFST frames

2.2.1 CFST Columns

A brief review of the behavior of concrete-filled steel tubular (CFST) members subject to axial load, is presented here. The discussion is focused on the basic behavior of columns. A lot of work on CFST columns have been done throughout the world in past few decades. Only few major theoretical and experimental studies performed have been discussed here.

2.2.1.1 Experimental Studies

Many studies have been carried out to investigate the behaviour of CFST columns subjected to various types of loadings. Furlong (1967), Knowles and Park (1969) and Neogi et al. (1969) are few of the earliest researchers who studied the behaviour of concrete filled steel tubular columns subjected to concentric compression and observed that the compressive strength enhances due to concrete confinement and the yield strength of steel tube decreases due to the development of hoop stresses in the steel tube. Knowles and Park (1969) proposed a value of 44 for KL/r (the ratio of effective length to radius of gyration) approximately equal to L/D of 12. Above this value confinement does not occur. Tomii et al. (1977) reported two failure modes, the overall buckling for slender columns and the crushing of concrete for short columns. The confinement effect decreases with the increase in column length. Shakir-Khalil and Zeghiche (1989) investigated full-scale rectangular CFST columns. Few studies carried out in past two decades are discussed below in brief:

Tomii (1991) found that the measured axial load carrying capacity of concrete filled steel tubes was greater than the nominal capacity which was defined as the sum of the compressive strength of the unconfined concrete and steel. This was related mainly to triaxial containment of the concrete and the strain hardening of the steel.

Ge and Usami (1992) conducted experimental work on concrete filled square box columns to determine the beneficial effects of filling thin-walled steel box columns with concrete. The main finding of the study was the delay of outward ***local buckling*** ascribed to specimens with longitudinal stiffeners.

Bergmann (1994) presented an experimental investigation of the compressive strength of CFST columns filled with high strength concrete (84 to 116 N/mm^2). Circular and square concrete filled tubes were tested under axial loading using different loading conditions. The test results indicated that the Eurocode-4 design provisions are applicable without modifications to the case of axially loaded circular tubes filled with high strength concrete.

Bridge et al. (1995) have suggested that a slenderness ratio (L/D) equal to 15 normally marks an approximate limit between short and long column behaviour.

O'Shea and Bridge (1997) conducted research on short CFST columns by considering the parameters as diameter to thickness ratio ranging from 55-200 and concrete of grades 50, 80 and 120 MPa and the results had shown an improvement in the buckling strength. Design methodologies were developed for thin-walled concrete filled steel tubes. The capacity of a short, thick-walled circular steel tube filled with medium strength concrete was determined using ACI 318 (1989) and EC4 (1992).

Kilpatrick and Rangan (1997) also presented an experimental and analytical investigation of the behaviour of concrete filled steel circular tubular columns and confirmed that the load carrying capacities of columns were considerably influenced by the slenderness of the tubes and the applied load eccentricity.

Schneider (1998) carried out concentric loading tests on 14 circular and rectangular composite columns with steel yield strength (fy) varying from 312 to 430 N/mm^2 and concrete cylinder strength (f'_c) between 24 and 31 N/mm^2. Results suggested that the behaviour was significantly affected by the shape of the cross-section and breadth to thickness ratio. Schneider also concluded from his test results that the concentrically loaded circular composite columns could have better post yield behaviour and larger stiffness than rectangular composite columns.

In an investigation into the design methods to predict the strength of concrete filled steel tubes, O'Shea and Bridge (2000) conducted tests on short circular thin-walled concrete filled steel tubes subjected to concentric loading with diameter to thickness ratios in the range of 60 and 220 and a length to diameter ratio of 3.5. They confirmed the enhancement of the concrete strength by the steel tubes, and it was

related to the type of loading conditions. Tan K. (2003) also performed similar tests with a length to diameter ratio of 3.5. Later, Lin and Tsai (2001) performed research on 18 specimens for double skinned CFST, considering parameters like diameter to thickness ratio and the hollowness ratio for an effective length of 1100 mm. They concluded that steel tube can improve the confinement of the concrete, and concrete infill can further postpone the incidence of local buckling of steel tube.

Uy (2001a) conducted an experimental programme undertaken for stocky short steel and composite columns fabricated with high strength steel plate. The experimental programme considered encased and concrete filled composite columns. All the columns were tested in pure compression and in order to estimate the capacity of the members an axial compressive strength model was proposed which considered the full capacity of both the steel and concrete.

Uy (2001b) performed experimental studies on two hollow short columns and nineteen short composite columns fabricated with high strength steel plate. The members were subjected to axial loading or uniaxial loading. The test results showed that the EC4 method overestimated the capacities of columns subjected to pure compression or pure bending. Hence, a conservative design model was developed, known as the mixed analysis approach.

Huang (2002), had studied the effects of cross section shapes, width to thickness ratios and stiffening arrangements on the ultimate strength, stiffness and ductility of CFT columns. He had conducted experiments with width to thickness ratio ranging from 40 to 150. Fourteen specimens with width to thickness ratio or diameter to thickness ratio of 40, 70, and 150 were tested. Results had shown a significant enhancement in the ultimate strength and ductility of square CFT columns.

Han (2002) performed tests on short rectangular columns with varying H/t or B/t ratios (16 to 52), and L/H ratio of 3 and concluded that the ultimate capacity is influenced by the confining factor, material properties and aspect ratio.

Liu et al. (2003) presented experimental results of a series of tests on twenty-two rectangular composite columns with a steel yield strength of 550 N/mm^2 and a concrete strength ranging between 61 N/mm^2 to 72 N/mm^2. Based on the test results, it was

suggested that the provisions in EC4, ACI and AISC moderately estimated the failure strength of the columns by 6, 14 and 16%, respectively. In further studies, Liu et al. (2003) presented the failure modes for different B/H ratios. It is observed that yielding occurs at both the faces simultaneously in case of square sections whereas longer face yields first in case of rectangular columns.

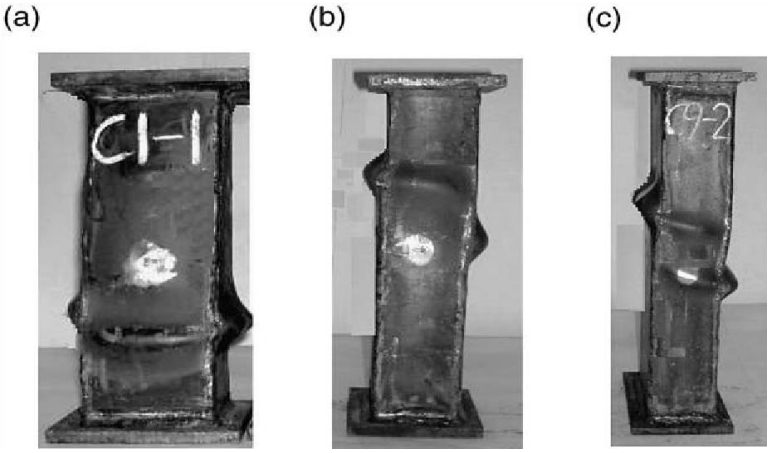

Figure 2.1 Typical Failure Modes of the Specimens (a) B/H= 1.0, (b) B/H = 1.5 and (c) B/H = 2.0 (Liu 2003)

Liu (2004) experimentally studied the behaviour of 12 high strengths rectangular concrete-filled steel hollow section columns subjected to eccentric loading keeping the cross-sectional aspect ratio, slenderness and load eccentricity as primary test parameters. The experimental ultimate capacities of the specimens were compared with the design strengths predicted by the codes. Comparison of results exhibited that Euro code 4 overestimated the ultimate capacities of the columns with a difference of 3%. ACI and AISC, conservatively predicted the failure loads by 11% and 25%, respectively.

Fujimoto et al. (2004) reported eccentric loading tests on 33 circular and 32 square composite stub columns. The test variables were material strengths (f_y = 262–853 N/mm^2; f'_c = 25–85 N/mm^2). Ductility improvement due to the confinement by the steel section was observed in the tests.

Sakino et al. (2004) investigated thirty-six circular and forty-eight square steel composite tubes subjected to concentric loading for deformation behaviour. Test parameters used in the study included material strengths (f_y = 262–853 N/mm^2; f'_c =

25–91 N/mm^2) and volumetric steel to concrete ratio (0.09–0.26). Test results showed a strength increase for square composite columns more than circular columns.

Giakoumelis & Lam (2004) and **Gupta et al. (2007)** concluded that concrete confinement increases as diameter-to-thickness ratio decreases. In addition, CFST columns were found to exhibit more local buckling and crushing of concrete for higher diameter-to-thickness ratio.

Zeghiche & Chaoui (2005) and Oliveira et al. (2009) concluded from their studies that axial capacity of CFST columns increases with steel and concrete material strength, as expected.

Han et al. (2011) examined tensile behaviour of CSFT sections considering steel ratio and type of concrete as parameters of experimental studies. Improvement in tensile strength was observed in the test results obtained.

Yang and Han (2009 & 2012) investigated the behaviour of CFST under partial compression. Test parameters considered were; cross-sectional shape, slenderness ratio and partial compression area ratio.

Abed et al. (2013) performed tests on 16 CFST short columns filled with normal and high strength concrete having a compressive strength of 44 MPa or 60 MPa considering the diameter-to-thickness ratios of 20, 32 and 54 in the experimental investigation. Test results indicated that the ultimate axial strength of CFST columns increased with an increase in the concrete compressive strength. Increase in the diameter-to-thickness ratio reduced the stiffness and ultimate axial strength of axially loaded CFST short columns.

Erramma and Niranjan (2014) studied the compressive behaviour of rectangular and triangular fluted reinforced CFST columns with varying slenderness ratio, experimentally and analytically. Analytical results were obtained using codes EC-4, ACI-318and ASCI and experimental results were observed to be higher than analytical results.

Han et al. (2014) reviewed the development of the family of concrete-filled steel tubular structures and presented a research framework on CFST members. The research

development on CFST structural members in most recent years, is summarized. The current design approaches from various countries are examined briefly. Comparative compressive behaviour of CFST stub columns is presented in Figure 2.2 which clearly shows that ultimate strength of CFST specimens is larger than the simple summation of the strength of steel tube and reinforced concrete. Schematic failure modes for the stub concrete-filled steel tubular column and the corresponding steel tube and concrete have been presented in Figure 2.3. It can be seen that both inward and outward buckling is found in the steel tube, and shear failure is exhibited for the plain concrete stub column. For the concrete-filled steel tube, only outward buckling is found in the tube, and the inner concrete fails in a more ductile fashion.

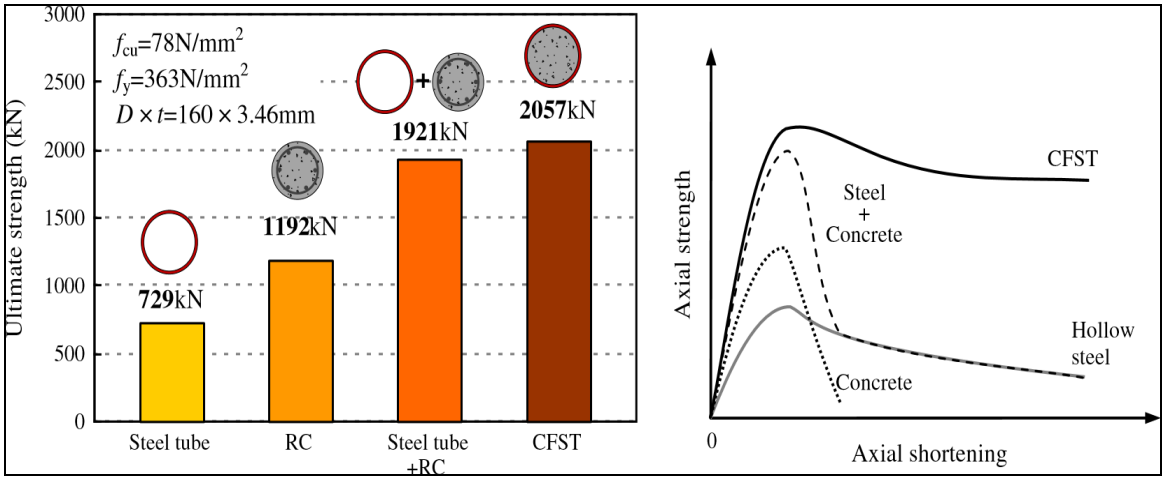

Figure 2.2 Axial Compressive Behavior of CFST Stub Column (Han et al. 2014)

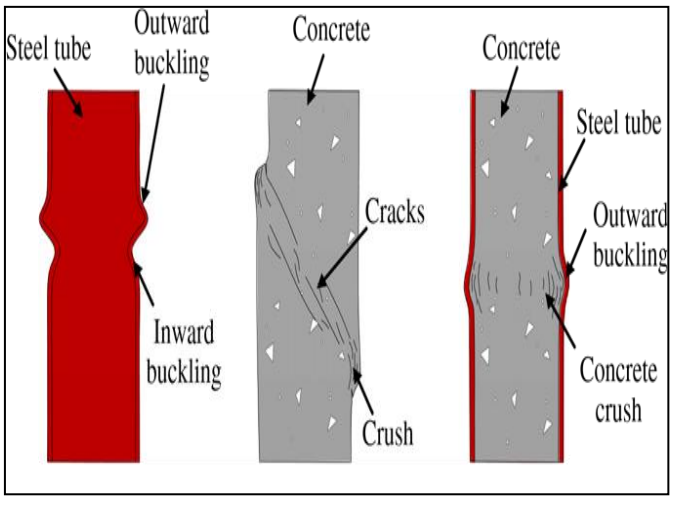

Figure 2.3 Schematic Failure Modes for Steel Tube, Concrete and the Stub CFST Columns (Han et al. 2014)

Jayaganesh et al. (2015) investigated the structural behavior of square and circular Concrete Filled Steel Tubular (CFST) stub columns subjected to axial partial/local compression. It was found that the elastic modulus(stiffness) and the ultimate bearing capacity of the CFST column decreased with the increase in local compression ratio.

It can be seen from the past experimental investigations that the behavior of uniaxially loaded short rectangular CFST columns has been adequately investigated. Literature review on nonlinear analysis for envisaging the behavior of CFST columns under axial load is provided in the following section.

2.2.1.2 Numerical Studies

Few researchers have executed numerical analysis of CFST column using nonlinear finite element methods.

Schneider (1998) developed a 3-D nonlinear finite element model for concrete-filled tubular columns using the ABAQUS program. The unconfined uniaxial stress–strain curve for concrete provided was used as five segments linear curves.

Hu et al. (2003) developed a nonlinear finite element model to simulate the behaviour of CFST columns using the ABAQUS. The steel tubes were simulated using an elastic-perfectly-plastic model with associated flow theory whereas an elastic plastic theory with associated flow and isotropic hardening rule was used to model the concrete. The von Mises yield criterion was employed to define the elastic limit of the steel tubes subjected to multiple stresses. The concrete confinement was achieved by matching the numerical results by trial and error by parametric study.

Hu et al. (2005) further elaborated the study by analyzing concrete-filled tubular columns subjected to an axial compressive force in combination with bending moment by using the ABAQUS, using the same material constitutive models used in the previous study.

Ellobody et al. (2006) also analyzed the behaviour of normal and high strength concrete-filled tubular columns using the ABAQUS using same parameters as used by Hu et al. (2003).

Zhao et al. (2008) simulated CFST column by the nonlinear finite element program

ANSYS/LS-DYNA in order to study the mechanical behaviour of the CFST column under blast load. The results indicate that CFST column has excellent ductility and blast resistance.

Han et al. (2011) presented a uniaxial compression stress–strain relation for confined core concrete of CFST member for ABAQUS, and the plastic damage concrete model was used to simulate the core concrete to predict the load versus deformation relationship. The experimental results matched well with the results that obtained from the finite element model using ABAQUS.

Xiamuxi and Hasegava (2012) conducted parametric study to clarify the effect of confinement on concrete core and propose evaluation equation for axial compressive strength of RCFT columns, numerical analyses of RCFT columns are conducted using non-linear finite element method (FEM) software–ADINA by matching the numerical results with experimental results via parametric study.

Zhou et al. (2012) experimentally investigated the behaviour of a special shaped column composed of concrete-filled steel tubes (SCFST column) subjected to a constant axial load and a cyclically varying flexural load. The experimental results were coMPared with the results from finite element analysis.

Patel et al. (2012) carried out experimental and numerical research on full scale high strength thin-walled rectangular steel slender tubes filled with high strength concrete. Experimental ultimate strengths and load deflection responses of CFST slender beam columns tested by other researchers were used to verify the accuracy of the numerical model. The verified numerical model was further utilized to investigate the effects of local buckling, column slenderness ratio, and depth-to-thickness ratio, concrete compressive strengths and steel yield strengths on the behaviour of CFST columns.

Yang and Han (2012) and **Evirgen et al. (2014)** also studied CFST sections considering various cross-sectional shapes like circular, hexagonal, rectangular and square. Experimental study was carried out by varying B/t (Breadth to thickness) ratio and grades of concrete and validated the results numerically using ABAQUS software.

Singh and Gupta (2014) presented a numerical investigation into the short CFST

columns performing 3D non-linear finite element analysis using ABAQUS. The parameters considered were different geometries of sections and different grades of infill concrete.

Serras et al. (2015) presented a simple and efficient analytical model for strength capacity the of circular concrete-filled steel tubes (CFST) under axial load and varying flexural loading. An accurate nonlinear finite element model is created using the ATENA software and the model is validated by comparing its results with those of experimental data published in the literature.

2.2.1.3 Closure

It has been observed from the literature review that relatively few researchers have performed finite element analysis of square/rectangular CFST sections. So, there is a requirement of FEM based numerical model to model and investigate the true behaviour of these incredibly useful sections.

2.2.2 CFST Beams

Many researchers have investigated the concrete filled tubular sections subjected to flexural loads for better prediction.

Zhang and Brahmachari (1994) had used cold-formed rectangular hollow sections in their experiments to predict flexural behaviour of CFST members.

Zhao and Grzebieta (1999), Elchalakani et al. (2001), **Zhao (2002**) and **Han (2004)** conducted experiments on concrete filled steel tubes. They obtained that filling of steel hollow tube with concrete increased the flexural strength.

Liang et al. (2005) used the finite element method to investigate the flexural and shear strengths of simply supported composite beams under combined bending and shear.

The test conducted by **Prabhavathy and Samuel Knight (2006)** in filled frames, showed that concrete in-filled beams give additional stiffness, which further delays the failure of the columns.

Han and Yang (2006) further tested total of 36 composite beam specimens filled with self-consolidating concrete to study the flexural behaviour of concrete-filled steel tubes.

The main parameters varied in the tests are: sectional types (circular and square); steel yielding strength (from 235 to 282 MPa), the ratio of tube diameter (or width) to wall thickness, D/t (from 47 to 105), and the ratio of shear span to depth (from 1.25 to 6).

Failure modes of CFST circular sections obtained by Han et al. (2006) in experimental testing are presented in Figure 2.4.

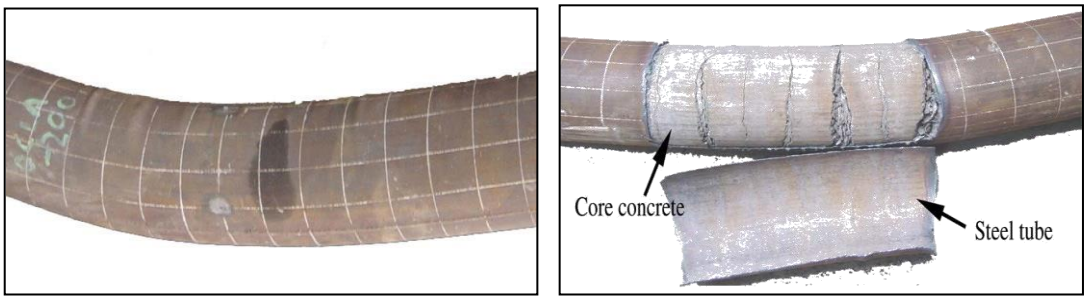

Figure 2.4 Failure modes of CFST Members in Bending (Han and Yang 2006)

Kang et al. (2007) carried experimental investigations of the flexural behavior of concrete-filled steel tubes, with variety of the filling material to evaluate their application as continuous girders and concluded that concrete-filled steel tube girders have good ductility and maintain their strength up to the end of the loading.

Arivalagan and Kandasamy (2008) and Arivalagan (2010) experimentally studied the behaviour and ultimate moment capacity of unfilled and concrete-filled rectangular hollow sections subjected to cyclic reversible loading to study the effect of filler materials, section slenderness, load-deflection response, moment-strain behaviour, ductility, stiffness degradation and energy absorption of concrete –filled RHS beams. From this study, it is understood that void filling increases the capacity of the section. Arivalagan (2010) also presented nonlinear finite element (FE) model for rectangular hollow sections filled with high strength concrete when used as a beam.

Gupta and Kataria (2014) compared the effects of size of the section on the bending capacity of square CFST beams testing six specimens. The main parameter was equal increment in sectional area of steel tube and in concrete of CFST beams. Fiber element analysis model was used for nonlinear analysis of flexural behaviour CFST beams. It was concluded that moment capacity of CFST beams increases in nonlinear incremental manner with increase in the sectional area of composite materials.

Han et al. (2014) presented the comparison of failure modes of CFST members with hollow steel tube and concrete beam subjected to bending as shown in Figure 2.5.

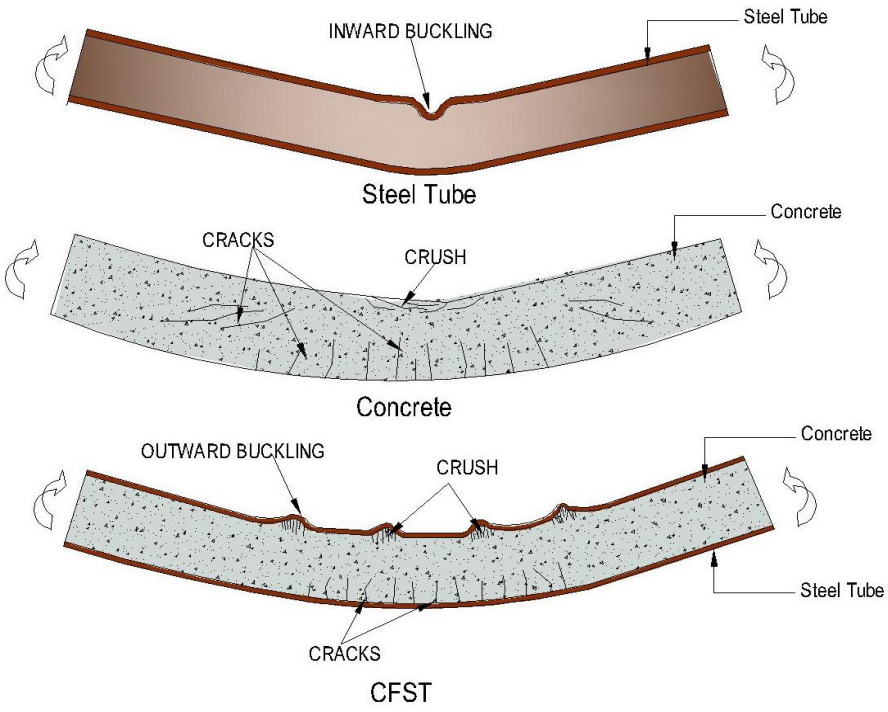

Figure 2.5 Behaviour of CFST Members in Bending (Han et al. 2014)

2.2.2.1 Closure

It can be established from the literature review that filling of steel hollow tube with concrete increased the flexural strength and ductility. Concrete in-filled beams give additional stiffness, which further delays the failure of the columns. Despite of this fact CFST sections as beams have not been explored as part of CFST frames.

2.2.3 CFST Beam-Column Joints

Beam-column joints construct a vital part of any structure and are designed more conservatively than individual members. Behaviour of beam-column joints is complex than that of individual members but the CFST connections are more complex to analyze and the deviation between analysis and actual behavior is large. Further, in case of overloading, the failure confined to individual members is preferred rather than in connections, which could affect many members. Beam-column connections comprise a huge part of the cost of structure steelwork and hence their design is of key importance

for the economy of the structure.

Connections are the most vulnerable in steel structures. Bolted connections using black bolts tend to slip, which reduces their energy dissipation capacity under cyclic loading and so are to be avoided. HSFG bolts perform better. The cost of various types of connections commands the lateral load resisting system used in steel framed structures. Simple connections (Figure2.6) are not expected to carry any moments (Neves et al. 2002 and 2003) and so only rigid and semi rigid connections will be discussed. Rigid connections are usually strengthened to an extent that their rotations /deformations are negligible compared to that of the members being connected. This is because in conformity with the capacity design philosophy, it is advantageous to ensure the development of plastic hinges in beams away from the beam column connection.

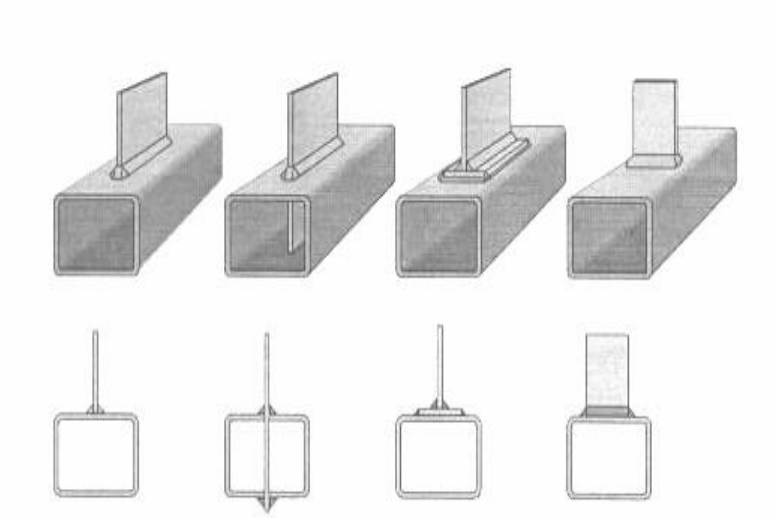

Figure 2.6 Typical Simple (No-Moment) and Rigid Joint Details (Neves et al. 2002)

2.2.3.1 Various Type of Connections

A wide array of beam-CFT column connections have been studied over the past few decades. Chen et al. (2015) reviewed a variety of connection details to concrete-filled rectangular tubular (CFRT) columns that have been developed by different researchers. A most convenient connection involves attaching the steel beam directly to the outer surface of the steel tube for simple connections [Dunberry et al. (1987) and Shakir and Mahmoud (1995). Alostaz and Schneider (1996)] investigated

seismic performance two types of connection details:

- Through beam
- Through column

Beams passing through panel zone are referred as through beam connections and beams connected to continuous columns are referred as through column connections. Test results showed that through beam connections enhance the seismic performance. Elremaily and Azizinamini (2001) investigated through beam connections for shear strength in the panel zone of CFST connections. But due to its complex nature in the panel zone these connections have difficulties in construction whereas through column connections can facilitate the field construction, Cheng et al. (2000) and Fujimoto et al. (2000) also studied the connections details to improve its seismic performance.

End plate type bolted connections (Figure2.7), are being extensively used in steel structures (Kaushik et al., 2013). Bolted end-plate I-beam to RHS column joints have been studied by several authors: France (1997); Lu et al. (1993); Lu & Wardenier (1998); Mourad et al. (1996); Neves et al. (2002 and 2003); Silva et al. (2003). They are often used as moment-resistant connections. Due to simple fabrication techniques and speedy erection, have made end plate connection one of the most popular methods of connecting members in structural steelwork frames. Extended end plate connections to rigid column stubs using bolts, also provides fairly good hysteretic loops but leads to abrupt failures

Another type of connections discussed in literature are seat angle connections. These connections have the advantages of easy quality control and less assembly time than welded connections. Pirmoz et al. (2008**)** studied the behaviour of bolted top-seat angle connections with web angles using 3D parametric models. Seat angles are attached to beam section on both sides and these angles are bolted to the CFST column (Figure 2.8). Bolted angle connections with top and seat angles as well as web cleats leads to pronounced pinching of hysteretic loops due to deformation of the angles.

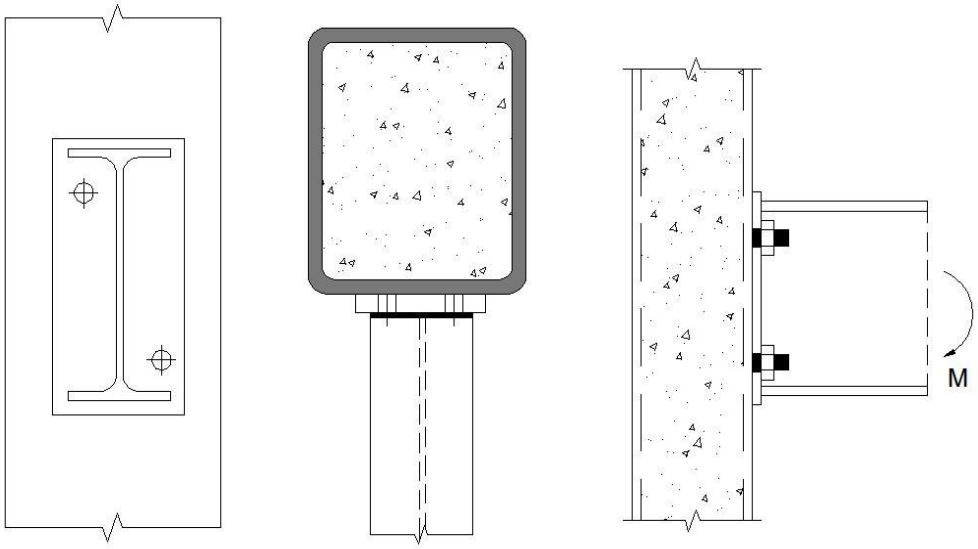

Figure 2.7 Typical End Plate Type Connection

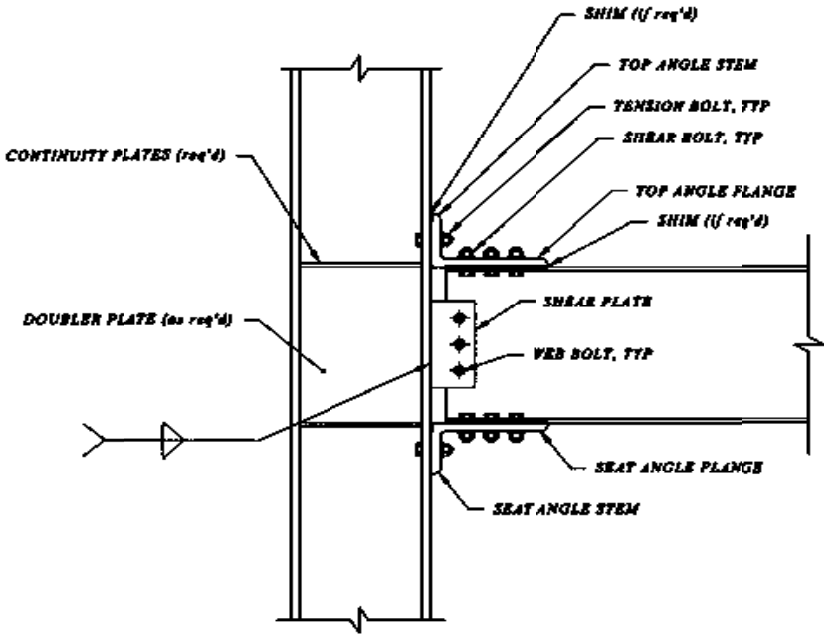

Figure 2.8 Typical Top and Seat Angle Type Connection (Pirmoz et al. 2008)

Hu et al. (2011) in their research, integrated three structural design concepts: the use of composite concrete-filled tube (CFT) columns, the use of partially restrained (PR) connections and the introduction of innovative materials (shape memory alloys) in the

design of smart connections (Figure 2.9). These concepts are used to enhance the robustness and performance of composite-special moment frames.

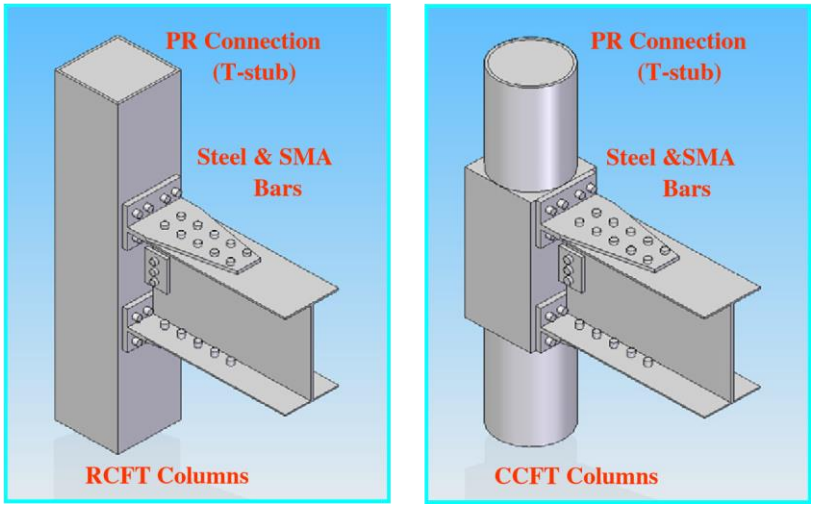

Figure 2.9 New Smart PR-CFT Connections (Hu et al. 2011)

The connection behaviour of various connections like fully restrained/rigid , partially restrained/ semi-rigid bolted connections has been presented in Figure 2.10.

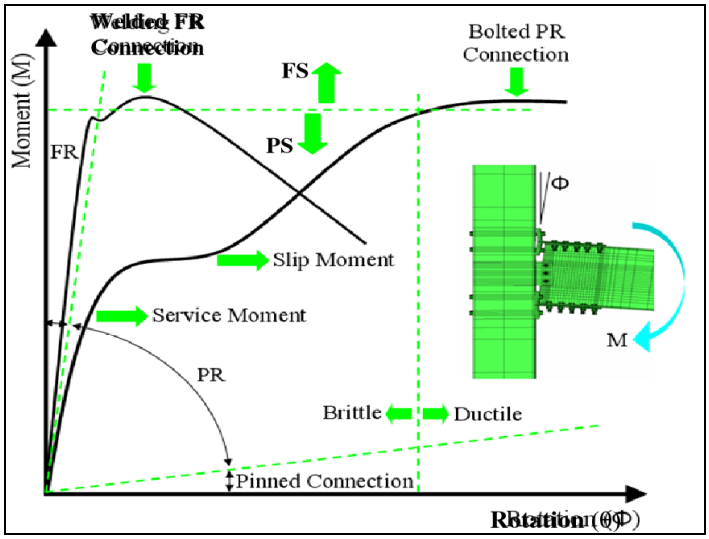

Figure 2.10 Characteristic of Connection Behavior : Fully Restrained Versus Partially Restrained Connection (Hu et al. 2011)

The innovative PR connections utilized the re-centering properties of super-elastic shape memory alloy tension bars and the energy dissipation capacity of low-carbon steel tension bars, as figured out in Fig 2.11. Simplified user joint elements based on the mechanical modeling approach were formulated in an effort to simulate the realistic behavior of bolted connections. The performance of the proposed frame was compared with the conventional welded frame in terms of time history response, residual roof drifts and inter-story drift ratios. It was observed that frames with the PR composite connections showed superior performance.

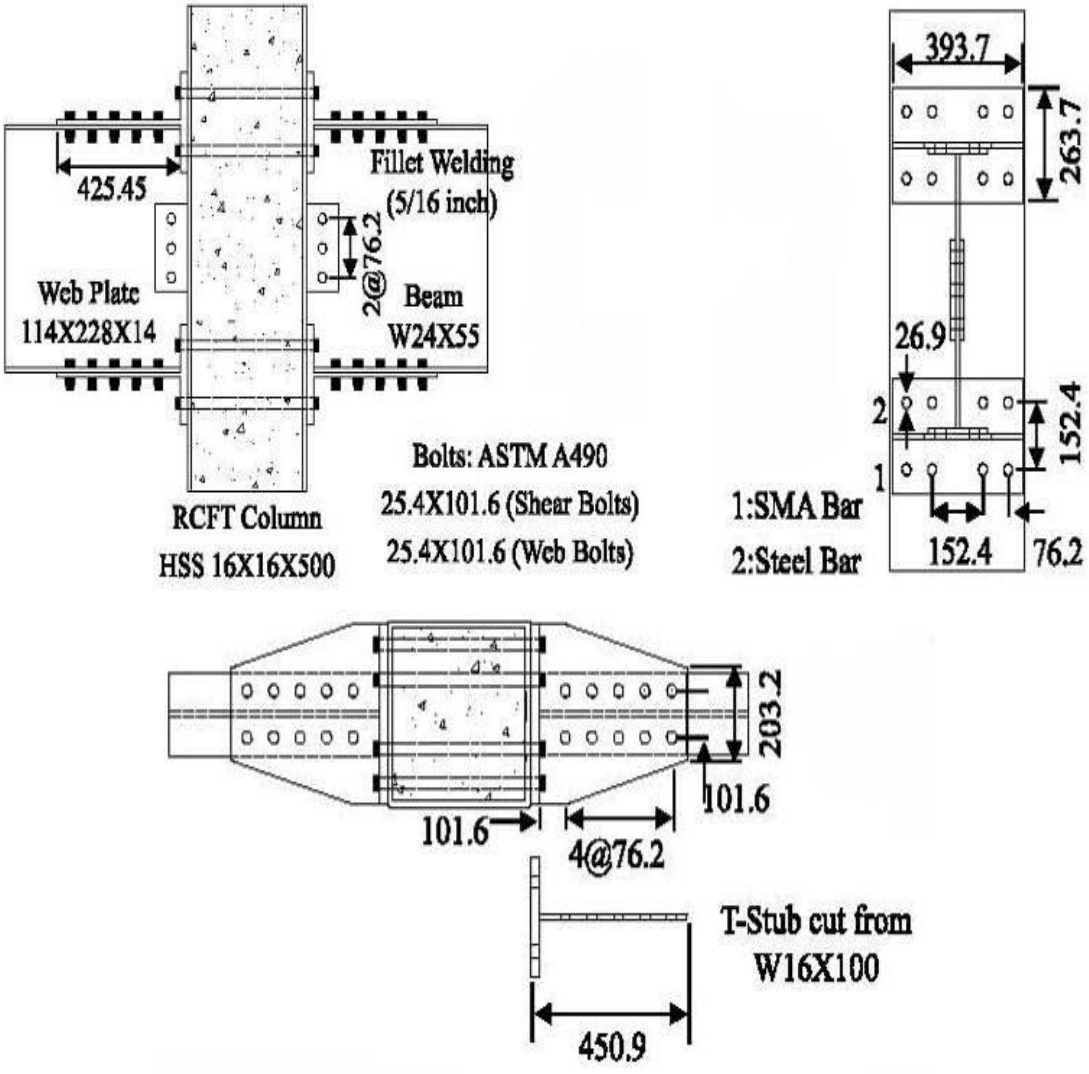

Fig. 2.11. Smart PR-CFT Connection Model (T-Stub Connection Detail) (Hu et al. 2011)

2.2.3.2 Experimental Studies of End Plate Beam-Column Connections

A brief review of work done by various researchers on CFST beam-column joints using end plate bolted connections has been presented below:

France (1997) conducted a test programme to obtain experimental data on the behaviour of end plate beam to column connections, made by using end plates bolted directly to the column face with ordinary bolts screwed into threaded holes formed using the flow drill process. Results obtained from tests are compared with those from a parallel series of tests in which the tubes were unfilled. Significant differences in strength and stiffness were observed

Beutel et al. (2001) conducted an experimental investigation into the behaviour of composite column-to-beam connections using ten large-scale connections under monotonic loading and under cyclic loading and presented the details and results of the preliminary monotonic tests.

Wang et al. (2008) presented the results of experimental program for bolted moment connection joints of circular or square concrete filled steel tubular (CFST) columns, and H-shaped steel beams using high-strength blind bolts. Moment rotation relationships were obtained and their performance was evaluated in terms of their stiffness, moment capacities and ductility. The test parameters varied were the column section type and the thickness of the end plate. The results showed that the proposed blind bolted connection satisfies the ductility requirements for earthquake-resistance in most seismic region for moment-resisting composite frame structures. Wang et al. (2008) also reported the mechanism of composite frames with square CFST columns based on the experimental research presented by Han et al. (2008) to investigate the influence of axial load on the structural behavior of composite frames. It was observed that the ultimate lateral load and displacement ductility decrease with increasing axial load level. Beam failure was observed first in all the frames. The lateral load-carrying capacity, ductility coefficient of composite frame decreased as the axial load level in the column increased.

Wang and Guo (2012) carried out an experimental study on the structural behavior of blind bolted end plate connections between CFTST columns and steel beams under monotonic loading to develop an easy to use bolted moment connection in the thin-

walled structures. The proposed connection was evaluated for the failure modes, moment– rotation relationship and connection rigidity.

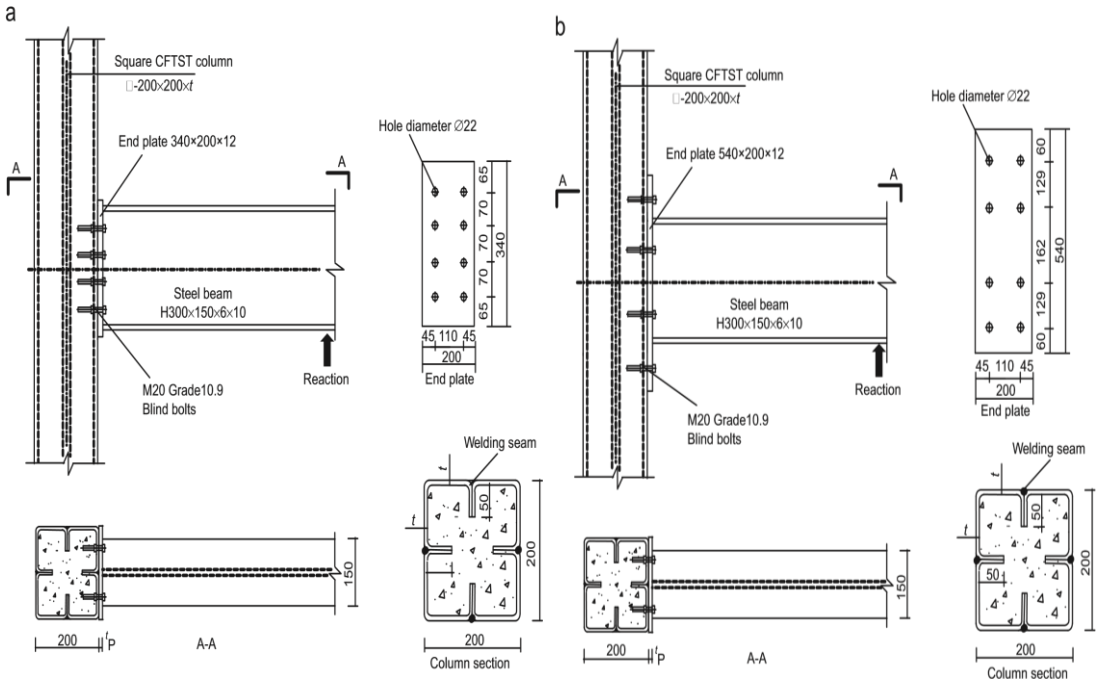

(a) Flush end plate connection (b) Extended end plate connections

Figure 2.12 Design Details of Test Specimens (Wang and Guo 2012)

Wang et al. (2012) investigated the seismic performance of the composite joint consisting of square concrete filled thin-walled cold-formed square tube CFTST column and steel beam with end plate and blind bolts. The CFTST column connection was fabricated by seam welding together four pieces of lipped angle with nominal wall thickness 1.5 mm or 3 mm. Four exterior joint specimens were tested under axially compressive load on the top of the columns and cyclic loads on the beam tip. The experimental parameters in the study were the thickness of the steel tube and the type of end plate. The seismic response of the blind bolted moment joints to CFTST columns was analyzed and evaluated in terms of the hysteretic behavior, failure modes, stiffness and strength degradation, ductility, and energy dissipation capacities of the joints. To improve the tension behavior of the blind bolted moment connections to the thin tube wall, the anchorage action of reinforcing rebar welded to the bolts with concrete-filled steel tubes was also investigated to consider the effect of cyclic loading

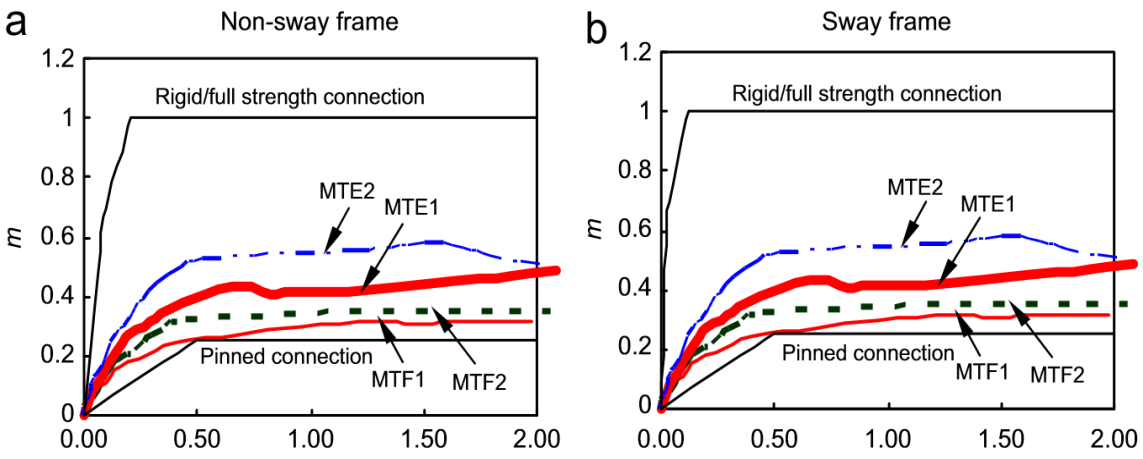

Figure 2.13 Classification of Tested Connections (Wang and Guo 2012)

Sheet et al. (2013) tested four half-scale interior connections with steel beams and concrete filled tubular (CFT) under cyclic displacement-controlled load. Square and circular steel tubular columns were considered with two different types of connections, flat and curved extended end-plates bolted to the CFT column with steel rods passing through the column and a through beam connection type, the experiments demonstrated the ductile failure of joints, large displacements with no apparent signs of local distress in the tube wall.

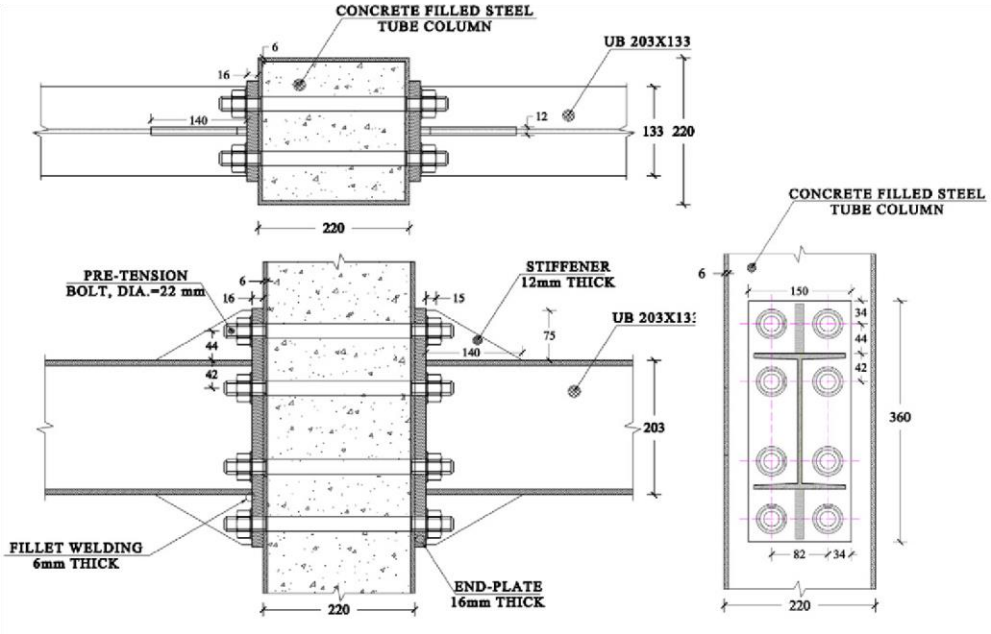

Figure 2.14 Flat End Plate Connections (Sheet et al. 2013)

2.2.3.3 Numerical Studies

Kaushik et al. (2013) used the finite element method approach (FEM) to analyze the fatigue behavior of bolted beam to column end-plate connection in the structural steel framework subjected to static loading. The study was elaborated for fatigue behavior of bolted beam to column end-plate connection subjected to static loading.

Wang et al. (2013) further elaborated his investigations with the finite element analysis (FEA) by modeling the tested specimens and comparing the results obtained from the FEA modeling against those from the test results. The feasibility of connecting an end plate to the steel beam using an alternative method to improve the joint behavior has been explored by the FEA studies.

Wang and Spencer (2013) conducted experimental tests and numerical analyses to study the behavior of the blind bolted end plate joint with concrete-filled square hollow section columns to steel beam. The behaviour was evaluated by testing four full-scale sub-assemblages' representative of interior or exterior beam-to-column joints.

Tizani et al. (2013) reported on the bind bolt connection type and executed an experimental programme to measure the connection stiffness. The programme tested eight full size connections, principally varying the connection endplate type, column thickness and concrete strength. The data was cross validated with a finite element model. The paper assessed the performance of this connection using connection stiffness classification methods. It concludes that the connection is able to develop the required stiffness for it to be used as a rigid connection in braced frames.

Hassan et al. (2014) investigated the behaviour of steel beam-CFST column joints with endplate connections, using blind bolts by performing finite element (FE) analysis. The FE model is verified with comparison of simulation results with test data. The effect of various types of blind bolts and binding bars on the joint behaviour is also analysed.

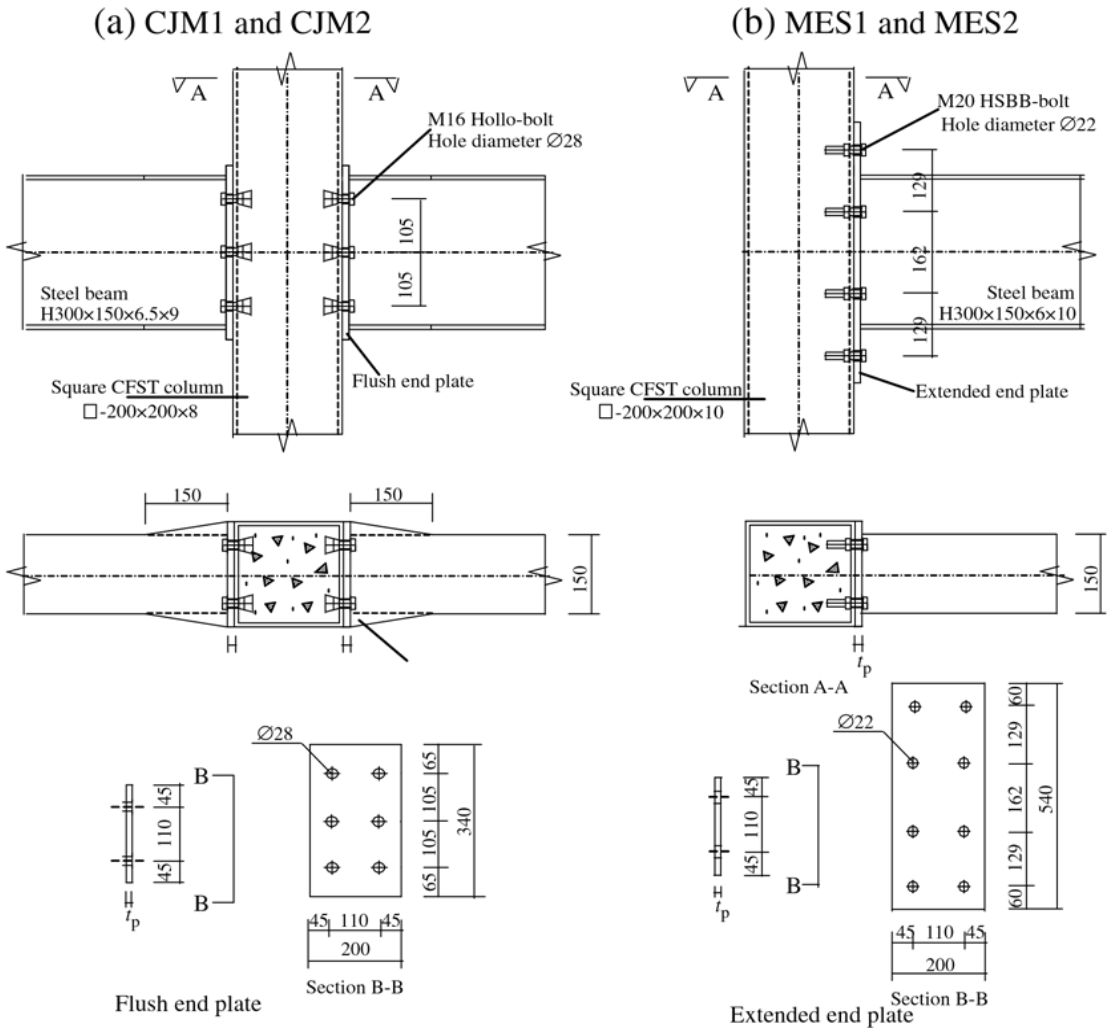

Figure 2.15 Extended End Plate Connections using Hollo Bolts (Wang and Spencer 2013)

Wang and Lee (2015); Wang et al. (2017) studied a mixed diaphragm in which a penetrated diaphragm and an exterior diaphragm are used at the beam-to-column connections of circular CFST columns to enhance the concrete filling property of the columns. Then the study was elaborated by considering rectangular CFST columns. The study was conducted based on the optimal dimensions of the mixed diaphragm and the validity and superiority of the mixed diaphragm at the connections of the rectangular CFST structure were then confirmed. The size of the rectangular CFST column, of which the yield moment is larger than that of the beam, was selected. Finite element analysis (FEM) was used to select the type of rectangular CFST.

2.2.3.4 Closure:

The advantages of utilizing concrete-filled tubular columns may still remain underutilized due to the lack of design guidelines on suitable cost-effective and construction-efficient connections between concrete-filled tubular columns and steel beams. This dearth of information is even more noticeable with regards to connections to CFST rectangular columns (Chen et al. 2015).

- Many researchers have reviewed the extensive theoretical and experimental works on the behaviour of CFST beam–columns and concluded that the understanding of the behaviour of CFST beam–columns joints is complex and its design has not been sufficiently verified. Therefore, more studies are required to improve the design for the beam-to-column connections to avoid connection failure before the ductility of the beam, column, and the panel zone is developed.
- It is understandable from the literature available that most of the previous studies are based on CFST column and steel beams (not concrete filled). No study of the behaviour of CFST column connected to CFST beams is available.
- End plate type bolted connections are extensively used in steel structures and CFST frame structures. Though being easy in their use, bolted endplates are extremely complex in their analysis and behavior. Hence, to analyze the forces to which these are subjected to is very critical.
- Furthermore, lack of efficient numerical modelling is also observed from the literature review.

2.2.4 CFST Frames

Multi-storey composite frames are extensively being used in high rise buildings in China. These frames are commonly composed of columns of structural steel members made composite with concrete and steel beams. In fact, most multi-storey steel construction makes use of composite action in the column members. Therefore, in order to consider the exact behaviour of the CFST frame, the composite action between steel and concrete is considered in such structures. The design of frames with CFT columns is similar to frames using structural steel sections for columns in which it is essential to

make a hinging beam joint. Thus, the ability to accurately compute the CFT column and joint strengths is imperative. Previous research on advanced analysis in steel framed structures is limited in its application. The effects of concrete infill have not been considered. Unfortunately, there also are severe limitations in the application of CFST, because the behavior of CFT elements is quite different than steel or concrete elements. Further, connections between CFT columns and steel members are also different than those used in ordinary steel construction.

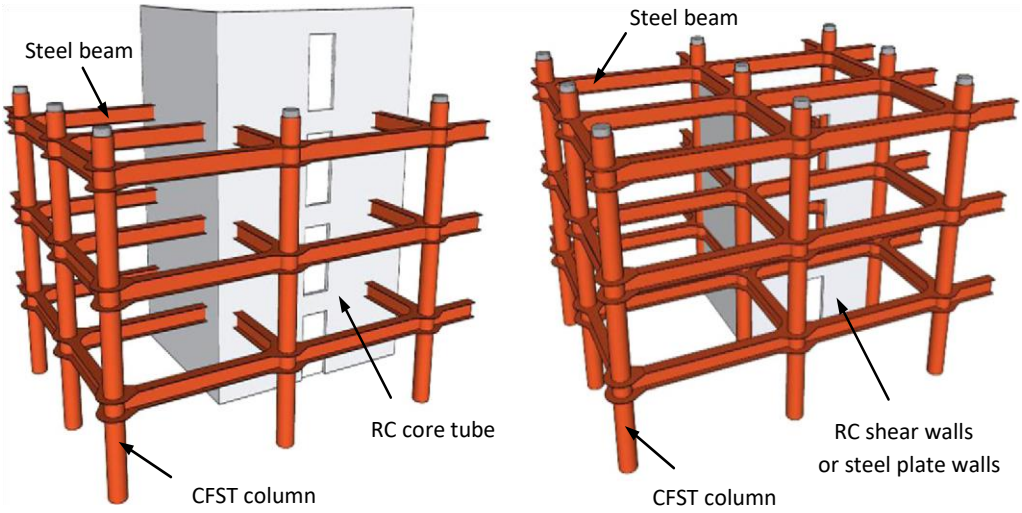

Figure 2.16 Existing CFST Hybrid Structural Systems (Han et al. 2014)

Whilst there has been considerable research into the behaviour of steel frames, composite frames have received less attention until recently (Liew and Uy, 2001). Little research has been done to investigate the behaviour on the CFST frame, especially the theoretical research by accurate model. Few of the studies available in literature have been presented here.

Eurocode 4 makes no mention of this type of analysis procedure.

Chen and Toma (1994) developed a thin-walled beam-column element, allowing for the advanced modelling of concrete core-walls and their interaction with the surrounding steel frames.

Matsui (1995) performed tests on square CFST frames with varying parameters viz width-to-thickness ratio of the column tube, diaphragm type, and loading histories. It is

concluded that the CFST frame showed excellent load carrying capacity under horizontal loads and the limiting value of the width-to-thickness ratio of the CFST column could be magnified to about 1.5 times that for the unfilled sections owing to the better local buckling strength and post buckling behaviour of the in-filled sections.

Kawaguchi et al. (1997) performed experiments on four portal frame specimens consisting of concrete-filled square hollow section (SHS) steel tubular columns and an H-shaped steel beam with through-type diaphragms under the constant axial load and cyclic horizontal load. The CFST frame exhibited excellent earthquake resistance. The axial load level of columns is generally small, the maximum value is 0.3.

Liew et al. (2001) have developed an advanced inelastic analysis technique and applied it to multi-storey steel buildings with composite beams.

Tsai et al. (2003) carried out a pseudo-dynamic test of a full scale 3-story composite frame using CFST columns and steel beams consisting 3-bays with buckling restrained braces in the middle span. The test result showed the excellent seismic capacity of the composite frame.

Schneider et al. (2004) discussed an economical connection for a steel girder to a concrete-filled steel tube (CFT) column. The joint consisted of a structural steel wide-flange shape penetrating continuously through a composite concrete-filled steel tube (CFT). Examples of two joint types were considered: One in which the girder was attached to the column in the field, and the second consisting of shop fabrication of the critical joint. The anticipated behavior during a seismic event, and some critical issues in the design of the connection, were presented.

Herrera (2005) predicted the seismic behaviour of CFST composite frame by performing the nonlinear analysis using software DRAIN-2DX. The analysis was based on the fiber beam–column element theory.

Han et al. (2008) presented the behaviour of the composite frame with concrete-filled square hollow section (SHS) columns to steel beam. Finite element modeling (FEM) was developed to carry out the behaviour of composite frames under a constant axial load on columns and a lateral cyclic load on the frame. Accurate material and geometrical nonlinear for confined concrete and steel were considered in the analysis. The finite element program ABAQUS was adopted. A damage plastic model for

concrete and elasto-plastic model for steel were used respectively. Six composite frame tests were carried out to verify the FE model. Each test frame specimen consisted of two concrete-filled SHS columns and a steel beam to represent an interior frame in a building. The results obtained from the finite element model were verified against those obtained from the experimental results.

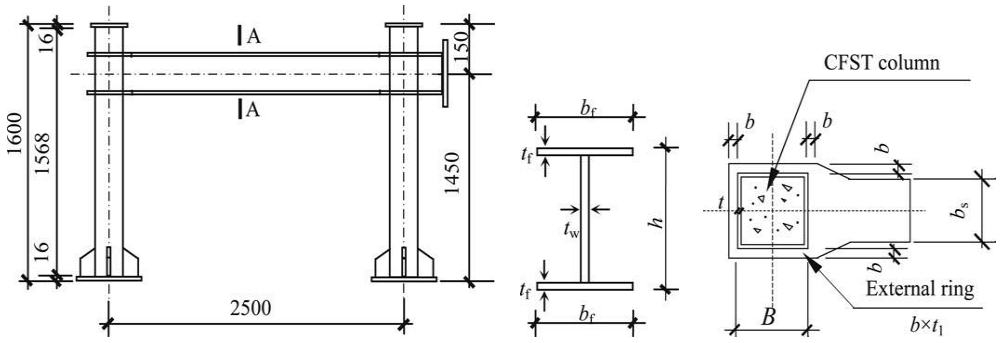

Figure 2.17. Frame Configuration (Unit: mm) (Han et al. 2008)

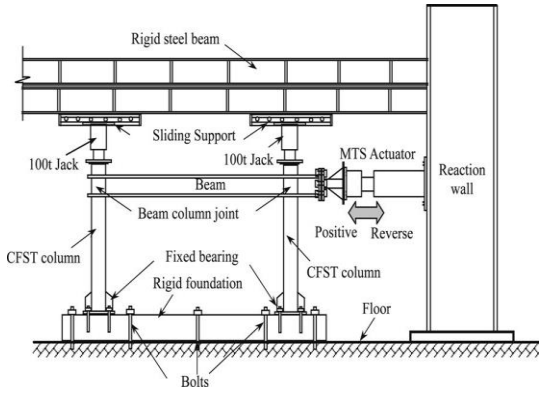

Figure 2.18. Arrangement of Test Set-Up (Han et al. 2008).

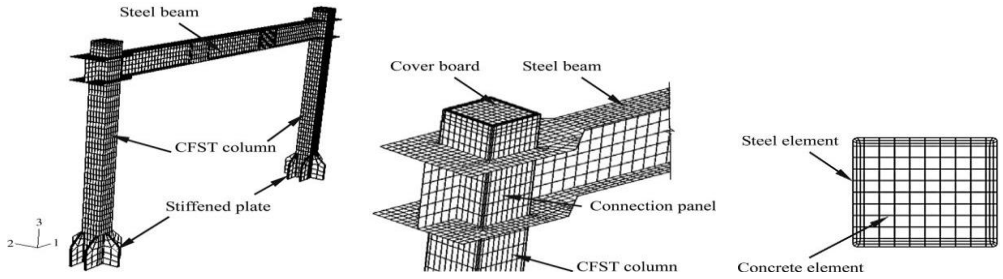

(a) The whole FEA model. (b) Steel beam discretization. (c) Section discretization.

Figure 2.19. Typical Finite Element Model of Composite CFST Frames (Han et al. 2008)

Han et al. (2011) presented the study on the behavior of composite frames with circular concrete filled steel tubular (CFST) columns to steel beam. Six composite frames represent an interior frame were tested under a constant axial load on the CFST columns and a lateral cyclic load on the frame. A finite element analysis (FEA) model was developed to verify the results against the experimental results. Detailed analysis was carried out on longitudinal stress in steel beams, axial stress distribution in concrete, concrete stress along the column height and at the connection panel. Parametric studies were conducted to investigate the influence of axial load level, beam to column linear stiffness ratio on the structural behavior of composite frames.

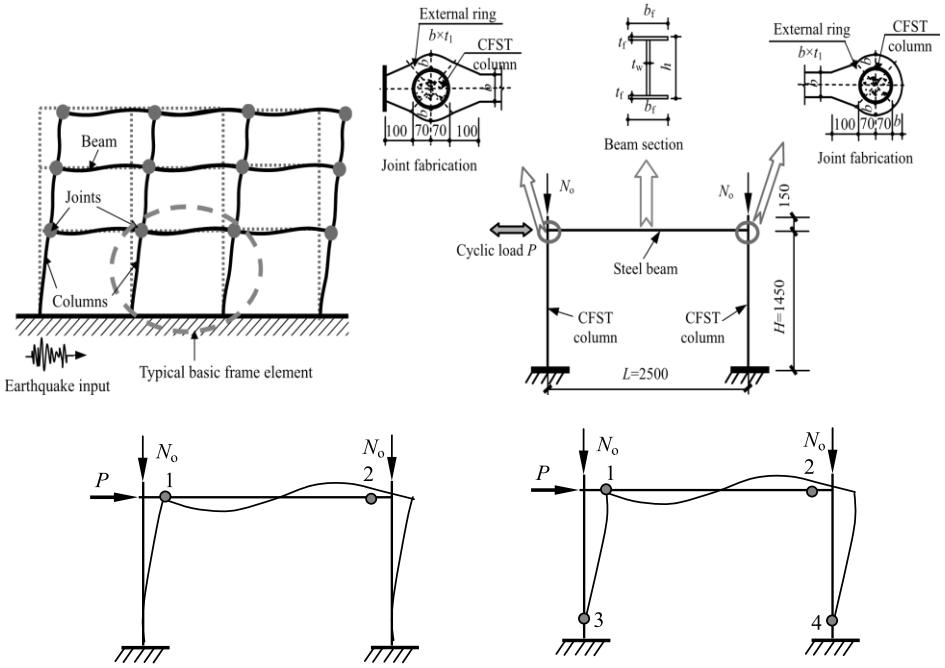

(a) Typical failure process and sequences of the plastic hinges.

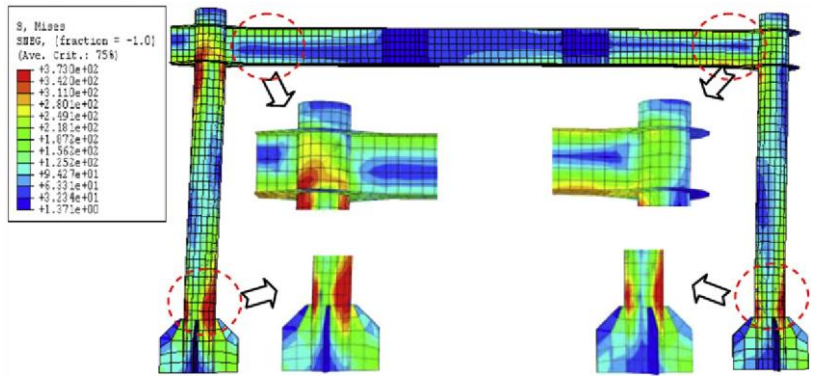

(b) Stress distribution (Stage 1).

Figure 2.20. Schematic View of Frame Models and Failure Modes (Han et al. 2011)

Zhao (2016) described an approach of simplified macro-modelling for composite frames consisting of steel-concrete composite beams and CFST columns and presented the performance evaluation procedure based on the pushover nonlinear analysis results. A four-story two-bay composite frame underground was selected as a study case. The establishment of the macro-model of the composite frame was guided by the characterization of nonlinear behaviors of composite structural members. Pushover analysis was conducted to obtain the lateral force versus top displacement curve of the overall structure. The identification method of damage degree of composite frames has been proposed.

2.2.4.1 Closure

Several state-of-the-art reports or papers have been published on CFST structures, such as Shams and Saadeghvaziri (1997), Shanmugam and Lakshmi (2001), Gourley et al. (2001) and Nishiyama et al. (2002) Whereas many studies have been done to assess the performance of CFST sections subjected to flexural loads. But the behaviour of composite frames is not fully understood hence the requirement for accurate and reliable analysis of a composite frame is very clear.

Though few experimental and numerical studies are available for analysis of CFST composite frames in which CFST columns and steel beams are part the frame, no study is available in literature where CFST members are used as both beam and columns as part of CFST composite frame. Little success has been achieved so far in developing an accurate model due to the complexity in modeling the concrete confinement effect for concrete-filled steel tubular members. Set against this background, to determine the behaviour of the composite frames with concrete-filled square hollow section (SHS) steel tubular columns to CFST beams, numerical studies are proposed to be carried out.

2.3 USE OF ULTRASONIC GUIDED WAVES FOR MONITORING DEGRADATION

In an infinite isotropic solid medium, only two types of independent wave propagation exist, i.e., compressional and shear waves. Both the waves propagate with

constant velocities and are non-dispersive. When geometry constraints are introduced and the dimensions are close to the wavelength, the wave becomes dispersive and is called a guided wave (**Reis et al. 2005**). In an infinite bulk of a perfectly elastic material, ultrasonic waves travel as bulk waves, decaying in amplitude because of the spread of the wave front. However, in a finite perfectly elastic medium, the sound wave is reflected from the structure boundaries, and the energy is contained within the elastic medium as a guided wave, which propagates with constant amplitude.

Ultrasonic Guided Wave inspection and structural health monitoring are being considered today in such natural wave guide structures as plates, multi-layer structures, rods, rails and pipes. An increased understanding of the basic physics and wave mechanics associated with guided wave inspection has led to an increase in practical nondestructive evaluation and inspection problems. A principal advantage of guided waves is inspection over long distances with excellent sensitivity from a single probe position. There is also an ability to inspect hidden structures and structures under water, coatings, insulations, and concrete.

The wave is termed "**guided"** because it travels along the medium guided by the geometric boundaries of the medium. Since the wave is guided by the geometric boundaries of the medium, the geometry has a strong influence on the behavior of the wave [Redwood (1960) and Achenbach (1975)]. In contrast to ultrasonic waves used in conventional ultrasonic inspections that propagate with a constant velocity, the velocity of the guided waves varies significantly with the wave frequency and the geometry of the medium. In addition, at a given wave frequency, the guided waves can propagate in different wave modes and orders (Kim et al. 1991). Guided waves travel either at boundaries (Surface Waves) or between the boundaries (Lamb Waves). Guided waves are highly dependent on wavelength and frequency, and propagating guided waves can only exist at specific combinations of frequency, wave number and attenuation.

2.3.1 Guided Waves for Monitoring Degradation of Structures

Guided waves have been exploited by researchers recently for monitoring various types of damages like Corrosion, notches and debond etc. But most of the work is done on simulated corrosion studies only on RCC, steel plates and pre-stressed members only a few research works are available on CFST members.

2.3.1.1 Monitoring of Steel in Concrete Structures

A wide range of ultrasonic techniques have been reported in the literature that may be suitably employed for the monitoring of steel in concrete structures for the purpose of diagnosing the cause and extent of damage in the form of fractures and corrosion.

Na et al. (2002) studied the feasibility of detecting and quantifying delamination at the interface between steel bar and concrete using ultrasonic guided waves. These waves can propagate a long distance in the reinforcing steel bar or concrete beam as they are sensitive to interface bonding between the steel bar and concrete. It was observed that traditional ultrasonic methods are good for detecting large voids in concrete but are not efficient for capturing delamination at the interface. In further studies, Na et al. (2002) utilized both high (1 MHz) and low frequencies (150 kHz) to study the effect of varying bond levels at the steel-concrete interface and debond location in RC beams on the received waveforms. It was concluded that debond resulted in an increase in signal for both low and high frequencies.

Na et al. (2003) investigated the feasibility of detecting interface degradation and separation of steel bars in concrete beams using Lamb waves. A special coupler between the steel bar and ultrasonic transducers was used to launch guided waves in the steel bar. The investigation revealed that the Lamb wave inspection technique was an efficient and effective tool for health monitoring of reinforced concrete structures.

Rose et al. (2004) discussed theoretical and experimental issues of acquiring dispersion curves for bars of arbitrary cross-section. The fundamental data as phase velocity, group velocity, and wave structure for each guided wave mode was presented for structures with complicated cross-sectional geometries as a rail. It was concluded that it was possible to inspect large lengths (10+ ft.) of the embedded rod using an ultrasonic guided wave pulse-echo technique. Guided waves can be used efficiently, both for measuring the length of a rod embedded in concrete and for estimating the amount of delamination between a steel and concrete. To determine the length of the embedded rod, guided wave modes at higher frequencies must be used. Lower frequencies are better for estimating delamination.

Reis et al. (2005) estimated the corrosion damage in a steel reinforced mortar using fundamental flexural mode at low frequencies below 250 kHz. Debond defects were simulated by wrapping a tape around the rebar. The loss of bond between steel and surrounding concrete has been detected and evaluated. Effect of corrosion has mainly been viewed as a loss of interfacial bond. The higher signal strength at the receiving end has been indicative of debond and corrosion as debond barricades the leakage of wave signals into concrete.

He et al. (2006) studied the effect of debond on signals in cylindrical specimens using frequencies between 1 MHz and 2 MHz and found the lower frequencies sensitive to the change in bond.

Ervin and Reis (2008) and Ervin et al. (2009) also used both low (<200 kHz) and high (2–9 MHz) frequencies to ultrasonically monitor the accelerated corrosion experiments. Few modes were found sensitive to the effect of bond weakening and stiffness reduction in mortars while few modes related well to the change in cross-sectional area.

Sharma and Mukherjee (2009) studied the use of ultrasonic guided waves with frequencies in the range of 1-4 MHz for damage detection in bars in air. Two ultrasonic testing techniques, pulse echo and pulse transmission, were used to monitor healthy as well as damaged bars. The amplitude of received signal in both pulse-echo and pulse transmission was a measure of the extent of the damage. The two techniques when used in combination can predict the existence, location as well as the extent of damage.

Sharma and Mukherjee (2010 a, b and c); Sharma et al. (2011) studied a nonintrusive corrosion monitoring technique for early detection of damages in steel embedded in concrete. Longitudinal guided ultrasonic waves were utilized to monitor notch and debond defects in steel bars in concrete simulating pitting and delamination phenomena caused by corrosion. The developed methodology was successfully applied for real-time monitoring of RC beam specimens undergoing accelerated chloride corrosion. Guided waves were further used for monitoring difference in progression of rebar corrosion in concrete in varying chloride and oxide environments.

Sharma and Mukherjee (2013) reported the effect of rates of corrosion in the two environments on the ultrasonic signals. Surface and core-seeking guided wave modes

were used to monitor beams undergoing accelerated impressed current corrosion in the presence of chloride corrosion and absence of chlorides (oxide corrosion). An effective combination of guided wave modes could relate to the differences in corrosion mechanisms and rates in the two environments.

Sharma and Mukherjee (2015a) demonstrated an ultrasonic in-situ monitoring technique for freshly poured concrete. The solidification and curing of freshly poured concrete was monitored through the propagation of ultrasonic waves in waveguides such as steel reinforcing bars.

Sharma et al. (2015) used ultrasonic guided waves as a non-destructive tool to monitor the initiation and progression of corrosion in reinforcing bars in concrete after repairing with bonded FRP sheets. Guided waves were able to discern the corrosion protection offered by the FRP.

Garg et al. (2016) used Lamb wave modes for complete inspection of various types of manufacturing defects during manufacturing of FRP. Service induced damages like notches and surface defects were also studied and evaluated. Quantitative evaluation of ultrasonic signal in defect ridden FRPs vis-à-vis healthy signal has been used to relate the extent of damage in FRPs and the technique has been found to have the potential to develop into a quick, real time health monitoring tool.

2.3.1.2 Monitoring of Corrosion in Pipes

Na et al. (2002) studied the feasibility of using ultrasonic guided waves for underwater inspection. of pipes filled with concrete. A special coupling mechanism for transmitting the guided waves has been introduced for underwater inspection of concrete-filled steel pipes. Incident angle adjustment and frequency sweep technique were used to generate, propagate, and receive the guided waves through the pipes in water. An analytical study was carried out to identify the cylindrical guided wave modes that are sensitive to the mechanical defects. The new transducer holder and its coupling mechanism have potential to be used for underwater pipe inspection.

Na and Kundu (2002) used electro-magnetic acoustic transducers (EMATs) for transmitting and receiving cylindrical guided waves through concrete-filled steel pipes. EMATs) give relatively consistent results in comparison to piezoelectric transducers

since they do not need any coupler. Through time history curves and wavelet transform, it is observed that EMAT-generated cylindrical guided wave techniques have good potential for the interface inspection of concrete-filled steel pipe.

Satyarnarayan et al. (2008) discussed the ultrasonic guided waves of higher order modes traveling along the circumferential direction and its interaction with defects in pipe support regions. These circumferential guided waves were produced in mild steel pipe specimens comprising artificially created axial notches (simulating axial cracks) and pinholes (simulating pinhole-like defects) of different sizes in order to simulate conditions such as cracking and corrosion under pipe supports. These higher frequency modes were tested for their capability to detect the defect location along the circumference. The defect size was assessed using the amplitude data.

Vesiljevic and Kundu (2008) analyzed the time history after the arrival of the first defect signal, and after different wave modes have propagated through the pipe. It is observed that the defective pipe can be identified by analyzing these ultrasonic signals. This paper also highlights difficulties associated with the interpretation of the recorded time histories due to mode conversion by the defect. The design of electro-magnetic acoustic transducers used to generate and receive the guided waves in the pipe. is described.

Rose et al. (2009) highlights the successes of guided waves and challenges for their applications in aircraft, composite materials and pipeline inspection. Various Guided wave imaging methods such as a line of sight, tomography, and guided wave C scan, phased array, and ultrasonic vibration methods have been discussed. Applications outlined encircles lap splice, bonded repair patch, fuselage corrosion, water loaded structures, delamination and crucial aspects of pipeline inspection.

Ahmad and Kundu (2012) investigated the effectiveness of Fourier transforms and Wavelet analysis in detecting defects in steel pipes. Cylindrical Guided waves are generated by piezo-electric transducers and propagated through the pipe wall boundaries in a pitch-catch system. Fourier transforms of received signals give information regarding the propagating guided wave modes which help in detecting

defects by selecting appropriate modes that are affected by the presence of defects. Continuous wavelet coefficients are found to be sensitive to defects.

Han et al. (2012) studied the performance of CFST members with square sections under both loading and chloride corrosion. The parameters were loading ratio during corrosion and corrosion conditions (no corrosion, and fully or half immersed into corrosive solution, respectively). According to the test, the effects of both loading and corrosion on the behavior of CFST and reference hollow steel tubular members were analyzed. It was observed that the CFST specimens behaved in a ductile manner. In the calculations, the steel wall thickness and cross-sectional area after corrosion were used.

Xu et al. (2013) proposed a novel active interfacial debonding detection method for rectangular CFST sections based on the wavelet packet energy spectrum of measurement of patches.

Sharma and Mukherjee (2014, 2015b) reports a non-contact, in-situ and non-destructive corrosion monitoring methodology for submerged plates using ultrasonic guided waves. A combination of the selected guided wave modes could effectively discern various corrosion mechanisms occurring in plates.

2.3.1.3 Closure

The research in the last two decades has shown the possibility of using Ultrasonic Guided Waves for monitoring various kinds of damages. But most of the work is done on simulated corrosion studies only on RCC and pre-stressed members; a very few research works have been reported on corrosion monitoring of CFST members. A more elaborate and detailed investigation of various kinds of damages in CFST sections is still required to develop a complete damage monitoring methodology for the same. These sections are liable to corrode from inside because of the presence of porous concrete and it is susceptible to environmental degradation with steel on the outside. It is hence, proposed in this research work to investigate ultrasonic guided waves for monitoring degradation due to corrosion in CFST sections.

2.4 GAPS IN THE RESEARCH AREA

From the literature survey following notable gaps/observations have been made:

2.4.1 CFST Columns

- The experimental investigations carried out by several researchers shows that the behavior of uniaxially loaded short rectangular CFST columns has been adequately investigated.
- Relatively few researchers have performed finite element analysis of square/rectangular CFST sections. So, there is a requirement of FEM based numerical model to model and investigate the true behaviour of these incredibly useful sections.
- Little success has been achieved so far in developing an accurate model due to the complication in modeling the confinement effect for concrete-filled steel tubular members.

2.4.2 CFST Beams

- From the literature review, it can be established that filling of steel hollow tube with concrete increased the flexural strength, stiffness and ductility which further delays the failure of the columns.
- Despite of their various advantages, CFST sections as beams have not been explored as part of CFST frames.

2.4.3 CFST Beam-Column Joints

- Extensive theoretical and experimental investigations have been carried out by many researchers on the behaviour of CFST beam–columns.
- It has been concluded that understanding of the behaviour of CFST beam–columns is intricate and its design has not been sufficiently verified. So, further studies are joints required to improve the design for the beam-to-column connections to avoid connection failure before the ductility of the beam, column, and the panel zone is developed.
- Most of the past studies are based on CFST column and steel beams. No study of the

behaviour of CFST column connected to CFST beams is available.

- End plate type bolted connections are widely used in steel structures and CFST frame structures. Despite of their simple fabrication, bolted end plates are extremely complex in their analysis and behavior.
- Furthermore, lack of efficient numerical modelling is also observed from the literature review.

2.4.4 CFST Frames

- The behaviour of composite frames is not fully understood hence the requirement for accurate and reliable analysis of a composite frame is very clear.
- Few experimental and numerical studies are available for analysis of CFST composite frames in which CFST columns and steel beams are part the frame but no study is available in literature where CFST members are used as both beam and columns as part of CFST composite frame.
- Set against this background, to determine the behaviour of the composite frames with concrete-filled square hollow section (SHS) steel tubular columns to CFST beams, numerical studies required to develop an accurate model.

2.4.5 Ultrasonic Guided waves for Monitoring Degradation

- The research in the last two decades has shown the possibility of using Ultrasonic Guided Waves for monitoring various kinds of damages.
- Most of the work is done on simulated corrosion studies only on RCC and pre-stressed members; a very few research works have been reported on corrosion monitoring of CFST members.
- A more detailed investigation of various kinds of damages in CFST sections is still required to develop a complete damage monitoring methodology for the same as these sections are liable to corrode from inside because of the presence of porous concrete and it is susceptible to environmental degradation with steel on the outside.

CHAPTER-3

BEHAVIOUR OF RECTANGULAR CFST COLUMNS UNDER AXIAL LOADS

3.1 GENERAL

A lot of work on concrete filled steel tubular (CFST) columns have been done throughout the world in past few decades and the usefulness of CFST sections (Figure 3.1) as compression members under axial loads is well recognized (Section 2.1.1). Several state-of-the-art reports or papers have been published on CFST sections, such as Shams and Saadeghvaziri (1997), Shanmugam and Lakshmi (2001) and Han et al. (2014). It has been observed from the literature review that relatively few researchers have performed Finite Element Analysis (FEA) of square/rectangular CFST sections. Comprehending the importance of these sections, the behaviour of square CFST sections has been investigated experimentally considering the influence of various parameters like slenderness ratio, cross-sectional aspect ratio (B/t), varying concrete and steel strength. This study mainly focusses at the numerical investigation of CFST sections subjected to axial loads. An FE model is developed and validated by comparison with experimental results of few studies selected from literature.

3.2 EXPERIMENTAL INVESTIGATIONS

It is an established fact that square/rectangular columns are preferred over the circular columns by the architects/structural designers' due to architectural reasons despite the fact that circular CFST columns have better mechanical and post-yield behaviour than square CFST columns (Schneider 1998). Also, the beam to column connections are more convenient for square/ rectangular CFST columns and the stiffness of square CFST columns is more. Sakino et al. (2004) investigated 36 circular and 48 square steel composite tubes subjected to concentric loading for deformation behaviour. Test results showed a strength increase for square composite columns more than circular columns. Considering the previous investigations and studies, square/rectangular sections have been selected for study.

Previous studies (Schneider 1998, Huang 2001, Han 2002 and Han et al. 2014**)** establish that various parameters such as confinement factor, slenderness ratio L/B, B/t ratio and H/B ratio are the key parameters which greatly influence the behaviour of these sections. Shape of the cross-section (Schneider 1998) and material strengths also influence the load carrying capacity of CFST columns (Fujimoto et al. 2004 and Sakino et al. 2004). Hence, in the present experimental work, the various parameters selected for the investigation of the test specimens are the slenderness ratio L/B, B/t ratio, H/B and strength of concrete and steel. In order to prevent the steel hollow section of the CFST column from local buckling, the limit of width-to-thickness (B/t) or (H/t) ratio of the steel hollow section with f_y in N/mm^2 set by EC-4 given below is followed.

$$H/t \leq 52\sqrt{\frac{235}{f_y}} \tag{3.1}$$

The permissible limit of H/t ratio specified in American Institute of Steel Construction (AISC, 1994) and American Concrete Institute (ACI, 2002) as follows, is also considered.

$$H/t \leq \sqrt{\frac{3E_s}{f_y}} \tag{3.2}$$

Herein E_s and f_y are the modulus of elasticity and the yield stress of steel, respectively.

Geometry of steel sections used as CFST specimens is shown in Figure 3.1.

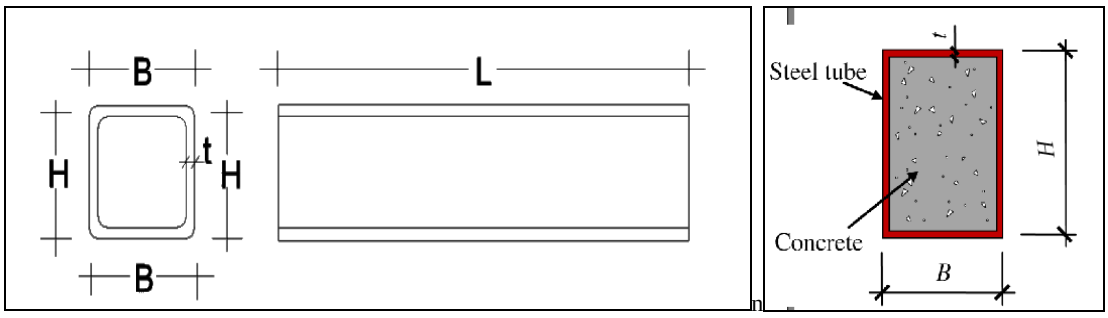

Figure 3.1 Geometry of CFST Sections

3.2.1 Specimen Details

Square/rectangular steel hollow sections of Grade Yst-240 and Yst-310 (Minimum yield strength 240 N/mm^2 and 310 N/mm^2) respectively with Modulus of elasticity of steel (E_s) as 2.1 x10^5 N/mm^2 conforming with IS 4923:1997, have been used in the experiment. The sizes of square hollow sections (SHS) have been selected as 72 mm x 72 mm x 3.2 mm, 72 mm x 72 mm x 4.8 mm with (B/t) ratios of 22.5 and 15 respectively and rectangular hollow sections (RHS) have been selected as 96 mm x 48 mm x3.2 mm. and 24 for rectangular hollow sections (RHS) 96 mm x 48 mm x 2.0 mm. These values satisfy the permissible limit of B/t ratio specified in AISC and ACI. To obtain the basic properties of steel sections, three tensile coupons have been extracted from the flat surface of each type of tube. The tensile coupon tests have been conducted according to IS 1608:1972. The SHS beams have yield stress ($f_{y)}$ of 260 N/mm^2 and ultimate stress (f_u) of 410 N/mm^2. The RHS beams have yield stress (f_y) of 350 N/mm^2 and ultimate stress (f_u) of 500 N/mm^2. Various details of the test specimens are illustrated in Table 3.1 and Table 3.2. The prepared test specimens are presented in Figure 3.2.

Figure 3.2 CFST Test Specimens

Table 3.1 Nomenclature of Test Specimens

Sr. No.	Specimen Label	Length 'L' (mm)	Details
1.	SH-1	300	Square hollow section (SHS)
3.	S-1-25	300	Square hollow section 3.2mm thick, filled with M-25 concrete
4.	S-1-40		Square hollow section 3.2mm thick, filled with M-40 concrete
5.	S-2-25		Square hollow section 4.8mm thick, filled with M-25 concrete
6.	S-2-40		Square hollow section 4.8mm thick, filled with M-40 concrete
7.	S-3-25	450	Square hollow section 3.2mm thick, filled with M-25 concrete
8.	S-3-40		Square hollow section 3.2mm thick, filled with M-40 concrete
9.	S-4-25		Square hollow section 4.8mm thick, filled with M-25 concrete
10.	S-4-40		Square hollow section 4.8mm thick, filled with M-40 concrete
11.	R-1-25	300	Rectangular hollow section 2.0mm thick, filled with M-25 concrete
12.	R-1-40		Rectangular hollow section 2.0mm thick, filled with M-40 concrete

Table 3.2 Geometric and Material Properties of Test Specimens

Specimen Label	B (mm)	H (mm)	B/H	B/t	f_{cu} (MPa)	f_y (MPa)	Area of concrete (mm^2)	Area of Steel (mm^2)
SH-1	72	72	1	22.5	-	240	-	854
S-1-25	72	72	1	22.5	35.5	240	4303.36	854
S-1-40	72	72	1	22.5	56.4	310	4303.36	854
S-2-25	72	72	1	15	35.5	240	3893.76	1231
S-2-40	72	72	1	15	56.4	310	3893.76	1231
S-3-25	72	72	1	22.5	35.5	240	4303.36	854
S-3-40	72	72	1	22.5	56.4	310	4303.36	854
S-4-25	72	72	1	15	35.5	240	3893.76	1231
S-4-40	72	72	1	15	56.4	310	3893.76	1231
R-1-25	48	96	2	24	35.5	240	3727.36	854
R-1-40	48	96	2	24	56.4	240	3727.36	854

3.2.2 Mix Design Proportions

Concrete of two different grades of M-25 and M-40 has been used for the test specimens. Properties of cement and details of mix proportions are as given below in Table 3.3, Table 3.4 and Table 3.5 respectively.

Table 3.3 Properties of Cement

Sr. No.	Property	Experimental Value
1.	Consistency	35%
2.	Specific Gravity	3.12
3.	Average 3 days Strength	22.05 MPa
4.	Average 7 days Strength	34.40 MPa

Mix proportion by mass for M 25 concrete for filling CFST sections are given below in Table 3.4.

Water content:175.00 kg/m^3 Cement Content: 396.00 kg/m^3

Table 3.4 Mix Proportions of Ingredients for M-25 Concrete

w/c ratio	Cement	Fine Aggregates	Coarse Aggregate — I (20 mm)	Coarse Aggregate — II (10 mm)	Average Strength (7 Days)	Average Strength (28 Days)
0.442	1	1.375	1.539	1.510	26.53 MPa	35.5 MPa

Mix proportion by mass for M 40 concrete for filling CFST sections are given below in Table 3.5.

Water content:170.0 kg/m^3 Cement Content:435.0 kg/m^3

Table 3.5 Mix Proportions of Ingredients for M-40 Concrete

w/c ratio	Cement	Fine Aggregates	Coarse Aggregate — I (20 mm)	Coarse Aggregate — II (10 mm)	Average Strength (7 Days)	Average Strength (28 Days)
0.391	1	1.003	1.803	1.178	40.58 MPa	56.4 MPa

3.2.3 Methodology

After casting concrete inside the steel hollow sections, the specimens have been left for 14 days for the concrete to set. A layer of high-strength cement mortar (ratio 1:2) has been added at top and bottom surface to provide a flushed surface to core concrete with the steel tube because the concrete shrinks over time. Steel plates of 2 mm thickness have been welded at both ends of the specimens to ensure the composite action of steel and infilled concrete during loading, uniform distribution of load and to control the local yielding of the steel tube. All the specimens have been tested to failure in compression using the Universal Testing Machine (UTM) of 5000-kN capacity

[Hungto, Taiwan Make] (Figure 3.3). The specimens have been centrally positioned in the rig to ensure that the applied compressive load is concentric. Each specimen is tested to failure under axial loading.

Figure 3.3. Test Set-Up for Axial Compression Testing

The requirement of FEM based numerical model to investigate the true behaviour of these incredibly useful sections has been established by many researchers. To reduce the expensive experimental study, parametric study has been taken up to complement the experimental results. Hence, the study mainly focusses at the numerical investigation of such sections by using software ATENA. The developed FE model is validated by comparison with some selected experimental results from literature.

3.3 FINITE ELEMENT MODELLING OF CFST COLUMNS

Finite element method (FEM) is a numerical process to find reasonably accurate solutions for boundary value problems. It is suitable for superimposition of material models for the components of a composite material. In the present study, numerical modelling has been done in a finite element code ATENA-5.4-1, with various

extraordinary features for non-linear analysis of composite materials. It enables virtual testing of structures which is the present trend in the research. As material properties have a vital role to play in the modeling of structural elements, each material in the program has been defined specifically. A numerical model has been developed taking various material models as detailed below:

3.3.1 Modeling of Confined Concrete

When concrete is subjected to lateral confining pressure, the uniaxial compressive strength f_c and the corresponding strain ε_{cc} are much higher than the values corresponding to unconfined concrete. Many models are available to model confined concrete, amongst these Mander's model (Mander et al. 1988) is the most used one. The relations between f'_{cc}, f'_c and between ε_{cc}, ε_c are estimated by the following equations

$$f'_{cc} = f'_c + k_1 f_1 \tag{3.3}$$

$$\varepsilon_{cc} = \varepsilon_c \left(1 + k_2 \frac{f1}{f'_c}\right) \tag{3.4}$$

where f_1 represents the confining pressure around the concrete core. The values of constants k_1 and k_2 are set on the basis of experimental data. The lateral confining pressure f_l drop off with increasing values of width-to-thickness ratio B/t.

Solid brick element having minimum 8 and maximum 20 nodes having three degrees of freedom at each node, is used for modeling of concrete. This element is able to capture plastic deformation and cracking in same directions (*ATENA Theory Manual*). Confinement effect is being automatically considered in the material models available in the material catalogue of ATENA. A more detailed sensitivity towards confinement is implemented in the Non-linear Cementeous-3 model which considers multidimensional failure surfaces in the material model. The IS 456:2000 stress-strain relationship has been used for calculating the basic material properties used in analysis

The failure of concrete is governed by the compressive failure surface expanding with increasing hydrostatic pressure, since the confining effect causes the concrete core to behave in a triaxial compressive stresses due to interaction between steel tube and concrete in a CFT column. Hence, a suitable model that describes the triaxial strength of concrete is the hardening/softening plasticity model (Menetrey and

Willam,1995). This model can be used to simulate the concrete cracking, the crushing under high confinement and the crack closure due to the crushing in other material directions. In ATENA, this confinement is taken into account by a multiplier for plastic flow β which determines the return flow. If is $\beta < 0$ material is being compacted against crushing, if $\beta = 0$ material is confined If $\beta > 0$ material is dilating. After performing parametric study on β, a value of 0.5 has been adopted in the analysis. The Poisson's ratio μc of concrete under uniaxial compressive stress is assumed to be 0.2.

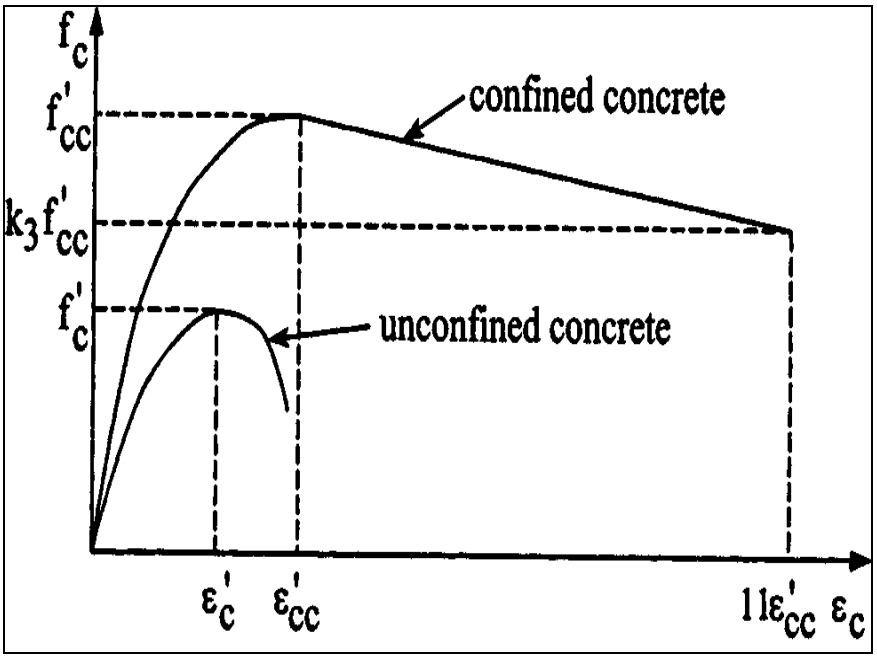

Figure 3.4 Typical Stress–Strain Curves for Confined Concrete (Mander et al. 1988)

3.3.2 Steel Tube

The steel tube is modeled by eight-sided solid brick element to make it complementary at junctions of concrete core and steel tube. Once the stress in steel reaches yield surface, it becomes perfectly plastic without carrying further loading prior to entering into strain hardening zone. The Von-Mises yield criterion flow rule constitutes the most realistic description of the plastic behaviour of metals (Chakrabarty, 1998). An elastic-plastic model 3D-Von Mises yield criterion (Figure 3.5) is adopted to describe the constitutive behaviour of steel tube to analyze the

behaviour of the steel in the plastic hardening range. Tubes can be represented by shell elements. as well as solid brick element.

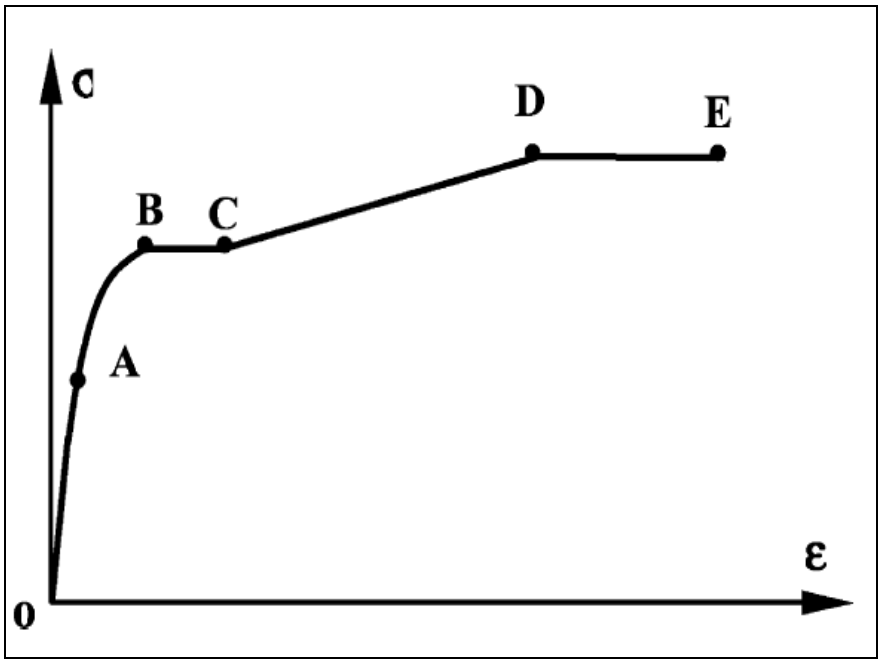

Figure 3.5 Typical Stress–Strain Curve for Steel with Strain Hardening

3.3.3 Boundary Conditions, Interface Modelling and Loading

In order to simulate the test set-up in properly both ends have been fitted with steel plates. Bottom plate is restrained against displacement in all three directions. The load/displacement is applied on top plate. In ATENA, the interface material model can be used to simulate contact between two materials such as for instance a contact between concrete and steel. Though ATENA interface provides an intelligent interface modelling but the risk of related computational problems can be avoided by using perfect connection to model interface for composite action of steel tube and core concrete

. The simulation of interaction between steel tubular column and confined concrete is modeled by a special 8-node interface element, called gap element available in ATENA material library. It uses an accurate model, which illustrates the actual

contact behavior between steel tube and concrete. The contact pressure acts on the characteristic surfaces and frictional stress occurs in the direction tangential to the contact surface. This type of behavior is based on Mohr-Coulomb criterion with cut-off. The constitutive relation for a general three-dimensional case in given in terms of tractions on interface planes and relative sliding and opening displacements, is given as:

$$\begin{Bmatrix} \tau_1 \\ \tau_2 \\ \sigma \end{Bmatrix} = \begin{bmatrix} K_{tt} & 0 & 0 \\ 0 & K_{tt} & 0 \\ 0 & 0 & K_{nn} \end{bmatrix} \begin{Bmatrix} \Delta\upsilon_1 \\ \Delta\upsilon_2 \\ \Delta\upsilon_u \end{Bmatrix} \tag{3.5}$$

wherein τ is the shear stress, σ the normal stress, Δ_v and Δ_u are the relevant sliding and opening displacement respectively. K_{nn} and K_{tt} denote the initial elastic normal and shear stiffness respectively and they are assumed to be equal to 10^5 MPa (Hajjar et al. 1998). Additionally, it is assumed that the contact surfaces are not allowed to penetrate each other, the friction between the two faces with a coefficient equal to 0.4 is maintained as long as the surfaces remain in contact and no tension strength exists between the two faces, thereby allowing the contact surfaces to separate.

CFST stub columns are independent of end friction, hence end friction has not been taken into consideration. Various values viz. concrete yield strength, concrete modulus of elasticity and steel yield strength and steel modulus of elasticity are entered in definition material type. After performing analysis and plotting of results is done in the post-processor phase.

3.3.4. Validation of Proposed Model

The accuracy of the proposed FE model has been assessed by comparing the results obtained from FE analysis with the experimental results of researchers like Han (2002), Liu et al. (2003) and Huang (2002). The parameters studied are peak load and deformed shape of columns. Table 3.6 presents the results obtained with the proposed model for experimental studies carried out by various researchers and it is evident from the comparison that the proposed model predicts the peak load very closely with the experimental results. Hence, the proposed FE model is further used for study of experimental validation and parametric analysis.

Table 3.6 Comparison of Experimental (from Literature) and FE Model Results

Specimen Label	Literature Reference	Section Details (in mm)	Length (mm)	f_Y (MPa)	f_C (MPa)	E (GPa)	Peak Load (Exp.) $P_{Exp.}$ (kN)	Peak Load (FE model) P_{Sim}(kN)	$P_{Sim.}/P_{Exp.}$ Ratio
RC-4-1	Han (2002)	150X135X2.86	450	228	59.3	182	1420	1428.0	1.0056
RC-6-1	Han (2002)	100X75X2.86	300	228	59.3	182	640	648.2	1.0128
RC-8-1	Han (2002)	140X105X2.86	420	228	59.3	182	1044	1216.2	1.1649
RC-10-1	Han (2002)	160X120X2.86	480	194	59.3	194	1820	1932.0	1.0615
RC-11-1	Han (2002)	130X85X2.86	390	228	59.3	182	760	953.4	1.2544
A-4-1	Liu et al (2003)	130X100X5.8	390	300	83	203	1601	1520.0	0.9490
A-5-1	Liu et al (2003)	130X100X5.8	390	300	106	203	1854	1781.0	0.9606
A-8-1	Liu et al (2003)	180X100X5.8	300	300	106	203	2287	2358.0	1.0310
A-10-1	Liu et al (2003)	150X100X4	390	495	55	206	1815	1781.0	0.9812
A-14-1	Liu et al (2003)	190X100X4	390	495	55	206	2038	1998.0	0.9803
SS-40	Huang et al. (2002)	200X200X5	840	265.8	27.15	-	2311.5	2349.0	1.0162
SS-70	Huang et al. (2002)	280X280X4	840	272.6	31.15	-	3401.1	3344.0	0.9832
SS-150	Huang et al. (2002)	300X300X2	840	341.7	27.27	-	3061.5	3000.0	0.9799
Mean									1.029
Standard Deviation									0.0873

3.4 ANALYTICAL MODEL

EC4 is the latest international code in composite construction which covers concrete filled steel section sections with or without reinforcement. Whereas the formula used by American Concrete Institute (ACI) for calculating the ultimate load doesn't capture the effect due to concrete confinement into account the ultimate axial force of a square column given by EC4 is: -

$$P_{Euro} = A_c f_c + A_s f_s \quad (3.6)$$

where A_s and A_c are the area of steel and concrete respectively, f_s and f_c are the strength of steel and strength of concrete respectively.

Previous studies reveal that EC4 predicts closely while AISC and ACI underestimated the critical loads (Schneider 1998). Hence in this study the ultimate capacity of different CFST sections with various parameters have been obtained according to EC4, is presented in Table 3.7.

3.5 RESULTS AND DISCUSSIONS

Various specimens detailed in Table 3.2 have been tested to failure in axial compression load in the Universal Testing Machine with various parameters. The obtained test results have been validated by FE analysis. The finite element investigations are also elaborated considering more parameters which have not been considered experimentally. Results obtained from experimental tests under axial loading and comparative analysis are discussed below.

3.5.1. Experimental Investigations

Test specimens have been tested under increasing axial compressive load. Load-deflection behaviour and failure modes of test specimens obtained from the experimental testing is discussed here.

3.5.1.1 Load–deflection behaviour

The typical load–deflection curves for the specimen group S-1 & S-2 with length 300mm and specimen group S-3 & S-4 with length 450mm, are illustrated in Figure 3.6 and Figure 3.7. It clearly indicates that increase in length results in drop in load carrying capacity of short columns. The critical loads of the tested specimens are summarized in

Table 3.7 as P_{Exp}. Loads obtained from FEA results and analytically are summarized as $P_{Sim.}$ and P_{Euro} respectively. The comparison of analytical and experimental results shows that EC4 underestimates the ultimate capacity of test specimens.

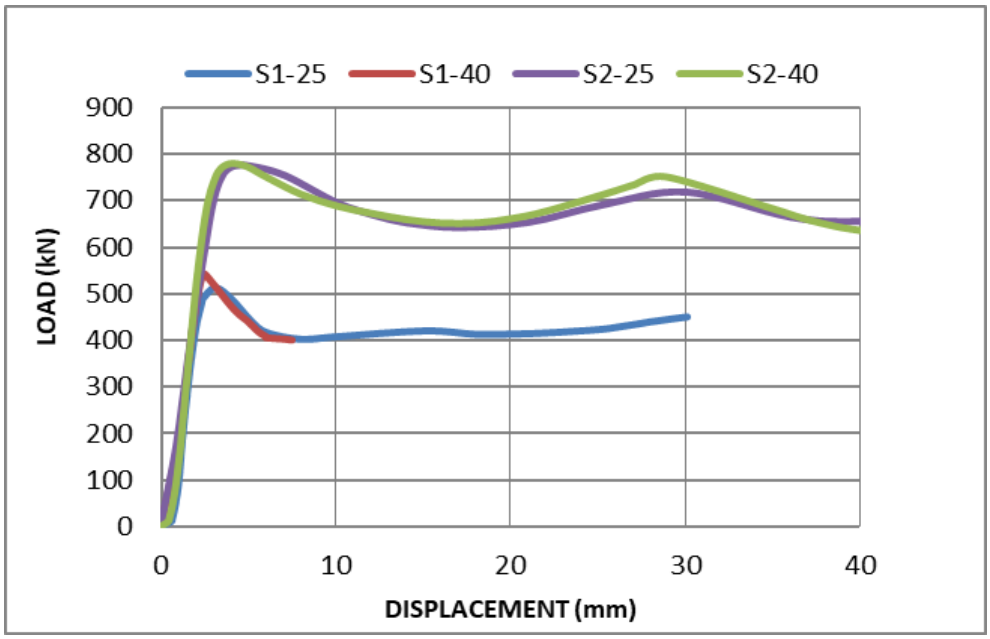

Figure 3.6 Load-Deflection Curves for Different Specimens of Length 300 mm

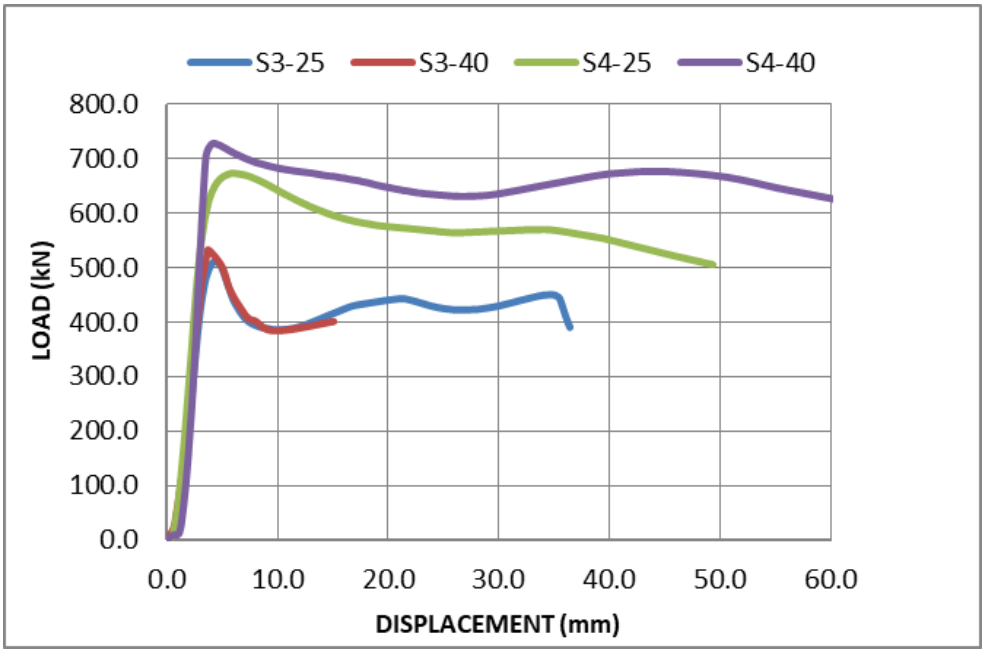

Figure 3.7 Load-Deflection Curves for Different Specimens of Length 450mm

Table 3.7 Comparisons of Experimental Results with Numerical and Analytical Results

Specimen Label	Experimental Load $P_{Exp.}$ (kN)	Numerical Load $P_{Sim.}$ (kN)	Analytical Load P_{Euro} (kN)	$P_{Sim}/ P_{Exp.}$
SH-1	235	250	204.96	1.06
S-1-25	513	540	327.18	1.05
S-1-40	542	620	399.13	1.14
S-2-25	735	740	492.19	1.01
S-2-40	779	780	557.30	1.00
S-3-25	509	515	327.18	1.01
S-3-40	537	560	399.13	1.04
S-4-25	672	680	492.19	1.01
S-4-40	727	760	557.30	1.05
R-1-25	213.5	252	285.20	1.18
R-1-40	267	285	347.52	1.07
MEAN				1.04
ST.DEV.				0.04

3.5.1.2 Failure modes

In square CFST columns, an outward buckling of steel tube at the bottom and mid height of the column has been observed under compressive load as shown in Figure 3.8. The steel tube directly carries the applied load and provides confinement to the concrete infilled in the tube. This composite action leads to the buckling of steel tube. The failure mechanism of the specimens is thus recognized as the material yielding of steel hollow sections and the crushing of core concrete. The welds at the corners of the specimen have been found undamaged as no cracking of concrete occurs on the top surface of the CFST column. The tested specimens with different geometric parameters have shown different failure modes, are illustrated in Figure 3.8 and 3.9.

Major observations regarding failure modes are as discussed below: -

- Material yielding has appeared almost simultaneously at every face of CFST columns with the H/B ratio equal to unity (Figure 3.8 and 3.9). It occurs as outward buckling of steel tube at the bottom and mid height of the column.
- Material yielding has appeared at wider face of CFST columns with the H/B ratio equal to 2 (refer part c of Figure 3.9). Yielding of tube has been observed near the bottom of specimen which can be characterized by uneven confinement exerted by the tube on core concrete.
- Most of the specimens have exhibited excellent post-yield behaviour.
- Increase in thickness of steel results in better ductility performance of the columns.
- Specimens with lesser thickness (3.2 mm) experience more deformations which can be characterized by the crushing of concrete inside.
- The specimens with higher thickness (4.8 mm) experienced lesser deformations indicating that thickness/area of steel affects the ductility performance of sections.
- Buckling at the bottom has been observed in specimens of longer length. Localized buckling is observed in case of presence of eccentricity.

(a) **(b)** **(c)**

Figure 3.8. Failure Modes of Test Specimens (a) Buckling at Centre (b) Buckling at Bottom and (c) Localized Buckling due to Eccentricity

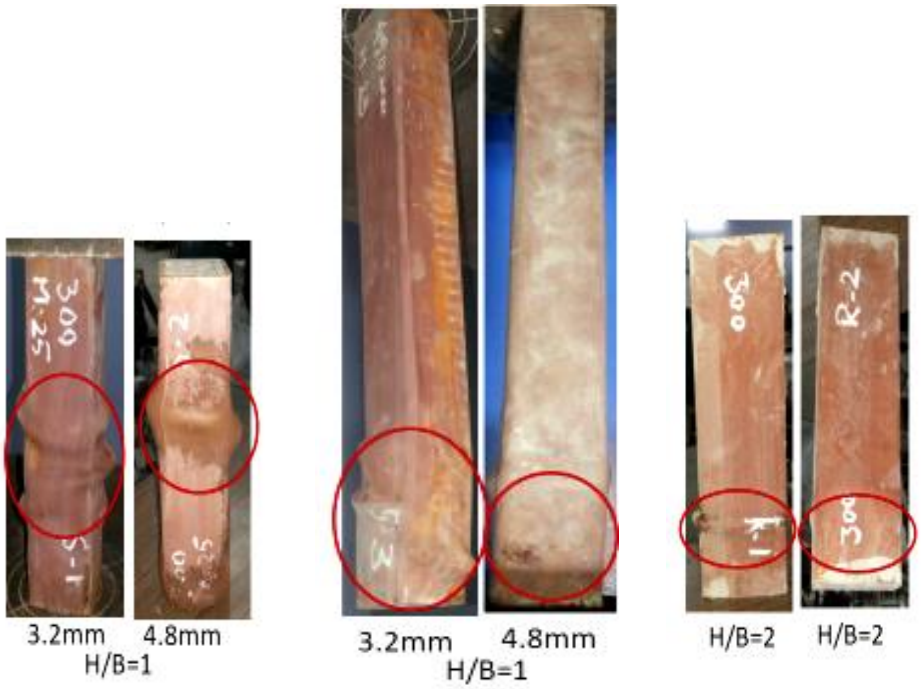

(a) **(b)** **(c)**

Figure 3.9. Failure Modes of Specimens with H/B Ratio 1 And 2 (a) Outward Buckling at Centre of Column (300mm), (b) Buckling at Bottom of Column (450mm) and (c) Outward Buckling at Bottom of Column (300mm)

3.5.2. Finite Element Analysis

Comparison of results obtained from Finite Element analysis in post processer mode of ATENA and experimental results for columns with different grades of concrete and steel with different geometrical parameters considered, is carried out and presented in Table 3.3 and Figure 3.10. Comparisons of peak loads clearly shows that FE analysis yielded very close results to experimental results. Mean ratio of simulated to experimental peak load is obtained as 1.04 (Table 3.7).

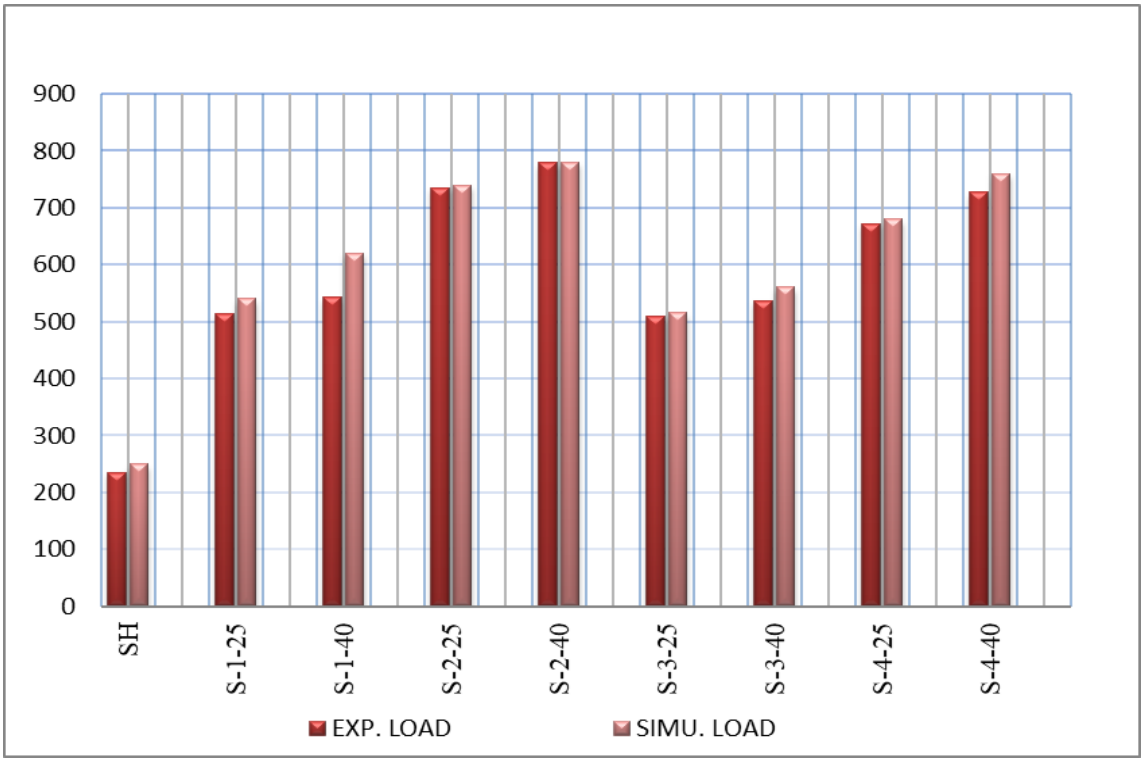

Figure 3.10 Experimental V/s Simulated Load with Varying Thickness of Steel Tube and Grade of Concrete

Failure modes: Comparison of failure patterns of experimental and FE model is presented in Figure 3.11. Here in the plotted iso-area diagrams, the darker areas indicate compression and the lighter signify tensile stress The FE failure modes/patterns are found to be very similar and in good agreement with the experimental results.

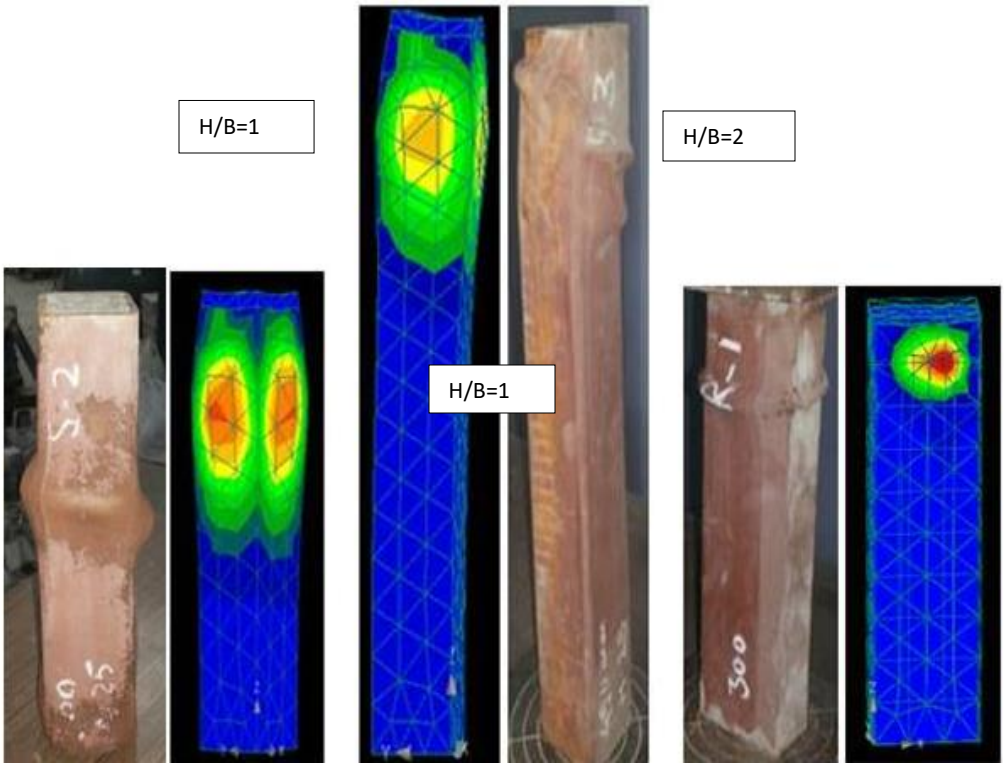

Figure 3.11 Failure Modes of Specimens (Experimental and FE Model) with Varying H/B Ratio

3.5.3 Analytical Investigations

The comparison of analytical results with experimental results is presented in Table 3.7. It shows that EC4 has underestimated the ultimate capacity of the CFST sections. Peak loads obtained in experimental tests are relatively higher.

3.5.3.1 Performance Index (PI)

To evaluate the performance of CFST columns, a Performance Index, is calculated.

$$PI = \Delta_u/\Delta_y \quad (3.7)$$

Herein, Δ_u is deflection at ultimate load and Δ_y is deflection corresponding to load at yielding respectively.

Performance indices of various specimens are given in Table 3.8 and Figure 3.12. It is observed that the performance index increases with increase in sectional area

of steel or with decrease in B/t. It can be characterized by increase in confinement pressure exerted by steel tube. For specimens with H/B = 2, lower value of PI is obtained due to unequal confinement pressure exerted by steel tube.

Table 3.8 Ductility Index (DI), Performance Index (PI) and Strength Index (SI) of Various Specimens

Specimen Label	Experimental Load $P_{Exp.}$ (kN)	Deflection At Ultimate Load Δ_u (mm)	Ductility Index (DI)	Performance Index (PI) Δ_u/Δ_y	Strength Index (SI) P_{Exp}/ P_{Euro}
SH-1	235	10.7	1.78	1.33	1.15
S-1-25	513	3.03	1.32	2.76	1.57
S-1-40	542	2.50	1.59	2.90	1.36
S-2-25	735	3.32	1.71	4.28	1.49
S-2-40	779	4.08	1.59	3.24	1.40
S-3-25	509	4.315	1.21	2.05	1.56
S-3-40	537	4.02	1.18	2.49	1.35
S-4-25	672	6.185	1.65	2.19	1.37
S-4-40	727	4.25	1.62	4.25	1.30
R-1-25	213	2.495	1.19	2.10	0.75
R-1-40	267	3.63	1.21	2.13	0.77
MEAN			1.315	2.83	1.39

3.5.3.2 Strength Index (SI)

A Strength Index is computed to calculate the strength of CFST sections.

SI = P_{Exp} / P_{Euro} herein P_{Euro} is the section capacity as per Eurocode 4.

The strength index degrades with increase of B/t or decrease of area of steel as the constraining factor of the steel tube decreases the composite action of steel tube and core concrete. It can be seen from Figure 3.13 that strength index of the CFST section is higher than 1 for all the test specimens.

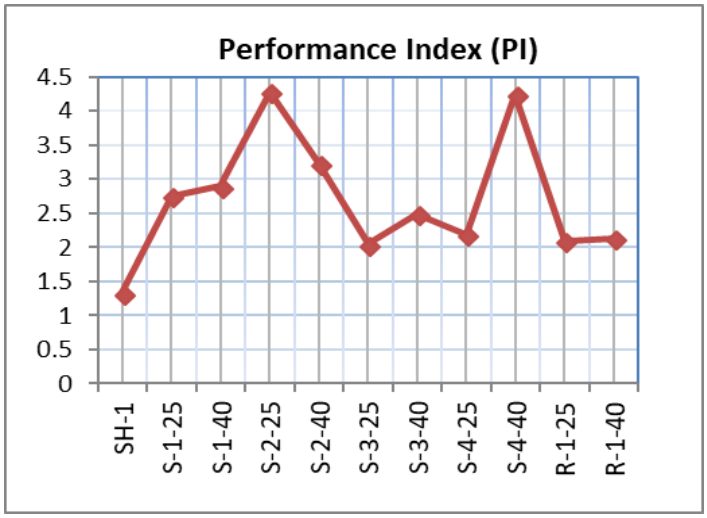

Figure 3.12. Performance Index of Various Specimens

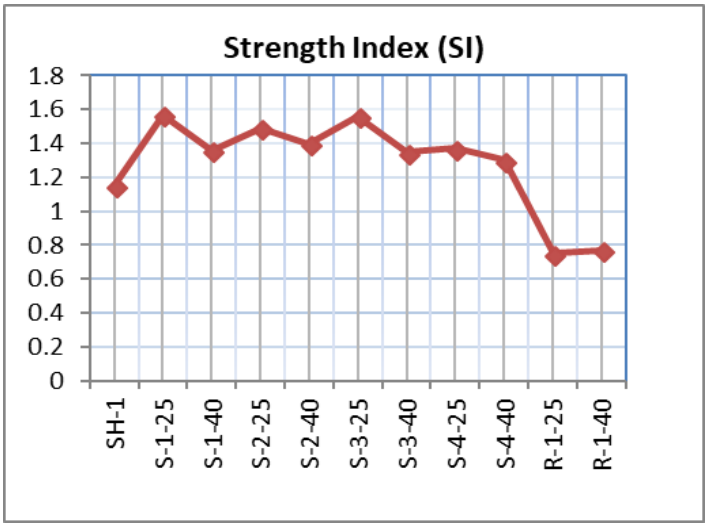

Figure 3.13. Strength Index of Various Specimens

3.5.3.3 Ductility Index (DI)

Ductility index is used to calculate the ductility of section. It is the ratio of strain at 95% of the ultimate load to the strain at the ultimate load. The increase in B/t is characterized by the decrease in ductility index and vice versa. Ductility indices so calculated for various specimens are listed in Table 3.8 and comparison is presented in Figure 3. 14.

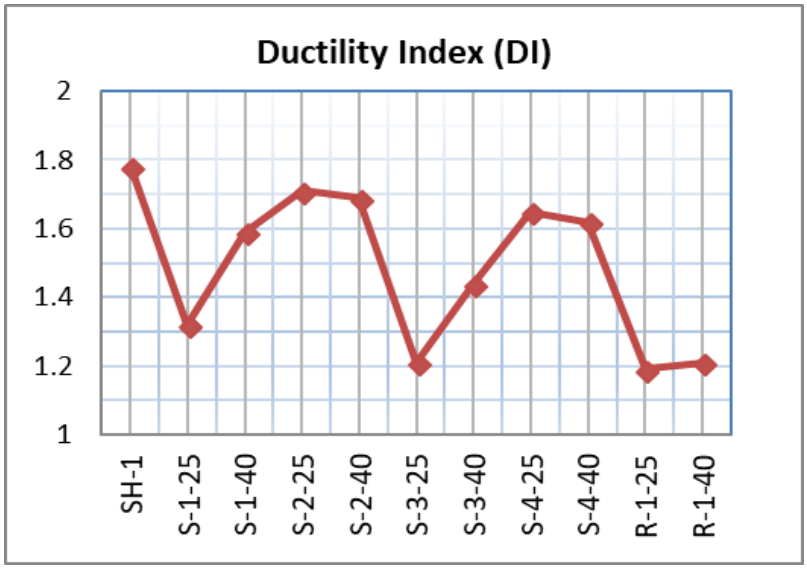

Figure 3.14. Ductility Index of Various Specimens

3.6 PARAMETRIC STUDIES

Effect of various parameters on the load carrying capacity of CFST columns is presented in this section.

3.6.1. Slenderness Ratio

The slenderness ratio of the column significantly influences the failure mode of concrete-filled columns which is characterized by yielding of steel tube followed by concrete failure. Experimental results reveal that the decrease in slenderness ratio enhances the load carrying capacity of the CFST column which is due to increase in confinement. Comparing the experimental peak loads of group S-1 and S-2 (slenderness

ratio 4.16) with group S-3 and S-4 (slenderness ratio 6.25), decrease in strength with increase in length (increase in slenderness ratio) of test specimens is clearly observed (Table 3.7). Effect of slenderness ratio has also been investigated numerically by considering length of section as 300mm, 450mm, 600mm and 900mm. Results of parametric study are presented in Figure 3.15. The results specify that increase in slenderness ratio results in decrease in load carrying capacity of CFST columns. Hence, both the experimental and numerical results indicate that load carrying capacity decreases with increase in slenderness ratio. It validates the numerical FE model developed for CFST sections.

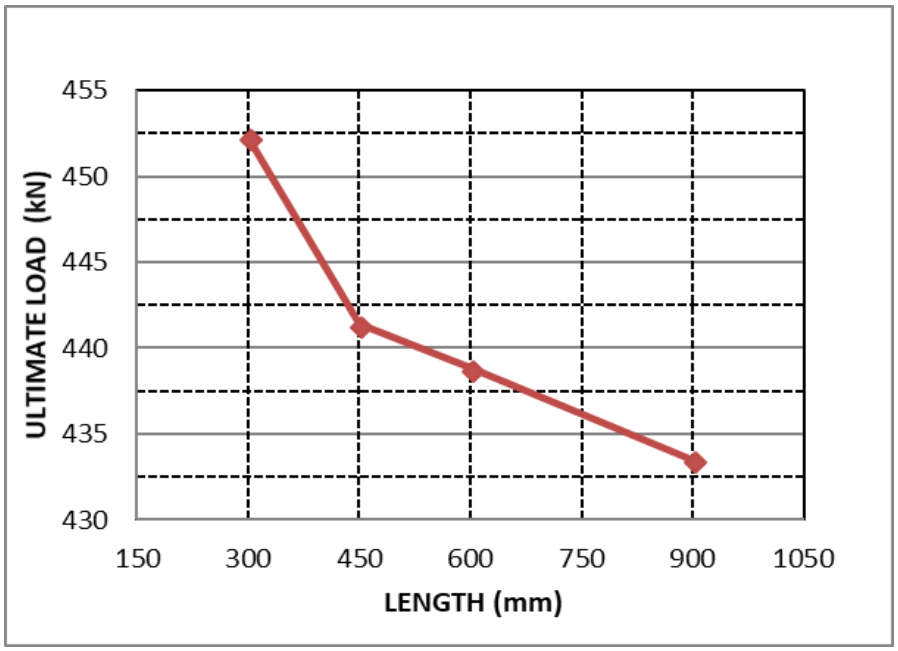

Figure 3.15 Effect of Change in Length on Load Carrying Capacity

3.6.2 Thickness of Steel Tube

The variation of thickness of steel tube significantly influences the ultimate load carrying capacity of concrete-filled columns as well as failure modes. Comparison of load carrying capacity of different sections reveal that increase in thickness enhances the load carrying capacity of the CFST column which is due to increase in confinement. Results obtained from experimental study are presented in Figure 3.16.

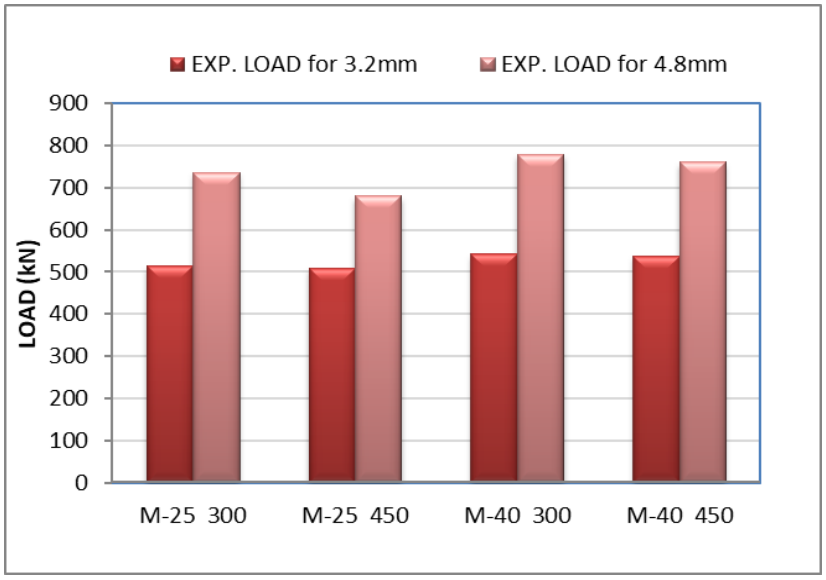

Figure 3.16 Variation in Strength with Change in Thickness of Steel Tube

3.6.3 Width to Thickness (B/t) Ratio

The width to thickness ratio (B/t) represents the aspect ratio of the section. The increase in B/t ratio may be either due to the increase in width or due to the decrease in thickness of the section. Hence this parameter is analyzed by keeping the width constant and varying the thickness (3.2mm, B/t=22.5 and 4.8mm, B/t=15). The decrease in B/t ratio represents the increase in cross-section of the steel tube which leads to greater load carrying capacity.

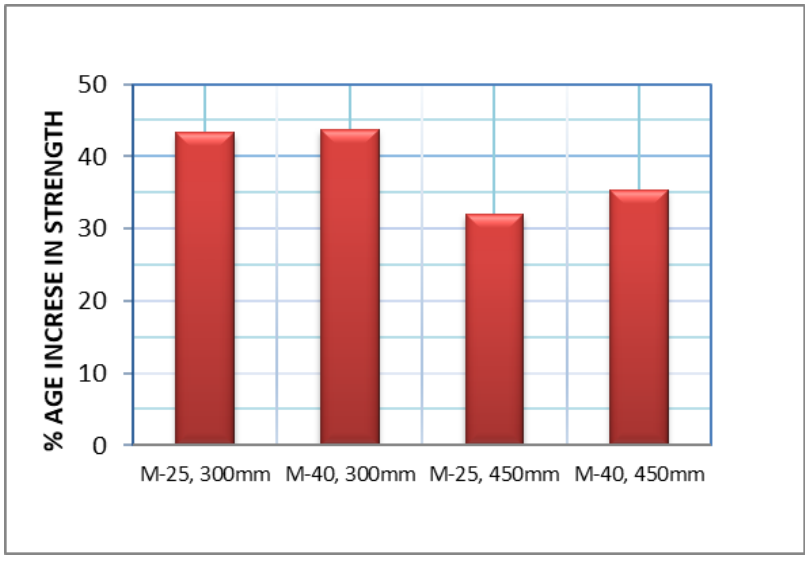

Figure 3.17. Effect of B/t Ratio

For specimens of 300 mm length, the increase in capacity of section is found to be 43% whereas an average increase of 33% is observed in specimens of 450 mm length (Figure 3.17). Hence, it can be concluded that increase in thickness enhances the strength of section but this increase in strength drops with increase in length or slenderness ratio.

3.6.4 H/B Ratio

Samples of H/B=1 (with aspect ratio 22.5) and 2 (with aspect ratio 24) and with same area of steel have been considered in the present study. The increase in H/B ratio of rectangular sections resulted in decease in strength of columns. The experimental load of rectangular sections (H/B=2) has been found to be lesser than analytical load in contrast to the square sections (H/B =1) Square CFST sections have larger experimental load than analytical loads probably due to decrease in confinement effect. Yielding of the wider face has been observed first and then in the shorter side (Figure 3.9).

3.6.5 Grade of Concrete

Infill concrete significantly increases the load carrying capacity of sections (Figure 3.18). The strength of concrete core influences the stiffness of CFST columns and increases with increase in concrete strength. But the columns fail by crushing of concrete exhibiting brittle behaviour when filled with high strength concrete. But in case of CFST sections of higher thickness this phenomenon vanishes as increased cross-sectional area of steel resulted in improved confinement. It is proved in experimental results that infill concrete increases the strength significantly, for any value of B/t ratio (Table 3.9). Further, the increase in concrete core strength increases the strength to a larger extent, for any value of B/t ratio

Table 3.9 Influence of Infilled Concrete on Load Carrying Capacity

Specimen Label	Slenderness Ratio	Experimental Load (kN)	% Increase in Strength
SH-1-300	4.167	235.4	0.00
S-1-M25-300	4.167	513	117.9
S-1-M40-300	4.167	541	129.8

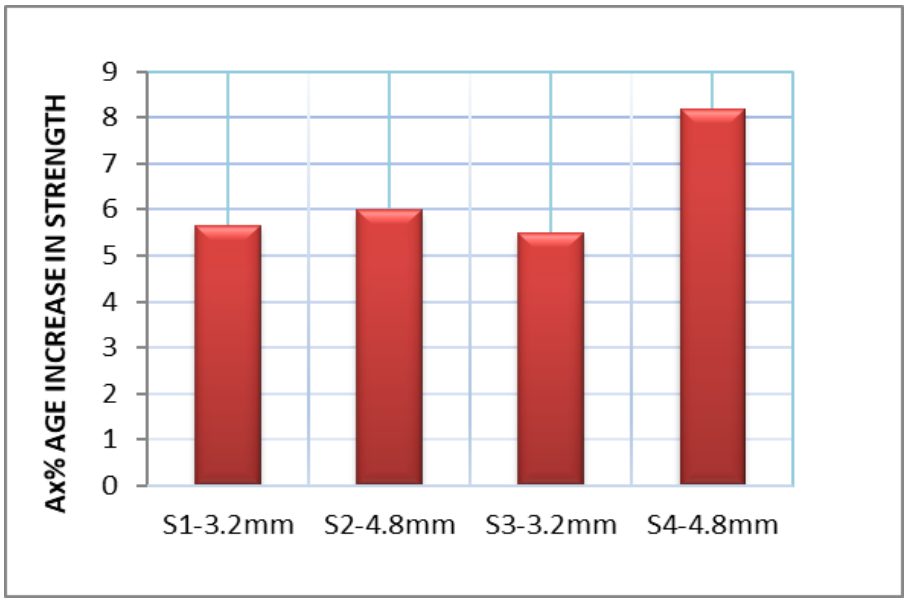

Figure 3.18 Effect of Strength of Concrete

The similar trends are seen in case of results obtained from FE investigations carried to study the influence of varying grade of concrete (M-20, M-25, M-30, M-35, M-40, M-45 and M-50) and steel (f_y 250 MPa, f_y 310 MPa and f_y 410 MPa) respectively on ultimate load carrying capacity of CFST sections (Figure 3.19 & 3.20).

3.6.5 Grade of Steel

It is observed that strength of the sections is increased with increase in grade of steel. Results obtained from numerical investigations to study variation in ultimate load with varying grade of concrete and steel are presented in Figure 3.19 & 3.20. It is observed that grade of steel significantly influences the load carrying capacity of the CFST columns. Results also indicate that the rate of enhancement in strength is more in case of sections with higher thickness (4.8 mm) than that of the sections with thinner thickness (3.2 mm). This means that increase in strength depends on B/t ratio also, for lesser B/t ratios the increase of strength is more.

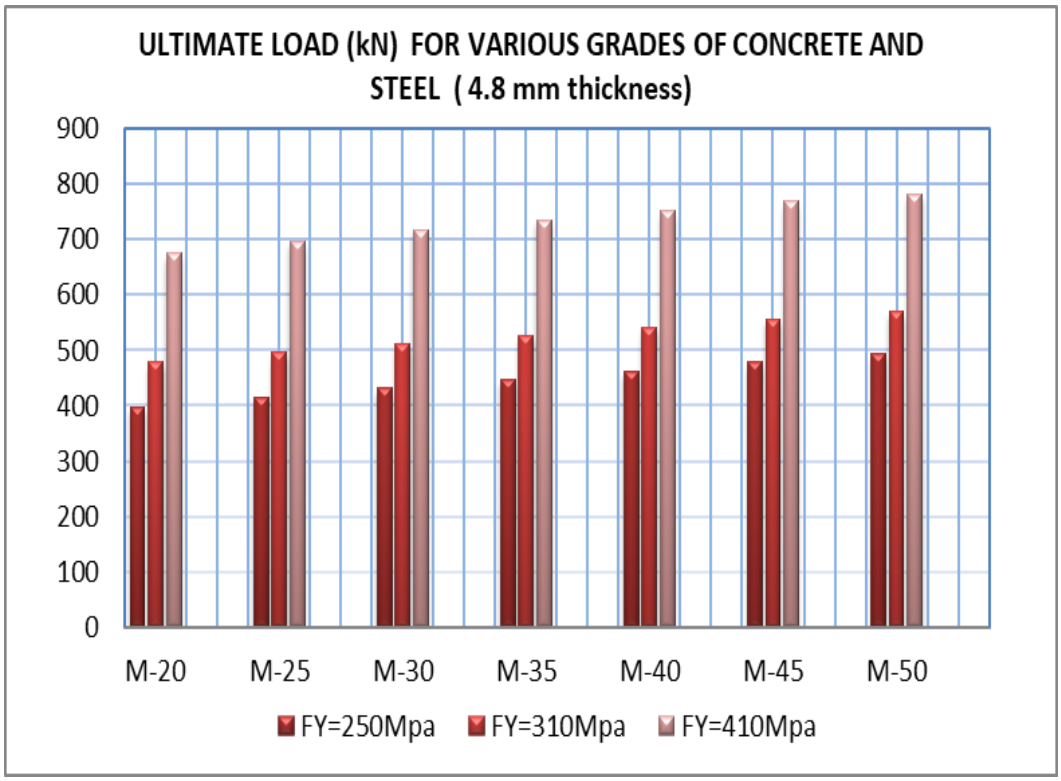

Figure 3.19 Variation in Ultimate Load with Varying Grade of Concrete and Steel

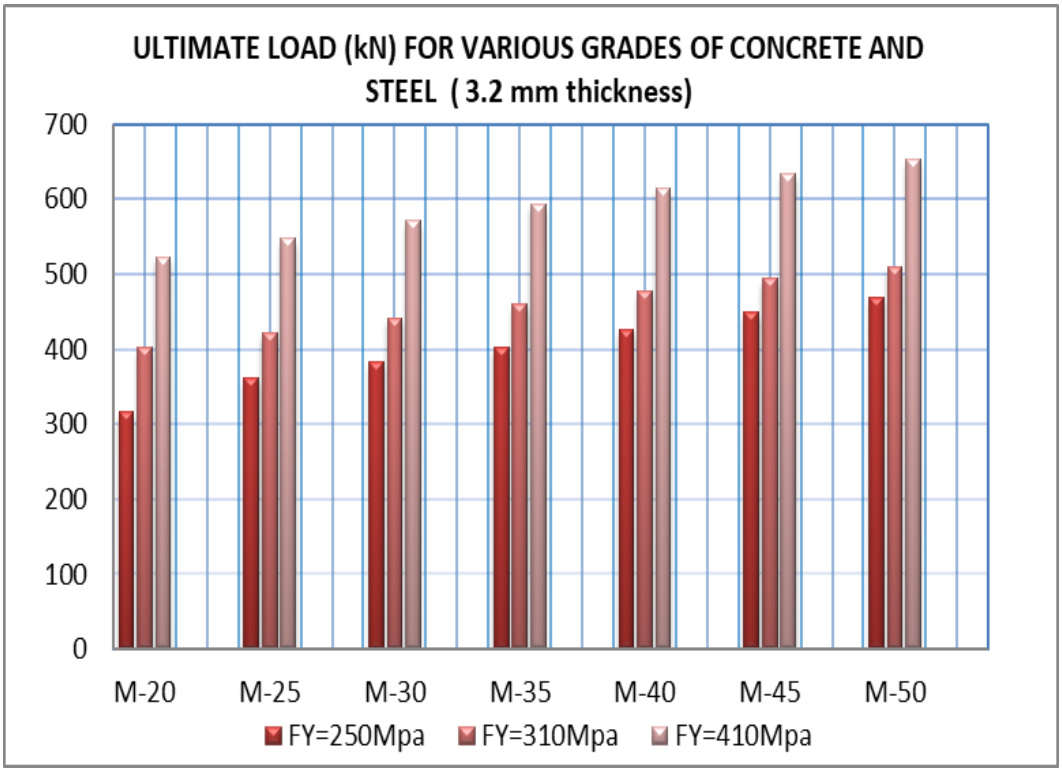

Figure 3.20 Variation in Ultimate Load with Varying Grade of Concrete and Steel

3.7 CLOSURE

It has been observed from the experimental and numerical investigation of various CFST specimens that load carrying capacity of the CFST columns is significantly influenced by various parameters such as slenderness ratio (L/B), thickness of steel tube (B/t ratio), depth to width ratio (H/B), grade of concrete and steel etc. Decrease in B/t ratio represents enhancement in cross section of steel tube and results in increase in the load carrying capacity of the CFST columns due to increase in the confinement pressure. Increase in slenderness ratio reduces the load carrying capacity of the column. Sections filled with higher grade of concrete and of higher grade of steel exhibit higher load carrying capacity. This increase is applicable to all values of B/*t* ratio or H/B ratio. Increased H/B ratio of or more aspect ratio results in decease in the strength of columns and earlier yielding of wider side of specimens.

Comparison of experimental results and results obtained from FE analysis for CFST columns with various parameters shows appreciable closeness. It can be concluded that proposed FE model is capable of predicting the column behaviour very efficiently.

CHAPTER 4

BEHAVIOUR OF CFST BEAM-COLUMN JOINTS: EXPERIMENTAL AND NUMERICAL INVESTIGATIONS

4.1 GENERAL

The usefulness of concrete filled steel tubular (CFST) sections as compression members is established by many authors (refer section 2.1.1 of Chapter 2). While few of the researchers have documented their utility as flexural members and proved their effectiveness under flexural loads (section 2.1.2 of Chapter 2). The results of previous studies conclude that filling of steel tube with concrete infill enhances the load carrying capacity, flexural strength, moment carrying capacity and stiffness of section. The improvement in the flexural strength and ductility further delays the failure of the columns. In all the previous studies, these sections have been tested either under axial compressive loads or under flexural loads. Though many studies are available on beam-column connections in which CFST columns were connected to steel beams, limited study on the behaviour of CFST columns connected to CFST beams is available (section 2.1.3 of Chapter 2). It is a well-known fact that beam-column joints (which are the integral part of a frame), are very important part of any structure and the constituent members behave differently as part of frame. Most importantly, in case of CFST beam-column joints, the connection type is expected to play a crucial role as is done in case of CFST column and steel beam joints. Hence, this chapter aims to explore effectiveness of CFST sections as part of CFST frame structures. For this purpose, CFST beam-column fabricated using CFST columns and beams have been selected as focus of study.

In the present chapter experimental investigation of beam-column joints has been presented. The objective of the study is, experimental investigation of proposed types of exterior-joints of frame considering various parameters for load-deflection behaviour, moment-rotation curves, failure modes and to get the classification of the joints as per EC-3. To identify the best type of connection out of various proposed

connections on the basis of these parameters, is also a part of study. The chapter also presents Finite Element (FE) modelling of proposed connections and comparison of FE results with corresponding experimental investigations. The model is further proposed to be used as part of full CFST frame for numerical investigations.

4.2 TYPES OF CONNECTIONS AND PARAMETERS TO BE STUDIED

It is observed from the literature review carried in section 2.1.3 that various types of connections; simple connections [(Dunberry et al. (1987) and Shakir and Mahmoud (1995)] ;extended-end plate connections [(France (1997); Lu et al. (1993); Lu and Wardenier (1998); Neves et al. (2002 and 2003); Kosteski and Packer (2003); Silva et al. (2003); Wang and Guo (2012); Sheet et al. (2013)] and many more; web angle connections (Hu et al. 2011) and top & bottom seat angle connections (Pirmoz et al. 2008) are mainly used in CFST frames. But in all these studies, CFST columns are connected to Steel beams. No study with CFST beams attached to CFST columns is available. As it is needed to provide connections for CFST beams and columns, various types of existing connections have been considered.

A simple connection involves attaching the steel beam directly to the skin of the steel tube. However, Alostaz and Schneider (1996) have observed that severe tube wall distortions can prohibit the development of the plastic bending capacity of the beam and cause very large stresses and strains on the flange weld and tube wall. It is observed by Neves et al. (2002 and 2003) that simple connections are not expected to carry any moments and so only rigid and semi rigid connections should be considered. It is important to mention here that in rigid connections, rotation angle between beam and column remains constant. Bending moment along with axial and shear force is also transferred from beam to column whereas semi-rigid connections are designed to transmit shear force fully and partial transmitting of the bending moment from beam to the joint is allowed. The analysis of frames with such kind of joints is more complex. In contrast with simple connections, bolted connections which are combinations of field bolting and shop welding connections have performed well (Leon et al. 1998), as they avoided problems related to the brittle weld failure observed in the 1994 Northridge and 1995 Kobe earthquakes. Further, it is advantageous to ensure the development of

plastic hinges in beams away from the beam column connection. A remedial measure, based on limited experimental investigations has been proposed in FEMA 267 with the intention of moving the location of the plastic hinge away from the face of the column. Reinforcing the connection with cover plates is a typology to move the plastic hinge away from the column flange (Yu et al. 2006). The results of investigations conducted by Wang et al. (2009) show that the end plate bolted connections, behave in a semi-rigid manner according to the EC3 specification. The experimental studies by Wang and Guo (2012) demonstrated that end plate bolted connections to CFTST columns are able to provide similar or even more favorable performance than their fully rigid counterparts. The usage of semi-rigid bolted forms also eradicates the potential problems associated with weld fracture in full-rigid arrangements.

Hence, considering all the above-mentioned points and constrains of the CFST sections as beams (e.g. web angle cannot be used in the case of CFST beams), two types of connections have been proposed for the present study: -

(i) Extended-end plate bolted connections

(ii) Seat-angle bolted connections

As end-plate bolted connections are extensively used in steel structures (Kaushik et al. 2013) and seat angle connections have the advantages of easy quality control and less assembly time than welded connections (Pirmoz 2006 and Pirmoz et al. 2008). Typical view of end plate and seat angle connections are presented in Figure 4.1. In these types of connections, bolts play a pivotal role on the behaviour of joints. The connections with black bolts tend to slip, which reduces their energy dissipation capacity under cyclic loading and so are to be avoided. HSFG bolts perform better. Hence, HSFG bolts have been used in the purposed connections. To evaluate the influence of other parameters e.g. size, grade and anchorage length of bolts, connections with full length bolts (termed as through bolts), bolts with partial length (normal bolts), bolts of diameter 10mm of grade 10.9 and 8mm of grade 8.8 have been considered. Other parameters considered in the study are; size of end plate, size of seat-angle and geometry of the beam section.

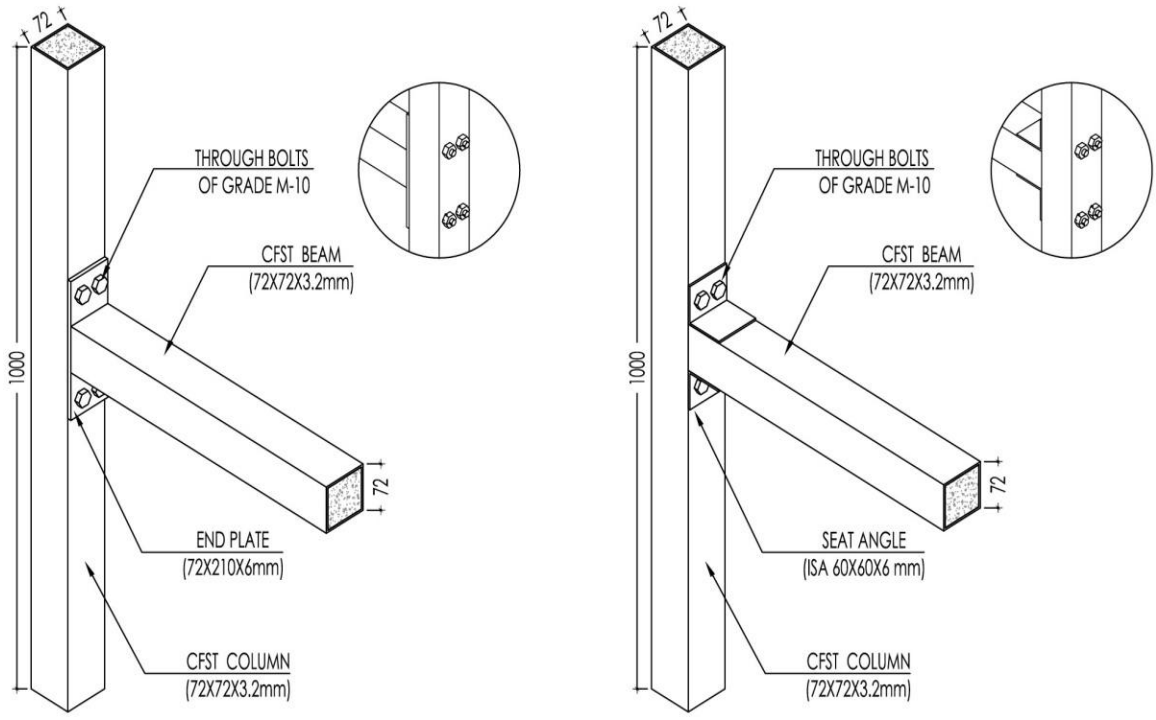

(a) **(b)**

Figure 4.1 Typical View of (a) End Plate and (b) Seat Angle Through Bolted Connections

4.3 EXPERIMENTAL INVESTIGATIONS

4.3.1 Material Properties

Steel hollow section: Square and rectangular steel hollow sections of TATA Structura and APPOLO make of Grade Yst-240 (with minimum Yield strength 240 N/mm^2) conforming IS 4923, have been used in the experiment. Modulus of elasticity of steel, E_s is taken as 2.1 x10^5 N/mm^2. In tensile coupon tests, conducted according to the Indian standard specification IS: 1608-1972, average yield strength has been found to be 260 N/mm^2.

Core concrete: Concrete of M-25 grade has been used for the test specimens as the same mix has been used in test specimens tested as short CFST columns in Chapter 3 and in specimens prepared for monitoring degradation using ultrasonic waves. For

details of mix proportions refer section 3.2.1 of Chapter-3. Six concrete cubes (150X150X150 mm) have been prepared and crushed to failure to determine the actual 28 days' compressive strength. The average 28 days' compressive strength of the concrete has been found to be 35.5 N/mm^2. The equivalent cylinder strengths fc' has been determined as being 28.4 N/mm^2. The IS 456:2000 stress-strain relationship has been used for the purpose of calculating the basic material properties used in analysis.

Bolts: High strength bolts (conforming IS:1364-2003) of the Grade 10.9, M10 having ultimate strength and yield strength of 1000 N/mm^2 and 900 N/mm^2, respectively, have been used in all samples. Two sets of sub assemblages have been connected with bolts of the Grade 8.8 M-8 having ultimate strength and yield strength 800 N/mm^2 and 640 N/mm^2, respectively.

To ensure bond behaviour, a pilot study has been conducted on joints using normal concrete mix and the joints have been observed to be weak and bond slip occurred at lower loads in case of specially in case of bolts of smaller anchorage length. Hence to ensure proper bond of anchor bolt with concrete, Injection mortar FIS V has been used. This is an approved material suitable for rebar connections in Concrete C20/25 to C50/60 (f_{ck} between 20 to 60 N/mm^2). The FIS V (Fischer brand) is a-component injection mortar based on vinyl ester hybrid. Resin and hardener are stored in two separate chambers and are not mixed and activated until extrusion through the static mixer. The injection cartridges are quick and easy to use with the Fischer dispensers.

4.3.2 Description of Test Specimens

In the present study CFST members are used as both beam and column to explore their potential in CFST framed structures. Square and rectangular concrete filled steel tubular sections as beams and columns have been selected for study because it's a proven fact that the rectangular sections are preferred over their circular counterparts by the designers' due to architectural reasons and most importantly more convenient connectivity between the beam and column.

The test specimens have been fabricated in a T-shape to simulate the external region of a semi-continuous frame. Depending upon the parameters discussed above,

total ten sets (two specimens for each set) of each type of connection; five with extended end plate and five with seat angle (Figure 4.1) using 10 mm diameter bolts, have been fabricated and tested for monotonic loading applied at the beam tip.

Two sets of specimens of with extended end plate using 8 mm diameter bolts, have been made. The size of square hollow section of cross-section 72 mm X 72 mm X 3.2 mm is selected to be used as column part, meanwhile, SHS of cross-section of 72 mm X 72 mm X 3.2 mm and RHS 48 mm X 96 mm X 3.2 mm have been used as beams. The size of the sections is selected due to their availability in the market. Table 4.1 and Table 4.2 summarizes the detail of the specimens. Figure 4.2, Figure 4.3, Figure 4.4 and Figure 4.5 provide the design details of the proposed beam-to-column connections. The columns for all specimens have been concrete filled square steel tubes of 1000mm height, whereas, the beams of two types i.e. concrete filled square steel tubes of 500 mm length with cross-section 72 mm X 72 mm X 3.2 mm in specimens named as SS-EPTB and SS-EPAB-1 and SS-EPAB-2 and rectangular steel tubes with cross-section 48 mm X 96 mm X 3.2 mm in specimens SR-EPTB and SR-EPAB have been used (Figure 4.4 and Figure 4.5). End plates and seat angles have been connected to CFST beams with the help of fillet weld of 6mm size.

Based on the present study, the behaviour of the joints in terms of load-deflection behaviour, moment-rotation curves and failure modes, has been evaluated and the viability of connecting an extended end plate and seat angle to the CFST beam with CFST column using through bolts and normal high strength bolts to improve the joint behaviour has been explored.

Table 4.1 Nomenclature of Test Specimens

Sr. No.	Specimen Label	Detail of Specimen
1.	SS-EPTB	Square column Square beam- End plate through bolted
2.	SS-EPAB-1	Square column Square beam - End plated anchor bolted
3.	SS-EPAB-2	Square column Square beam - End plate anchor bolted
4.	SS-SATB	Square column Square beam - Seat angle through bolted
5.	SS-SAAB-1	Square column Square beam - Seat angle anchor bolted
6.	SS-SAAB-2	Square column Square beam - Seat angle anchor bolted
7.	SR-EPTB	Square column Rectangular beam- End plate through bolted
8.	SR-EPAB	Square column Rectangular beam - End plate anchor bolted
9.	SR-SATB	Square column Rectangular beam - Seat angle through bolted
10.	SR-SAAB	Square column Rectangular beam - Seat angle anchor bolted

Table 4.2 Summary of Test Specimen Data

Specimen Label	**Column section b x b x t (mm)**	**Column height (mm)**	**Beam Section b x h x t (mm)**	**Beam Length (mm)**	**End plate Size**	**Bolt dia (mm)**	**Seat Angle size**
SS-EPTB	72 X 72 X3.2	1000	72 X 72 X3.2	500	72 X 190 X 6	10	
SS-EPAB-1	72 X 72 X3.2		72 X 72 X3.2		72 X 190 X 6	10	
SS-EPAB-2	72 X 72 X3.2		72 X 72 X3.2		72 X 170 X 6	8	
SS-SATB	72 X 72 X3.2		72 X 72 X3.2		-	10	60 X 60 X 6
SS-SAAB-1	72 X 72 X3.2		72 X 72 X3.2		-	10	60 X 60 X 6
SS-SAAB-2	72 X 72 X3.2		72 X 72 X3.2		-	8	50 X 50X 6
SR-EPTB	72 X 72 X3.2		48 X 96 X3.2		72 X 210 X 6	10	
SR-EPAB	72 X 72 X3.2		48 X 96 X3.2		72 X 210 X 6	10	
SR-SATB	72 X 72 X3.2		48 X 96 X3.2		-	10	60 X 60 X 6
SR-SAAB	72 X 72 X3.2		48 X 96 X3.2		-	10	60 X 60 X 6

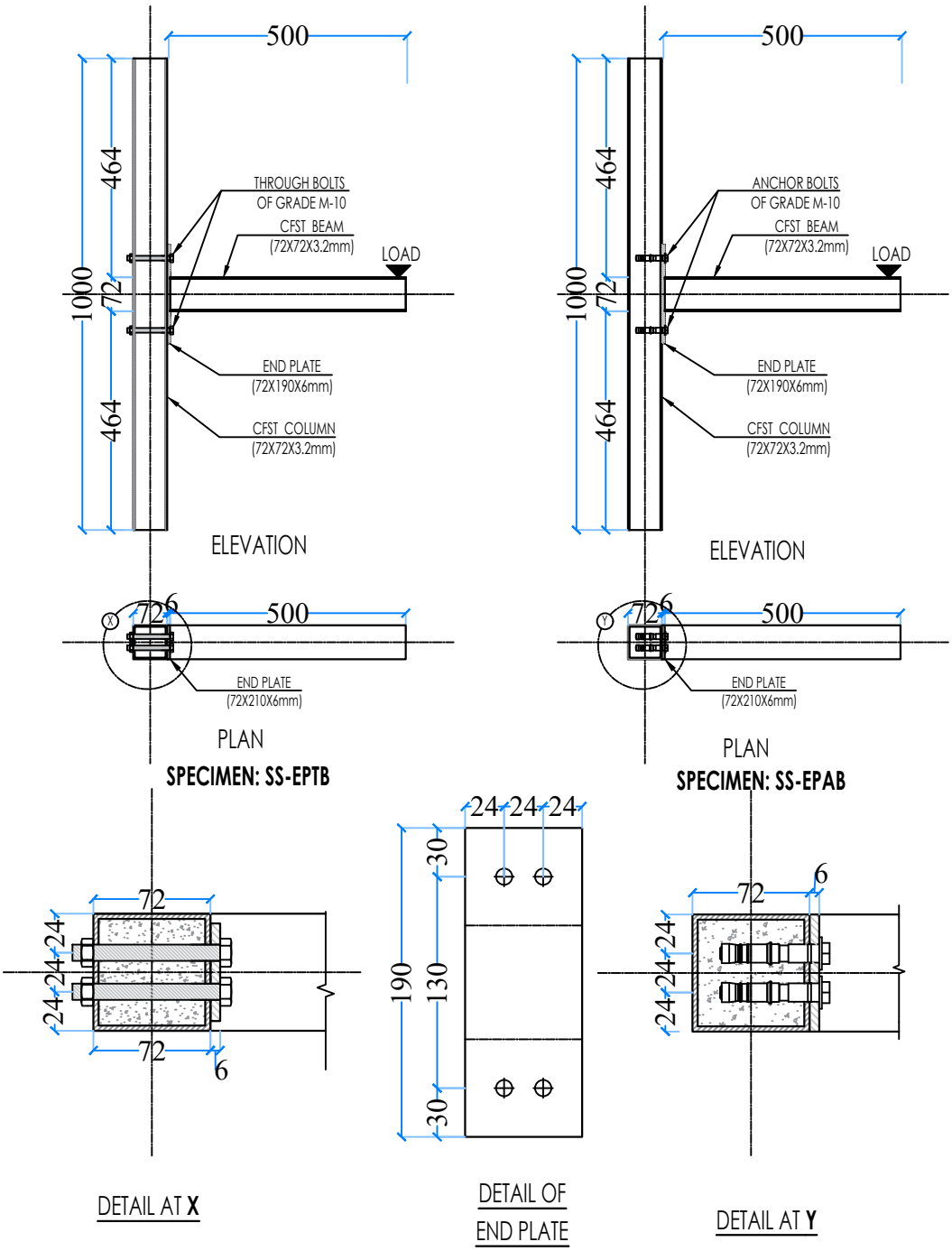

(Note: All Dimensions are in mm and drawings are NTS)
Figure 4.2 Design Details of SS-EPTB, and SS-EPAB Connections

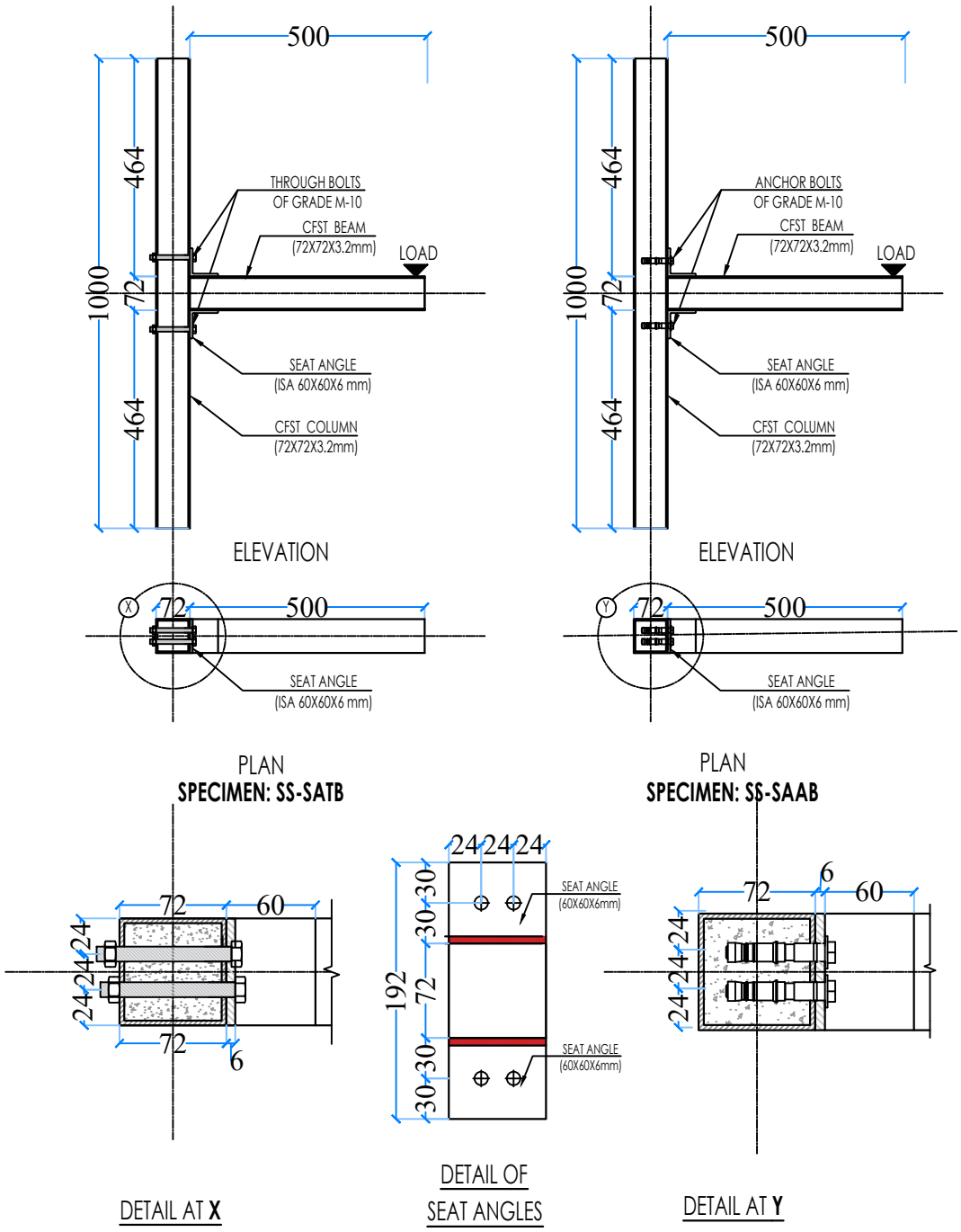

(Note: All Dimensions are in mm and drawings are NTS)

Figure 4.3 Design Details of SS-SATB and SS-SAAB Connections

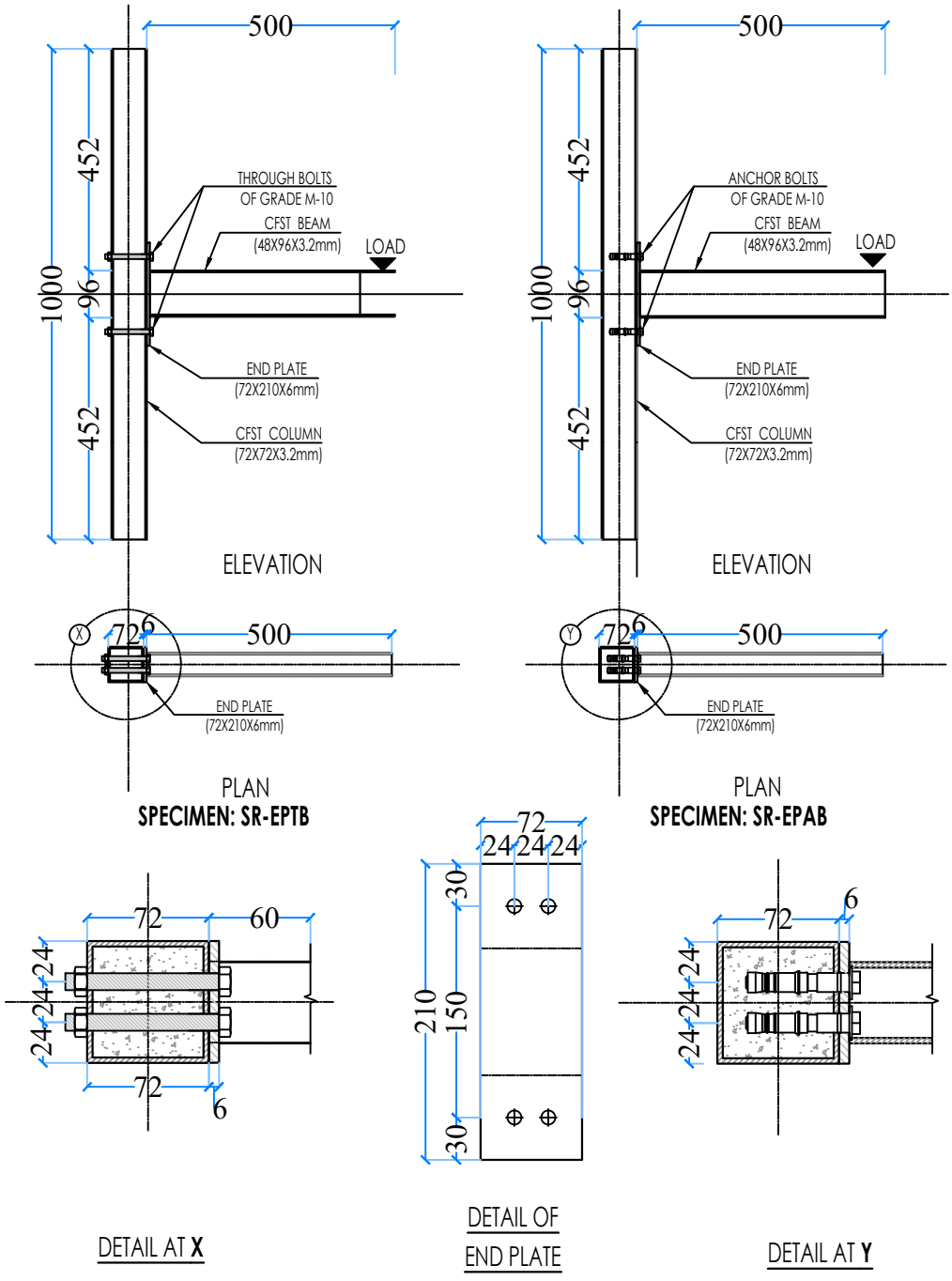

(Note: All Dimensions are in mm and drawings are NTS)

Figure 4.4 Design Details of SR-EPTB and SR-EPAB Connections

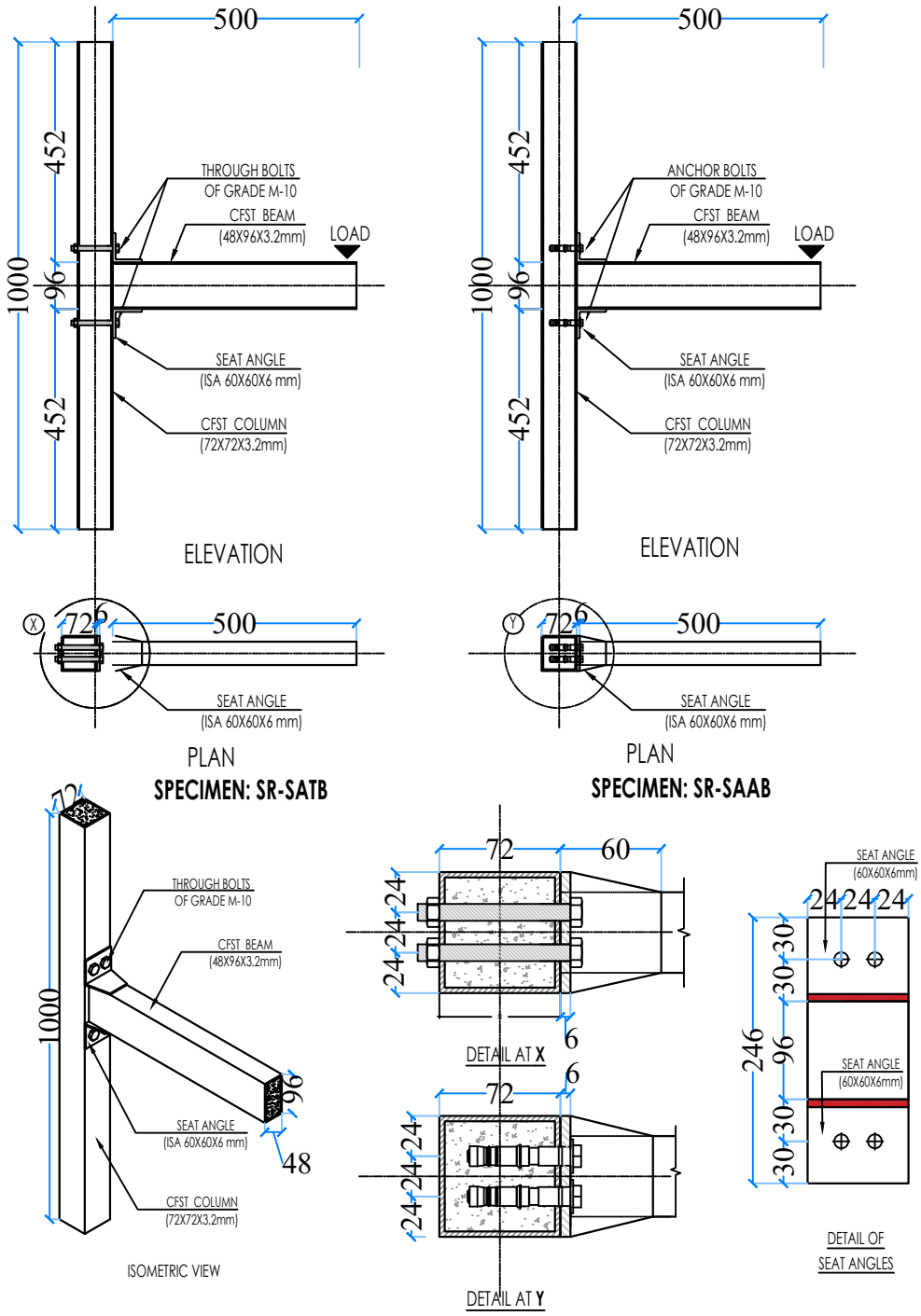

(Note: All Dimensions are in mm and drawings are NTS)

Figure 4.5 Design Details of SR-SATB and SR-SAAB Connections

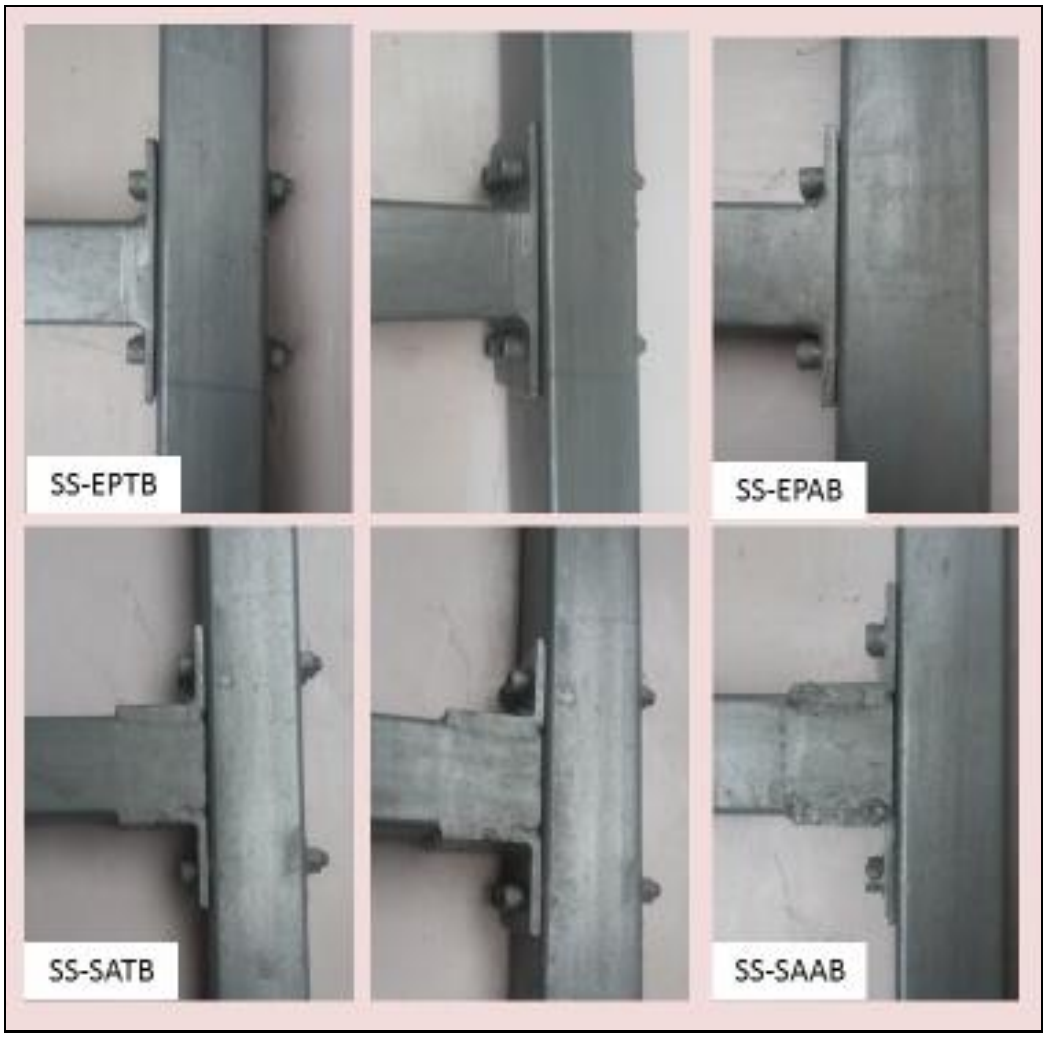

(a) Prepared Specimens

(b) Specimens During Fabrication

Figure 4.6 Specimens of Various Beam-Column Connections

4.3.3 Experimental Setup and Loading Procedure

The general arrangement of the test setup is illustrated in Figure 4.7. Load has been applied with the help of a hydraulic jack of 600 kN capacity. It has been applied at the beam end in the vertical direction. In order to investigate the behaviour of various bolted connections under monotonically increasing loads. in the pre-loading phase, all the measurement channels (Linear Variable Displacement Transducers) have been checked to record the initial readings before the application of load. Then, the loading jacks have been increased by 0.2 kN and after a while all the readings have been reduced to zero. In the formal loading phase, the test has been performed in the load control mode. Test has been performed till the failure load achieved. Each beam tip displacement has been automatically recorded by two Linear Variable Displacement Transducers (LVDTs) mounted acting on each beam tip and 100 mm away from tip.

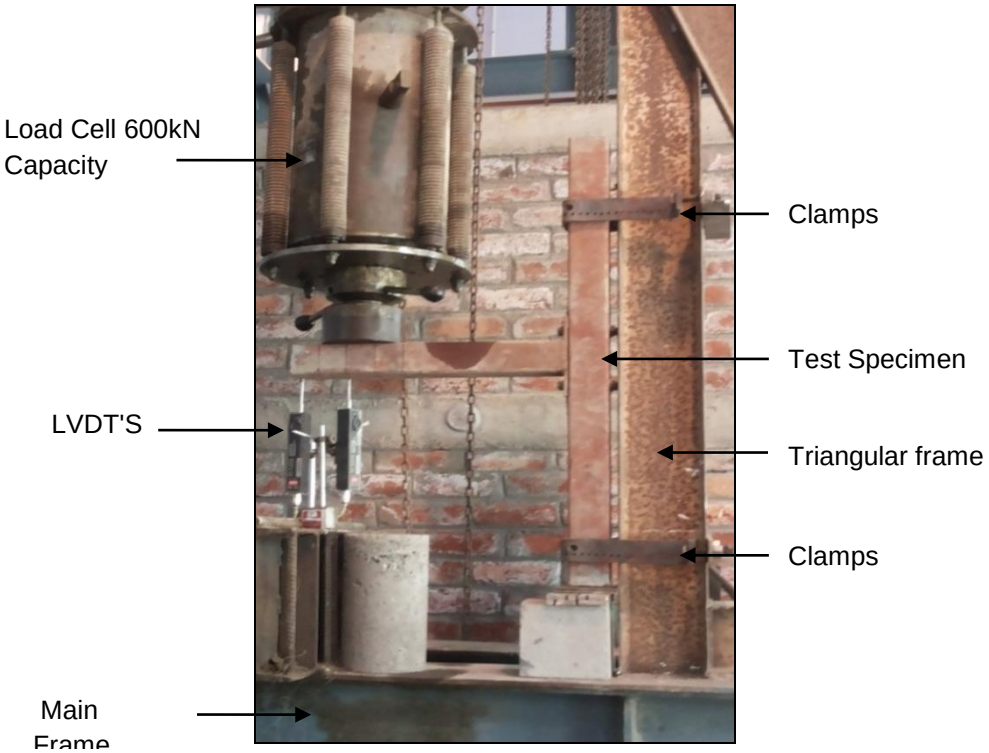

Figure 4.7 Experimental Set-up

Considering the pilot studies executed and material properties used in the experiments, FE models of various test specimens have been developed and analyzed to study the load-deflection and failure behaviour of all the experimental test models.

4.4 NUMERICAL MODELLING OF CFST BEAM COLUMN JOINTS

The Finite Element Method (FEM) is a popular tool for validating and predicting the physical performance of complex engineering structures. In recent years, large-scale general-purpose finite element codes with more and more perfect functions have developed speedily. This has made the application of finite element analysis possible on different kinds of bolted connections. In the present study, during the finite element analysis, the interaction between the end-plate and column wall as well as geometric and material nonlinearities have been considered by an appropriate method. The nonlinear behavior of Concrete Filled Steel Tubular (CFST) beam-column joints using FE modelling under the static load has been carried out, to study the response and load carrying capacity of exterior concrete-filled steel hollow tubular section beam-column joints using non-linear finite element analysis with software ATENA-3D.

Modeling related problems such as the concrete confinement effects, interface between the concrete core and the steel tube, end plate and steel of tube column interaction, the definition of boundary conditions and material representation etc. are investigated using a comprehensive parametric study. Then the proposed model is validated by comparing with experimental results. A numerical model has been developed in ATENA-5.4-1, a general-purpose finite element code with many special features for non-linear analysis of plain and reinforced concrete structures. Based on the results of FEA, the loading resistance of these connections, and the influence of connection details on the connection behavior has been discussed.

4.4.1 Concrete

Solid brick element having minimum 8 and maximum 20 nodes is taken for concrete element in modeling of concrete used in ATENA 3D. This element has three degree of freedom (X, Y, Z) directions at each node. It is also capable of capturing plastic deformation and cracking in same directions. Confinement effect (increase of the compressive failure stress due to compressive stresses in other directions) is being

automatically considered in the material models available in ATENA. A more detailed sensitivity towards confinement is implemented in the Non-linear Cementeous-3 model which considers multidimensional failure surfaces in the material model.

4.4.2 Steel Tube

The steel tube is modeled by eight-sided solid brick element to make it compatible at junctions of concrete core and steel tube. Once the stress in steel reaches yield surface, it carries no further loading and becomes perfectly plastic before entering into strain hardening zone (Figure 4.8). The Von-Mises yield criterion flow rule represents the most realistic description of the plastic behavior of metals (Chakrabarty 1998). So, an elastic-plastic model 3D-Von Mises yield criterion is adopted to describe the constitutive behavior of steel tube to analyze the behavior of the steel in the plastic hardening range.

4.4.3 Modelling of Bolts

The simplest way to model a headed anchor (bolt) is to activate no slip for the bar end with head. For more precision, a combination of 1-D and volume element has been used in this analysis. Here the bolt shank has been modeled as reinforced bar with bond and bolt head has been modeled as steel plate of very small size. Various interfaces need to be carefully handled. Hence the steel-concrete contact at shank area has been modeled as bond model (Figure 4.8). Properties of good bond has been given as bolts used were threaded bolts. Interface between outer side of end plate and bottom side of steel plate (head) is simplified as no connection whereas shank top and head as perfect connection. Mesh refinement has been done for steel plate used as bolt head.

4.4.4 Interface Modelling

The interface material model can be used to simulate contact between two materials such as for instance a construction joint between two concrete segments or a contact. In the tested connections, there are so many interfaces which need to be modeled carefully. Though ATENA interface provides us intelligent interface modelling but the work required to define the interface material parameters and the risk of related problems can be avoided by using perfect connection and no connection.

Perfect connection is used to model interface for composite action of steel tube and core concrete as the focus of study being connection part. Interface between outer surface of with bond CFST column and core concrete filled in CFST beam top surface seat angle joints have been modeled as no connection. Contact element has been used to model interface between end plate and outer of column steel plate.

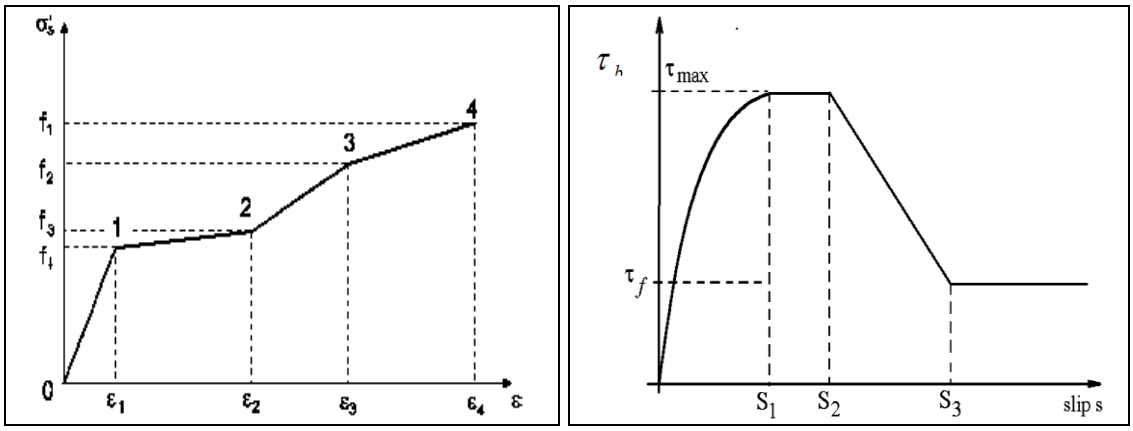

(a) **(b)**

Figure 4.8 (a) Typical Stress–Strain Curves for Steel with Strain Hardening and (b) Bond-Slip Law by CEB-FIB Model Code 1990 (ATENA 2012)

4.4.5 Boundary Conditions and Loading

In order to simulate the test set-up in better way both ends of column part have been fitted with steel plates. CFST column is restrained against displacement in all three directions. Monotonically increasing load is applied at steel plate modeled at the beam end. Values of concrete yield strength, concrete modulus of elasticity and steel yield strength and steel modulus of elasticity, are entered in definition material type and analysis is run in preprocessor mode. Modeling of few connections has been illustrated in Figure 4.9.

4.4.6 Description of FE Model

Following the experimental tests, FE analysis of the various connections is carried out. Material non-linearities are considered and Newton-Raphson incremental method is applied in the solution. The elements are chosen from ATENA library. All

steel parts and core concrete are modelled using the solid element (brick). The structural meshing technique is used to have a proper element shape. Denser mesh and low order elements have been used. Mesh refinement is applied to sensitive areas like end plates. A monotonic load is applied to the beam-tip. The displacements in x, y direction on the top base are kept constrained.

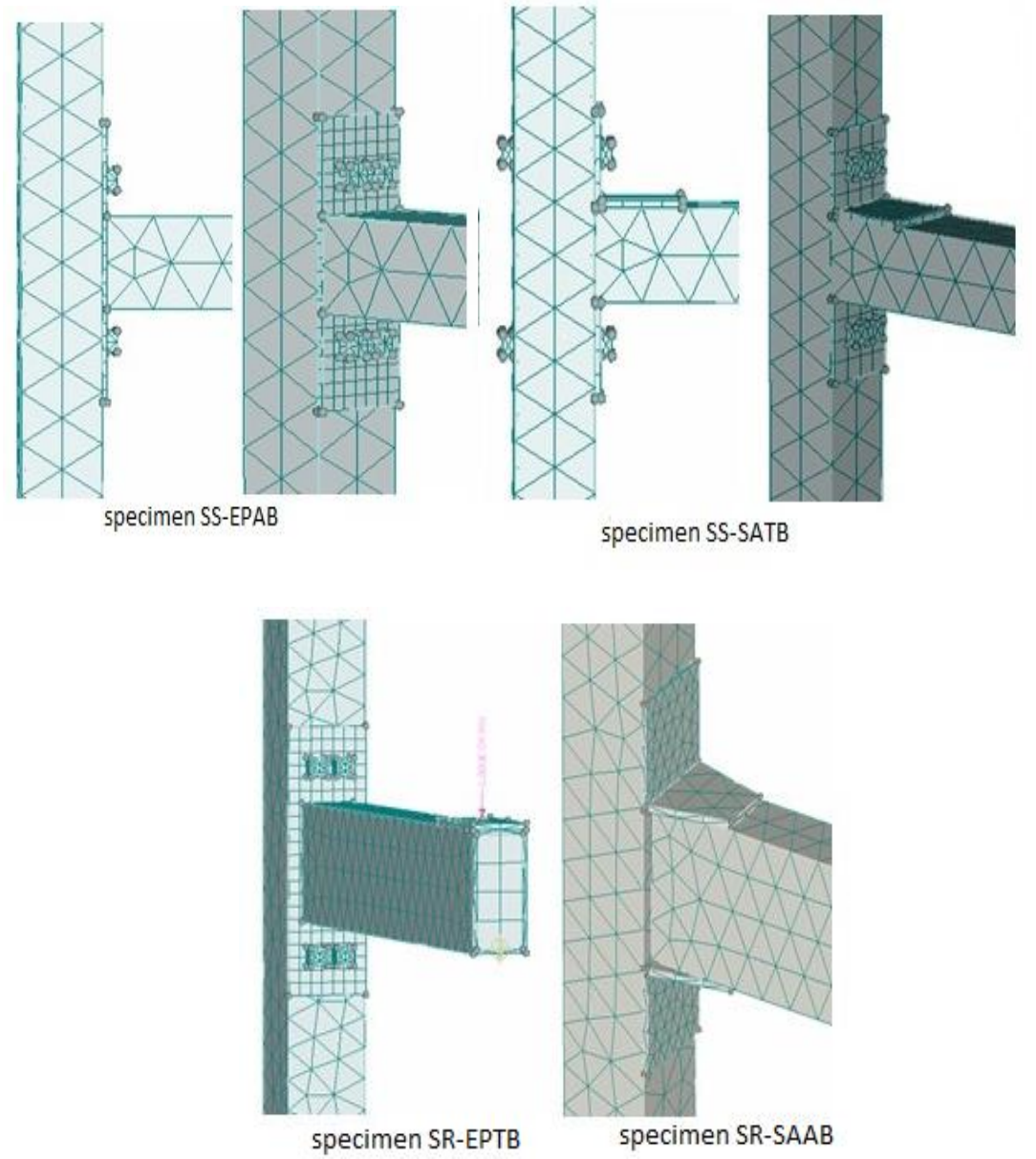

Figure 4.9 FE Modeling of Various Connections

4.5 RESULTS AND DISCUSSIONS

In order to investigate the behaviour of various bolted connections under monotonically increasing loads, various specimens have been tested by applying load at the beam tip with the help of a hydraulic jack of 600 KN capacity. Test has been performed till the failure load achieved. For each beam tip displacement has been automatically recorded by two Linear Variable Displacement Transducers (LVDTs) mounted acting on each beam tip and 100 mm away from tip. The results obtained are discussed in this section. Load-displacement and deformation behaviour of extended end-plate bolted Connections and seat angle bolted connections are discussed in Section 4.5.1 and Section 4.5.2 respectively. It is followed by a discussion on various failure modes and comparative studies. Finally, the FE analysis results are discussed.

4.5.1 Load-Displacement and Deformation Behaviour of Extended End-Plate Bolted Connections

Test specimens have been divided in two groups: connections with square beam and connections with rectangular beams connected to square CFST columns. Results are discussed in the same order.

4.5.1.1 Square Beam with Square Column

Specimen SS-EPTB: Specimen SS-EPTB has rectangular end plate of 72 mm X 190 mm X 6 mm size, connected to the square CFST columns with the help of high strength through bolts of Grade 10.9 M-10. The load displacement curve presented in Figure 4.10) indicates that behaviour of specimen is elastic before the displacement achieved a level of 7.42 mm to a load value of 4.5 kN. Further as the load is increased, a typical sound has been released from the connection zone at the load value of 8.64 kN and displacement of 28.14 mm. It can be characterized by the bond failure of bolts in tension from the core concrete in column. The end plate of CFST beam started deviating from column face and the concrete around the shank has started to loosen. This bond failure occurred in the column face directly in line with the beam top portion leads to the reduction of moment capacity (Figure 4.10). Then again, the load starts increasing. The load attained is a maximum of 11.9 kN at displacement of 52.1 mm, and at this stage, failure of the connection has been evident. The specimen SS-EPTB test has

been terminated when larger deformations appeared without any further increase in load. Moreover, the end plate has started yielding. The upper part of end plate has got inclined and departed from the column wall without showing signs of deformation in the column wall (Figure 4.14). No sign of local deformation of beam portion of the connection has been observed.

Specimen SS-EPAB-1: Specimen SS-EPAB-1 has 6 mm thick rectangular end plate of size 72 mm X 190 mm to the square CFST columns with high strength bolts of Grade 10.9 M-10. The load displacement curve of the beam (Figure 4.10) has been observed to be same as that of specimen SS-EPTB. The deformation at the tip of beam corresponding to 10.5 kN load is about 47 mm and the specimen has reached a maximum load of 10.53 kN at displacement of 50.0 mm. The specimen SS-EPAB-1 test has been terminated at a displacement of 54.5 mm. The bolts in tension zone have shown slight anchorage failure from the column near the end plate of CFST beams and concrete around the shank area near the head of bolt lost its bond with concrete which further has led to the loss of moment capacity. The deformation of the end plate, which departed from the column face, is lesser in bending than that occurred in specimen SS-EPTB. The end plate in tension zone is deviated away by 4 mm from the column wall without causing any bending deformation of the column face-wall (Figure 4.14).

Specimen SS-EPAB-2: Specimen SS-EPAB-2 has 6 mm thick end plate 72 mm X 170 mm joined to the CFST columns with bolts of Grade 8.8 M-8. The maximum load achieved is 8.37 kN at displacement of 32 mm, as shown in Figure 4.10. After this point increase in displacement with decrease in load has been observed. In the test, no deformation in the column wall is detected. After the completion of test, the maximum deformation of the end plate has been found to be 5 mm (Figure 4.14) and the end plate is deviated from the column wall similarly in case in specimen SS-EPAB-1.

It can be concluded by comparing the behaviour of SS-EPTB (peak load 11.9 kN), SS-EPAB-1 (peak load 10.53 kN) and SS-EPAB-2 (peak load 8.37 kN) that length, diameter and grade of bolts considerably influence the capacity of the joint. Decrease in length, diameter and grade of bolts result in decrease in capacity of the joint.

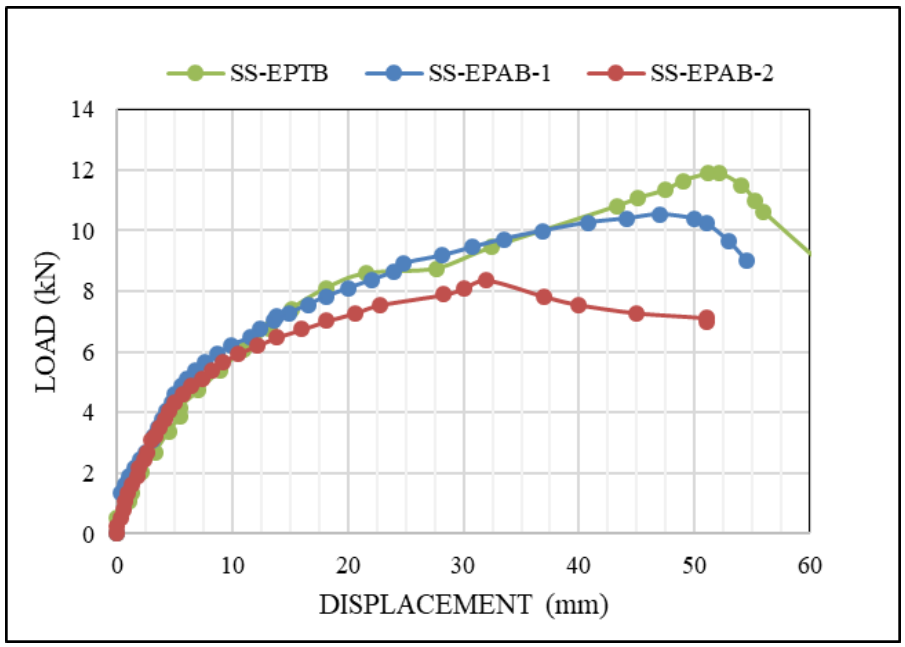

Figure 4.10 Load- Displacement Relationship of Specimen SS-EPTB, SS-EPAB-1 and SS-EPAB-2

4.5.1.2 Rectangular Beam with Square Column

Specimen SR-EPTB: Specimen SR-EPTB has rectangular end plate of 72 mm X 200 mm X 6 mm size, connected to the rectangular CFST beam to square CFST column with the help of high strength through bolts (120 mm long) of Grade 10.9 M-10. The load displacement curve of the beam (shown in Figure 4.12) is elastic at the displacement level of 3.42 mm corresponding to a load of 4.34 kN. Distinct cracking sounds have been emitted from the connection zone at 5.7 kN load and 9 mm displacement due to start of bond failure of bolts from the column by the end plate of CFST beams and the concrete around the shank area. This has led to the bond failure in the area of the column wall directly in line with the beam top flange. The failure mode is shown in Figure 4.17. The displacement attained at tip of beam corresponding to the maximum load of 12.32 kN was 32.6 mm, and evident failure of the connection is found to be started. After achieving displacement of 42mm against load value of 12.12 kN, drop in load has been observed. The specimen SS-EPTB test has been terminated at

displacement of 52 mm at the free end of beam. The end plate has started deforming and the upper part of end plate got separated from the column face with distinctive signs of bending deformation of end plate (Figure 4.14).

Specimen SR-EPAB

Specimen SR-EPAB has 72 mm X 200 mm X 6 mm rectangular end plate connected to the square CFST columns with high strength bolts of Grade 10.9 M-10. The trend of load displacement curve of the beam (shown in Figure 4.12) is initially same to specimen SR-EPTB. However, the deformation mode of the end plate in specimen SR-EPTB is clearly different to that observed in specimen SR-EPAB. The specimen SR-EPAB attained a maximum load of 11.83 kN at a displacement of 17.5 mm. After this point, the specimen SR-EPAB has shown continuous increase in deformation without any further increase in load. The bolts in tension has shown anchorage failure from the column by the end plate of CFST beams and concrete around the shank area near the bolt head, lost its bond with concrete. The maximum deformation of the end plate is about 4 mm; and the bending deformation of the end plate, which deviated from the column wall, is lesser than that of specimen SR-EPTB. It has been observed that the end plate near to the bolts in tension has been pulled away by 4 mm from the column wall. The whole end plate has inclined and its top part deviated from the column wall without showing any local failure of flange of beam (Figure 4.14).

4.5.2 Load-Displacement and Deformation Behaviour of Seat Angle Bolted Connections

4.5.2.1 Square Beam with Square Column

Specimen SS-SATB: Specimen SS-SATB has seat angles of size 60 mm x 60 mm X 6 mm connected to both sides of CFST beam further connected to the square CFST columns with high strength through bolts of Grade 10.9 M-10. The maximum load of specimen SS-SATB has been more than that of specimen SS-SAAB-1, as shown in Figure 4.11. The specimen has attained a maximum of 9.936 kN at a displacement of 47 mm. The test is stopped at a displacement of 54 mm. Moreover, the maximum

deformation of the connecting leg is about 5 mm from the column wall with noticeable crack at root of the seat angle (Figure 4.14).

Specimen SS-SAAB-1

Specimen SS-SAAB-1 has seat angles of size 60 mm x 60 mm x 6 mm connected to the square CFST columns with high strength bolts of Grade 10.9 M-10. The trends of load displacement curve of the beam (Figure 4.11) initially have shown better behaviour then specimen SS-SATB. However, the deformations of the seat angle in specimen are markedly more than those obtained in specimen SS-SATB. The specimen SS-SAAB-1 has attained a maximum load of 8.91 kN at a displacement of 34.63 mm and the bolts in tension exhibited slight anchorage failure near the connecting leg of seat angle of CFST beams and concrete around the shank near the head of bolt has lost its bond with concrete. The deformation at the tip of beam after 8.91 kN load has started increasing without any further increase in load. The connecting leg near to the bolts in tension has been pulled away by 4 mm from the column face (Figure 4.14).

Specimen SS-SAAB-2: Specimen SS-SAAB-2 has seat angles of size 50 mm x 50 mm x 6 mm connected to the square CFST columns with high strength bolts of Grade 8.8 M-8. Specimen SS-EPAB-2 has been terminated at 50 mm displacement. The maximum load achieved is 8.1 kN at a displacement of 42.7 mm, as shown in Figure 4.11. During the test, no cracking in the square steel tube column wall has been observed. After the completion of test, the maximum deformation of the connecting leg is found to be 5 mm and it has got inclined and deviated from the column wall similarly in case in specimen SS-SAAB-1.

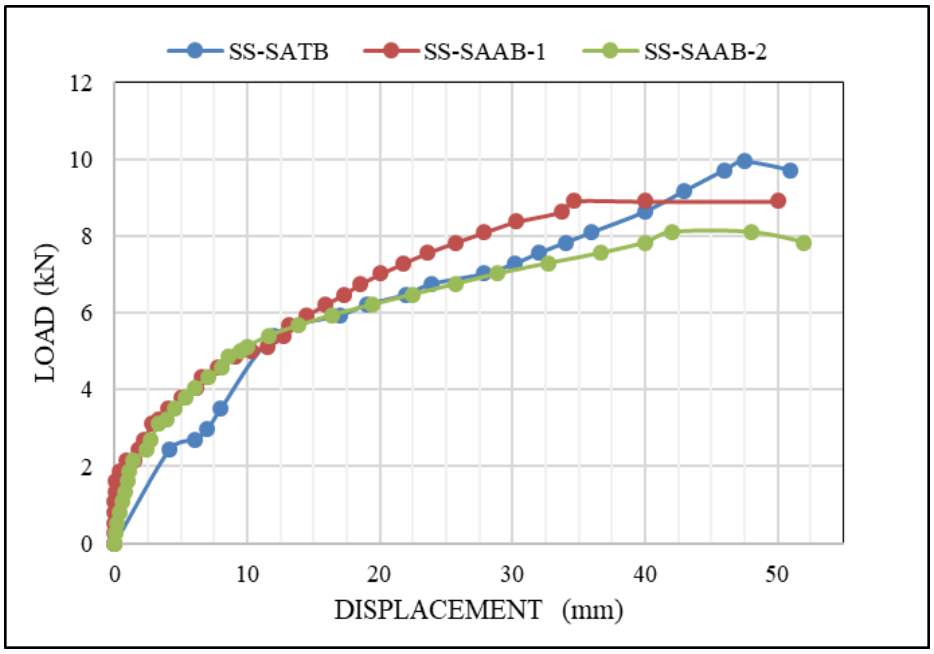

Figure 4.11 Load- Displacement Relationship of the Specimen SS-SATB, SS-SAAB-1 and SS-SAAB-2

4.5.2.2 Rectangular Beam with Square Column

Specimen SR-SATB

Specimen SR-SATB has seat angle 60 x 60 x 6 mm connected to CFST beam, connected to the square CFST columns with high strength through bolts of Grade 10.9 M-10. The maximum load of specimen SR-SATB has been more than that of specimen SR-SAAB, as shown in Figure 4.12. The specimen has attained a maximum of 9.73 kN at a displacement of 35 mm. The specimen SS-SATB test has been stopped at a displacement of 50 mm. Moreover, the maximum deformation of the connecting leg is about 5 mm from the column wall with noticeable bending deformation. Visible crack has been observed at root of connecting seat angle.

Specimen SR-SAAB

Specimen SR-SAAB has seat angles of size 60 mm x 60 mm X 6 mm connected to the square CFST columns with high strength bolts of Grade 10.9 M-10. The trend of load displacement curve of the beam (Figure 4.12) have shown behaviour similar to that

of specimen SR-SATB. However, ultimate load of the SR-SAAB specimen is found lesser. The specimen SR-SAAB has attained a maximum load of 8.75 kN at a displacement of 31.0 mm. The bolts in tension have exhibited slight anchorage failure from the column near the seat angle of CFST beams and concrete near the head of bolt lost its bond with concrete. A breakage at the root of the seat angle near to the bolts in tension and the connecting leg has been observed and it is pulled away by 5 mm from the column wall.

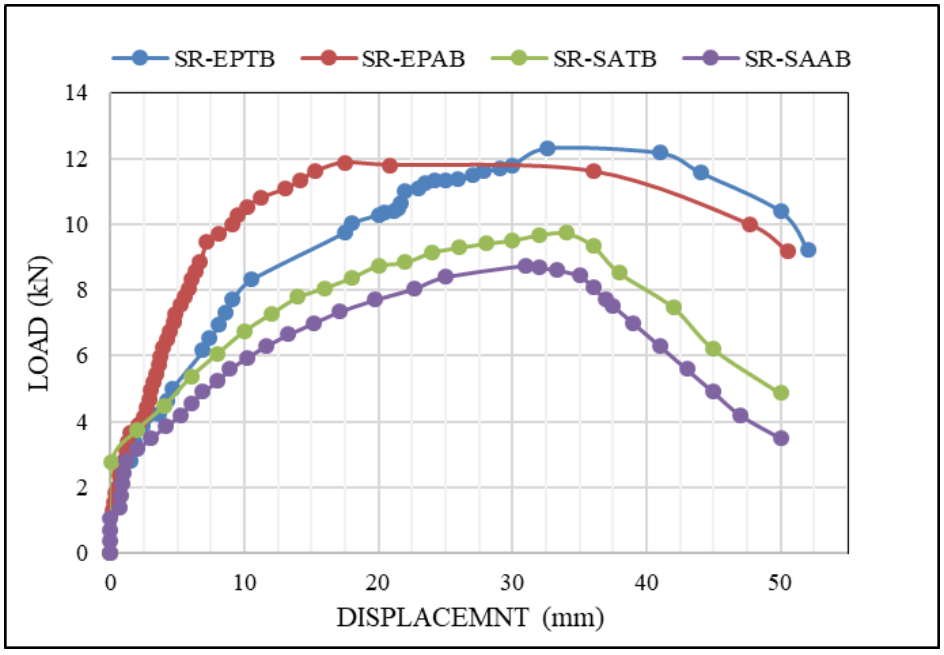

Figure 4.12 Load- Displacement Relationship of Specimen SR-EPTB, SR-EPAB, SR-SATB and SR-SAAB

4.5.3 Failure Modes

Based on the observations made during testing of various bolted connections, following failure modes have been witnessed:

I. Deformation of the end plate: In case of through bolt connections

II. Bond failure of bolts: In case of normal bolted connections

III. Seat angle failure in seat angle bolted connections

Schematic of various failure modes have been depicted in Figure 4.13. Different deformation modes of typical specimens tested have been presented in Figure 4.14. The deformation occurred in the end plate of specimen SS-EPTB is significantly more than that of specimen SS-EPAB and the ultimate load found to be more. The deformations in column face due to the deviation of end plates are not observed but the end plates got yielded in all type of end plated connections. The deviation of the end plate for specimen SS-EPTB and SS-EPAB is 4 mm and 6 mm, respectively. The main reason of increased outward deformation of the end plate is due to pulling out of the tensile bolts. The observed results show that the minor cracking of concrete appeared in the vicinity of tension bolts in the column face. Any sign of bending of the bolts has not been observed during tests and the entire range of extended end plate connections have performed satisfactorily and better than seat angled connections where the connecting leg of seat angle yielded and even crack at the root has been observed in case of through bolts connection. In case of square column-rectangular beams connections, Square column-rectangular beams connections with end plate have shown slightly higher load carrying capacity over their square column-square beam counterparts. Specimen SR-EPTB has attained 3.5% higher ultimate load than SS-EPTB.

It has been observed from the overall comparison of all the joints that through bolted connections with extended end plate perform better than the seat angle connections. In end plate connections, the yielding of plate in the tension zone happens whereas in seat angle connections, rupture at the root of connecting angle occurs. These connections have shown promising strength and ductility to be used as moment resisting connection. Various parameters viz. variation in size of end plate, dia and grade of bolts significantly affected the capacity of the joints. As far as overall caparison is concerned, connections with extended end plates have been found better, and the test results show the through bolted extended end plate connections exhibited favorable strength, stiffness and ductility for use in a moment resisting connection.

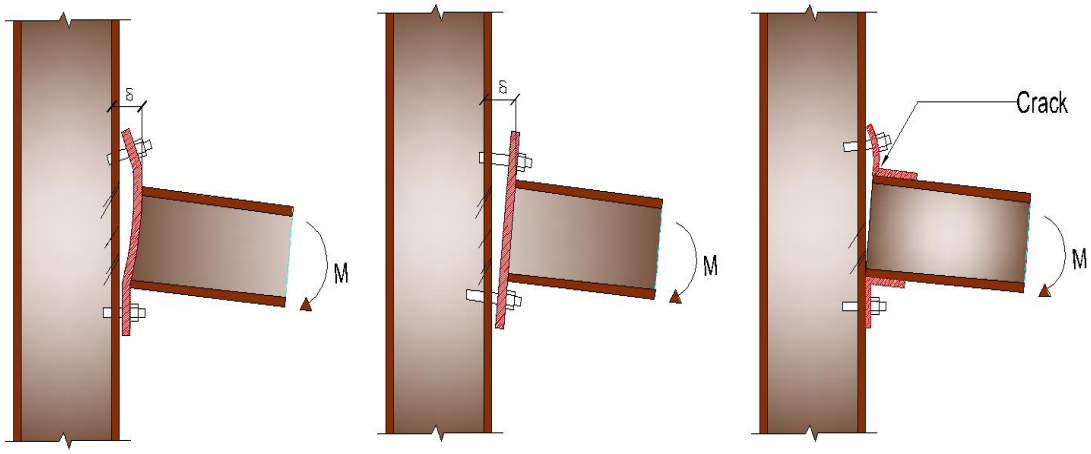

Figure 4.13 Schematic of Various Failure Modes from Left to Right (i) Yielding of End Plate (ii) Bond Failure of Bolts And (iii) Failure of Seat Angle

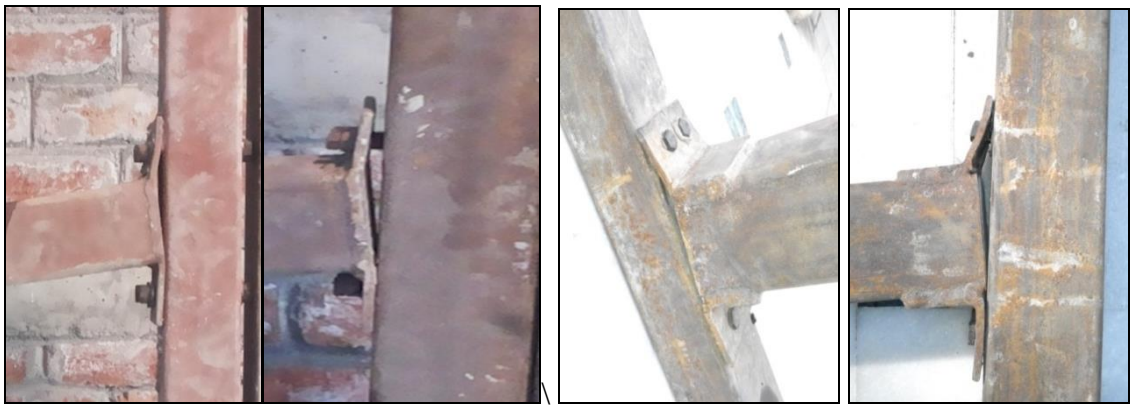

(a) **Endplate Deformation of SS-EPTB and SS-EPAB**

(b) Seat Angle Deformation of SS-SATB and SS-EPAB

(c) End Plate Deformation of SR-EPTB and SR-EPAB

Figure 4.14 Various Failure Modes

4.5.4 Comparative Studies

4.5.4.1 End Plate Bolted Connections V/s Seat Angle Connections

It is clearly visible from the Figure 4.15 that specimens with extended end plate exhibited better load carrying capacity over specimens with seat angle connections. These connections have shown promising strength and ductility to be used as moment resisting connection. The stiffness and strength of connections is enhanced with the increase in size of plate. It is expected that the strength of the bolted connections may be affected with change in various parameters such as thickness of end plate and cross-section of steel tube. It is observed that:

- End plate connections performed better to their seat angle counterparts.
- In square beams to square column connections, specimen with end plate and through bolts (SS-EPTB) has shown 19.76 % higher strength over specimen with seat angle connection (SS-SATB).
- In square beams to square column connections, specimen with end plate and normal length bolts (SS-EPAB) has shown 18.18 % higher strength over specimen with seat angle connection (SS-SAAB).
- In rectangular beams to square column connections, specimen with end plate and through bolts (SR-EPTB) as shown 26.6 % higher strength over specimen with seat angle connection (SR-SATB).
- In rectangular beams to square column connections, specimen with end plate and normal length (SR-EPAB) bolts has shown 35.7 % higher strength over specimen with seat angle connection (SR-SAAB).

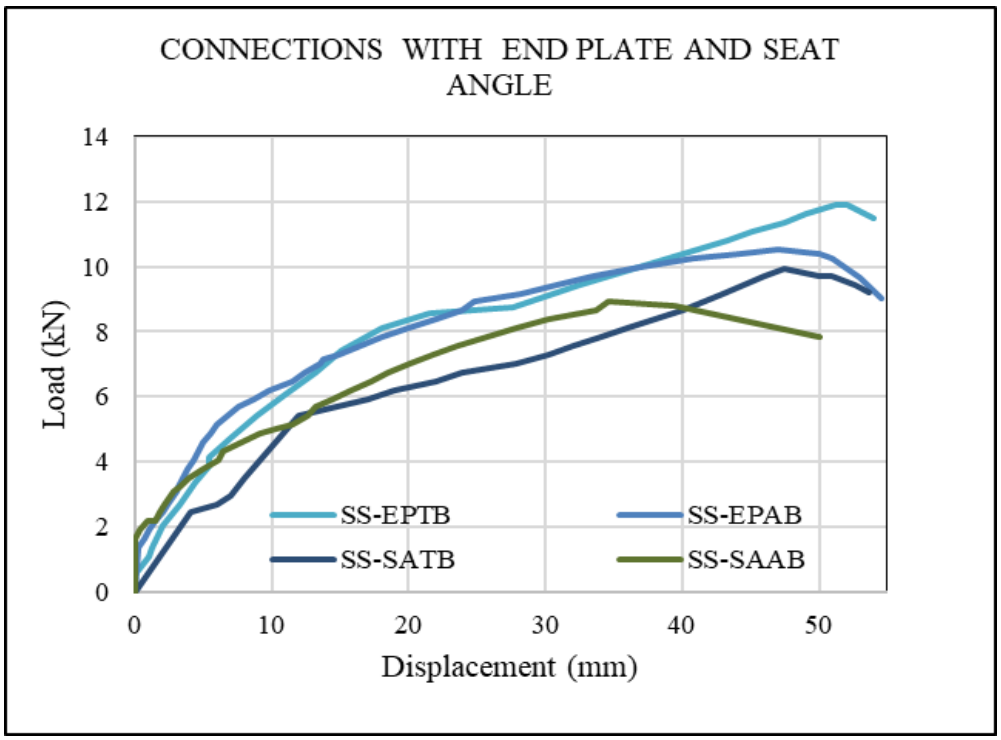

(a) Square Beam to Square Column

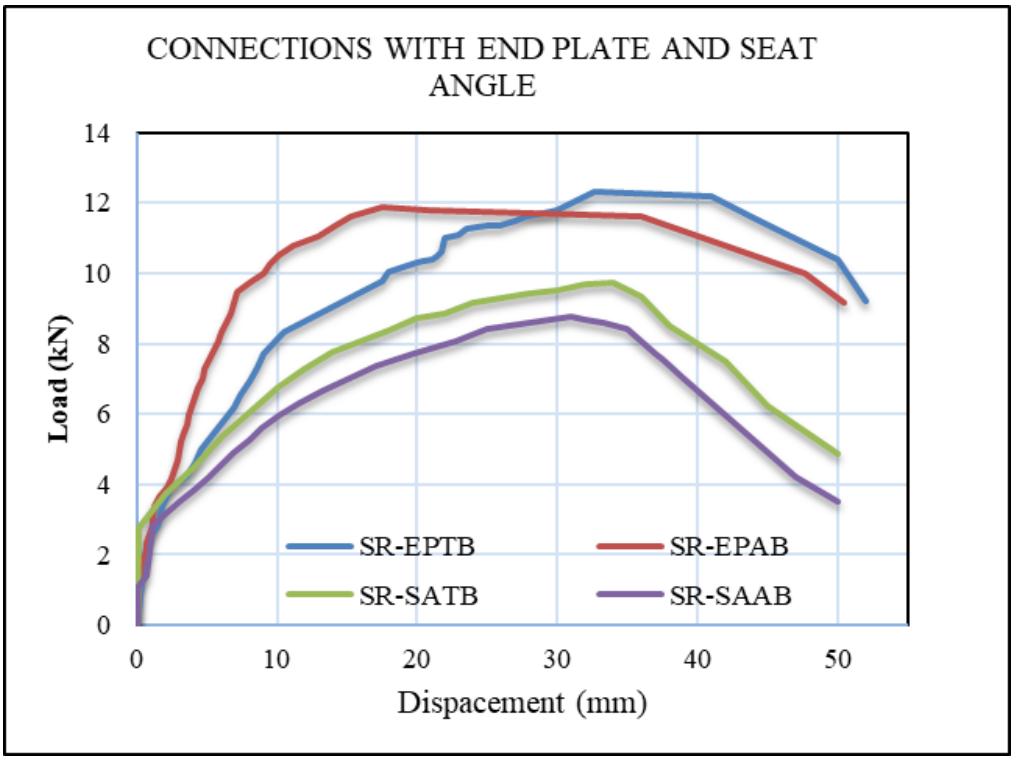

(b) Rectangular Beam to Square Column

Figure 4.15 Behaviour of End Plate Connections V/s Seat Angle Connections

4.5.4.2 Influence of Length, Size and Type of Bolts

Connections with through bolts V/s normal length bolts: The extended end plate connections with through bolts exhibited better behaviour in terms of load carrying capacity and ductility over connections with bolts of 60mm length (Figure 4.16). The same behaviour has been exhibited by seat angled connections. It is observing that:

- In end plate connections, specimens with through bolts (SS-EPTB) have shown 13.3 % higher strength over connections with normal anchor length bolts (SS-EPAB-1). Similarly, in seat angle connections, specimen SS-SATB has shown 11.51 % higher strength over SS-SAAB-1.
- In group of rectangular beams to square columns, specimens with through bolts (SR-EPTB and SR-SATB) have shown 4.14% and 11.2% higher strength than specimens with normal length bolts (SR-EPAB and SR-SAAB) respectively.
- Hence, it can be concluded that through bolted connections are better than the connections with normal length bolts.

Size and type of bolts: The behaviour of connections using 10 mm dia bolts have been compared with connections with 8 mm dia bolts. Figure 4.17 clearly shows that diameter of the bolts significantly affects the behavior of joints. Specimen SS-EPAB-1 and SS-SAAB-1 with 10mm dia bolts of grade 10.9 has shown 25.7% and 10% higher strength over SS-EPAB-2 and SS-SAAB-2 using 8mm dia bolts of grade 8.8 respectively. Hence it can be concluded that dia and grade of bolts considerably influence the capacity of the joint.

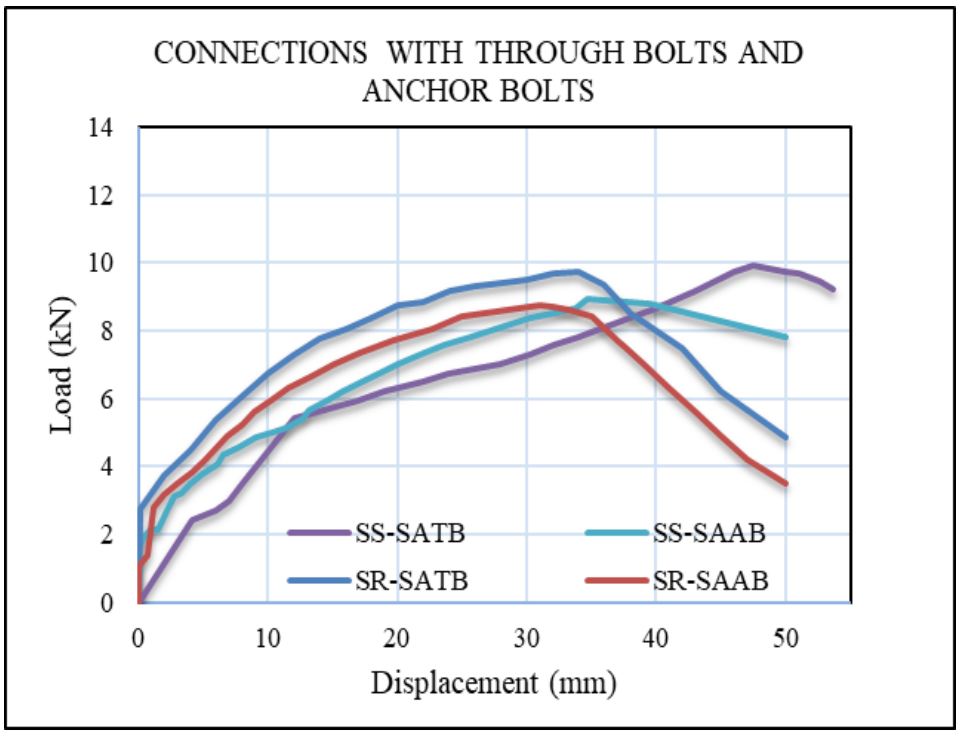

(a) Seat AngleConnections

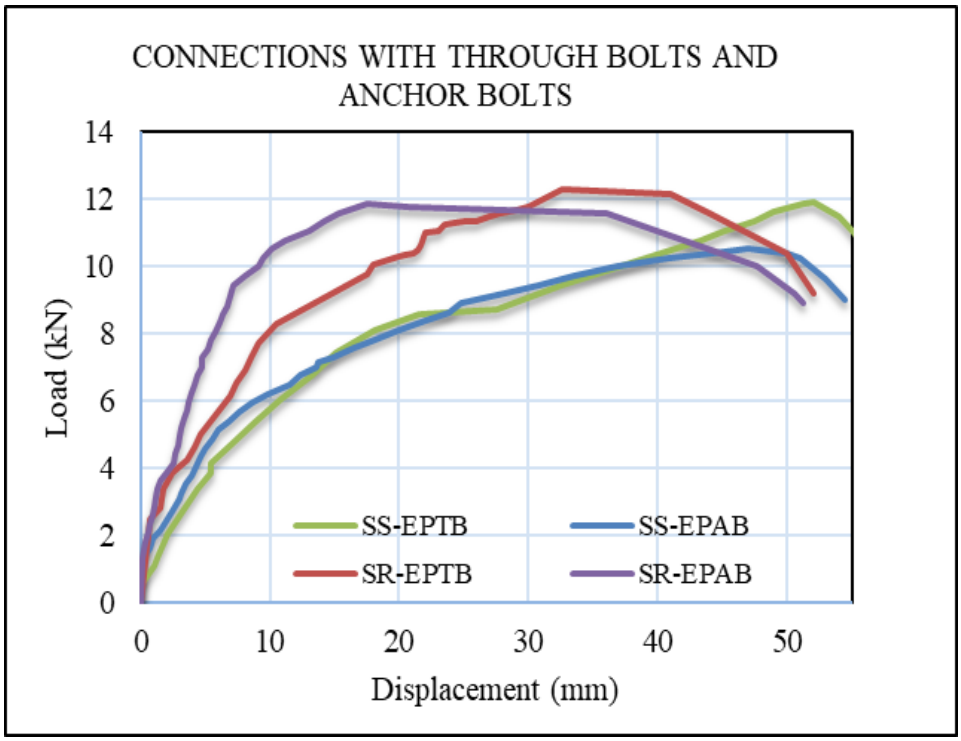

(b) End Plate Connections

Figure 4.16 Behaviour of Connections with Through Bolts V/s Connections with Normal Length Bolts

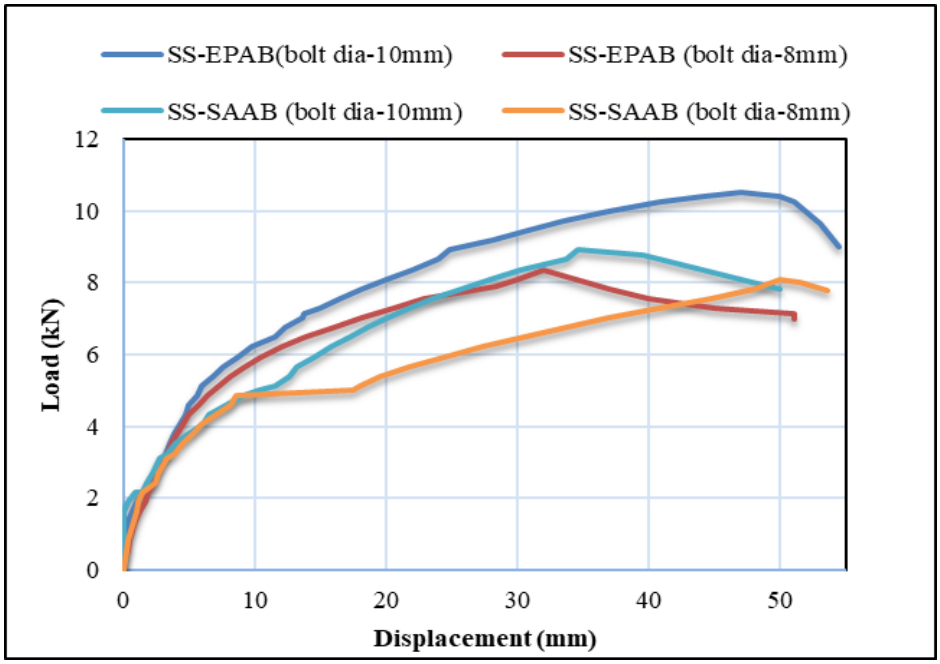

Figure 4.17 Load- Displacement Relationship of Connections with Varying Bolt Diameter

4.5.4.3 Geometry of Beam Section

Specimen SR-SATB and SR-SAAB which have square column-rectangular beam connections, have attained higher ultimate load than SS-EPTB and SS-EPAB. Connections of rectangular beams of same cross section area as used in case of square beams with square columns using end plates, exhibited slightly (3.5%-12.5%) higher strength.

4.5.5 Finite Element Analysis Results

4.5.5.1 Comparison of Ultimate load of experimental and FE results

Comparison of experimental and simulated Load-Displacement behaviour of various connections, obtained using the non-linear finite element analysis is presented in Figure 4.18 and Figure 4.19. All the specimens have been tested and analysed under identical conditions in the laboratory and the numerical modelling, respectively. In the case of experimental testing, the specimens have been tested by applying concentrated load at the tip of free end of the beam, while in numerical study; a monotonically increasing load was applied gradually at the free end. All test specimens have been

tested following an identical procedure described in the experimental program. Majority of the specimens exhibited the satisfactorily identical behaviour as depicted in experiments except few specimens.

Specimen SS-EPAB, SS-SATB, SS-SAAB-1 and SR-EPTB exhibit very identical behaviour and very closer loads at various points. In case of Specimen SS-SATB overall higher loads have been obtained whereas specimen SR-EPTB initially exhibited very identical behaviour initially but obtained higher ultimate load in comparison to the experimental load. Behaviour of typical models is discussed here.

FE analysis of specimen SS-SAAB-1 has yielded very closer results. Simulated model experienced displacement of 36.75 mm corresponding to ultimate load of 9 kN whereas experimental model has got displacement of 34.6 mm at peak load value of 8.91 kN. At ultimate load value of 10 kN, larger displacements have been experienced by FE model without further increase in load.

Specimen SR-EPTB, has performed identically to the test model initially, up to a load value of 11.4 kN corresponding displacement of 22.14 mm. At ultimate experimental load of 12.32 kN, displacement value is very close. After which it increased to 15 kN but very speedy increase in displacements has been observed. Similar failure pattern has been observed in both test and FE model.

In case of specimen SR-SATB, FE analysis results are found in close agreement. Simulated model experienced identical displacement of 15.4 mm corresponding load of 8.25 kN. Test model has got displacement of 34 mm at peak load of 9.7 kN, corresponding to this displacement FE model observed load value of 11 kN.

FE model of specimen SR-SAAB has exhibited totally identical behaviour till a load value of 6.9 kN and displacement value of 12.37 mm. After this the load started increasing and specimen has achieved displacement of 31.8 mm at load of 9.89 kN corresponding to experimental value of 32 mm displacement at ultimate load of 8.76 kN. From a group of beam-column joints (square beam connected to square column), all the specimens except SS-EPTB has performed very closely (Figure 4.18) whereas from second group of beam-column joints (rectangular beam connected to square column), the specimens SR-EPTB, SR-EPAB and SR-SATB has performed very closely (Figure 4.19).

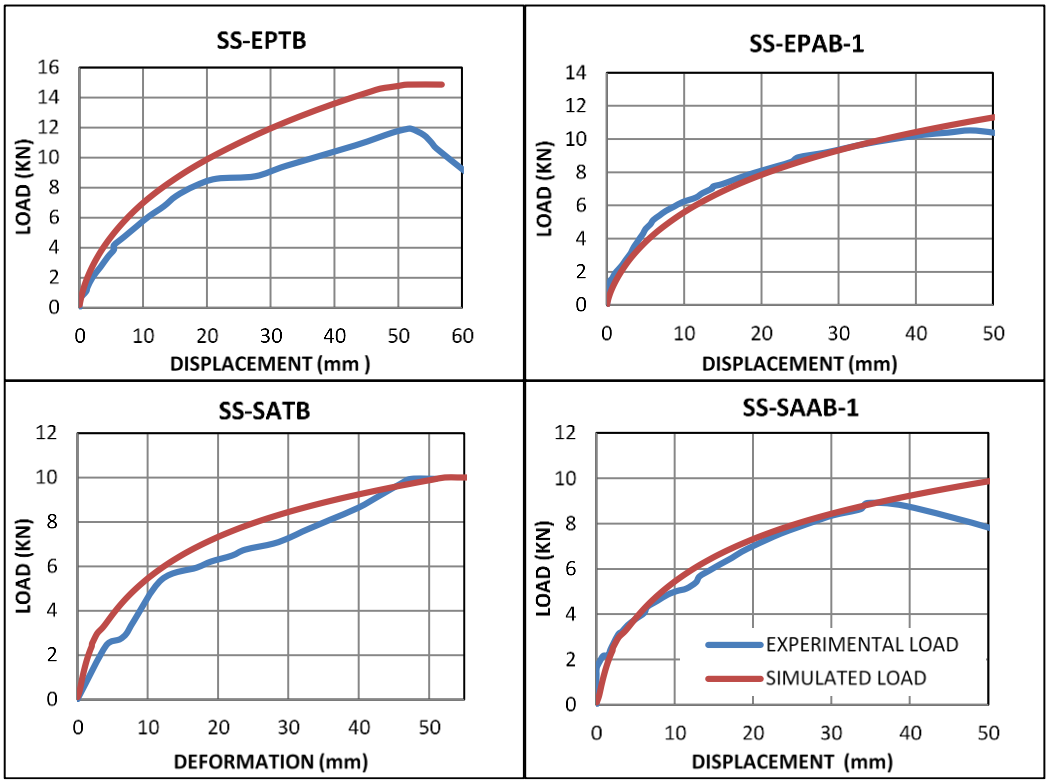

Figure 4.18 Comparison of Simulated and Experimental Load-Displacement Behaviour

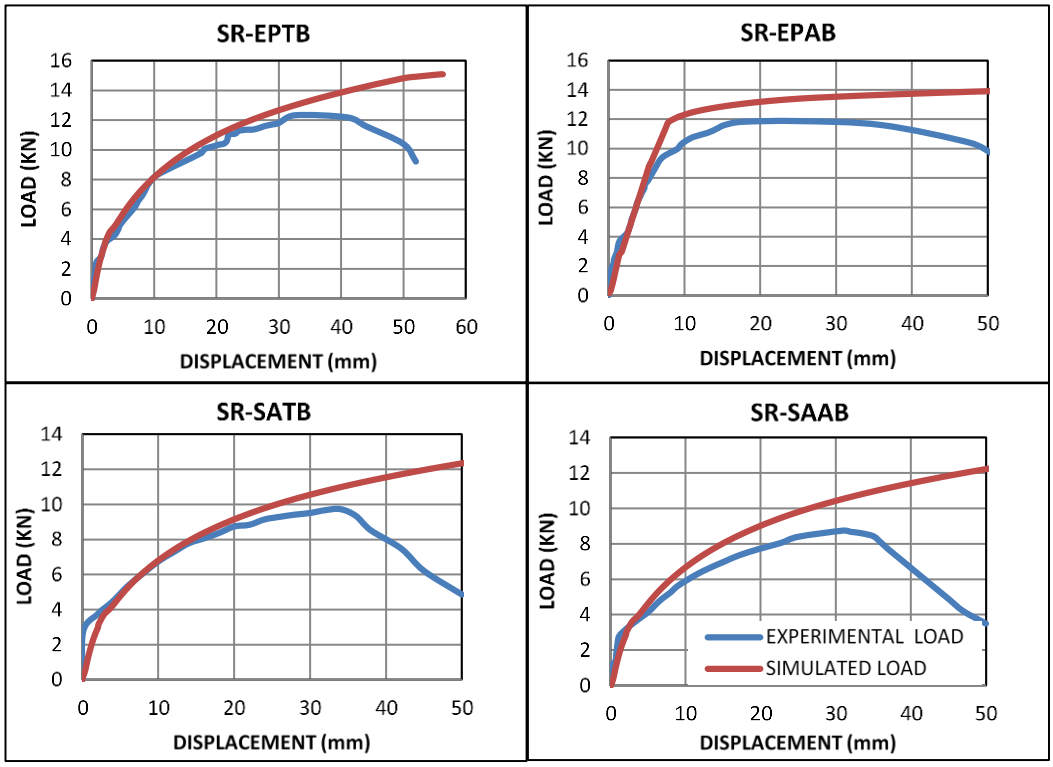

Figure 4.19 Comparison of Simulated and Experimental Load-Displacement Behaviour

4.5.5.2 Comparison of Failure Modes

After calculating and plotting iso-areas of normal stresses in the post-processor phase where darker areas indicate compression and the lighter for tensile stress, the typical comparison between the experimental and simulated failure modes are illustrated in Figure 4.20. Part (a) of Figure 4.20 represents bond slip failure mode of normal anchor bolted end plate connection, part (b) represents yielding of end plate near tension bolts in end plate connections using through bolts where as in part (c) failure mode of seat angle at root of seat angle anchor bolted connection, has been represented. It can be observed from the figures that majority of the specimens has experienced identical failure modes. It can be concluded on the basis of these observations that FE models are capable of depicting closer deformation/ failure behaviour.

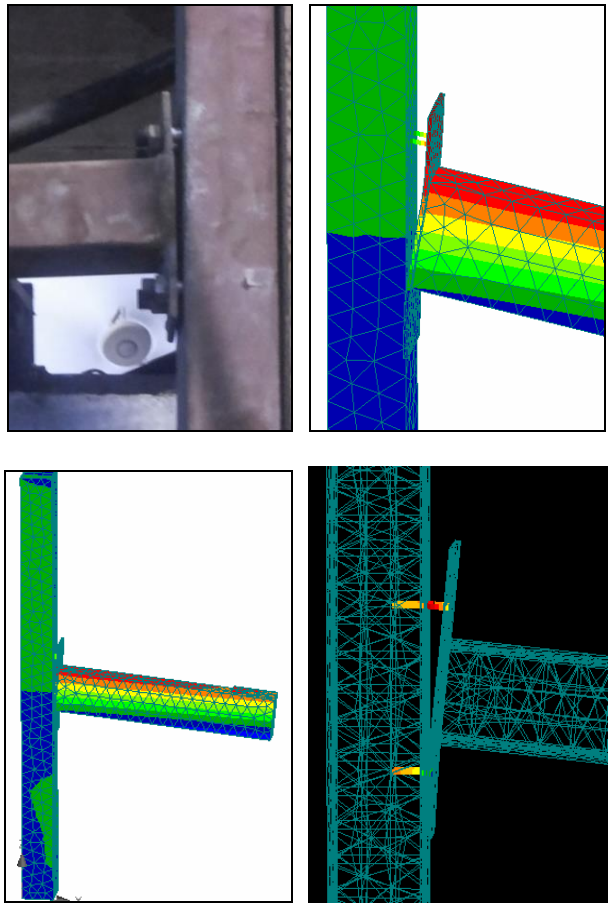

(a) Bond Failure of Tension Bolts in Specimen SS-EPAB-1

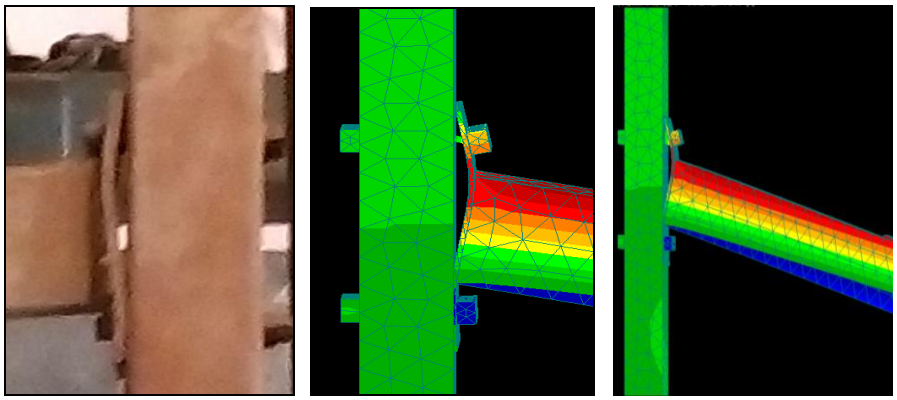

(b) Yielding of End Plate in Specimen SR-EPTB

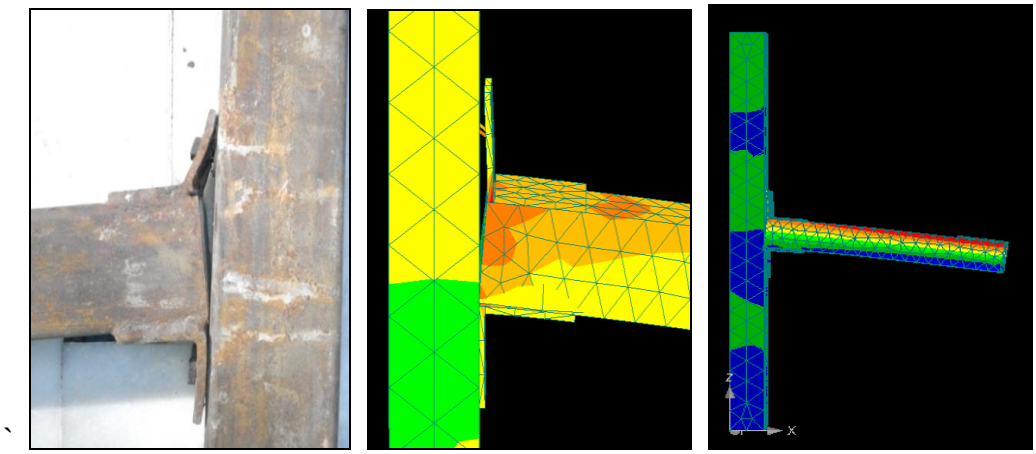

(c) Yielding of Connecting Leg of Seat Angle in Specimen SS-SAAB-1

Figure 4.20 Comparison of Simulated and Experimental Failure Modes

4.6 MOMENT- ROTATION RELATIONSHIPS

The behavior of beam-to-column connections is characteristically represented by M–θ_r curves that depict the relationship between the bending moment (M) and the corresponding rotational rotation (θ_r) of the connection. The bending moment of the connection corresponds to the acting load P, multiplied by the distance between the load application line and the beam end connected to the end plate. The connection rotation(θ_r) is defined as the change in angle between the center lines of the beam and the column. It has been calculated with the help of displacement measured at the tip of beam. The connection rotations corresponding to the connection moments are used to

make the moment–rotation curves for the connections shown in Figure 4.21 and Figure 4.22. For the extended end plate connections, the end plate has shown significant bending deformation and the maximum deformation of the end plate out of the column face is situated in the beam tensile area.

Table 4.3 Summary of Measured Test Results

Sr. No.	Specimen Label	P_u (kN)	Δ (mm)	M_u(kN-m)	θr,u (rad)	m	θ
1.	SS-EPTB	11.90	52.1	5.36	0.104	0.76	4.34
2.	SS-EPAB-1	10.53	47	4.74	0.094	0.67	3.92
3.	SS-EPAB-2	8.37	32	3.77	0.064	0.61	2.67
4.	SS-SATB	9.936	47.5	4.47	0.095	0.73	3.96
5.	SS-SAAB-1	8.91	34.63	4.01	0.069	0.65	2.89
6.	SS-SAAB-2	8.1	42	3.65	0.084	0.59	3.50
7.	SR-EPTB	12.32	32.6	5.54	0.065	0.79	3.62
8.	SR-EPAB	11.88	20.8	5.35	0.042	0.76	2.31
9.	SR-SATB	9.73	34	4.38	0.068	0.62	3.78
10.	SR-SAAB	8.75	31	3.94	0.062	0.56	3.44

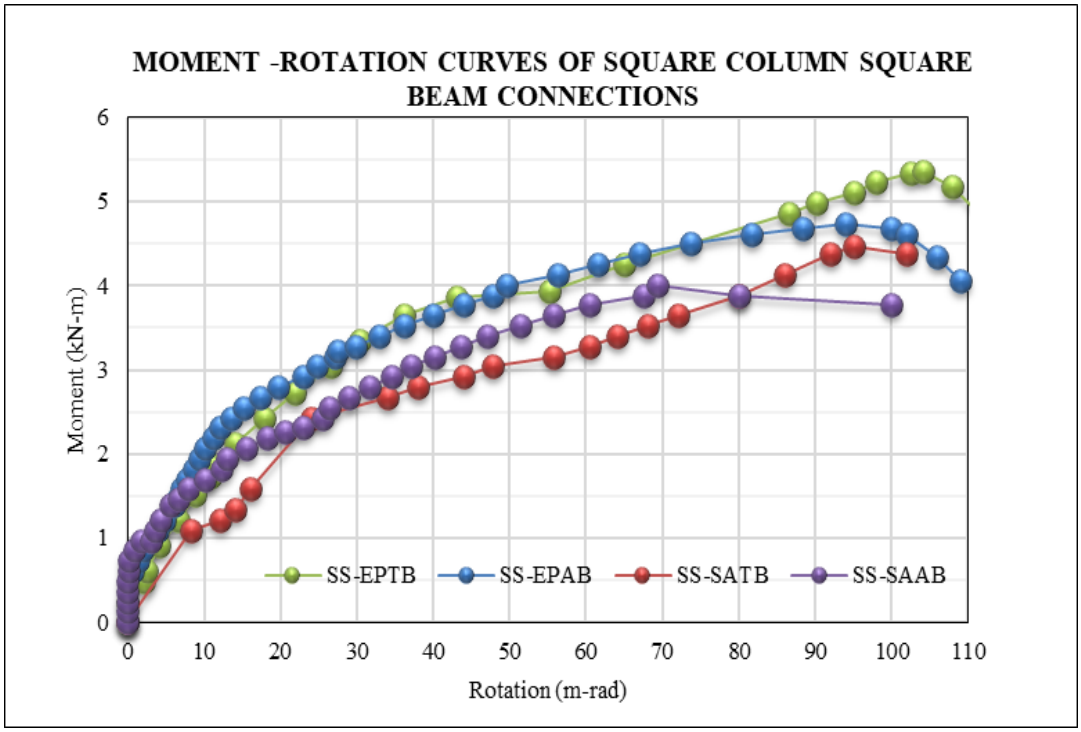

Figure 4.21 Moment–Rotation Relationship of Various Connections (Square Column to Square Beam)

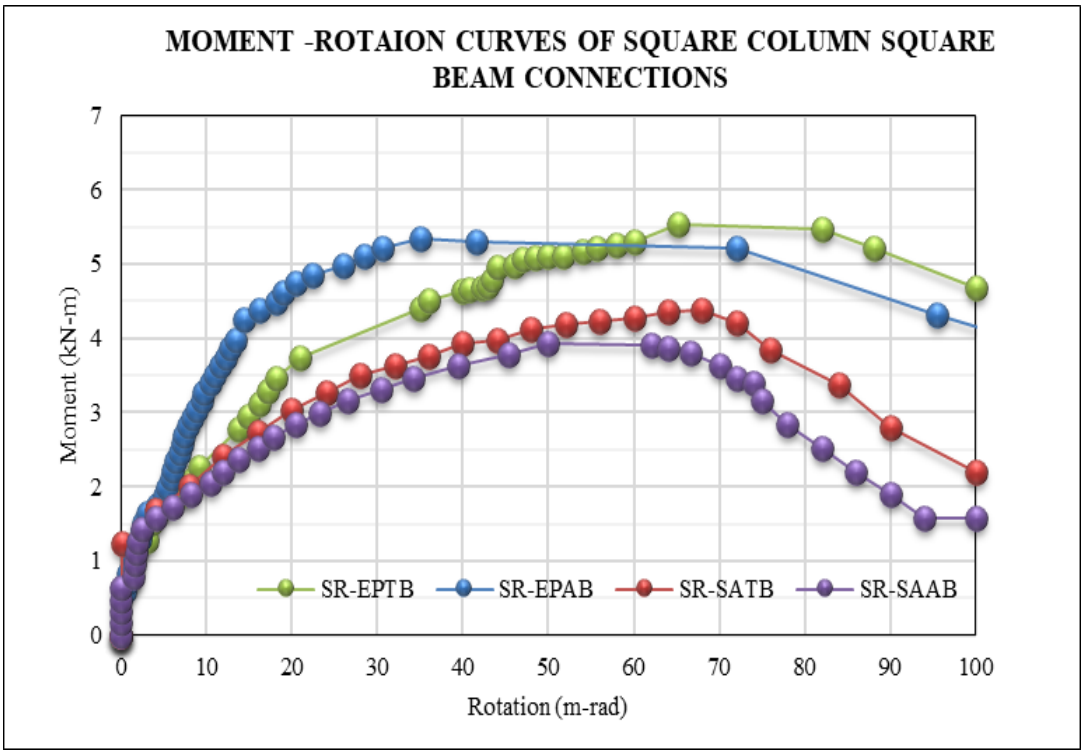

Figure 4.22 Moment–Rotation Relationship of Various Connections (Square Column to Rectangular Beam)

4.7 EVALUATION OF CONNECTION CLASSIFICATION

One of the objectives of the study is to get the classification of the joints as per EC-3. Hence, the classification of connections has been made using the approach given in EC3 Part 1-8 as given under:

Classification by rigidity

A connection can be classified as rigid, nominally pinned, or semi-rigid according to its rotational stiffness by comparing its initial stiffness with classification boundaries suggested in EC3 as

- rigid, if $S_{j,\ ini} = k_b\ EI_b/L_b$; where $k_b=8$ for non-sway frames and $k_b=25$ for sway frames.
- nominally pinned, if $S_{j,\ ini} \leq, 0.5\ EI_b / L_b$; otherwise, it is semi-rigid.

$S_{j,\ ini}$ is the initial stiffness of connection. EI_b is the flexural stiffness for the beam and L_b is the beam span.

Classification by strength

A connection can be classified as full-strength, nominally pinned, or of partial strength in terms of strength by comparing its moment resistance with the plastic moment resistance of the beam.

- full strength, if $M_u \geq M_{bp}$;
- nominally pinned, if $M_{ur} \leq 0.25\ M_{bp}$; otherwise, it is partial strength.

M_{bp} is the design plastic moment resistance of the beam is calculated as per EC4.

M_{bp} is calculated as per EC4:

$$M_{plrd} = m_{sq} \frac{h^2 b - (h - 2t)^2 (b - 2t)}{4} f_y \qquad (4.1)$$

Herein M_{plrd} is plastic moment of beam; m_{sq} is a correction coefficient for different ratios of h/b and grades of concrete.

According to the approach discussed above, the classification of connections has been done from strength criterion and the analysis results for connections of sway

frames are illustrated in Figure 4.23 and Figure 4.24. Here in to, horizontal ordinate θ, and vertical ordinate m, respectively indicate dimensionless connection rotation and moment.

$$m=\frac{M\,u}{Mbp} \tag{4.2}$$

$$\theta=\frac{\theta r}{Mbp}\cdot\frac{EIb}{Lb} \tag{4.3}$$

Herein, θ_r is rotational angle corresponding to load and θ_{ru} (in Table 4.3) is rotational angle corresponding to ultimate load. It is observed from Figure 4.23 and Figure 4.24 that the majority of bolted end plate connections in the specimens may be classified as semi-rigid and partial strength as per the EC3 specification and display good stiffness and strength. It is also found that the rotation capacities of all specimens satisfy the ductility requirement of not being less than 30 mrad for earthquake resistance, suggested by FEMA-350.

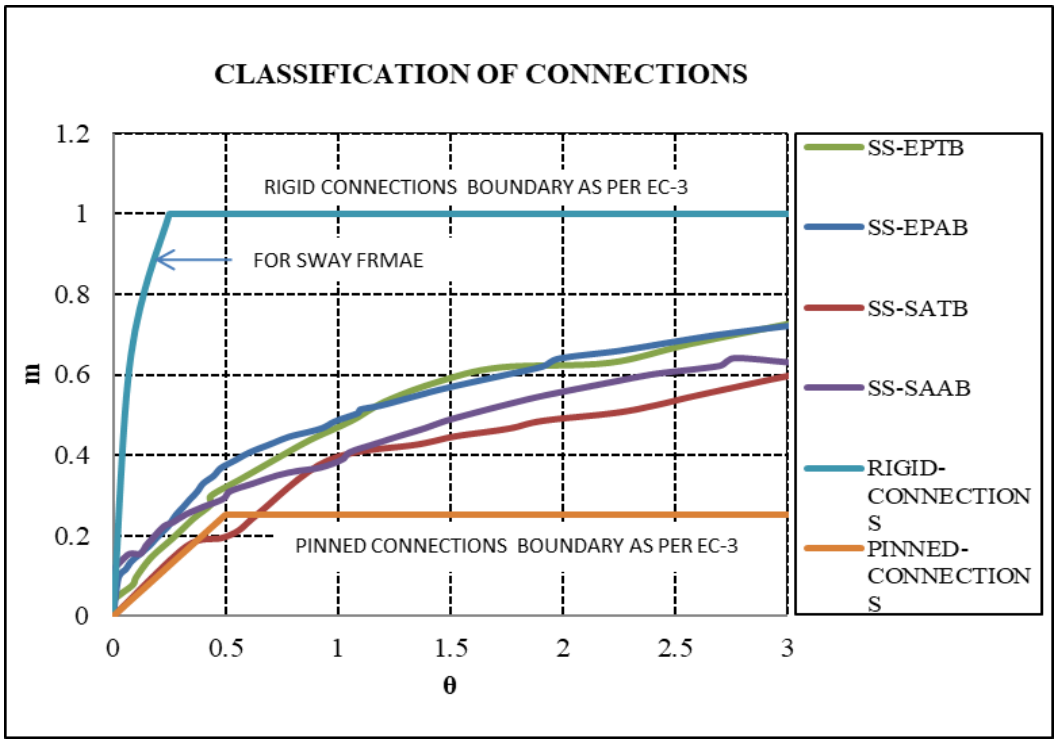

Figure 4.23 Classification of Tested Connections (Square Column to Square Beam)

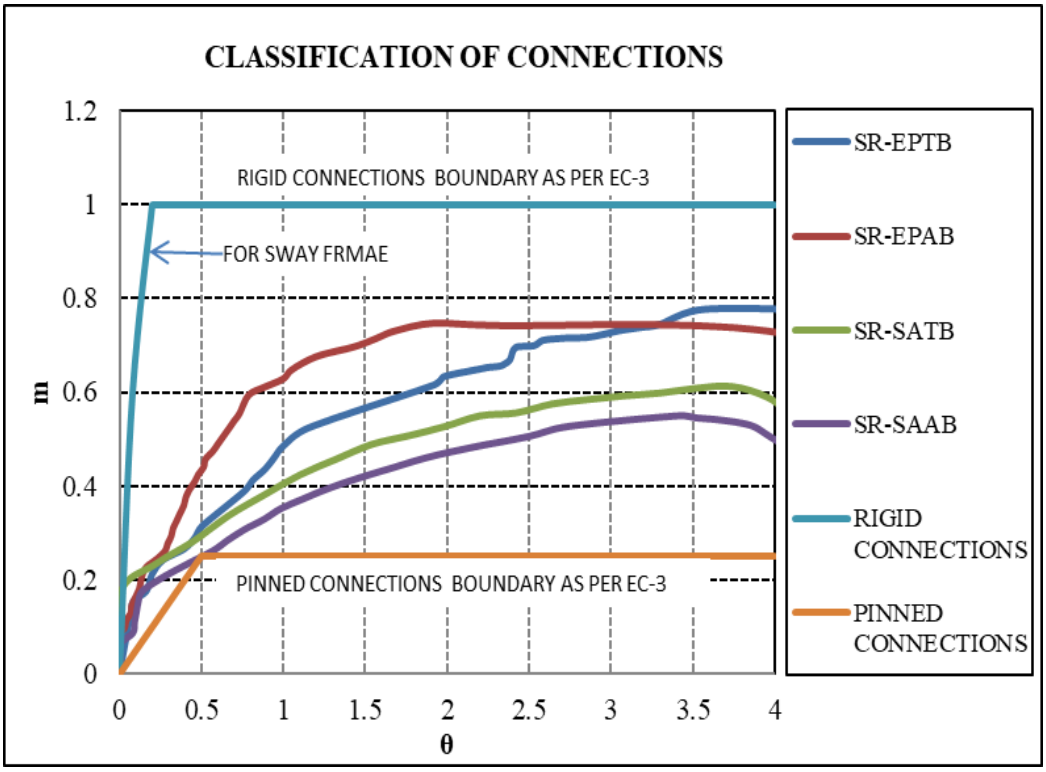

Figure 4.24 Classification of Tested Connections (Square Column to Rectangular Beam)

4.8 CLOSURE

In the present work, behaviour of CFST beam-column joints have been investigated experimentally as well as numerically. Based on the investigation, the following observations have been drawn:

i. The connections with extended end plate using through bolts have shown higher strength over seat angle through bolted connections. Specimen SS-EPTB has shown 19.76 % higher strength over SS-SATB and Specimen SR-EPTB has shown 26.6 % higher strength over SR-SATB.

ii. The connections with through bolts have exhibited better strength over connections with bolts of normal length. Specimen SS-EPTB has shown 13.3 % higher strength over SS-EPAB-1 and Specimen SS-SATB has shown 11.51 % higher strength over SS-SAAB-1. Similarly, specimen SR-EPTB has shown 4.14% higher strength than

SR-EPAB and SR-SATB has exhibited 11.2 % higher strength than specimen SR-SAAB.

iii. Connections of rectangular beams of same cross section area as used in case of square beams with square columns using end plates, exhibited slightly (3.5%-12.5%) higher strength.

iv. Specimen SS-EPAB-1 and SS-SAAB-1 with 10mm dia bolts has shown 25.7% and 10% higher strength over SS-EPAB-2 and SS-SAAB-2 using 8mm dia bolts respectively.

v. It is observed that variation in size of end plate, dia and grade of bolts and bond strength of the matrix significantly affected the capacity of the joints.

vi. The experimental results show that the proposed bolted connections behave as connections with partial strength as per the EC3 specification and display good stiffness and strength.

vii. The proposed FE model is capable to predict the behaviour of connections closely.

viii. The stiffness and strength of connections is enhanced with the increase in size of plate. It is expected that the strength of the bolted connections may be affected with change in various parameters such as thickness of end plate, the anchorage length of the bolt and cross-section of steel tube.

CHAPTER 5

NON-LINEAR INVESTIGATIONS OF CFST FRAME

5.1 GENERAL

As discussed in previous chapters, concrete filled steel tubes offer numerous advantages for seismic resistant design as they provide large axial stiffness and load capacity. Though there has been extensive research into the behaviour of steel frames, composite frames have received less attention [Liew and Uy (2001)]. Little research has been done to investigate the behaviour on the CFST frames [Han et al. (2008)]. Few of the studies available in the literature [Matsui (1995); Kawaguchi et al. (1997); Tsai et al. (2003) and Han et al. (2008)] concluded that CFST frames showed excellent load carrying capacity under horizontal loads. But the available experimental and numerical studies [Liew et al. (2001); Herrera (2005); Han et al. (2008) and Zhao (2016)] are for the analysis of CFST composite frames in which CFST columns and steel beams are part the frame, no study is available in literature where CFST members are used as both beam and columns as part of CFST composite frame. It is also a well-known fact that beam-column joints are vital part of any structure but the constituent members behave differently as part of a frame. Hence, the present study aims to explore the mechanical behaviour of the CFST composite frames with CFST beams and columns.

It is highly expensive and time consuming to conduct tests to study the effects of every parameter on the behavior of CFST frames. Additionally, the dimensions of the frame are usually large, hence it is impractical to experimentally investigate the effects of every parameter on the behaviour of CFST frames under various loading conditions. In such cases, verified nonlinear inelastic analysis techniques may be the cost-effective methods for determination of the behavior of CFST frames. Little success has been achieved so far in developing an accurate model of CFST frames due to the complexity in modeling the confinement effect for concrete-filled steel tubular members and various interfaces. So, set against the background, this study has been taken to

determine the behaviour of CFST frame with concrete-filled Square Hollow Section (SHS) steel tubular columns and beams using end plate type connections using FE modelling.

This section describes an approach of simplified macro-modelling for composite frames consisting of steel-concrete composite beams and CFST columns and presents the load-displacement behaviour based on the nonlinear analysis results. The main objective of this study is to develop an accurate finite element model to simulate the behaviour of the composite frames with concrete-filled square hollow section (SHS) steel tubular columns and CFST beams. In the study, various types of frames (2-D and 3-D) have been considered. A single & two- storey 2D frame and two- storey 3-D composite frames using end plate type beam-column connections, have been selected as for study. The finite element program ATENA has been used in the analysis. The effects of concrete confinement and the interface between concrete and the steel tube are considered in the analysis. The establishment of the macro-model of the composite frame is directed by the characterization of nonlinear behaviors of composite structural members. FE analysis is conducted to obtain the lateral force versus top displacement curve of the overall frame. The FEA predicted results indicate that the suitability of the FEA model to predict the P–Δ relations of CFST column frames.

5.2 DESCRIPTION OF CFST FRAMES

5.2.1 Selection of Beam-Column Connections

Connections being the most vulnerable components in composite structures, are the main parameter of the study. During the Northridge and Kobe earthquakes, observations on damaged connections in steel frames indicate that Bolted angle connections with top and seat angles as well as web cleats develop brittle fractures [(Bruneau and Bisson (1998)]. Therefore, semi-rigid connections are advantageous to provide some degree of flexibility in the connections. Extended end plate connections to rigid column stubs using bolts provides fairly good behaviour and fall under semi-rigid category of connections (Wang and Guo 2012). It has been observed from the results of experimental and numerical investigations carried for mainly two types of connections

(section 4.5 of Chapter 4) that connections with end plate have been proved better than their counterparts with seat angle. Hence, CFST frames with beam-column joints using extended end-plate are selected for analysis of 2D and 3-D frame with different number of storey. CFST frames with beam-column joints using HSFG through bolts (EPTB connections) and normal length bolts (EPAB connections) have been considered to study the effect of anchorage length. Each joint arrangement has been detailed to maintain the minimum use of welded joints in critical regions of the connection.

5.2.2. Details of Frames Considered

Design details, loading and boundary conditions of single storey CFST frame model are presented in Figure 5.1. Schematic view and various design details of double Storey CFST frame model are presented in Figure 5.2. The beam and column configuration and connection details are also shown in the figures. The column height and the beam span are kept 1500 mm and 2000 mm, respectively. Square steel hollow sections of size 72 mm x 72 mm x 3.2 mm of Grade Yst-240 conforming IS 4923, has been considered for the frame as the same sections has been used in the study of beam-column connections in chapter 4.

The frame models have been designed in accordance with the concept of strong-column/weak-beam, so beam failure mode is expected to occur. For that the beam to column linear stiffness ratio is taken as 0.75. The beam to column linear stiffness ratio is defined as $k=I_b/I_c$, where I_b and I_c are the linear stiffness of CFST beam and CFST column, respectively. The stiffness of rectangular CFST beam is defined as $(EI_b)/L_b$, where L is the length of beam. The stiffness of rectangular CFST beam (EI) is $E_sI_s+0.6E_cI_c$ (Han et al. 2011) where E_s and E_c are modulus of elasticity of steel and concrete, respectively, and I_s and I_c are moments of inertia for hollow steel cross section and core concrete cross section, respectively. I_c is defined as (EI)/H, where H is the height of column. Concrete of grade M-25 is considered as infill concrete.

Extended end plate bolted connections have been used for connecting beam column joints of CFST frame as these connections have exhibited better performance over seat angle connections (refer section 4.5.2, 4.5.3, and 4.5.4 and section 4.6). High strength bolts (conforming IS:1364-2003) of the Grade 8.8, M10 having ultimate strength and yield strength of 800 N/mm^2 and 640 N/mm^2, respectively, have been used (detailed properties of materials are discussed in Section 4.3.2 of chapter 4).

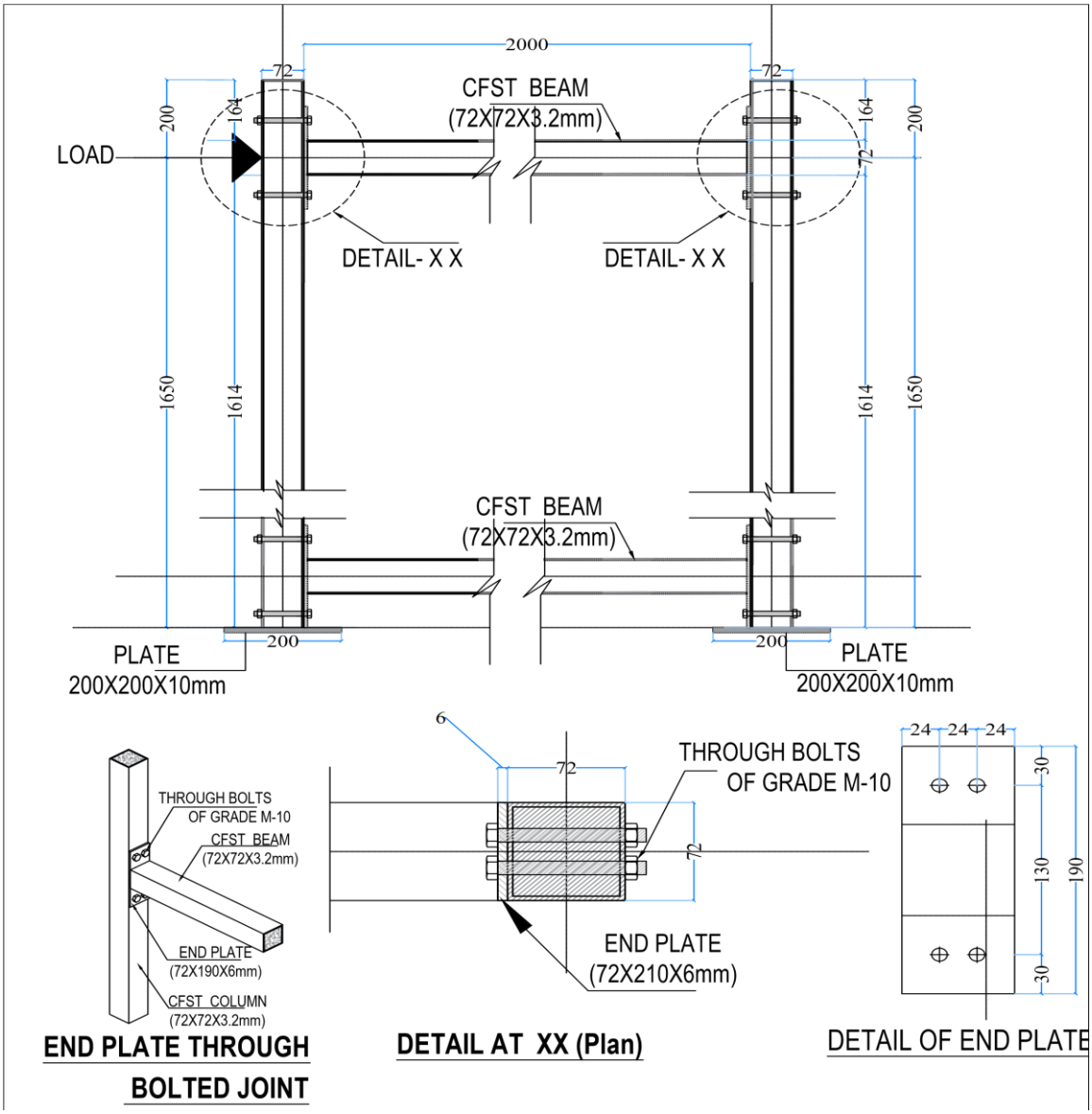

Figure 5.1 Schematic View of CFST Frame Model

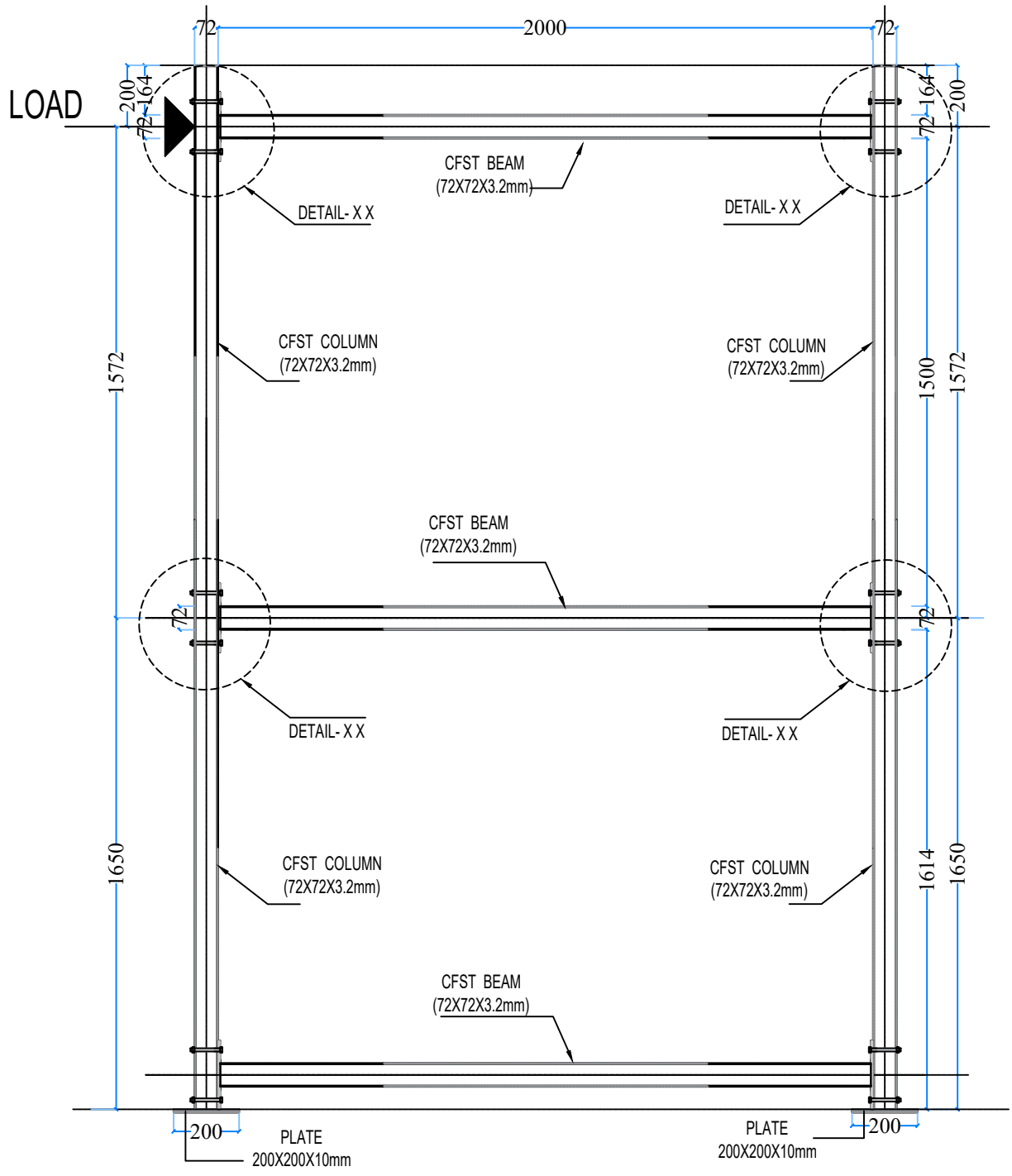

(a) Sectional Elevation of Frame

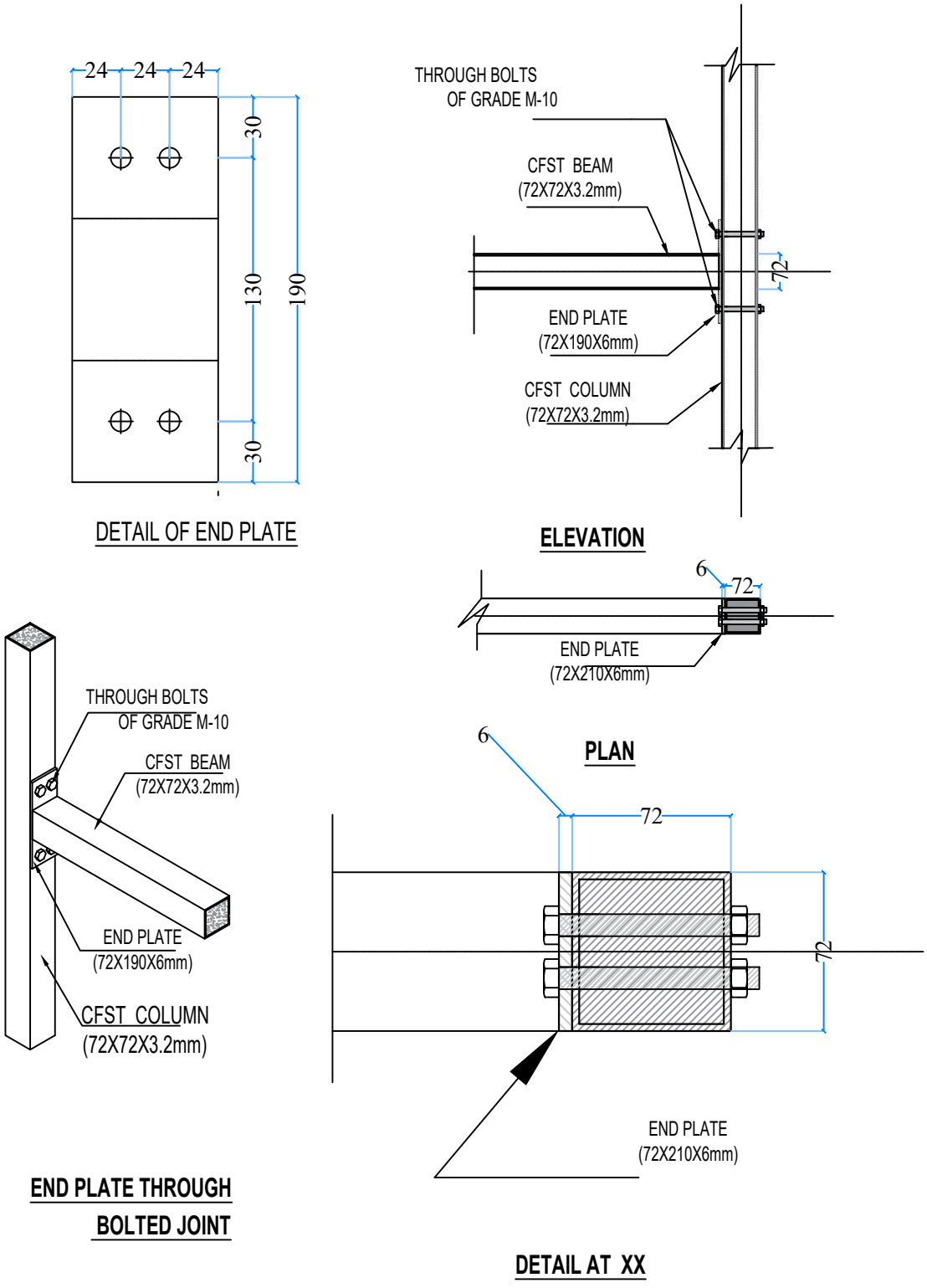

(b) Details of Connection used

Figure 5.2 Schematic View of Double Storey CFST Frame Model

5.3 NON-LINEAR FINITE ELEMENT MODEL OF CFST FRAMES

In order to accurately simulate the actual behaviour of frames with concrete-filled steel tube (CFST) square columns to concrete-filled steel tube (CFST) beam, the main five components of the frames need to be modeled. These components are the confined concrete of square columns, the interface and contact between the concrete and the steel tube, the steel tube, the connection details between columns to steel beam, and the CFST beam which further have sub-components like end plate/seat angle and bolts. In addition to these parameters, the choice of the element type, mesh size, boundary conditions and load applications that provide accurate and reasonable results are also important in simulating the behaviour of structural frames.

5.3.1 Material Modeling

Material modelling of has been discussed in detail in section 3.3 of Chapter 3 and in section 4.4 of Chapter 4. Each and every aspect of FE modelling of various materials used in CFST column and CFST joints has been discussed.

Concrete: 8-nodded brick element is considered for the modelling of concrete. (for detailed modelling refer Section 4.4.1 of Chapter 4).

Steel: Steel tubes are modeled as Von-Mies yield model. (refer Section 4.4.2 of Chapter 4)

Bolts: Bolts have been modelled as bar element in which properties of steel with hardening have been considered. (refer Section 4.4.3 of Chapter 4)

Interface modelling: Detailed modelling of interface between various interfaces have been discussed in Section 4.4.4 of Chapter 4.

Finite element type and mesh: Different element types have been tried in order to find a suitable element to simulate the behaviour of frames. Solid elements have been found to be more efficient in modeling the concrete as well steel, and steel tubes can be modeled with shell elements also. A fine mesh of three-dimensional eight-node linear brick for concrete and brick and tetra for steel tubes, is used. A typical joint, which consists of a concrete-filled steel tubular (CFST) column, a concrete-filled steel tubular (CFST) beam using extended end plate bolted connection, shown in Figure 5.1 and

Figure 5.2, is used in the analysis. These kinds of joints have been widely used in CFST frames (CFST columns and steel beams composite frames).

Boundary conditions and load application: The bottom surfaces of the concrete-filled steel tube columns have been fixed with a steel plate which has been further fixed against all degrees-of-freedom. The top of CFST columns subjected to an increasing horizontal load. The loads of CFST frame has been applied in the form of displacement under different increment steps option available in the ATENA library. The axial force is transferred to the composite column by an elastic rigid plate. The load step and displacement step are solved using static and general arithmetic with geometrical and material nonlinear methods available in the ATENA library.

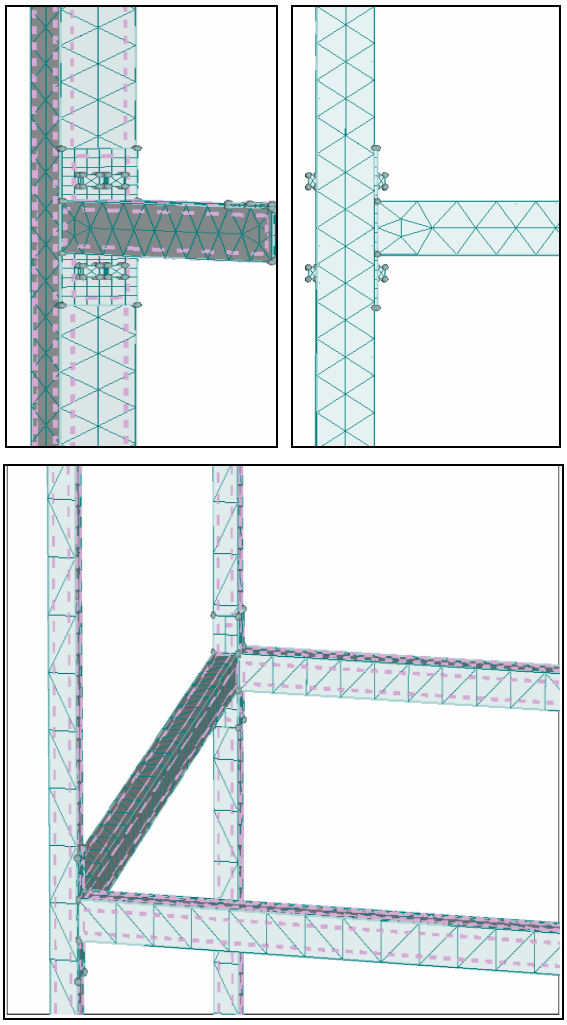

Figure 5.3 FE Modeling of Connections in CFST Frames

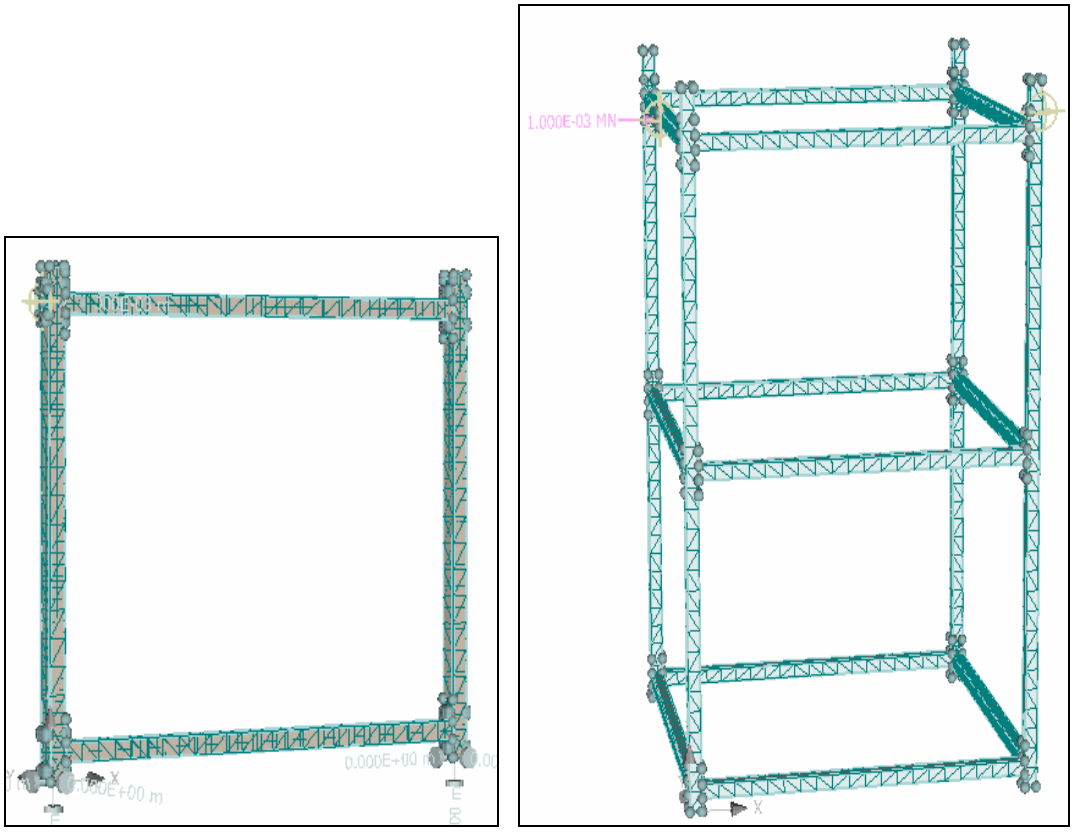

Single Storey CFST Frame **Two storey CFST Frame**

Figure 5.4 FE Modeling of CFST Frames

5.4 RESULTS AND DISCUSSIONS

This segment presents the results of Finite Element analysis of CFST frames. Finite element analysis of CFST frame under the static incremental loads, performed using ATENA software. The load deflection curves and the failure behaviour obtained from the analysis are presented.

5.4.1 FE Analysis Results of Single Storey 2-D CFST Frame

In the present study, non-linear response of CFST frame using end plate type beam-column connections with through bolts (EPTB connections) and normal length bolts (EPAB connections) have been modelled (as per details discussed in section 5.2.1 General Description of Structure) using FE Modelling under the incremental loading has been carried out. The objective of this study is to see the variation of load-

displacement graph and the failure modes at different values of the base shear. The effect of bolt length has also been considered. The load on the structure has been gradually increased in the steps till failure. When the FE non-linear analysis is completed, the results are shown in Post processer. The load-deflection values at every step have been recorded and further the failure pattern at every step has been studied.

5.4.1.1 Load V/s Deformation

Frame with EPTB connections: FE results obtained in the form of load-deflection curve at the top floor level of the frame has been plotted in Figure 5.5. It can be seen from that the structure behaved linearly elastic up to the value of base shear around 42 kN and displacement of 38 mm. After this point, there is a slight curvature in the plot and deflection started increasing with the load increments. After this point, the graph depicted non-linearity in its behaviour. At ultimate load value of 139.1 kN deflection has been observed to be 605 mm and a rapid increase in displacement is observed. After this point, there is constant increase in deflections and plot has become almost flat. Subsequently deflection started increasing and load started decreasing; it has reached to the value of 785 mm with the base-shear value 121 kN. It has been observed that after start of yielding load increased almost three times before attaining maximum value. The frame also showed significant post yield ductility.

Frame with EPAB connections: Initially the frame behaved linearly elastic up to the value of base shear around 52 kN and displacement of 64 mm. After this point, the graph showed non-linearity in its behaviour. At ultimate load value of 118 kN deflection has been observed to be 820 mm and increase in displacement is observed. After this point, there is constant increase in deflections and decrease in load has been noticed. Deflection curve at the top floor level of both the frames have been plotted in Figure 5.5.

5.4.1.2. Failure Modes

After calculating and plotting iso-areas of normal stresses in the post-processor phase where darker areas indicate compression and the lighter for tensile stress, the failure modes of simulated results are presented in Figure 5.6, 5.7 and 5.8. Figure 5.6 depicts displacements occurred in the frame. It can be observed from the figure that larger displacements have been experienced by the top members of the frame.

Maximum micro cracks have occurred at the base of columns on tension side, where yielding of tube seems to happen. Maximum size of crack is 0.6 mm (Figure 5.7). Figure 5.8 represents bond slip failure mode of bolted end plate connection on tension side of joint. No failure in members has been observed.

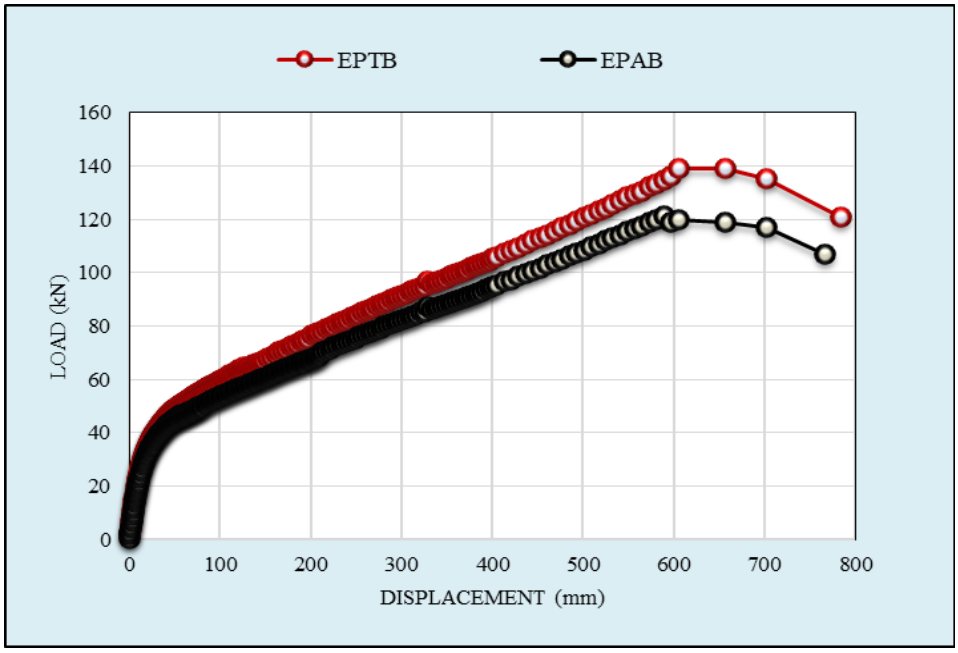

Figure 5.5 Load-Displacement Curves for 2D Single Storey CFST Frames

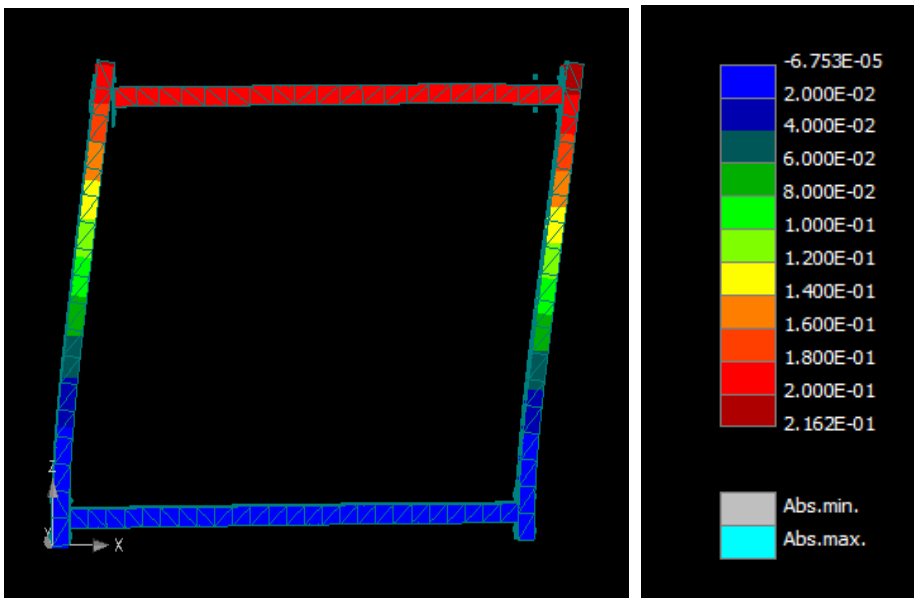

Figure 5.6 Displacements of Frame (values given in meters)

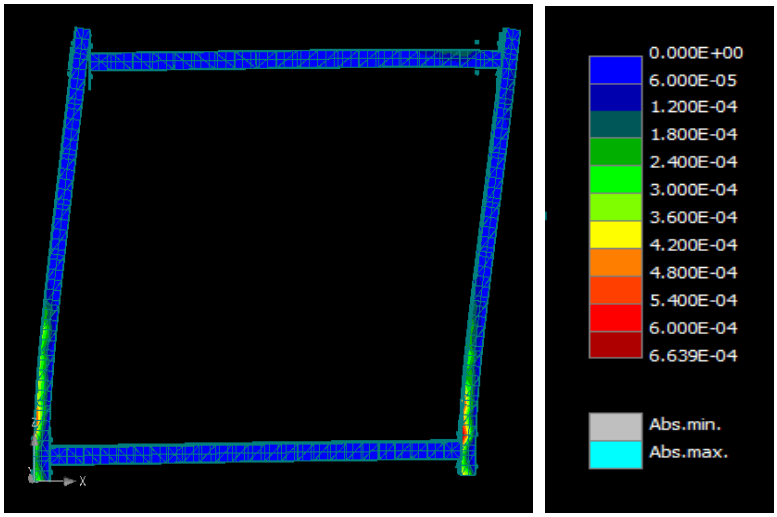

Figure 5.7 Crack Widths Obtained (values are given in meters)

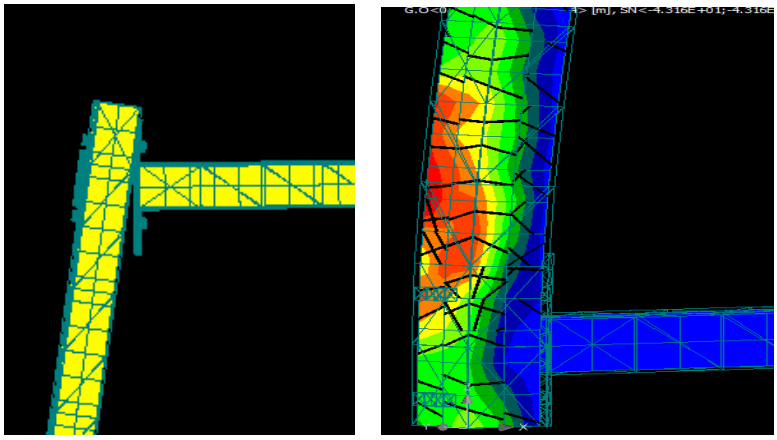

Figure 5.8 Failure Modes at Top and Bottom (Left Side) of Frame

5.4.1.3. Effect of Anchorage Length of Bolts on Behavior of CFST Frames

The CFST frame with extended end plate connections using through bolts have shown higher strength over connections with normal length anchor bolts. The frame with EPTB type connections has shown 17.5 % higher strength. The connections with through bolts have performed better in terms of stiffness over frame having connections with bolts of normal length. Failure occurred at lower part of end plates in both the frames. Initially both the frames behaved almost in similar manner. At a load value of 78 kN both the frames experienced displacement of 215 mm. After this point frame with EPAB type connections, started getting more displacements than the former frame. Both the frames experienced bond failure of bolts at lower part of end plates.

It can be concluded that frame with through bolted end plate connections performed better as it has been observed in case of testing of individual EPTB type connections under vertical monotonically increasing loads at beam tip. It can be projected that variation in size of end plate, dia and grade of bolts significantly affect the capacity of such frames.

5.4.2 FE Analysis Results of Two Storey 2-D CFST Frame

5.4.2.1 Load V/s Deformation

Deflections at the top floor level of both the frames are plotted in Figure 5.9.

Frame with EPTB connections: It can be seen from the graph that the frame behaved linearly elastic up to the value of 28 kN and displacement of 50 mm. After this point, there is a slight curvature in the plot and deflection started increasing with the load increments. After this point, the graph depicted non-linearity in its behaviour. At a load value of 52 kN deflection has been observed to be 530 mm. After this point, further increase in load has been observed depicting strain hardening. At ultimate load value of 94 kN deflection has been observed to be 1430 mm. After this point, there is constant increase in deflections and plot has become almost flat. Subsequently deflection started increasing and load started decreasing. It has been observed that after start of yielding load increased almost three times before attaining maximum value. The frame also showed significant post yield ductility.

Frame with EPAB connections: The frame behaved almost identical to the frame with EPTB connections but at lower load values. The frame behaved linearly elastic up to the value of 23 kN and displacement of 45 mm. After this point, there is a slight curvature in the plot and deflection started increasing with the load increments. After this point, the graph depicted non-linearity in its behaviour. At a load value of 46 kN deflection has been observed to be 550 mm. After this point, further increase in load has been observed representing strain hardening. At ultimate load value of 81 kN deflection has been observed to be 1463 mm. After this point, there is constant increase in deflections and plot has become almost flat. Subsequently deflection started increasing and load started decreasing. It has been observed that after start of yielding load increased almost

three times before attaining maximum value. The frame also showed significant post yield ductility.

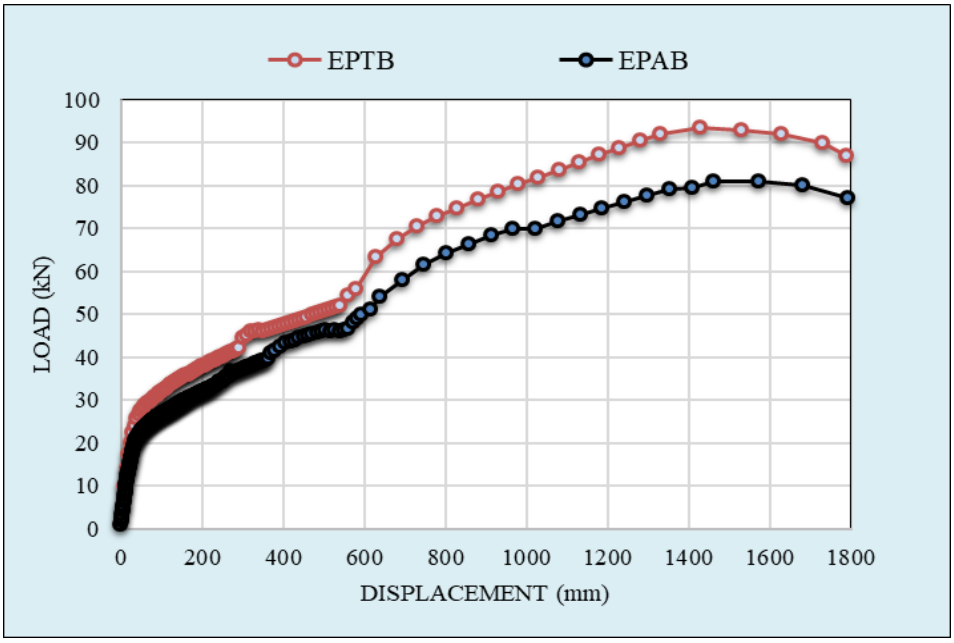

Figure 5.9 Load-Displacement Curves for Two Storey CFST Frame with EPTB Connections and EPAB Connections

5.4.2.2 Failure Modes

After calculating and plotting iso-areas of normal stresses in the post-processor phase where darker areas indicate compression and the lighter for tensile stress, the failure modes of simulated results are presented in Figure 5.10, 5.11 and 5.12. Figure 5.12 represents bond slip failure mode of bolted end plate connection.

5.4.2.3 Effect of Type of Connections on Behavior of CFST Frames

The CFST frame with extended end plate connections using through bolts have shown higher strength over connections with normal length anchor bolts. The frame with EPTB type connections has shown 16.05 % higher strength. The connections with through bolts have performed better in terms of stiffness over frame having connections with bolts of normal length. Failure occurred at lower part of end plates in both the frames. Initially both the frames behaved almost in similar manner. At a load value of 21 kN both the frames experienced displacement of 37mm. After this point frame with EPAB type connections,

started getting more displacements than the former frame. Both the frames experienced bond failure of bolts at lower part of end plates. Hence, it can be concluded that frame with through bolted end plate connections performed better similarly as observed when tested as individual EPTB type connection under vertical loads at beam tip.

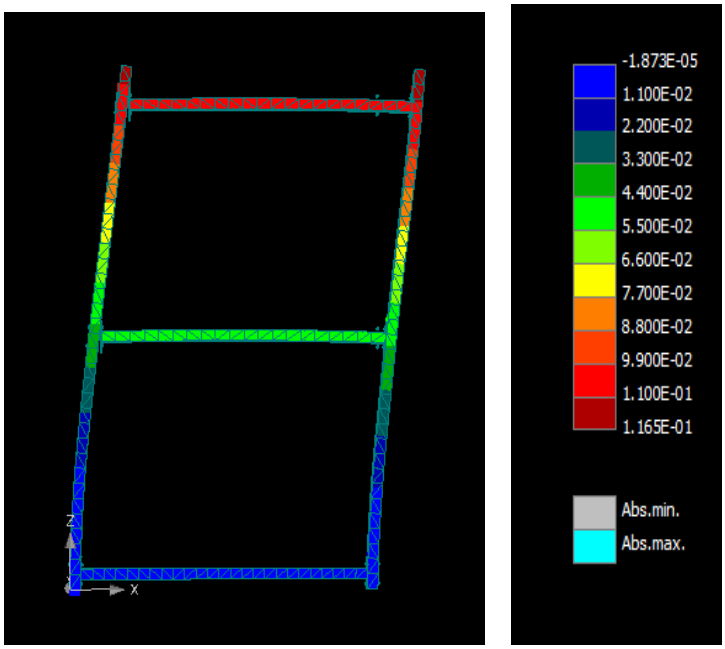

Figure 5.10 Stresses at Various Joints of CFST frame

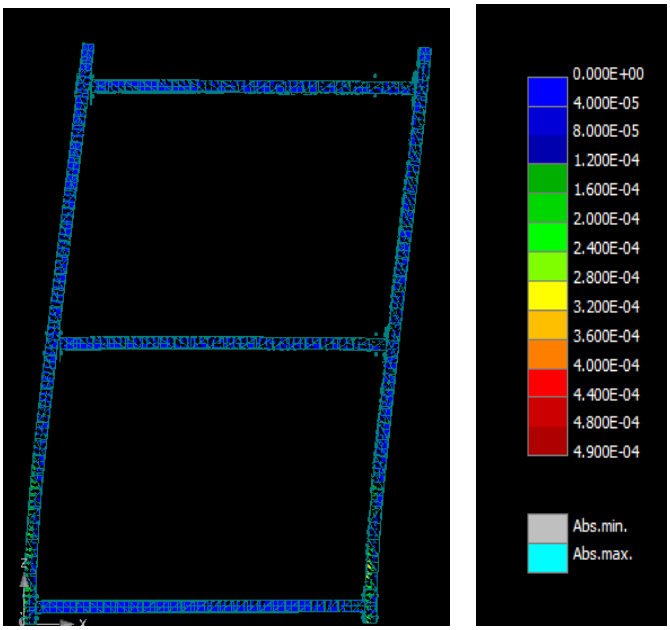

Figure 5.11 Development of Micro-Cracks in Infilled Concrete

(values are given in meters)

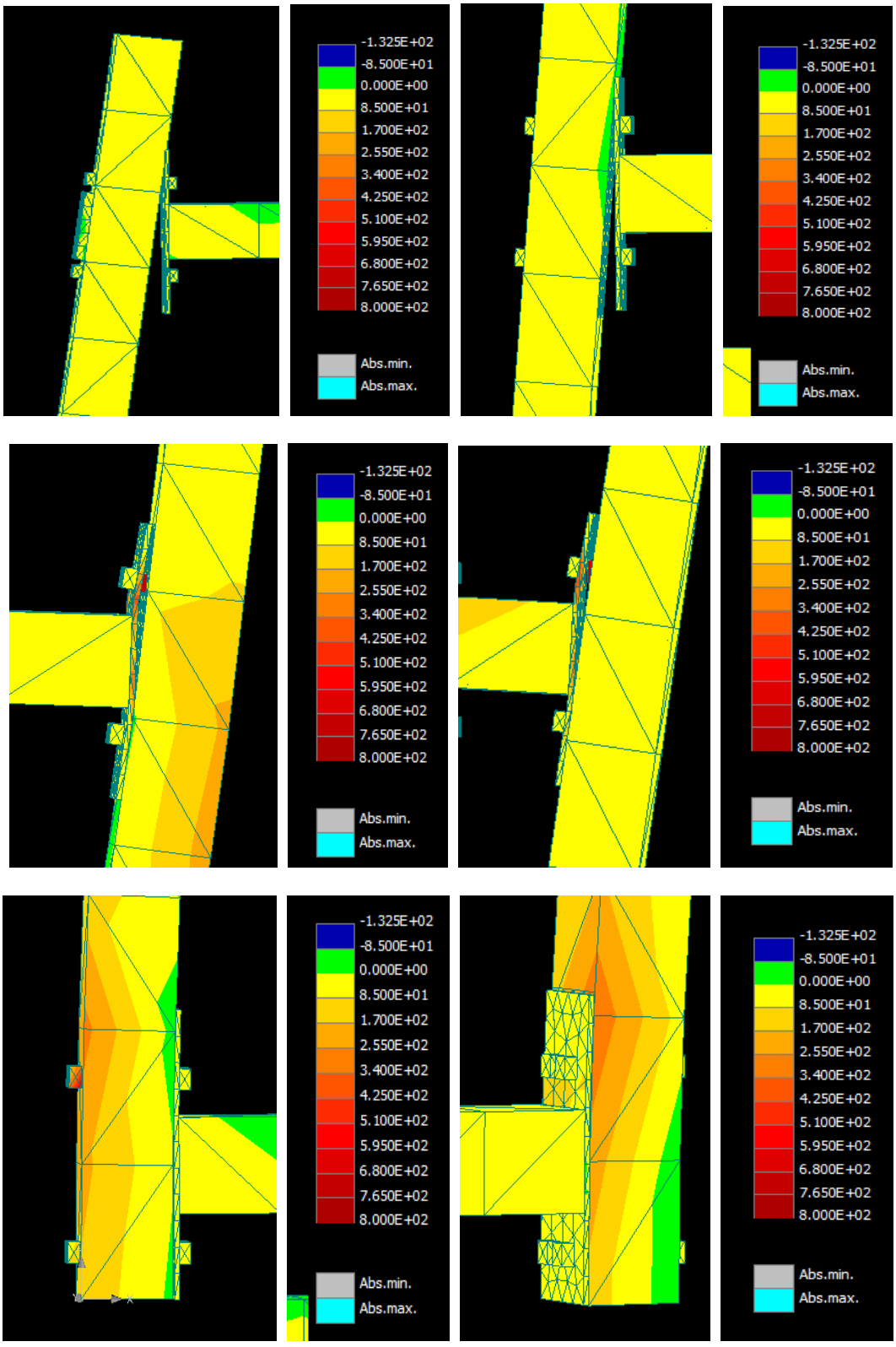

Figure 5.12 Failure Modes at Various Joints of CFST Frame

5.4.3 Two Storey 3-D CFST Frame

Two frames; with EPTB connections and EPAB connections have been analysed and results are discussed in this section.

5.4.3.1 Frame with EPTB connections

Load V/s Deformations: FE modelling of the frame has been depicted through Figure 5.4 and load-deformation curve is presented in Figure 5.13. It can be seen from load-deformation curve that floor level-1 has experienced the minimum deflection even though the damage experienced by this floor is maximum. The variation of load-deflection curve is same as per other floor levels. The maximum deflection as base shear 305 kN has been found to be 1412 mm which increases further, even after without any increase of load.

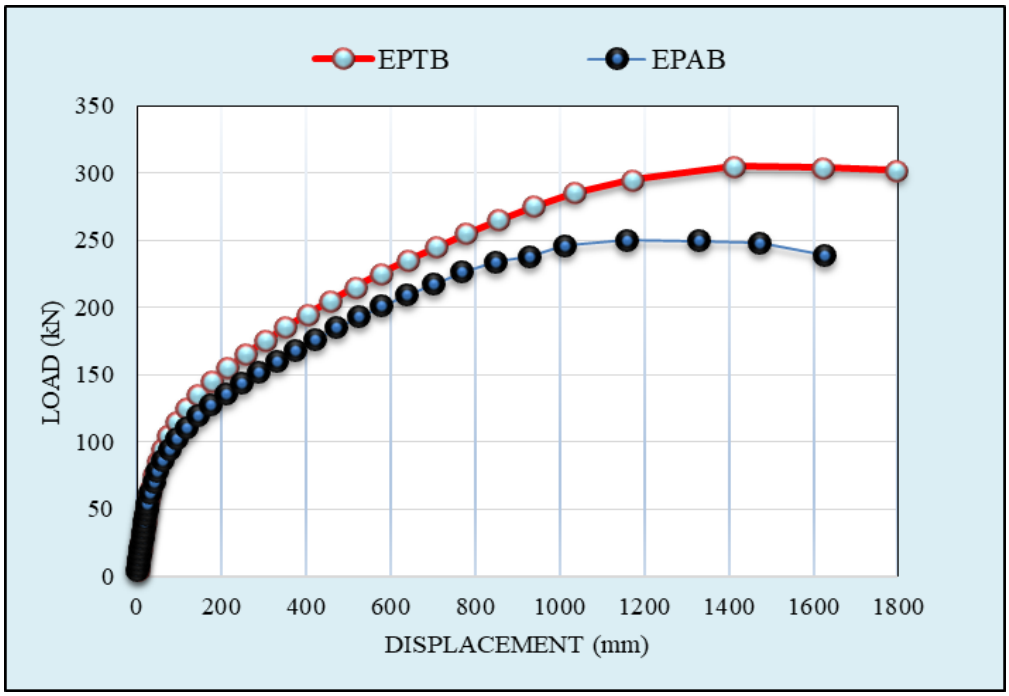

Figure 5.13 Load-Displacement Curves for Two Storey CFST Frame with EPTB and EPAB Connections

Failure Modes: The variation of crack patterns has been taken out from the post processer of ATENA and are plotted in Figure 5.14 to 5.15. The shape of deformed structure has been shown in Figure 5.14. In the deformed shape storey drift in the direction of loading at upper levels is evident. Maximum stresses have been observed by the elements at the top level. Figure 5.15 and Figure 5.16 show the deformations experienced and location of areas with deformations in steel tube. Similar patterns of deformations are observed at the base of columns on the loading side as observed in 2-D frames

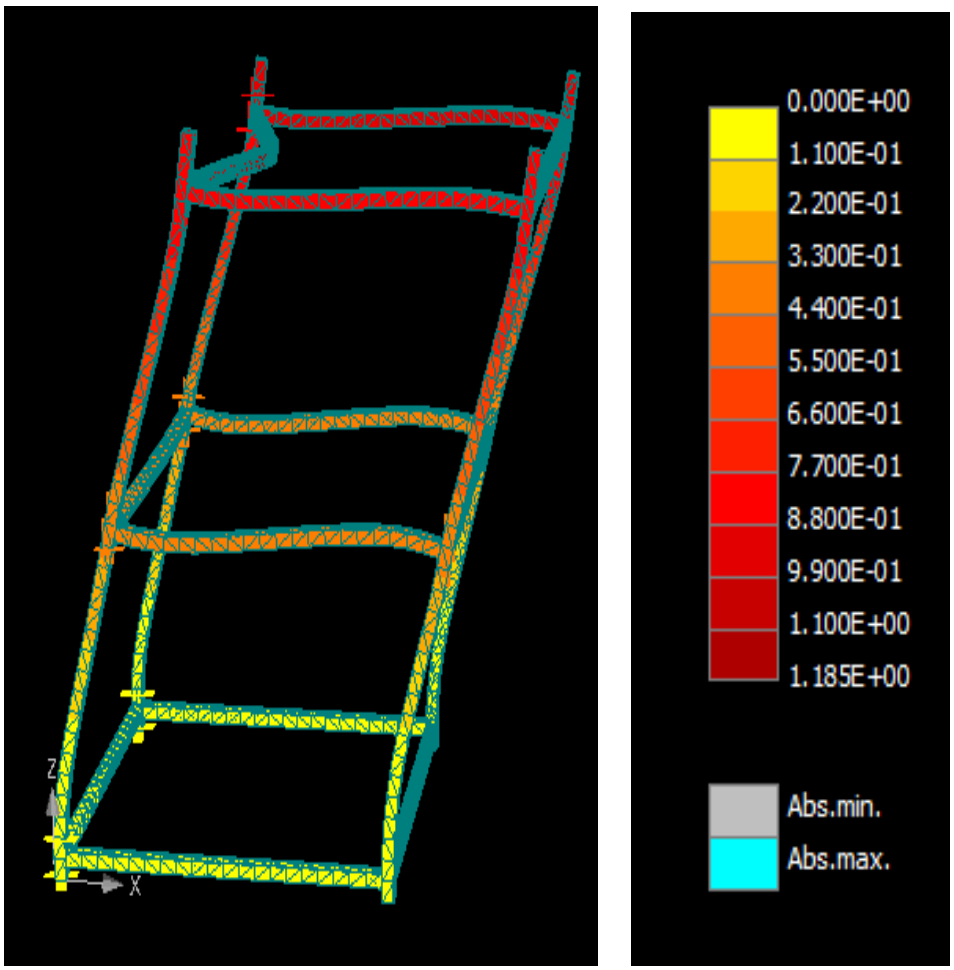

Figure 5.14 Displacements in CFST Frame with EPTB Connections

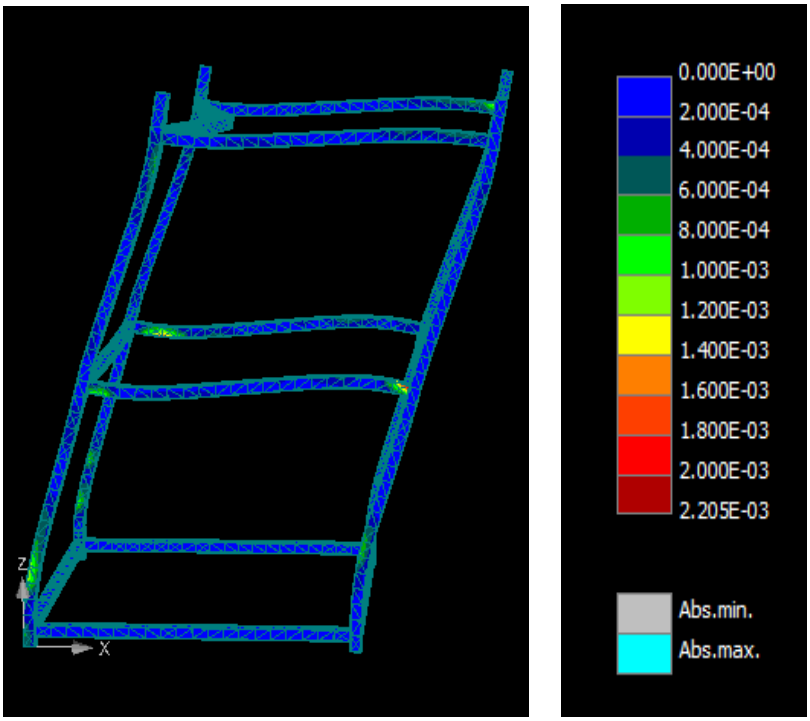

Figure 5.15 Crack Width Developed in CFST Frame with EPTB Connections (values are given in meters)

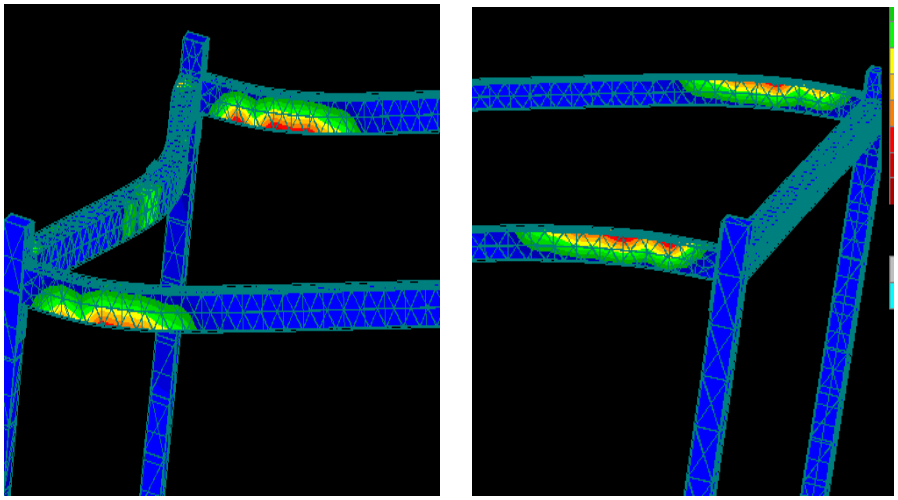

Figure 5.16 Failure Modes at Various Joints

5.4.3.2 Frame with EPAB connections

Load V/s Deformations: FE modelling of two storey 3-D frame has been depicted through Figure 5.4. of Load-displacement curve obtained from FE results is plotted in Figure 5.13. It is observed that floor level-1 has experienced the lesser deflection even

though the damage experienced by this floor is maximum. The variation of load-deflection curve is same as that on other floor levels. The maximum deflection at load value of 236 kN has been found to be 820 mm which increases up to 1380 mm, even after without any application of load. Deformations in end plates are also observed at this stage. On the left side of frame lower side of end plates have been observed to be pulled away from the columns and on the right side, top side of end plates have got deviations from the column walls.

Failure Modes: The variation of stresses and deformation/crack patterns has been obtained from the post processer of ATENA and are plotted in Figure 5.15. In the deformed shape storey drift in the X direction (direction of loading) at upper levels is clearly visible. Maximum stresses have been experienced by the members at the top level. At the base of columns tension stresses are observed on the loading side.

Comparison between frame with EPTB and EPAB connections shows that frame with EPTB type connections has shown 21.9% higher strength over frame with EPAB type connections. The connections with through bolts have performed better in terms of stiffness over frame having connections with bolts of normal length.

5.5 CLOSURE:

It has been observed that maximum value of displacement occurred at upper floors whereas at lower levels yielding of steel tube od CFST columns has been observed. The frames also showed significant post yield ductility.

The CFST frame with extended end plate connections using through bolts have shown higher strength over connections with normal length anchor bolts. The frame with EPTB type connections has shown 17.5% and 16.05 % higher strength for single storey and double storey 2-D frame respectively and performed better in terms of stiffness over frame having connections with EPAB type connections. Double storey 3-D frame with through bolt connection has exhibited 21.9 % higher strength over frame with EPAB connections. Failure occurred at lower part of end plates in both the frames. Hence, it can be concluded that frame with through bolted end plate connections performed better similarly as observed when tested as individual exterior connection under vertical loads at beam tip.

CHAPTER-6

GUIDED WAVES FOR MONITORING DEGRADATION IN CFST SECTIONS

6.1 GENERAL

The major flaw of structures made of CFST sections is their vulnerability to environmental attack causing corrosion. It can severely reduce the strength and life of these structures. Corrosion of steel confining the concrete is one of the major durability problems to maintain aging CFST structures. The problem accelerates since the inner surface of the steel tube is in contact with concrete which serves as an electrolyte for the initiation of corrosion. If the corrosion ingress starts, it further accelerates and can be catastrophic for the structures as it results in huge loss of life and property. The increased volume of the corrosion products induces stresses in the concrete that result in cracking and delamination of steel tube from the in filled concrete. As a result, it weakens the structure to a high degree. Also, corrosion due to chloride ingress results in the occurrence of pits in the steel tube which reduces the cross-sectional area of tube drastically and can be catastrophic.

The quality of concrete, the change of temperature, the shrinkage and creep of the mass concrete core, are some of the causes of the interfacial debonding defect between the steel and inner concrete core of CFST. The interfacial debonding defect can weaken the confinement effect of steel tube on the concrete core resulting into the loss of load-carrying capacity and in the ductility of the CFST under earthquake and cyclic loadings. Unfortunately, such debonding damage and the voids cannot be visually identified. Actually, these are almost unavoidable in CFST structures but such damages are most unfavorable (Xue et al. 2012).

Monitoring and detection of corrosion are very important for any industry. To this effect, Non-destructive Evaluation (NDE) techniques have a significant role to play in detection and monitoring of corrosion. Multidisciplinary efforts are important for manipulation of tremendous benefits offered by NDE in ensuring the damage assessment and life extension of any structure.

A wide range of non-destructive testing techniques has been reported in the literature that may be suitably employed for detection and monitoring of corrosion of steel in reinforced concrete structures for assessing the cause and extent of the corrosion. But most of the techniques are electrochemical techniques which relate corrosion rate and extent through an assessment on surrounding concrete medium. None of the techniques focus on corrosion monitoring through direct measurements on steel tube. The degradation due to corrosion accelerates and can be catastrophic unless early remedial action is taken. Therefore, it is necessary to develop a non-intrusive technique for early detection of damages in the form of cracks, debonds and corrosion in steel tubes in CFST members. Ultrasonic guided wave technique which is an active monitoring technique has gained popularity in recent years for detection of corrosion in reinforcing steel bars (Sharma and Mukherjee 2010c, 2013 and 2015). So, in this work, it is proposed to use ultrasonic guided waves for monitoring these damages in CFST sections. Guided waves have been used owing to their ability to scan through longer spans with sensitivity better than conventional non-destructive testing techniques. In addition, different frequencies and modes can be utilized for evaluation of different types of damages in RC structures.

6.2 ULTRASONIC GUIDED WAVES

In an infinite isotropic solid medium, only two types of independent wave propagation exist, i.e., compressional and shear waves. Both waves propagate with constant velocities and are non-dispersive. When geometry constraints are introduced and the dimensions are close to the wavelength, the wave becomes dispersive and is called a guided wave (Reis et al. 2005). In an infinite bulk of a perfectly elastic material, ultrasonic waves travel as bulk waves, decaying in amplitude because of the spread of the wave front. However, in a finite perfectly elastic medium, the sound wave is reflected from the structure boundaries, and the energy is contained within the elastic medium as a guided wave, which propagates with constant amplitude.

Ultrasonic guided wave inspection and structural health monitoring are being considered today in such natural wave guide structures as plates, multi-layer structures, rods, rails, piping and tubing, an interface, and curved or flat layers on a half space. An

increased understanding of the basic physics and wave mechanics associated with guided wave inspection has led to an increase in practical nondestructive evaluation and inspection problems. Computing power today is also making dreams come true, where only a vision was possible decades ago. A principal advantage of guided waves is inspection over long distances with excellent sensitivity from a single probe position. There is also an ability to inspect hidden structures and structures under water, coatings, insulations, and concrete.

An understanding of the basic wave mechanics and wave propagation principles for various sensors and mode types is essential, though, if one is to carry out some reliable tests. The most interesting one, of course, is to be able to inspect over long distances from a single probe position.

The wave is termed "**guided"** because it travels along the medium guided by the geometric boundaries of the medium. Since the wave is guided by the geometric boundaries of the medium, the geometry has a strong influence on the behavior of the wave (Redwood 1960 and Achenbach 1975). In contrast to ultrasonic waves used in conventional ultrasonic inspections that propagate with a constant velocity, the velocity of the guided waves varies significantly with the wave frequency and the geometry of the medium. In addition, at a given wave frequency, the guided waves can propagate in different wave modes and orders (Kim et al. 2001). Guided waves travel either at boundaries (Surface Waves) or between the boundaries (Lamb Waves). Guided waves are highly dependent on wavelength and frequency, and propagating guided waves can only exist at specific combinations of frequency, wave number and attenuation.

The research in the last two decades (Section 2.2 Chapter 2) has shown the possibility of using Ultrasonic Guided Waves for monitoring various kinds of damages. But most of the work is done on simulated corrosion studies only on RCC and pre-stressed members; a very few research works have been reported on corrosion monitoring of CFST members. As these sections are liable to corrode from inside because of the media in the form of concrete is there and from outside because of environmental reasons. As bolts are necessary elements of the most type of joints used in these types of structures, chances of ingression of water inside the members are there

resulting propagation of corrosion. Hence it is needed to explore the suitability of Ultrasonic Guided Waves for actual corrosion monitoring in CFST sections.

In this study, ultrasonic guided waves have been used in pulse transmission (PT) for monitoring two type of defects i.e. notches and delamination simulating loss of area and debond due to corrosion in CFST sections. Specific guided wave modes were used for investigating varying extents of notches and simulated delamination defects. PT signatures could relate to the percentage notch and delamination very efficiently. The method is further applied to CFST sections undergoing accelerated corrosion. It can successfully relate to the state of steel tube undergoing chloride corrosion and can be applied to real time corrosion monitoring of CFST sections.

6.3 GUIDED WAVES IN CFST SECTIONS

In this study, ultrasonic guided waves have been used in pulse transmission (PT) for monitoring two type of defects i.e. notches and delamination simulating loss of area and debond due to corrosion in CFST sections. Specific guided wave modes are used for investigating varying extents of notches and simulated delamination defects. PT signatures can relate to the percentage notch and delamination very efficiently. The method is further applied to CFST sections undergoing accelerated corrosion. It can successfully relate to the state of steel tube undergoing chloride corrosion and can be applied to real-time corrosion monitoring of CFST sections.

Guided waves are the waves which travel along the medium guided by the geometric boundaries which has a strong influence on the behavior of the wave (Redwood 1960 and Achenbach 1984). In contrast to ultrasonic bulk waves that propagate at a constant velocity, the velocity of the guided waves varies considerably with the wave frequency and the geometry of the medium. Also, at a given wave frequency, the guided waves can propagate in different wave modes (Rose 2003) The complex effect of the boundaries results in dispersion of the wave and generates different modes that have predictable frequency-dependent properties. The velocity-frequency relationships of guided waves can be displayed as dispersion curves (Pavlakovic and Cawley 2000). Ultrasonic Guided Wave inspection and structural health monitoring are being considered in such natural wave guide structures as plates,

multi-layer structures, rods, rails, piping and tubing (Rose et al. 2004) A major advantage of guided waves is inspection over long distances with excellent sensitivity from a probe position.

In CFST section, desired Lamb waves can be excited in the steel tube just as in the steel plates. The ultrasonic wave is reflected from its boundaries, and the energy is contained within the steel tube as a guided Lamb wave. The complex effect of the steel tube boundaries surrounded by air on the one side and concrete on the other results in dispersion of the wave and generates different modes. Various Lamb wave modes can be effectively generated by a pair of transducers arranged in a pitch-catch orientation and having an equal inclination with steel tube using water as coupling media. At a particular frequency, the different Lamb wave modes can be produced by varying the angle of the transmitting and receiving probes (Figure6.1), calculated by Snell's law as-

$$\theta=\sin^{1}(V_L/V_{ph}) \quad (6.1)$$

where,

V_{Ph}= Phase velocity of the desired Lamb Wave mode

V_L=Longitudinal velocity of the incident wave in the coupling media.

For generating specific ultrasonic guided wave mode, an acrylic tank of dimensions 350mm x 70mm x 70mm was fixed on the top of CFST specimen to maneuver the probes and water was used as coupling media to carry the incident energy from the probe to the tube surface (Figure 6.1(b)). The scanning of a particular length of CFST section was done in pitch catch orientation by the transmitter and receiver probes placed at a same angle of inclination with vertical (θ) as shown in Figure 6.1. Both the probes are kept at a same inclination with vertical to make the receiver most sensitive to the wavelength of the input frequency.

The specific Lamb waves transmit through the length of the tube and should be sensitive to various defects in the propagated span. Ultrasonic energy propagating through the steel tube leaks to concrete and water. The leakage into concrete depends on the relative elastic and damping properties of the concrete filled inside. The efficiency of steel–concrete interface bond can be effectively characterized by ultrasonic

investigations. The discontinuities and irregularities produced as a result of corrosion and other service related damages in CFST sections would result in scattering and reflections of the smooth wave guide resulting in mode conversions and signal attenuation. Another effect of debonding of steel from surrounding concrete is expected to reduce leakage into the surrounding concrete and signal rise. Therefore, it should be possible to characterize various defects as a result of various kinds of damages in steel tube and interface modifications. It is proposed in this study to utilize specific guided wave modes to monitor various kinds of damages in CFST sections using this non-contact guided wave technique.

6.4. EXPERIMENTAL PREPARATION AND METHODOLOGY

It is proposed to study the effect of area loss and debond of the steel tube from the surrounding concrete in CFST sections using ultrasonic guided waves. The changes in ultrasonic transmitted signal with increasing depth of the notches and with increasing length of delamination would lead to damage diagnosis of the CFST tube. Area loss is simulated as notches of varying depths in steel tube and increasing delamination is simulated as loss of bond between steel tube and concrete using a double-sided tape of increasing lengths.

6.4.1 CFST Sample Preparation

The square hollow steel tubes conforming to IS 4923 -1997 and IS 1161-1998 having a cross-section of 72mm x 72mm x 3.2mm, have been used in the study as these are easily available in the market. Moreover, the change in geometry (thickness) and material properties will not change the methodology overall. The length of the square hollow steel tubes is kept 600mm. These hollow steel tubes have been filled with commonly used M-25 grade concrete with design mix proportions of cement, sand and stone aggregates as 1:1.375 (FA):1.539 (20mm CA) :1.510 (10mm CA) by weight prepared with water cement ratio of 0.44. The 28 days' compressive strength of cubes is found to 38.7 N/mm^2.The steel tube has been left unfilled by 25mm on each side of the section for attaching clips to use it as anode and for easy handling of samples. Total twelve samples have been prepared to be used for different purposes. The CFST specimens have been cured for 14 days and left for drying in air for another 14 days.

6.4.2 Ultrasonic Testing System and Set-up Details

The ultrasonic testing (UT) system consists of DPR300 Pulser/Receiver system (Karl Dutsch Make) (Fig 6.1(a)), transducers (Olympus NDTT Immersion Probes), data acquisition system and display devices (Sharma and Mukherjee, 2015a and 2015b, Garg et al. 2016 and 2017). The compression transducers are driven by the PR system which generates ultrasonic pulses through the steel tube of CFST section. The ultrasonic excitation is a pulse obtained when PR is set at maximum input voltage amplitude of 475V. The ultrasonic waves generated by the transmitter probe travel through the surrounding water and intrude the tube of CFST specimen at an angle to generate the corresponding Lamb wave mode. The probes are to be placed at an appropriate distance from the plate specimen which is termed as *Water Path.* It is the distance traveled in water before the wave hits the top surface of the CFST section. Transmitter transducer sends the ultrasonic pulse to the specimen through a coupling medium (water) and is received by the receiving transducer. The received pulses are the pulse transmission signals displayed in the form of Voltage- time (V-t) signatures. In this study, non-contact transducers of 0.5 MHz and 1.0 MHz are used. The selection of typical frequencies for UT is discussed in the following section.

6.4.3 Selection of Optimum Mode and Frequency

Lower frequencies of 0.5 MHz and 1.0 MHz, have been initially selected for experimental study due to lesser dispersion at lower frequencies. The probes at these frequencies have been used for checking the signal fidelity and signatures are obtained at various angles of inclination of T and R probes. In order to avoid any bias in the experiment, P-R settings are kept constant during the study. The propagation span has been kept as 200mm and water path of 30μs has been chosen for both left transmitting and Right Receiver probe (Figure 6.2). Pulse transmitted signals obtained at 0.5 MHz by varying the incidence angles are shown in Figure 6.3(a) and the corresponding peak to peak voltage trends of the received PT signals are shown in Figure 6.4(a) respectively.

It is observed that as the angles of probes is varied from 12^o onwards upto16^o, signal strength rises significantly but further starts falling with an increase in angle

beyond 16°. From the observed signals and their trends, the best signal fidelity and pulse are obtained at 16°. From the phase velocity, angle of incidence with water and attenuation dispersion curves (Figure 6.5) plotted using software Disperse (Pavlakovic and Cawley 2000), for 3.2 mm thick steel plate with water on one side and concrete on the other, it is observed that the signal at 16° corresponds to S_o mode at 0.5 MHz.

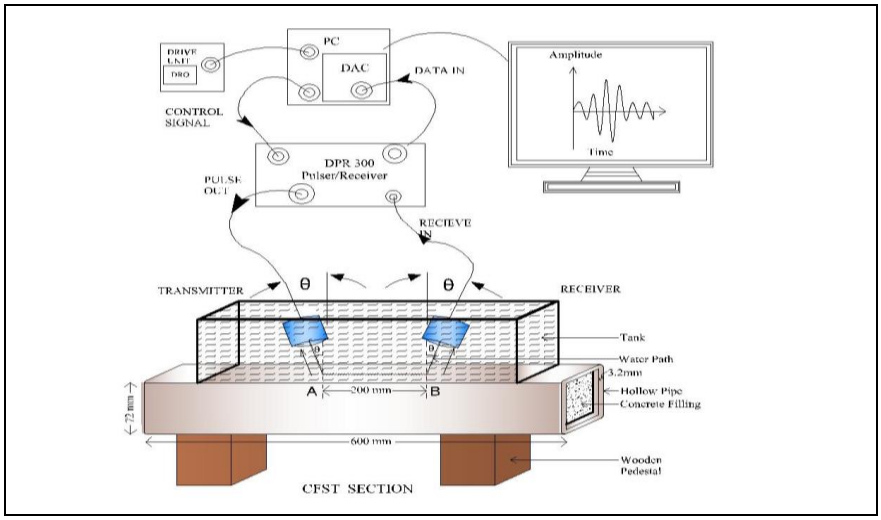

(a) Schematic of Ultrasonic Testing Set-Up

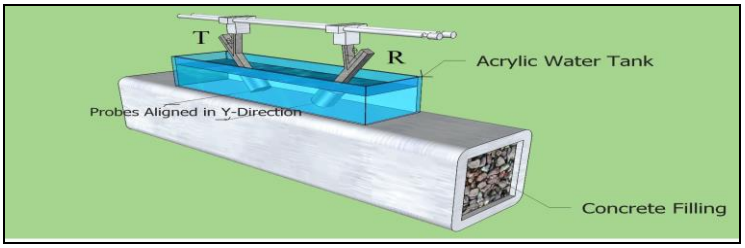

(b) Schematic of Probes

(c) Immersion probes (left) 0.5 MHz (right) 1 MHz

Figure 6.1 Experimental Set-up

Similarly, PT signatures at 1 MHz (Figure 6.3(b)) by varying the incidence angles and corresponding peak to peak voltage trends of the PT signals have been obtained (Figure 5(b)). The rise in signal strength is observed as the angles of probes is varied from 12^o onwards upto16^o which starts falling with further increase in angle. The best signal fidelity in healthy CFST tube is also obtained at around 14^o - 16^o from the observed signals and their trends. From the phase velocity and angle of incidence with frequency dispersion curves (Figure 6.5(b)), it is observed that the mode at 14^o -16^o corresponds to S_1 mode at 1 MHz

From the attenuation dispersion curves, also (Figure 6.5(c)), it is observed that the two modes are least attenuative at these frequencies. Hence, the two modes of S_0 at 0.5 MHz and S_1 at 1.0 MHz are used further for experimental investigations.

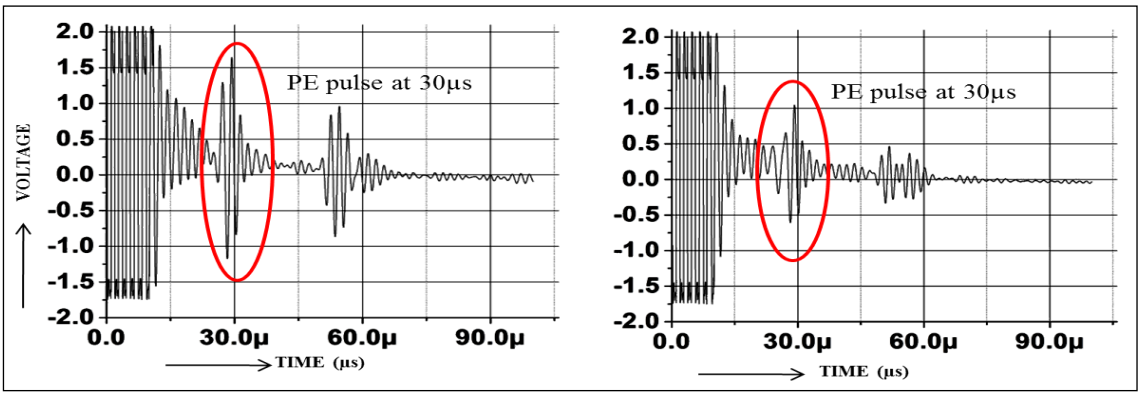

Left probe Right probe

(a) PE signatures at 0.5 MHz frequency

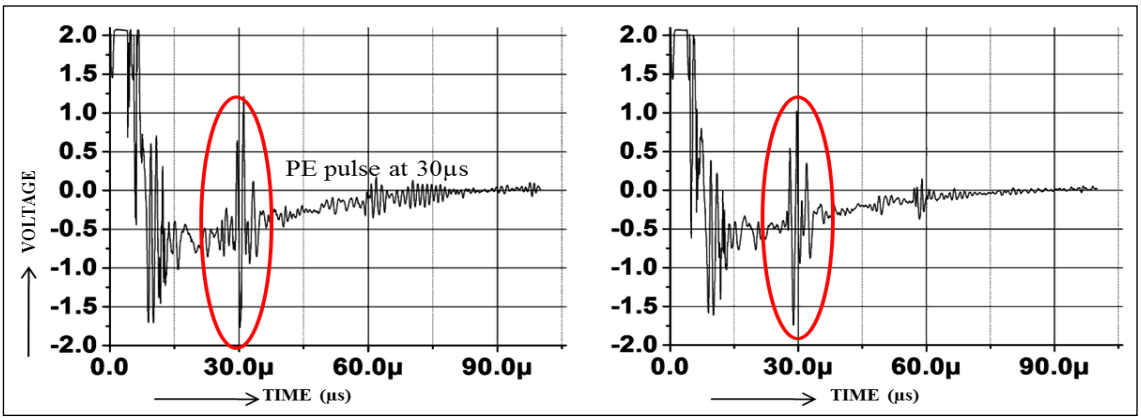

Left probe Right probe

(b) PE signatures at 1.0 MHz frequency

Figure 6.2 Typical PE Signatures to Set the Water-Path

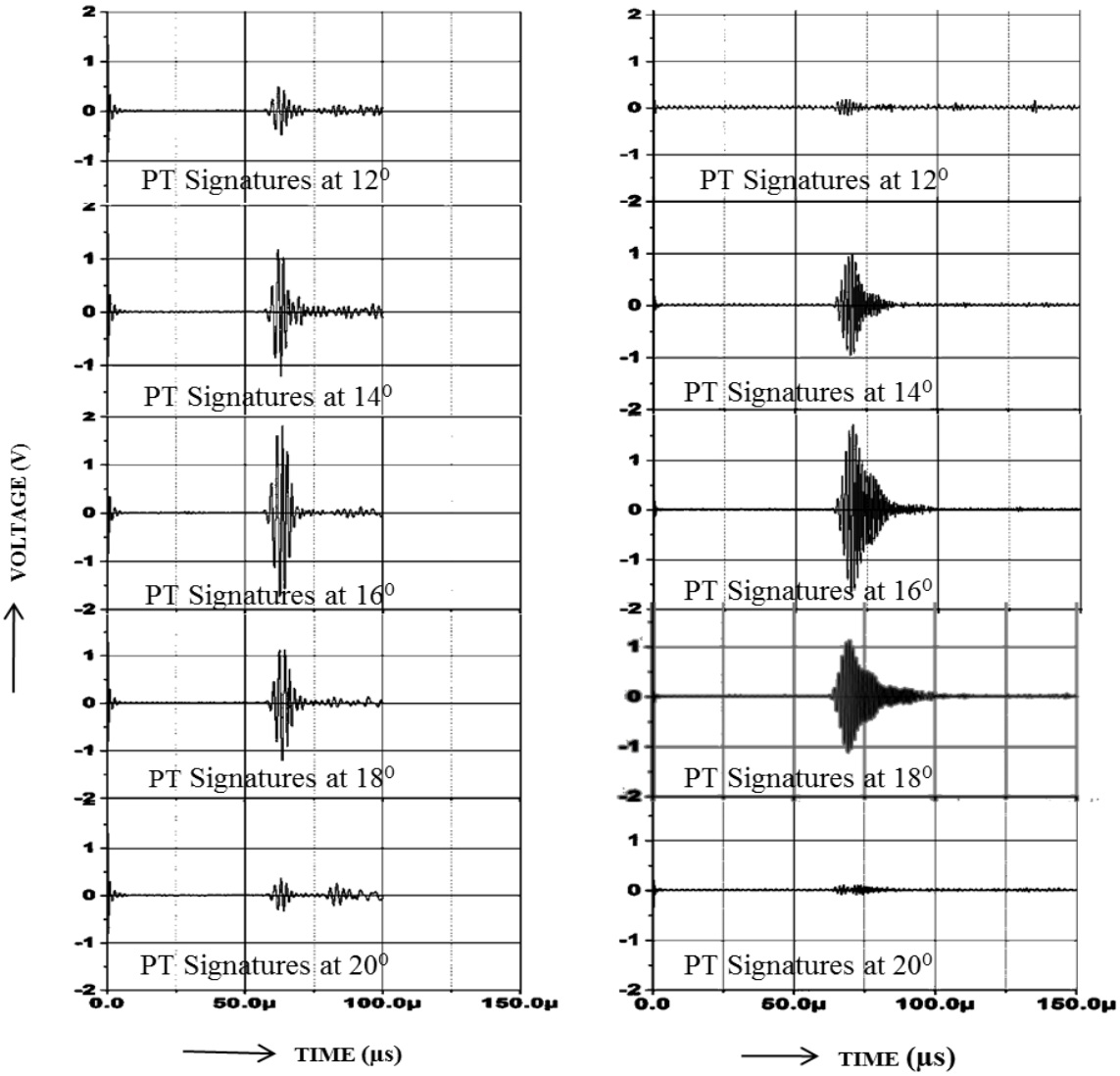

(a) 0.5 MHz (b) 1.0 MHz

Figure 6.3 PT signatures at Varying Angles (a) 0.5 MHz (b) 1.0 MHz

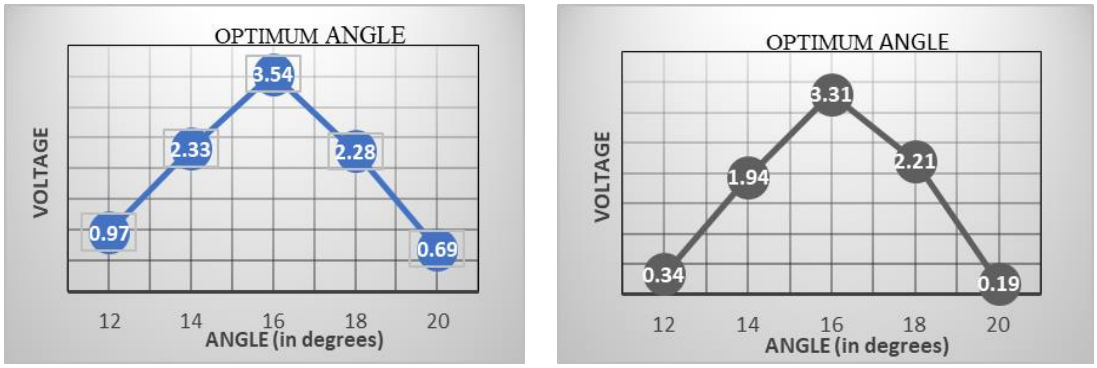

(a) 0.5 MHz (b) 1.0 MHz

Figure 6.4 Peak to Peak voltage trends at varying incident angles

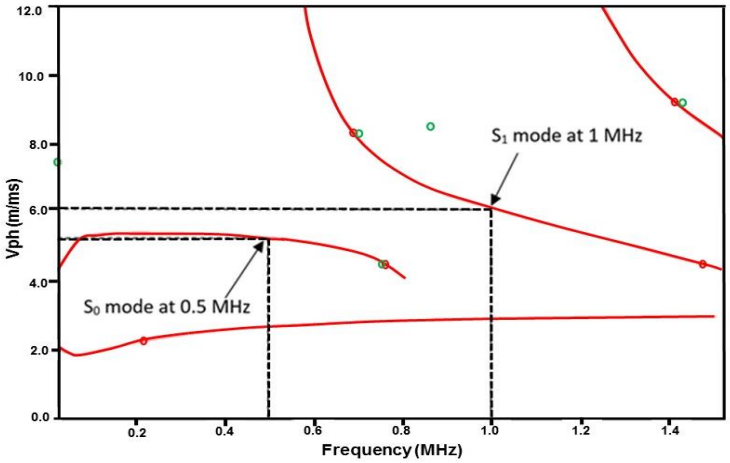

(a) Phase Velocity Vs Frequency

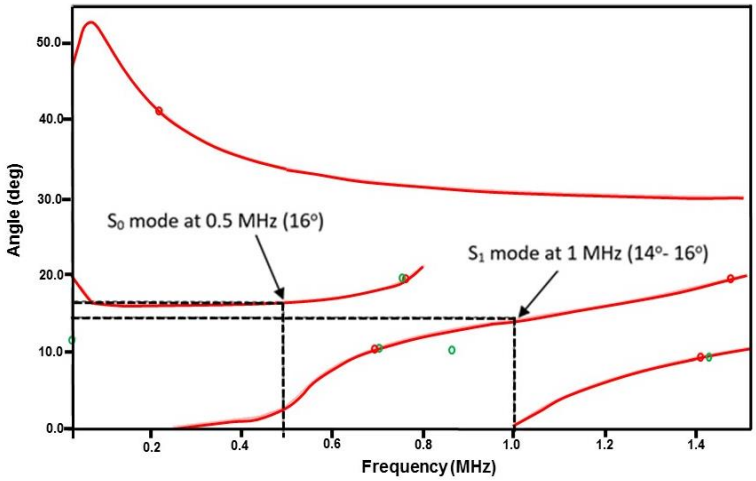

(b) Angle of Incidence with Water Vs Frequency

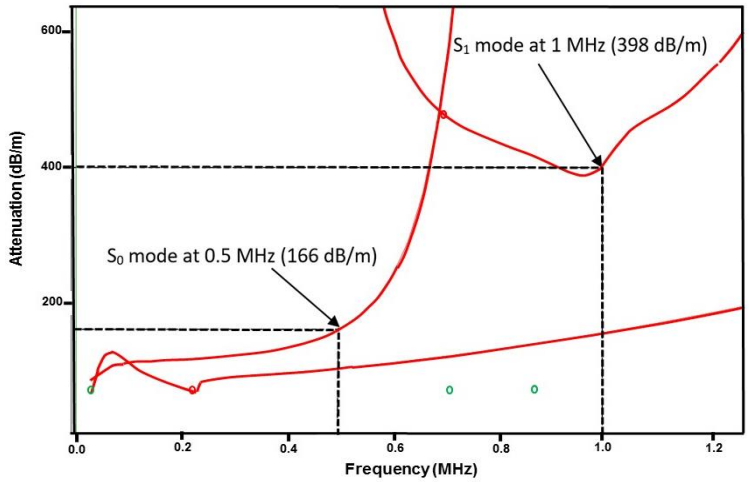

(c) Attenuation Vs Frequency

Figure 6.5 Dispersion Curves (Pavlakovic and Cawley 2000)

6.5. DAMAGE DETECTION IN CFST SECTIONS

6.5.1 Simulated Defects

6.5.1.1 Notches in Tubes

PT signatures in the healthy CFST specimens have been taken using the selected S_0 mode at 0.5 MHz and S_1 mode at 1.0 MHz frequencies respectively. Simulated defects in the form of machined notches of varying depths (1mm, 2mm, 3mm and 3.2mm) have been machined in the middle of the steel tube of CFST section as a through cut. A total of four specimens each reflective of a particular notch depth have been fabricated. The width of the notches has been kept constant of 2mm.To ensure repeatability of the experiments and the readings, the signatures have been taken on three locations marked on the steel tube as Loc-1, Loc-2 and Loc-3 (Figure 6.6). PT signatures corresponding to increasing depths of notches were recorded to study the effect of these damages on signal strength. Comparison of PT signatures of simulated notched specimens' vis-a-vis healthy specimens has been done to quantify the effect of notches on signal strength.

6.5.1.2 Debond/ Delamination of Steel Tube from Infilled Concrete

Another set of three specimens with increasing length of debond between tube and concrete and one specimen without debond (Healthy) has been prepared. Debonding between steel and concrete has been created by pasting square sized PVC sheets of various sizes 40mm x 40mm (S1), 50mm x 50mm (S2) and 70mm x 70mm (S3) to the inner surface of the hollow pipe in the middle portion of steel tube prior to filling the concrete inside (Figure 6.7). This indicated increasing debond between steel tube and concrete of CFST section. The PT signatures are also taken on these simulated debond samples and compared with a healthy signal to study the effect of delamination on PT signals. In this case, also, the signals are taken at three locations in a particular sample.

6.6. RESULTS AND DISCUSSIONS

6.6.1 Simulated Notch Defects

Using S_0 mode at 0.5 MHz frequency, ultrasonic pulse transmission signatures

are recorded at three different locations (Figure 6.6) at a gap of 25 mm (each side from centre line of sample) with increasing depths of notches. It is done to ensure whether at all locations fall in voltage amplitude is consistent or not, due to the presence of notch to mark repeatability of results. Dp was fixed as 200 mm with water path of 30 μs. PT signatures obtained with S_0 mode at 0.5 MHz with increasing depth of notches in simulated notch specimens are shown in Figure 6.8(a). The trends of the transmitted signals with respect to healthy voltage amplitudes are plotted in Figure 6.9(a).

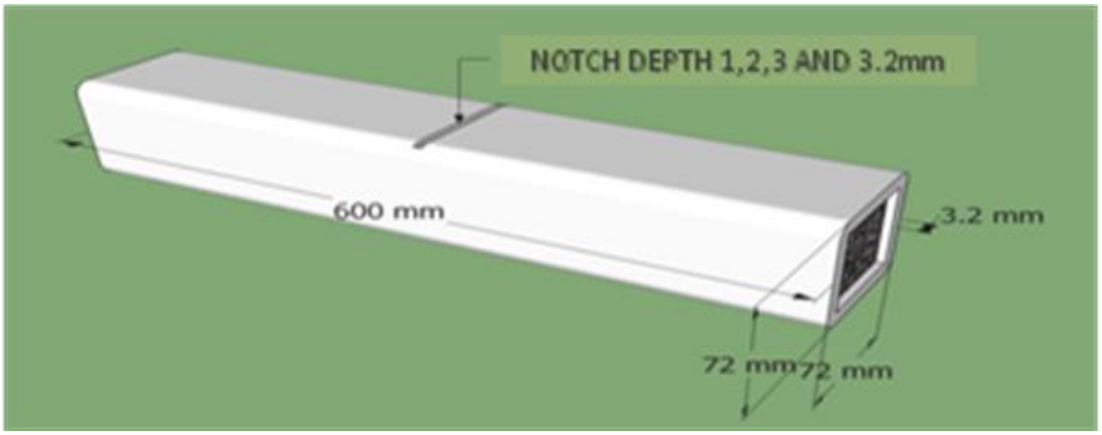

(a) Schematic

(b) Actual specimen

Figure 6.6 Simulated Notch Specimen (Notch in middle)

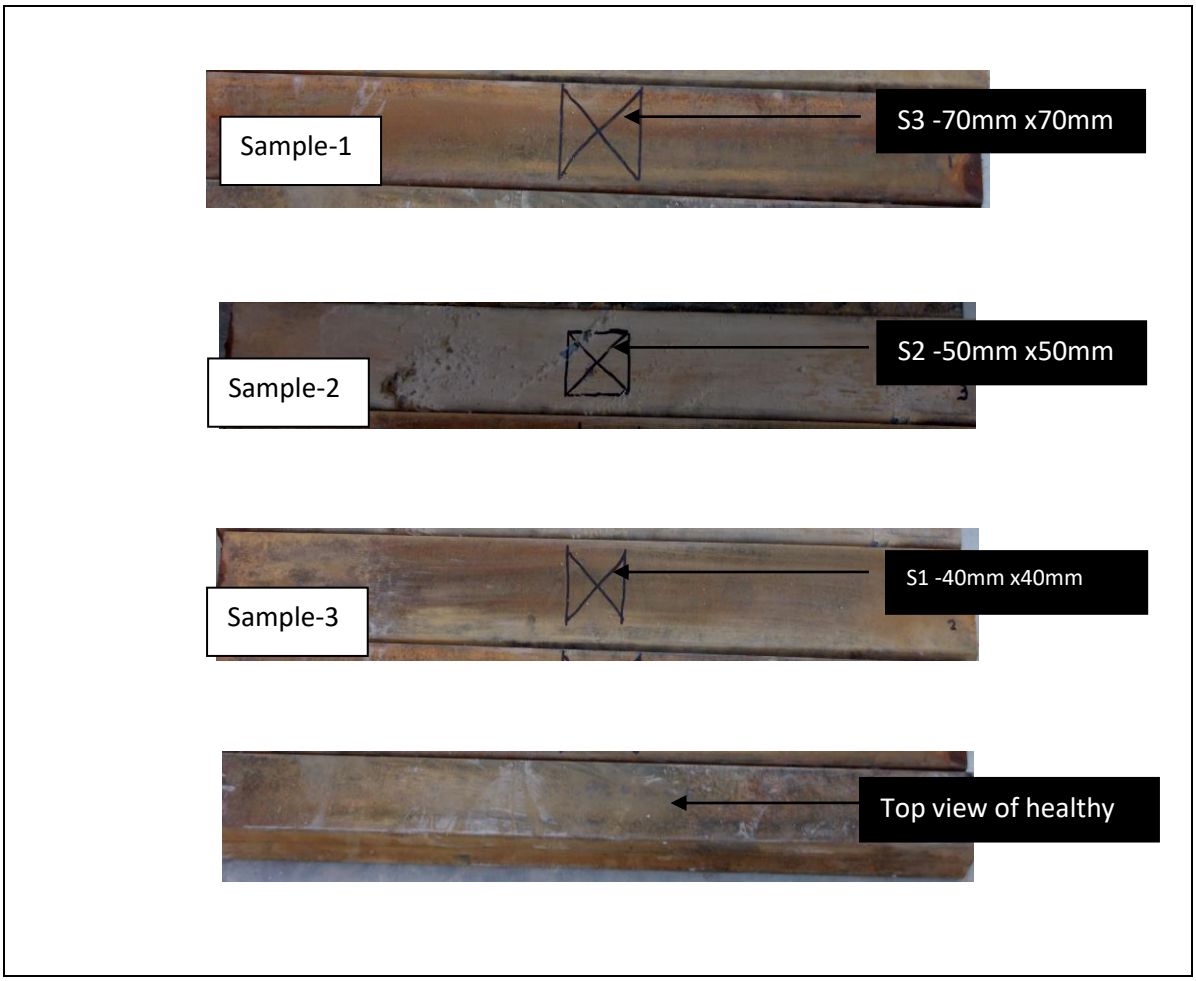

Figure 6.7 Simulated Debond Specimens

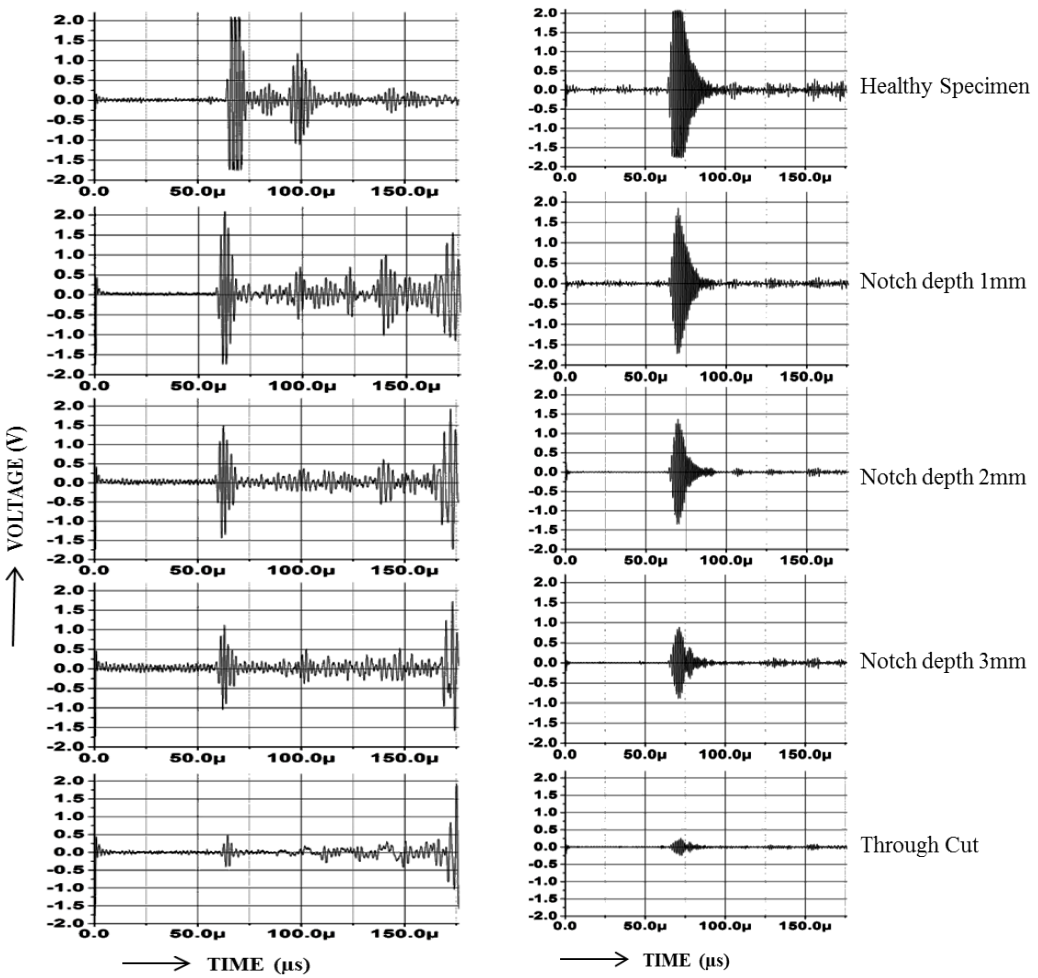

(a) S_0 mode at 0.5 MHz frequency (b) S_1 mode at 1.0 MHz frequency

Figure 6.8 PT Signatures in Simulated Notched Specimens

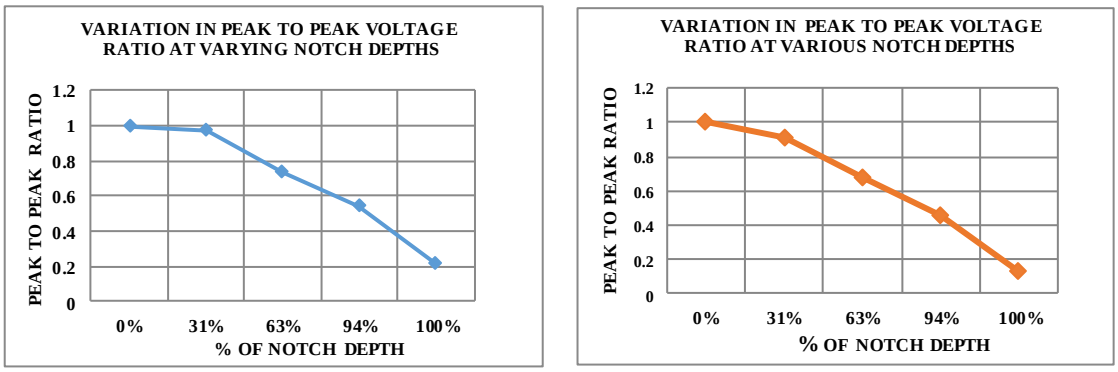

(a) S_0 mode at 0.5 MHz frequency (b) S_0 mode at 1.0 MHz frequency

Figure 6.9 Normalized Peak to Peak Voltages for Simulated Notched Specimens

From the transmitted signal strength (Figure 6.9(a)) in notched specimens, it is observed that there is drop in signal strength as the depth of the notch increases. This is due to increase in reflections from notch with increased depth and less energy being from notch with increased depth. The drop-in voltage amplitude of the received signal indicates the presence of notch as compared to the healthy signal. Also, with the increase in depths of the notch, signal strength constantly drops and here the comparison of healthy signals with signals obtained in the notched specimen can be used to quantify the extent of notch also.

Similarly, pulse transmission signals are recorded on the same specimens using S_1 mode at 1.0 MHz as shown in Figure 6.8(b). It is observed from pulse transmission signals that as the depth of notch increases there is a constant drop in signal amplitudes. At through cut, the signal received is of almost negligible magnitude.

From the PT signatures obtained using S_0 mode at 0.5 MHz and S_1 mode at 1.0 MHz, it is observed that the amplitude of the peak to peak voltage of the received signal decreases with increase in the depth of the notch. S_0 mode at 0.5 MHz shows a clear and significant peak and consistent drop in voltage amplitudes with increasing depth of notch defects. It is due to lesser signals attenuation and scattering at low frequencies. Hence, PT signals at S_0 mode at 0.5 MHz and S_1 mode at 1.0 MHz can be used to identify as well as quantify the notch defects and would be further used for identifying actual corrosion in CFST sections.

6.6.2 Simulated Debonds Defects

Ultrasonic pulse transmission signatures have been recorded in healthy CFST specimens and compared with the signatures obtained with increased debonding using both S_0 mode at 0.5 MHz and S_1 mode at 1.0 MHz respectively. PT signatures recorded using S_0 mode at 0.5 MHz with increasing debond are shown in Figure 6.10. Voltage amplitudes of the received signals with increased delamination with respect to healthy signals are plotted in Figure 6.11. It is observed that there is an increase in the

ultrasonic signal as the area of delamination increases. As the debond increases, there is a rise of 38.4 % in S1, 56.8% in S2 and 94.3% in S3 as compared to the healthy signal. This is due to a reduction in leakage of the signal with an increase in delamination causing rise in signal strength. Hence, increase in signal strength points towards delamination of the tube from surrounding concrete. Quantitative change in signal amplitude can be used to correlate with the extent of delamination. Similarly, PT signatures for S_1 at 1.0 MHz frequency by increasing area of delamination are shown in Figure 6.12 and Figure 6.13 respectively. The corresponding rise in signal amplitude is observed as 41.8 % in S1, 52.6% in S2 and 81.7% in S3 as compared to the healthy signal. Hence, increase in debond is marked by a rise in signal strength is well picked up by the low-frequency mode. The investigation using the two low-frequency modes are further used for picking up actual corrosion in CFST sections.

6.7. ACCELERATED CORROSION STUDIES

This study is further extended to monitor actual accelerated corrosion in CFST sections. The progression of ultrasonic guided waves in steel tubes undergoing corrosion in chloride environments is studied. Two guided wave modes used in the notch and debond studies were further used to evaluate their suitability in discerning different stages of corrosion in CFST sections. A brief discussion on the corrosion mechanism of steel is necessary to understand the proposed method.

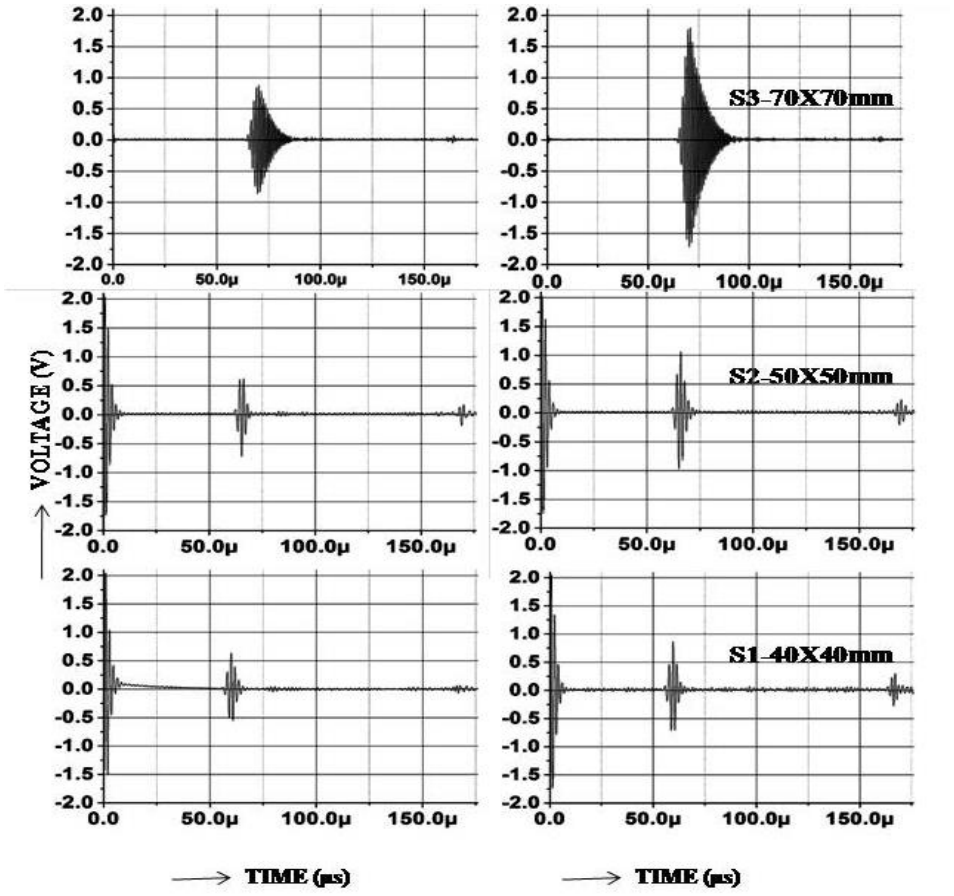

(a) Healthy specimens (b) Specimens with delamination

Figure 6.10 PT Signatures with Increasing Delamination (S_0 Mode at 0.5 MHz Frequency)

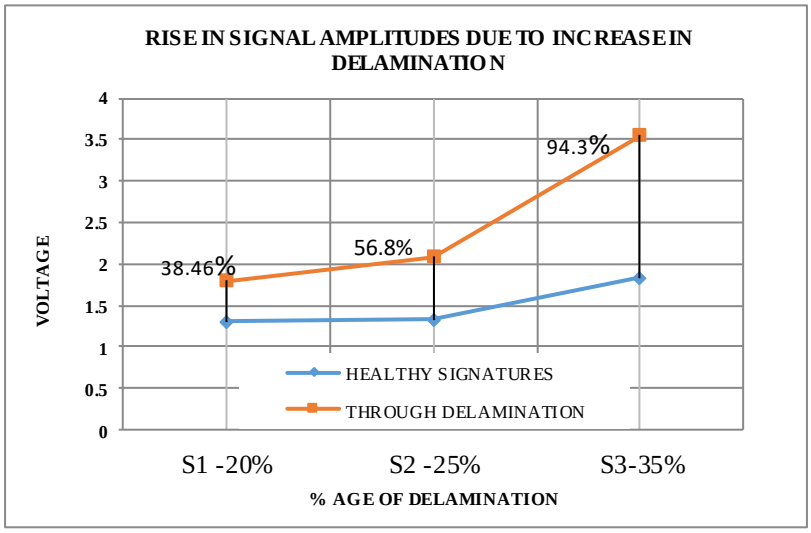

Figure 6.11 Comparison of Peak to Peak Voltages of PT Signals of Delaminated Specimens with Healthy Specimens (S_0 mode at 0.5 MHz Frequency)

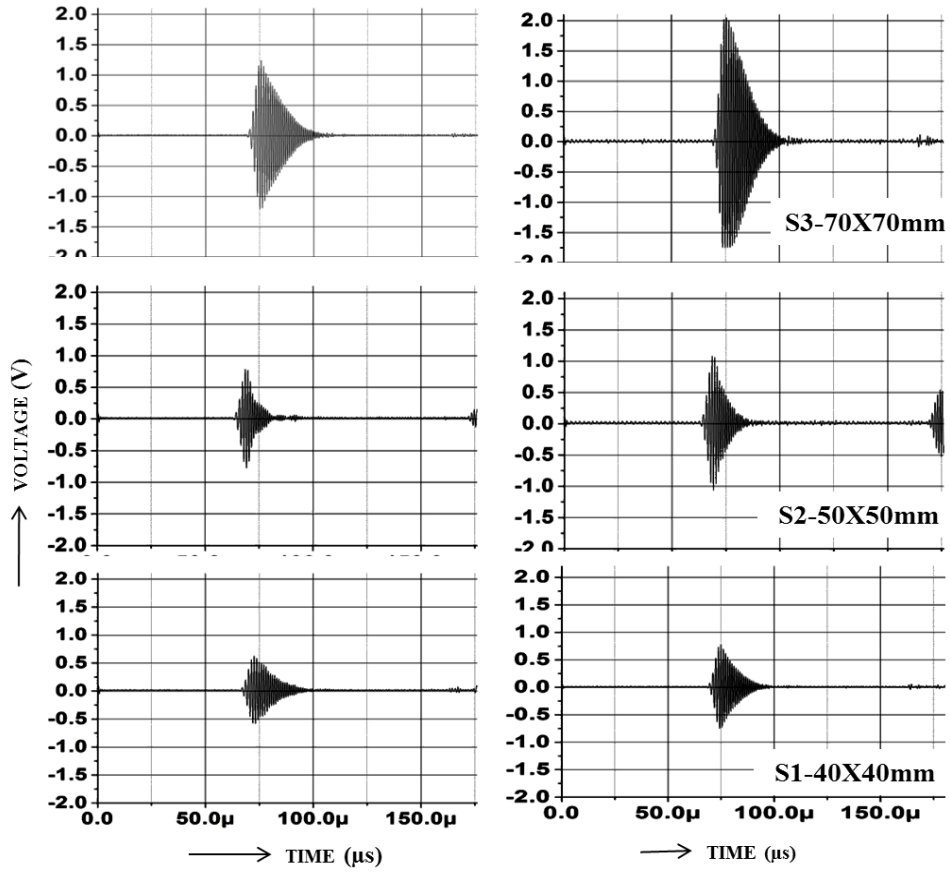

(a) Healthy specimens (b) Specimens with delamination

Figure 6.12 PT signatures with Increasing Delamination (S_0 Mode at 1.0MHz Frequency)

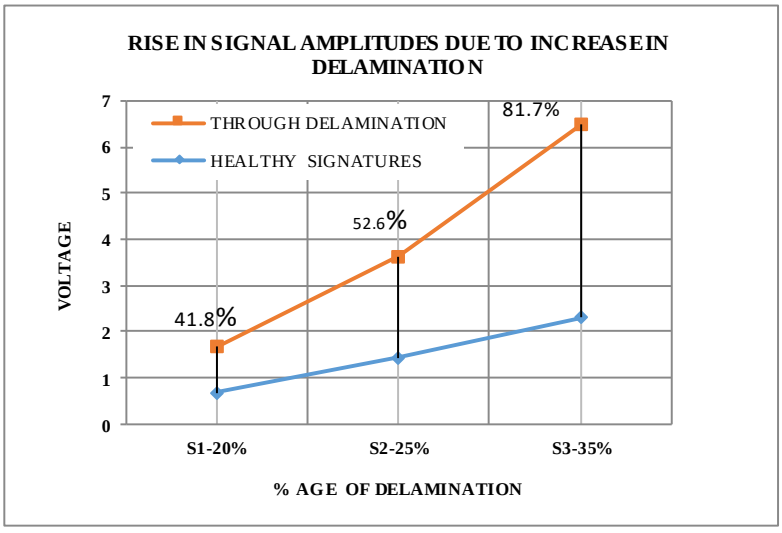

Figure 6.13 Comparison of Peak to Peak Voltages of PT Signals of Delaminated Specimens with Healthy Specimens (S_1 Mode at 1.0 MHz Frequency)

6.7.1 Corrosion in CFST Sections and Ultrasonic Investigations

Corrosion is a destructive phenomenon and, in some cases, causes material failure. Corrosion is the process of metal wastage produced by chemical action (oxidation). Natural corrosion takes a long time, hence accelerated corrosion has been used to corrode the CFST sections. Commonly used methods of accelerated corrosion are:

- Electrolysis corrosion/Impressed current corrosion method
- Dipping in acidic solution
- Salt mist chamber
- Alternate drying and wetting

Out of these techniques, the impressed current technique has been used because it is the fastest and quickest way of inducing corrosion. In impressed current corrosion technique, two dissimilar metals are kept in an electrolyte and also having external electrical contact with each other. At least one of the metals must have a positive oxidation potential. A potential difference due to the different oxidation potentials of the metals causes electrons to flow in the circuit. Oxidation (corrosion) occurs at the anode where metal is removed. Reduction (of electrolyte) occurs at the cathode.

Mild steel hollow square sections of dimensions and sizes as mentioned in Section 6.2.1 filled with concrete have been further exposed to accelerated corrosion environment. The weight of the healthy CFST sample has been recorded. Impressed current corrosion is done only for a localized area of 140mm X 50mm dimension. An acrylic pond of dimension (150mm X 60mm X 50mm) has been fixed at the top of the CFST section for restricted exposure to corrosion. The tank is sealed by epoxy to avoid any leakage of the electrolyte. The tank is filled with water with 3.5% NaCl solution to provide chloride environment and induce faster corrosion which is changed every day till the total duration of exposure. For accelerated corrosion, positive terminal of a constant power supply device (APLAB Make, 0-64V, 0-2 A) is attached to exposed unfilled part of CFST steel tube section and served as an anode. An external cathode of the copper strip (125 mm x 30 mm x 4 mm) is used as the cathode. This copper strip acting as a cathode is kept immersed in the acrylic tank within the top of CFST specimen. The copper plate is immersed such that it does not touch the surface of CFST

specimen. PT signatures have been recorded with S_0 mode at 0.5MHz and S_1 mode at 1.0MHz respectively with increasing days of corrosion exposure and compared with healthy signals.

Ultrasonic pulse transmission signatures have been recorded using S_0 mode at 0.5MHz and S_1 mode at 1.0 MHz respectively at different locations of the sections as shown in Figure 6.14. A constant voltage of 30V is maintained for accelerated corrosion and is continued for 24 hours. After 24 hours, the current has been recorded as 0.21A. The acrylic pond is dismantled and PT signatures have been taken at all locations and mass has been recorded. The acrylic pond is reconstructed and corrosion continued till it gives way to small pits in the top surface of steel tube of the specimens after 13 days. PT signatures have been taken after every day at all the marked locations (Figure 6.14) with increased exposure to corrosion.

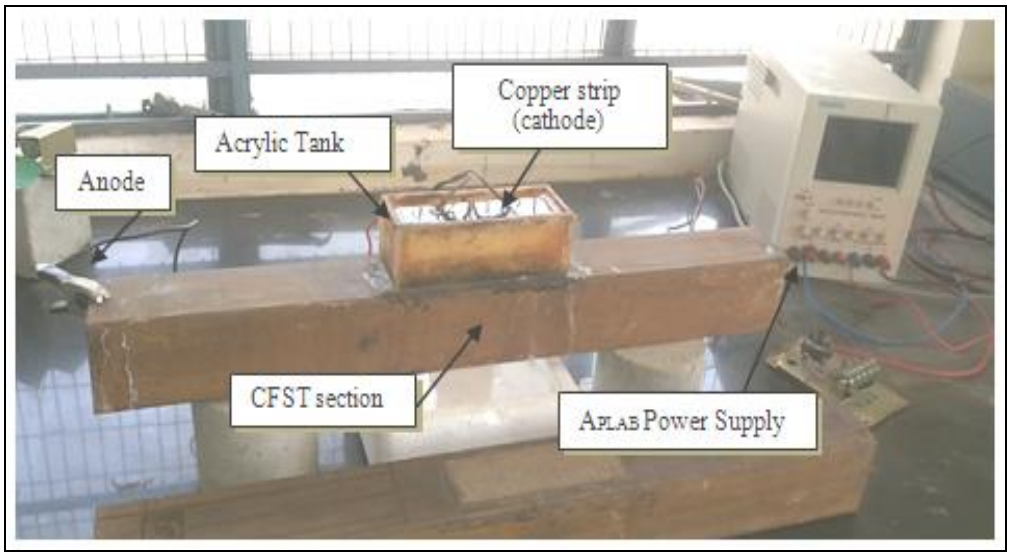

(a) Set- up for accelerated corrosion in CFST sections

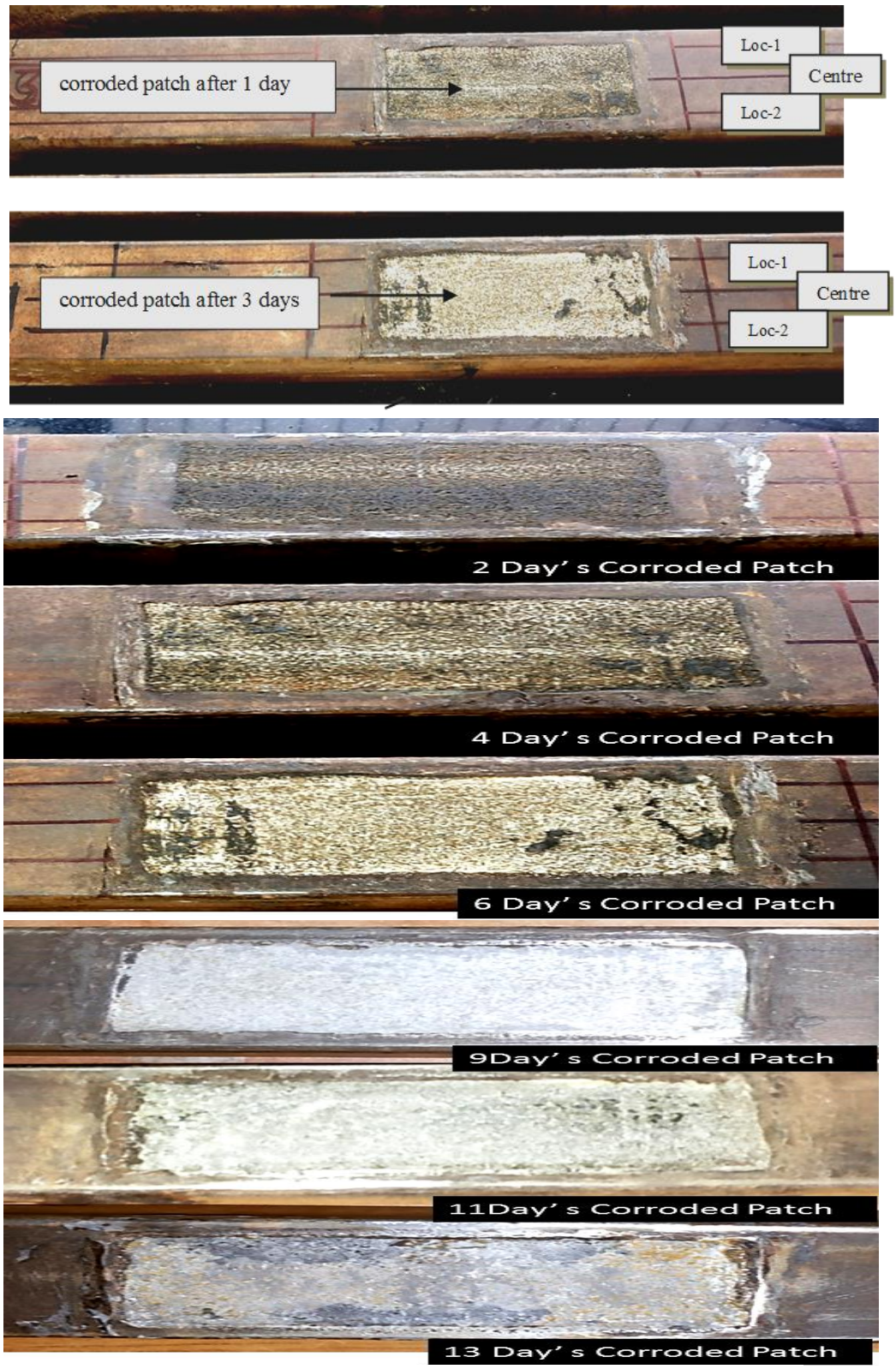

(b) Corroded patch after exposure of increasing days of corrosion

Figure 6.14 CFST Sections Subjected to Corrosion

The PT signatures using S_0 mode at 0.5 MHz and S_1 mode at 1.0 MHz are shown in Figure 6.16. PT trends of received voltage signals are shown in Figure 6.16, Figure 6.17, Figure 6.18 and Figure 6.19. From the signals, it is observed that in the healthy specimen, the signatures are characterized by a strong pulse. For the initial three days with S_0 mode at 0.5 MHz and initial 6 days with the S_1 mode at 1.0 MHz, there is no significant drop in signal. As the corrosion progresses further in both modes, drop in voltage of the transmitted signal is observed**.** It is noted that the maximum drop in voltage amplitude is observed at location Loc-1 marked at 25mm from center line (refer Figure 6.14). It suggests significant localized corrosion at this location. This can also be visually verified by the development of large sized localized pits at the same location. The drop in PT signal strength can be recognized as the corrosion in CFST sections in exposed part leading to the material loss in the form of pits on the specimen as in the case of notches. Initially, this voltage drop is found very sluggish but as the corrosion increases, this drop is significant due to initiation of formation of small pits at the exposed area. This continues till peak to peak voltage dropped to a very small value on a 13^{th} day when large pits appeared on the top surface. Hence, it is indicated that ultrasonic guided wave modes can successfully pick up deterioration due to corrosion in CFST sections. It is marked by severe signal attenuations with increased exposure to corrosion. It is analogous to the increased notch depth in simulated specimens where the signature drops significantly with the increased depth of the notch. Hence, chloride corrosion causes pits in steel section similar to notches which are indicated well by signal attenuation of selected guided wave modes. Hence, the damage in the form of simulated notches and debonds and actual corrosion in CFST sections are well picked up by ultrasonic guided wave modes using this non-contact guided wave monitoring technique.

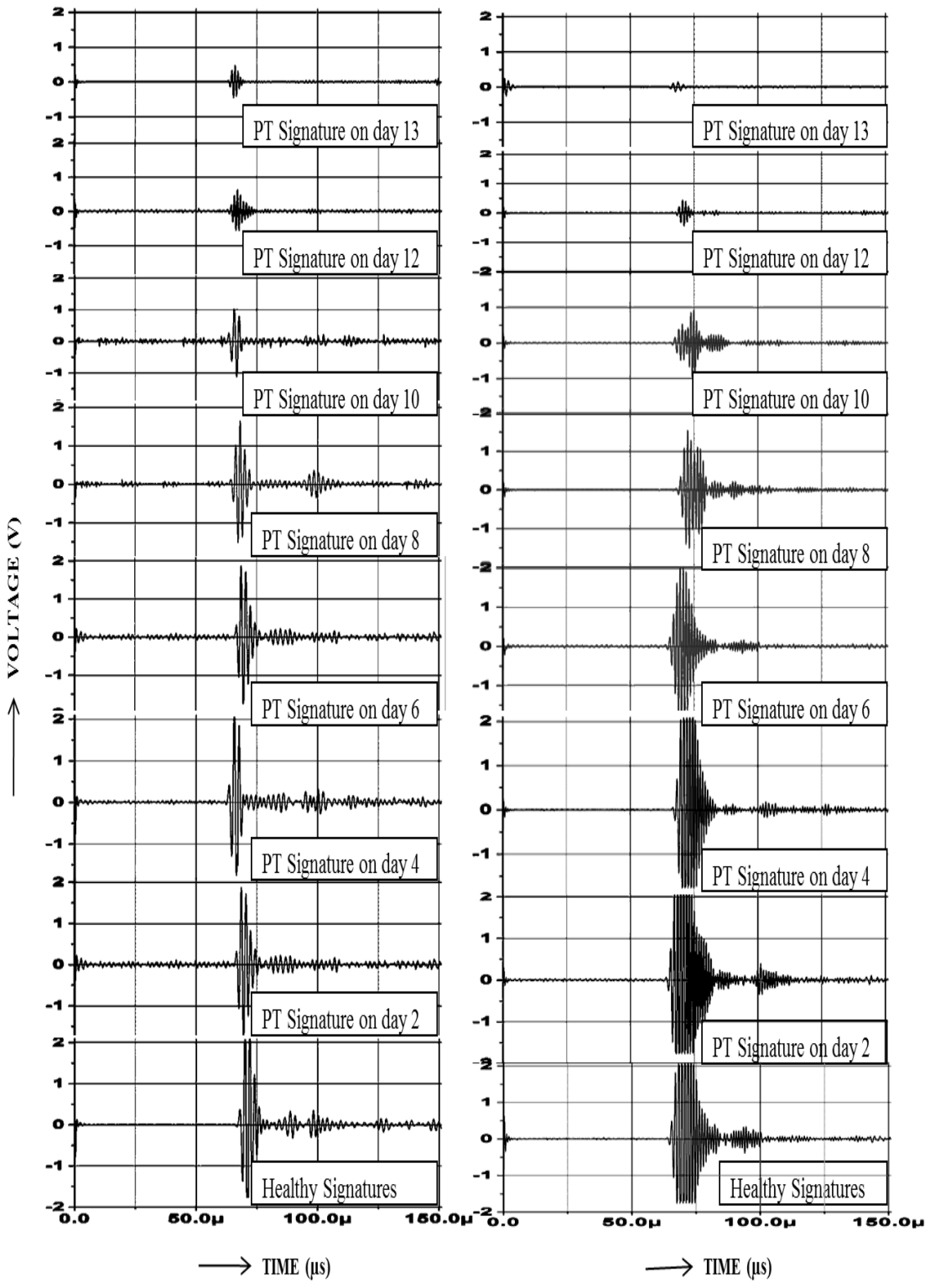

(a) S_0 mode at 0.5 MHz frequency (b) S_1 mode at 1.0 MHz frequency

Figure 6.15 PT signatures with Increasing Exposure of Corrosion

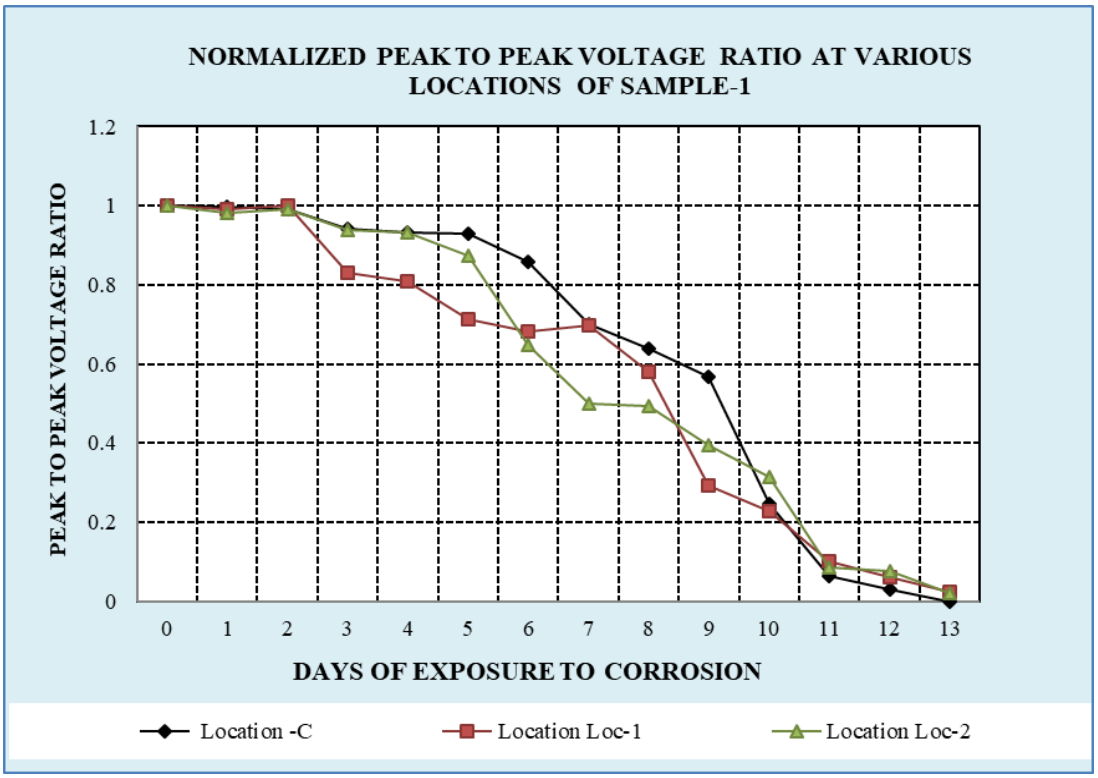

Figure 6.16 Trends of Normalized PT Signals for S_0 Mode at 0.5 MHz Frequency

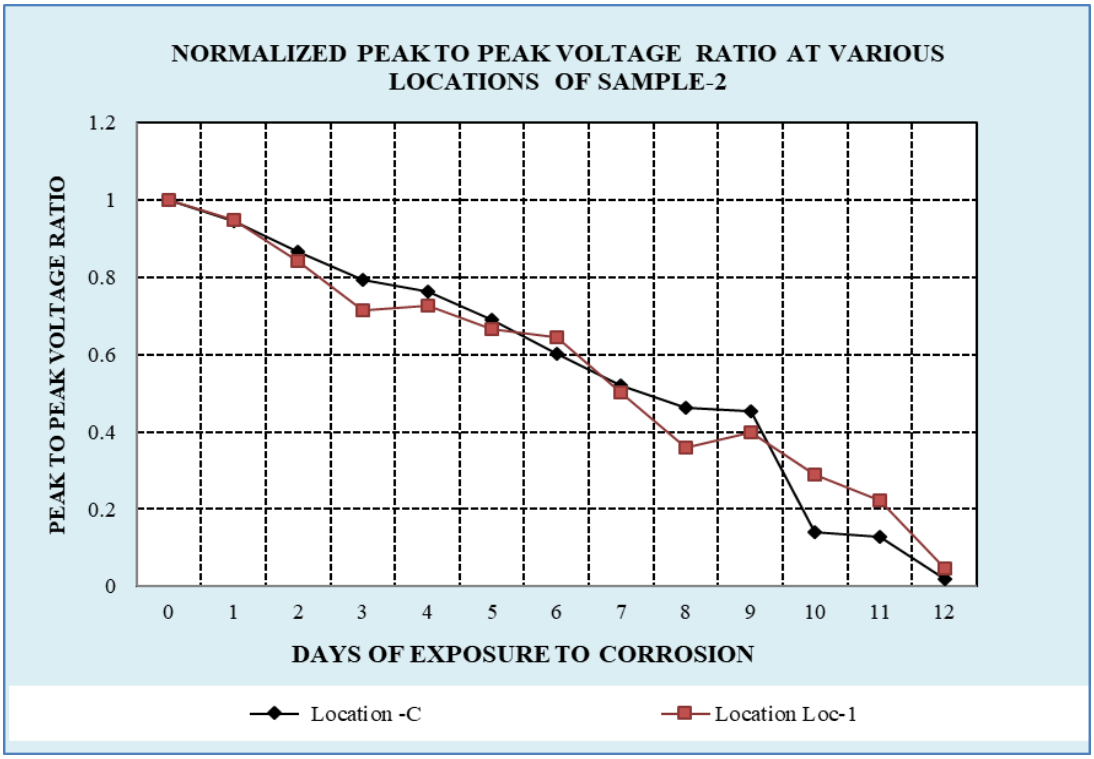

Figure 6.17 Trends of Normalized PT Signals for S_0 Mode at 0.5 MHz Frequency

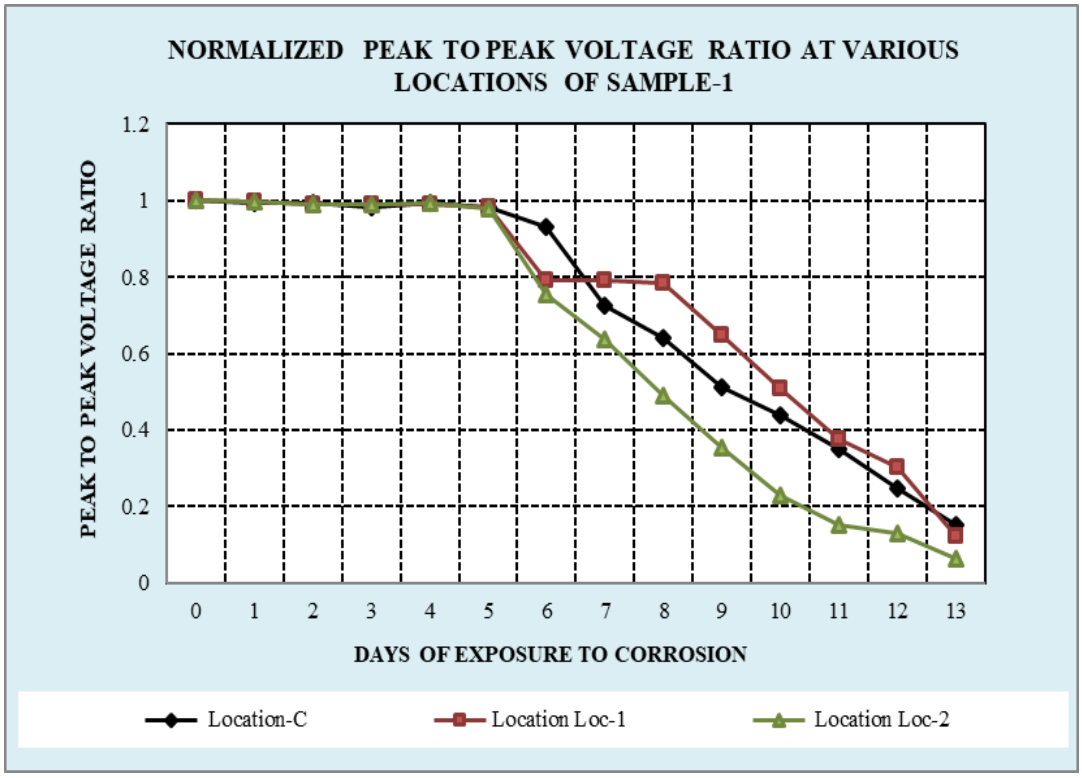

Figure 6.18 Trends of Normalized PT Signals for S_1 Mode at 1.0 MHz Frequency

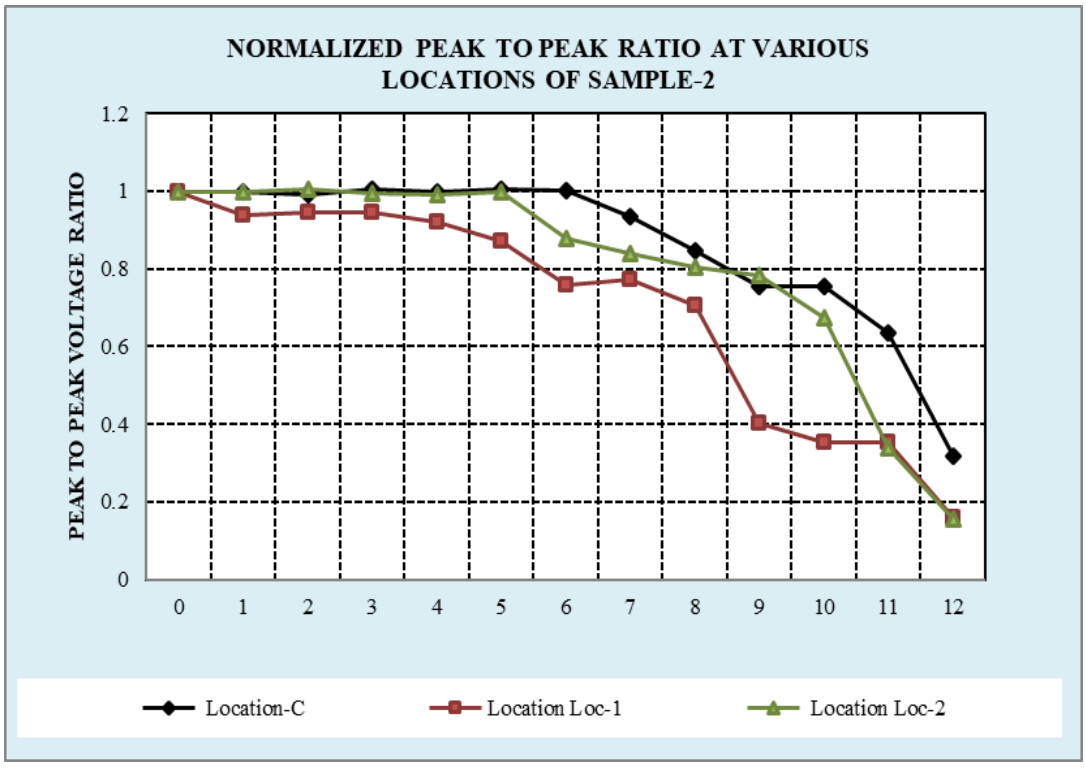

Figure 6.19 Trends of Normalized PT Signals for S_1 Mode at 1.0 MHz Frequency

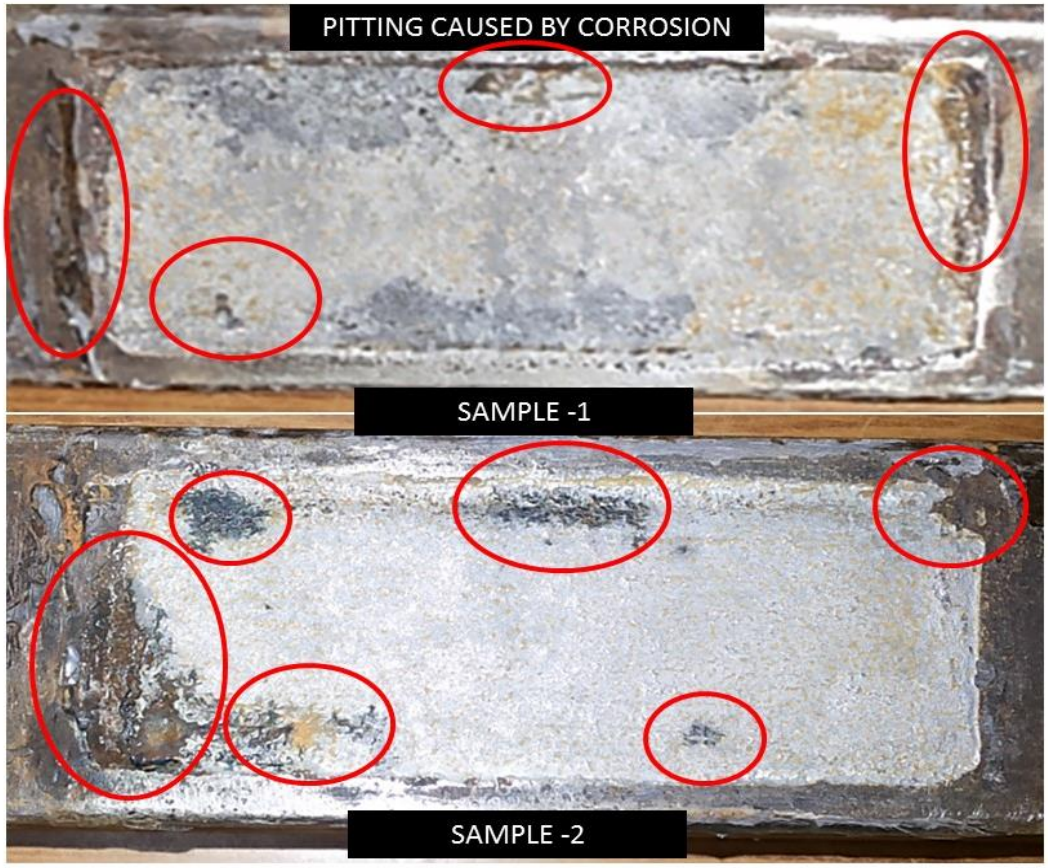

Figure 6.20 Formation of Pits Due to Corrosion in CFST Specimens

6.7.2 Destructive Testing

Along with the ultrasonic investigations, the samples undergoing corrosion have also been monitored for loss in mass with increasing every day. To investigate the effect of corrosion on CFST sections, destructive flexural tests have been performed on healthy and two corroded specimens with 6 days and 12 days' corrosion under two-point static loading. Figure 6.22 shows the load-deformation curves for healthy and corroded CFST sections. From the P-Δ curves, it has been observed that as the corrosion progressed, flexural strength dropped due to increasing pits and degradation. The flexural strength reduced by 9.82% with 6 days of exposure to accelerated corrosion in comparison to the healthy specimen. After 12 days of exposure, the flexural strength drops by 23.6% in comparison to the healthy beam. Visual inspection also confirmed that as the exposure to corrosion increases, beams experience severe and

widespread pitting (Figure 6.21). It is also observed that as exposure to corrosive environment increases, % loss in mass of the sample w.r.t mass of healthy sample increases. Initially mass is almost negligible at 7 days of corrosion. This signifies that the initial corrosion is slow and it does not lead to a significant mass loss. At the start of pitting, after the 7th day, there is a significant loss of mass and at 12 days 1.15% mass loss is observed. Results of destructive testing (set-up is shown in Figure 6.22) of the healthy specimen, 6 days corroded specimen and 12 days corroded CFST specimen are presented in Figure 6.24 and Table 6.1. P-Δ results (Figure 6.23) indicate the ductile behaviour of CFST sections. As corrosion increases, the ductility is reduced. It is observed that at peak load 61.42 kN, displacement is 7mm in healthy CFST sections, which increases to 15 mm at a load of 64.77 kN and still no crack was observed on the specimen. In partially corroded samples the peak load and displacement are 58.41 kN and 10.25 mm respectively and in fully corroded samples with increased corrosion, the strength falls to 49.46 kN and brittleness increases which can be very catastrophic if not monitored properly and at early stages. It indicates the importance of monitoring of progressive corrosion and other defects in CFST sections much before the sections completely collapse.

Table 6.1 Results for Flexural Testing of Corroded CFST Specimens

Sr. No.	**Results for testing of CFST specimens**			
1.	Exposure (days)	0 (Healthy)	6	12
1.	Days of Corrosion Exposure	0	6	12
2.	Mass Loss (%)	0	0.547	1.15
3.	Peak Strength (kN)	64.77	58.41	49.46
4.	Displacement (mm)	16.0	10.25	8.49

Figure 6.21 Flexural Testing Set-Up

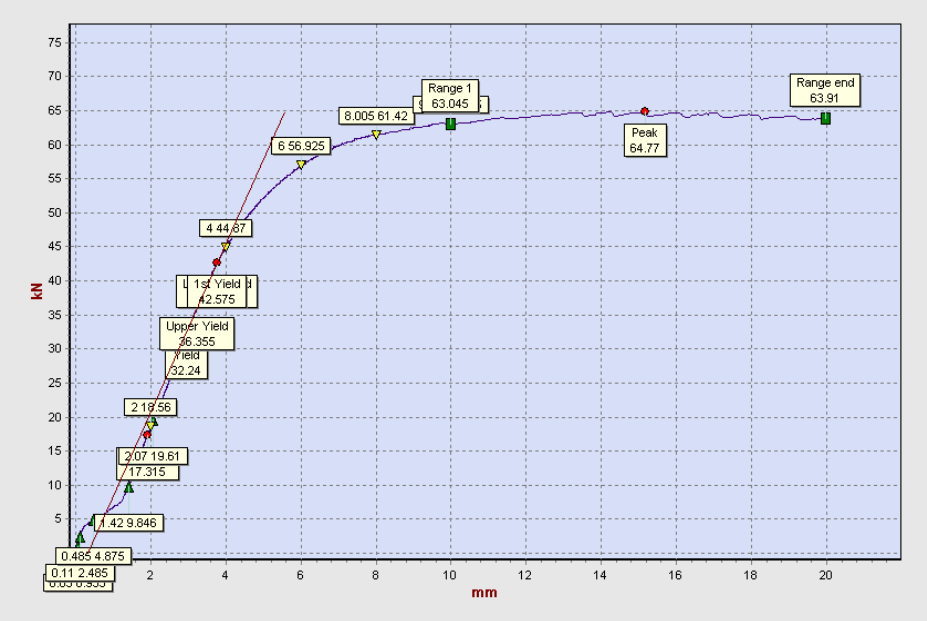

(a)

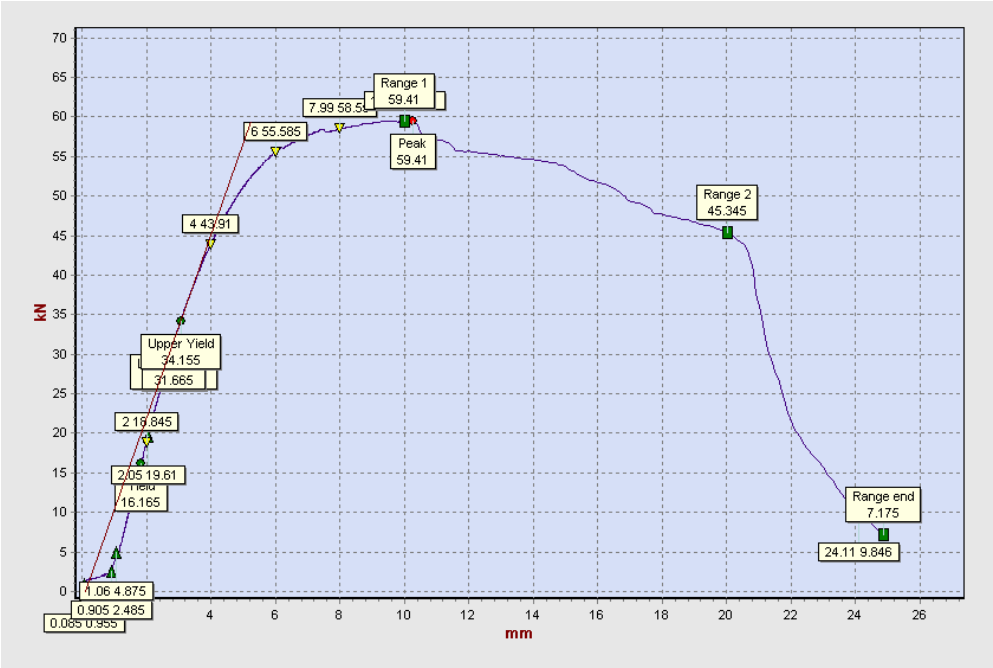

(b)

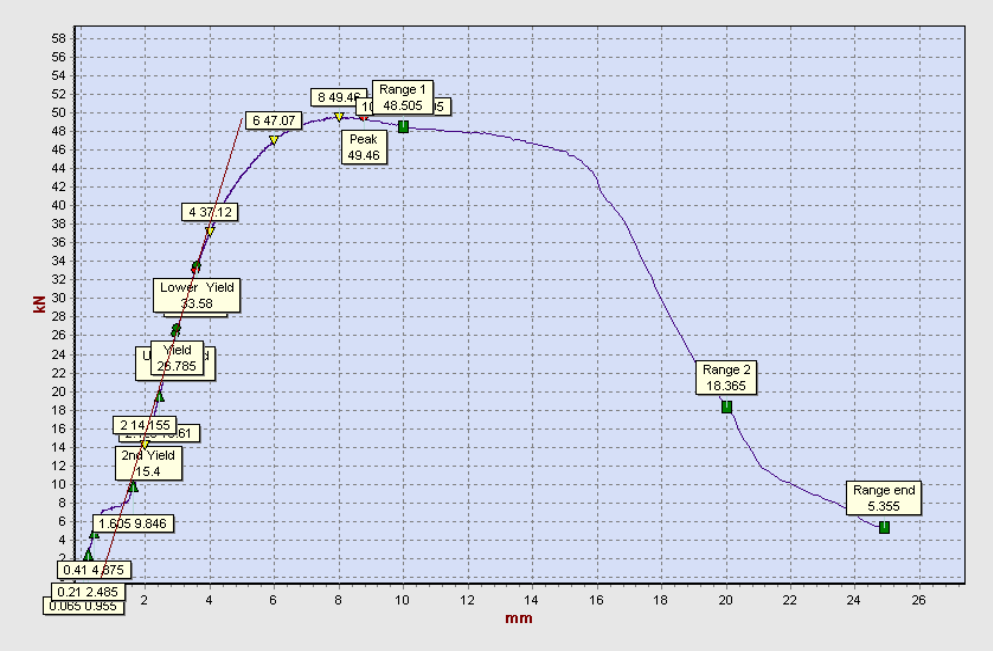

(c)

Figure 6.22 Load v/s Displacement Curves of (a) Healthy (b) 6 Days Corroded (c) 12 Days Corroded CFST Specimens

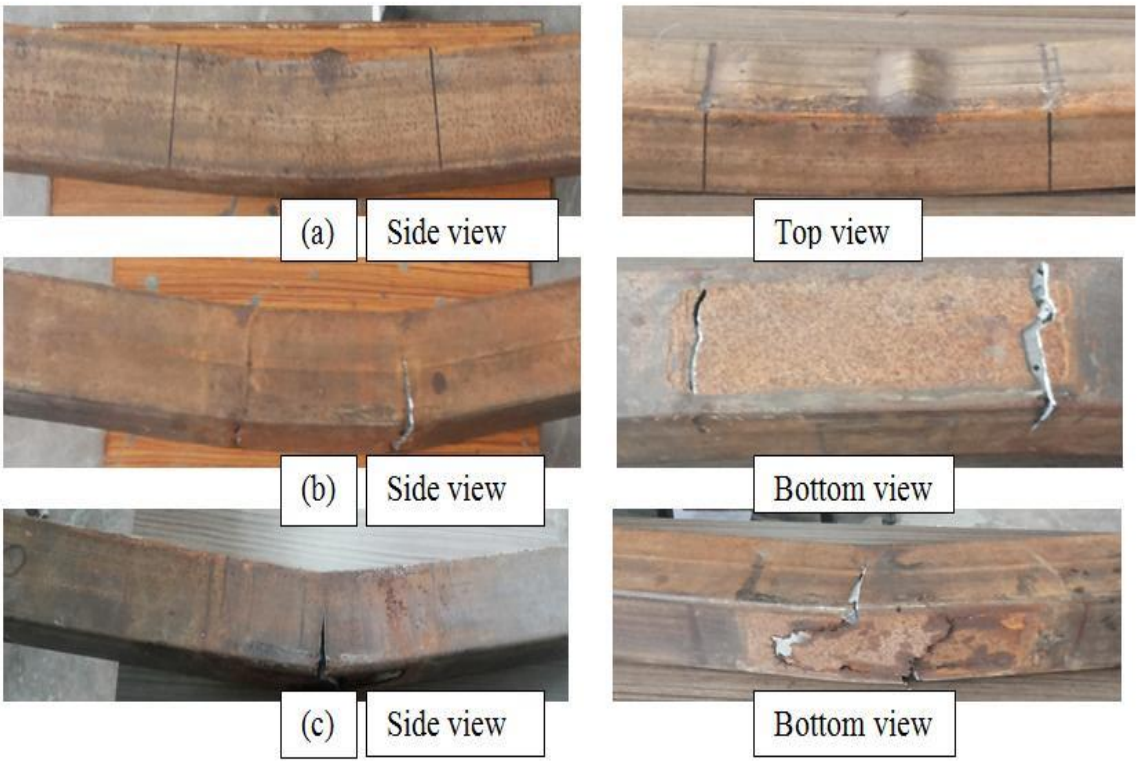

Figure 6.23 Flexural Testing of (a) Healthy (b) 6 Days Corroded (c) 12 Days Corroded CFST Specimens

6.8 CLOSURE

The present investigation illustrates a non-contact ultrasonic guided wave approach for detecting and quantifying various kinds of defects in concrete filled steel tubular sections, using a pair of mobile non-contact probes. Pulse transmission scanning of the CFST specimens helps in identifying the problem areas in the steel tube of CFST section due to various kinds of damage in the form of cracks, notches and corrosion. The reduction of the received signal with increased depth of notch could relate to the extent of the notch. Further the increase in the received signal strength with increased area of delamination points towards increased debond of steel tube from concrete causing less leakage and rise in signal strength. The methodology is further successfully applied to the CFST specimens undergoing with progressive accelerated corrosion. The attenuation of the received signal strength with increased corrosion points towards the significant area loss and pitting due to chloride corrosion and is well picked up this in-

situ and non-contact damage monitoring methodology. The technique developed in the study clearly suggests that non-contact ultrasonic guided wave approach can be used for degradation monitoring in CFST sections Practical application of the methodology would require further investigations of this noncontact procedure without using water as a couplant (Dry testing) and the research is underway and would be published further.

The experimental study carried out on CFST sections with simulated defects and corrosion damage shows the suitability of guided waves for detecting these damages. Different frequencies and modes have been explored to detect these damages in CFST sections. However, experimentally it has been established that lower frequencies exhibit better results as compared to higher frequencies. For detecting the notch damage (varying depth of notches), two modes S_0, and S_1 are used. Drop-in voltage amplitude with the increase in the depth of notch with all the modes at selected frequencies is observed. At 0.5 MHz frequency with S_0 mode, decrease in voltage is consistent and regular as the depth of notch increases. Whereas with S_1 mode at 1 MHz, the fall in the signal with the varying extent of defect has been found to be irregular and disproportionate. In corrosion study it is observed that There is fall in voltage amplitude with increase in corrosion exposure because the area of tube reduces and signal is consumed. For S_0 mode at 0.5 MHz, quick fall in voltage is observed at initial stage and sluggish response afterwards is noticed whereas for S_1 mode at 1 MHz, initially the fall in signals is sluggish but later on it is consistent. It has been established experimentally that lower frequencies exhibit better results as compared to higher frequencies.

CHAPTER-7

CONCLUSIONS

7.1 GENERAL

The present study has been conducted to examine the performance of beam-column joints in CFST frames experimentally. The study also includes the applications of FE modelling to predict the behaviour of CFST sections as columns and as part of. CFST frames. Health monitoring of CFST sections using ultra-sonic waves is also made part of the investigations.

As first step of the study CFST columns have been tested numerically and experimentally. Further, the behaviour of CFST beam-column joints have been investigated experimentally as well as numerically. Their performance as part of CFST frames, is also tested through numerical modelling. This is followed by demonstrating a non-contact ultrasonic guided wave approach for detecting and quantifying various kinds of defects in concrete filled steel tubular sections, using a pair of mobile non-contact probes.

The major conclusions drawn out of these experimental and numerical investigations, are summarized below:

7.2 CFST COLUMNS

1. The decrease in B/t ratio (increase in thickness) represents the enhancement in cross section of steel tube and results in enhancement of load carrying capacity of the CFST columns due to increase in the confinement pressure. Columns with B/t ratio of 15 have exhibited 43% (average) more load carrying capacity than the columns with B/t ratio of 22.5 for specimens of 300 mm length whereas 34% (average) increase has been observed in specimens of 450 mm length.

2. Increase in slenderness ratio (or L/B ratio) reduces the load carrying capacity of the column. Strength gain occurs in CFST columns only with the smaller slenderness ratio (L/B).

3. The strength of concrete core and grade of steel significantly influences the section capacity CFST columns. Sections (300 mm length) filled with M-40 concrete have exhibited 6% (average) higher strength than sections filled with M-25 grade of concrete. This increase is applicable to all values of B/*t* ratio or H/B ratio

4. Sections with higher grade of steel exhibit higher load carrying capacity irrespective of B/*t* ratio or H/B ratio.

5. The increased H/B ratio of or more aspect ratio results in deceased strength of columns and earlier yielding of wider side of specimens due to uneven spread of confinement pressure.

6. Comparison of experimental results and results obtained from FE model for CFST columns with various parameters exhibits appreciable closeness (only 4% average deviation has been observed from experimental values). It can be concluded that proposed FE model is capable of predicting the column behaviour very efficiently.

7.3 CFST BEAM- COLUMN JOINTS

1. The connections with extended end plate have shown higher strength over seat angle connections. In square beams to square column connections, extended end plate using through bolts and normal length bolts have shown 19.76 % and 18.18% higher strength over seat angle through bolted connections respectively.

2. In the category of rectangular beams connected to square columns, extended end plate connections using through and normal length bolts have shown 26.6 % and 35.7 % higher strength over seat angle connections respectively.

3. Through bolted connections have exhibited better strength over connections with bolts of normal length in all categories. End plate and seat angle connections using through bolts have exhibited 13.3 % and 11.51 % higher strength over connections with normal length bolted connections respectively.

4. In the category of rectangular beams connected to square columns similar trends are shown. Through bolted connections have shown has got 4.14% to 11.2 % higher strength than connections with normal length bolts.

5. It is observed that variation in size of end plate, dia and grade of bolts and bond strength of the matrix significantly affected the capacity of the joints. Specimens with 10 mm dia bolts have shown 10% to 25.7% higher strength over specimens with 8 mm dia bolts.

6. The experimental results show that the proposed bolted connections behave as connections with partial strength as per the EC3 specification and display good stiffness and strength.

7. The developed FE models have predicted the behaviour of connections very closely to the experimental test models.

7.4 NON-LINEAR MODELLING OF CFST FRAMES

1. The CFST frame with extended end plate connections using through bolts have shown higher strength over frame with connections using normal length bolts.

2. Single storey frame with end-plate through bolted connections has shown 17.5 % higher strength and performed better in terms of stiffness over frame having connections with bolts of normal length. Whereas double storey frame with end-plate through bolted type connections has shown 16.05 % higher strength and performed better in terms of stiffness over frame having connections with bolts of normal length.

3. 3-D double storey frame with end-plate through bolted connections has exhibited better strength (21.9% higher) over the frame with connections using normal length bolts.

4. Hence, it can be concluded that frame with through bolted end plate connections performed better similarly as it has been observed when tested as individual exterior connection under vertical loads at beam tip.

7.5 MONITORING CFST SECTIONS USING GUIDED WAVES

The experimental study using Pulse transmission scanning has been carried out on CFST sections with simulated defects and corrosion damage to explore the suitability of guided waves for detecting these damages. Different frequencies and modes have been explored to detect various kinds of damage in the form of cracks, notches and corrosion in CFST sections. However, experimentally it has been established that lower frequencies exhibit better results as compared to higher frequencies. The reduction of the received signal with increased depth of notch could relate to the extent of the notch. Further the increase in the received signal strength with increased area of delamination points towards increased debond of steel tube from concrete causing less leakage and rise in signal strength. The methodology is further successfully applied to the CFST specimens undergoing with progressive accelerated corrosion. The attenuation of the received signal strength with increased corrosion points towards the significant area loss and pitting due to chloride corrosion and is well picked up this in-situ and non-contact damage monitoring methodology. Conclusions of the study can be summarized as under.

7.5.1 Notch Defect Study

This study is carried out by inducing notch of varying depths 1,2, and through cut (3.2mm). Two modes are used for detecting the notch damage S_0, and S_1. Following conclusions are drawn from this study:

1. There is a drop-in voltage amplitude with the increase in the depth of notch with all the three modes at selected frequencies.
2. At 0.5 MHz frequency with S0 mode, decrease in voltage is consistent and regular as the depth of notch increases.
3. With S_1 mode at 1 MHz, there is a visible drop in signal with increase in depth of the notch. But the fall in the signal with the varying extent of defect has been found to be irregular and disproportionate.

7.5.2 Corrosion Study

1. There is fall in voltage amplitude with increase in corrosion exposure. It is because the area of tube reduces and signal consumption is more.

2. In comparison to simulated machined notches, with clear area reduction, corrosion being non-uniform and widespread, causes relatively less attenuation of signal.

3. For S_0 mode at 0.5 MHz, quick fall in voltage is observed at initial stage and consistent response afterwards is noticed.

4. For S_1 mode at 1 MHz, initially signal fall in signals is sluggish but later the fall is noticeable. Maximum drop in voltage is observed at Loc-1 and Loc-3 location of the section.

5. It has been established experimentally that lower frequencies exhibit better results as compared to higher frequencies

7.6 SCOPE OF FUTURE WORK

7.6.1 CFST Beam-Column Joints and Frames

The present study of CFST beam-column joints is just an awakening to the topic. The practical use of these joints as part of CFST frames needs a lot of detailed investigations

1. The future study needs to be elaborated to the detailed experimental investigation using full scale specimens subjected to monotonic and cyclic loads.

2. The effect of combined actions on the joint behavior namely bending, shear and axial action needs to studied experimentally.

3. Extended end plate connections with varying size and thickness can considered to evaluate the behaviour of such connections.

4. Various types of bolts can be tested especially blind bolts which are an innovation in this field.

5. Study of full-scale frames using end plate bolted connections using self-compacting concrete and considering various parameters can be carried out for

push-over loads and cyclic loads to assess their performance under seismic loads.

7.6.2 Use of Ultrasonic Guided Waves

Guided waves provide effective way of characterizing defects in various geometries. Therefore, it becomes important to obtain reliable results from this technique and to find out better implementation of this technique. The experimental methodology discussed in this work can further extended for:

1. Ultrasonic investigations using guided waves can be performed on various sections of varying thicknesses and configurations are required for practical application of the methodology.
2. Analytical model can be developed and correlated with non-destructive testing.
3. Detection of possible defects in connections of such structures such as welding defects and cracks can also be considered using guided waves.
4. Practical application of the methodology would require improvisation of set up for non-contact-based damage monitoring methodology eliminating the couplant media.

7.7 OVERVIEW

The concrete-filled steel tubular structure can be an efficient alternative system to the steel or the reinforced concrete system. Some queries on the feasibility of the CFST system should be completely evaluated for its extensive application. The thorough comparison of advantages and disadvantages of the CFST system with the traditional systems; the steel and RC system should be conducted in the future. The more detailed study of connection system, using self-compacting concrete, high performance concrete and more efficient bolts like blind bolts as well as the life-cycle performance evaluation should be considered in the future studies.

Guided waves with low frequencies can be successfully used for health monitoring of various damages in CFST sections. Practical application of the methodology would require further investigations on various sections of varying thicknesses and configurations.

REFERENCES

1. Abed, F., Alhamaydeh, M. and Abdalla, S. (2013). 'Experimental and numerical investigations of the compressive behavior of concrete filled steel tubes (CFSTs)', *Journal of Constructional Steel Research,* vol. 80, pp. 429-439.
2. Achenbach, J. D. (1975). *Wave propagation in solids*. Elsevier Science Publishers, 1975.
3. Achenbach, J. D. (1984). *Wave propagation in elastic solids*. New York: North-Holland Publishing Company.
4. Ahmad, R. and Kundu, T. (2012). 'Structural health monitoring of steel pipes under different boundary conditions and choice of signal processing techniques', *Advances in Civil Engineering*, vol. 2012, pp. 1-14. Article ID 813281.
5. Alostaz, Y.M. and Schneider, S.P. (1996). *'*Analytical behavior of connections to concrete-filled steel tubes*', Journal of Constructional Steel Research*, vol. 40, no. 2, pp. 95–127.
6. American Institute of Steel Construction. *Load and resistance factor design specification for structural steel buildings*, Chicago: American Institute of Steel Construction; 1994.
7. American Concrete Institution, ACI-318, *Building code requirements for reinforced concrete*, Detroit (MI) ACI, 2002.
8. Arivalagan, S. and Kandasamy, S. (2008). 'Flexural behaviour of concrete-filled SHS beams*', Journal of Civil Engineering and Management*, vol. 14, no .2, pp. 107-114.
9. Arivalagan, S. (2010). 'Finite Element analysis on the flexural behaviour of concrete filled steel tube beams*', Journal of Theoretical and Applied Mechanics*, Warsaw, vol. 48, no. 2, pp. 505-516.
10. Arivalagan, S. and Kandasamy, S. (2010). 'Study on Concrete–Filled Steel Member Subjected to Cyclic Loading', *International Journal of Civil and Structural Engineering*, vol. 1, no. 3. pp. 458-465.
11. ATENA (2012). *Advanced Tool for Engineering Nonlinear Analysis*, Version 4.3.1g, Cervenka Consulting Ltd., Prague, Czech Republic.

12. Bergmann, R. (1994). 'Load Introduction in Composite Columns Filled with High Strength Concrete', Tubular Structures VI, *Proceedings of the Sixth International Symposium on Tubular Structures*, Grundy, P., Holgate, A., and Wong, B. (eds.), Melbourne, Australia, 14-16 December 1994, A. A. Balkema, Rotterdam, The Netherlands, pp. 373-380.

13. Beutel, J., Thambiratnam, D. and Perera, N. (2001). 'Cyclic behaviour of concrete filled steel tubular column to steel beam connections', *Journal of Engineering Structures*, vol. 24, no.1, pp. 29–38.

14. Bridge, R.Q., O'Shea, M.D., Gardner, P., Grigson, R. and Tyrell, J. (1995). 'Local buckling of square thin-walled steel tubes with concrete in-fill', *In: Proceeding of. International Conference on Structural Stability and Design*, Sydney, pp. 307–14.

15. Bruneau, M. and Bisson, M. (1998). 'Hysteretic behavior of existing and retrofitted concrete-encased riveted stiffened seat angle connections', *Engineering Structures*, vol. 22, pp. 1086–1096.

16. Chakrabarty, J. (1998). *Theory of Plasticity*, 2nd edition, McGraw-Hill Book Co, Singapore.

17. Chen, W.F. and Toma, S. (1994). *Advanced analysis of steel frames*, Boca Raton, Florida: CRC Press. 1994.

18. Chen, Z., Qin Y. and Wang, X. (2015). 'Development of connections to concrete-filled rectangular tubular columns', *Advanced Steel Construction*, vol. 11, no. 4, pp. 408-426.

19. Cheng, C.T., Hwang, P.S., Lu, L.Y. and Chung, L.L. (2000). 'Connection behaviors of steel beam to concrete-filled circular steel tubes*', In: Proceeding of 6th ASCCS Conference*, Los Angeles, USA. pp. 581–589.

20. Cervenka, V., Jendele, L., Cervenka, J. (2000). *ATENA Theory Manual*, Part-1, Prague.

21. Dunberry, E., LeBlanc, D. and Redwood, R.G. (1987). 'Cross-section strength of concrete-filled HSS columns at simple beam connections', *Canadian Journal of Civil Engineering*, vol. 14, pp. 408–17.

22. Elchalakani, M., Zhao, X.L. and Grzebieta, R.H. (2001). 'Concrete-filled circular steel tubes subjected to pure bending', *Journal of Constructional Steel Research,* vol. 57, no.11, pp. 1141-1168.

23. Elchalakani, M., Zhao, X.L. and Grzebieta, R.H. (2004). 'Concrete filled steel circular tubes subjected to constant amplitude cyclic pure bending', *Engineering Structures*. Vol. 26, pp. 2125-2135.

24. Ellobody, E., Young, B., and Lam, D. (2006). 'Behaviour of normal and high strength concrete-filled compact steel tube circular stub columns', *Journal of Constructional Steel Research,* vol. 62, no.7, pp. 706-715.

25. Elremaily, A. and Azizinamini, A. (2001). 'Experimental behavior of steel beam to CFT column connections', *Journal of Constructional Steel Research*, vol. 57, no.9, pp. 1009–19.

26. Eramma, H. and Niranjan, B.R. (2014). 'Experimental Investigation on Reinforced Concrete Filled Steel Rectangular Fluted Columns', *International Journal of Scientific & Engineering Research,* vol. 3, no. 11.

27. Ervin, B.L. and Reis, H. (2008). 'Longitudinal guided waves for monitoring corrosion in reinforced mortar', *Measurement Science & Technology,* vol. 19, no.1, pp. 1–19.

28. Ervin, B.L., Kuchma, D.A., Bernhard, J.T. and Reis, H. (2009). 'Monitoring corrosion of rebar embedded in mortar using high frequency guided ultrasonic waves', *Journal of Engineering Mechanics,* vol. 135, no.1, pp. 9–19.

29. Evirgen, B., Taskin, K. and Tuncan, A. (2014). 'Structural behavior of concrete filled steel tubular sections (CFT/CFST) under axial compression', *Thin-Walled Structures,* vol. 80, pp. 46–56.

30. Eurocode 3 (1992). *Design of steel structures,* Part 1.1, General rules and rules for buildings, London.

31. Eurocode 3 (2001). *Design of steel structures,* Part 1-1, General structural rules. 1993-1-1: 2001.

32. Eurocode 4 (2004). *Design of composite steel and concrete structures*. Part 1-1, General rules and rules for buildings, CEN, 2004.

33. Eurocode 4 (2005). *Design of composite steel and concrete structures,* Part 1-1,

General rules and rules for buildings, CEN, 2005.

34. FEMA 267. *Interim guidelines: evaluation, repair, modification and design of welded steel moment frame structures*. Federal Emergency Management Agency; 1995.

35. FEMA-350, *Recommended seismic design moment-frame buildings*. Federal Emergency Management Agency; 2000.

36. France, J.E. (1997). 'Bolted Connections between Open Section Beams and Box Columns'. PhD Thesis, University of Sheffield, U.K.

37. France, J.E., Davison, B.J. and Kirby, P.A. (1999). 'Moment-capacity and rotational stiffness of endplate connections to concrete-filled tubular columns with flow drilled connectors', *Journal of Constructional Steel Research*, 1999, vol. 50, no. 1, pp. 35-48.

38. Fujimoto, T., Nishiyama, I., Mukai, A. and Baba, T. (1995). 'Test results of eccentrically loaded short columns square CFT columns', *In: Proc. of the Second Joint Technical Coordinating Committee Meeting on Composite and Hybrid Structures*, Hawaii, June, 1995, pp. 26–28.

39. Fujimoto, T., Nishiyama, I. and Mukai, A. (1997). 'Test Results of CFT Beam-to-Column Connection', *US-Japan Cooperative Earthquake Research Program: Composite and Hybrid Structures*, Monterey, California, USA.

40. Fujimoto, T., Inai, E., Tokinoya, H., Kai, M., Mori, K., Mori, O., and Nishiyama, I. (2000). 'Behavior of Beam-To-Column Connection of CFT Column System Under Seismic Force', *Composite and Hybrid Structures, Proceedings of the Sixth ASCCS International Conference on Steel-Concrete Composite Structures*, Xiao, Y. and Mahin, S. A. (eds.), Los Angeles, California, March 22-24, 2000, Association for International Cooperation and Research in Steel-Concrete Composite Structures, Los Angeles, California, pp. 557–564.

41. Fujimoto, T., Mukai, A., Nishiyama, I. and Sakino K (2004). 'Behavior of eccentrically loaded concrete-filled steel tubular columns', *Journal of Structural Engineering*, ASCE, vol. 130, no. 2, pp. 203-12.

42. Furlong, R.W. (1967). 'Strength of steel encased concrete beam-columns', *Journal of the Structural Division Proc. American Society of Civil Engineers*, vol. 93 (ST5), pp. 115–30.

43. Garg, M., Sharma, S., Sharma, S. and Mehta, R. (2016). 'Non-contact damage monitoring technique for FRP laminates using guided waves', *Smart Structures and Systems,* vol. 17, no.5, pp. 795-817.

44. Garg, M., Sharma, S., Sharma, S. and Mehta, R. (2016). 'Non-contact damage monitoring technique for FRP laminates using guided waves', *Smart Structures and Systems,* vol. 17, no.5, pp. 795-817.

45. Garg, M., Sharma, S., Sharma, S. and Mehta, R. (2017). 'Effect of hygro-thermal aging on GFRP composites in marine environment', Steel and Composite Structures, vol. 25, no. 1, pp. 93-104.

46. Ge, H. and Usami, T. (1992). 'Strength of concrete-filled thin walled steel box columns: Experiments', *Journal of Structural Engineering,* ASCE, vol. 118, no.11, pp. 3036-3054.

47. Giakoumelis, G. and Lam, D. (2004). 'Axial capacity of circular concrete filled tube columns*', Journal of Constructional Steel Research,* vol. 60, no. 9, pp. 1049-1068.

48. Gourley, B.C., Tort, C., Hajjar, J. F. and Schiller, P.H. (2001). 'A Synopsis of Studies of the Monotonic and Cyclic Behavior of concrete-Filled Steel Tube Beam-Columns', *Structural Engineering Report No ST-0-4,* Department of Civil Engineering Institute, Technology University of Minneapolis MN, USA, pp. 262.

49. Gourley, B.C., Tort, C., Denavit, M.D., Schiller, P.H. and Hajjar, J.F. (2008). 'A synopsis of studies of the monotonic and cyclic behavior of concrete-filled steel tube members, connections and frames', *Report No. NSEL-008, NSEL Report Series. Department of Civil and Environmental Engineering,* University of Illinois at Urbana-Champaign.

50. Gupta, P.K. Sarda, S.M. and Kumar, M.S. (2007). 'Experimental and computational study of concrete filled steel tubular columns under axial loads', *Journal of Constructional Steel Research,* vol. 63, pp. 182-193.

51. Gupta, P. K. and Katariya, S. K. (2014). 'Effect of Cross-Section on Flexural Capacity of Square Concrete-Filled Steel Tube (CFST) Beam', *International Journal of Applied Engineering Research*, vol. 9, no. 7, pp. 783-789.

52. Hajjar, J. F., Schiller, P. H. and Molodan, A. (1998). 'A Distributed Plasticity Model for Concrete-Filled Steel Tube Beam-Columns with Interlayer Slip', *Journal of Engineering Structures*, vol. 20, no.8, pp. 663-676.

53. Hajjar, J.F. and Tort, C. (2010). 'Mixed finite-element modeling of rectangular concrete-filled steel tube members and frames under static and dynamic loads', *Journal of Structural Engineering, ASCE,* vol. 136, no.6, pp. 654–64.

54. Han, L.H., (2002). 'Tests on stub columns of concrete-filled RHS sections', *Journal of Constructional Steel Research,* vol. 58, no. 3, pp. 353-72.

55. Han, L.H. (2004). 'Flexural behaviour of concrete-filled steel tubes', *Journal of Constructional Steel Research*, vol. 60, no.2, pp. 313-337.

56. Han, L. H. and Yang, Y. F. (2006). 'Cyclic Performance of Concrete-filled Steel CHS Columns under Flexural Loading', *Journal of Constructional Steel Research,* vol. 61, no. 4, pp. 423-452.

57. Han, L.H., Yao, G.H. and Tao, Z. (2007). 'Performance of concrete-filled thin-walled steel tubes under pure torsion', *Thin-Walled Structures,* vol.45, no.1, pp. 24–36.

58. Han, L. H., Wang, W. D. and Zhao, X. L. (2008). 'Behaviour of steel beam to concrete-filled SHS column frames: Finite element model and verifications', *Engineering Structures*, vol. 30, no. 6, pp. 1647-58.

59. Han, L. H., Wang, W. D. and Zhong, T. (2011). 'Performance of circular CFST column to steel beam frames under lateral cyclic loading', *Journal of Constructional Steel Research,* vol. 67, pp. 876-890.

60. Han, L.H., Hou, C. and Wang, Q.L. (2012). 'Concrete filled steel tubular (CFST) members under loading and chloride corrosion: experiments', *Journal of Constructional Steel Research,* vol.71, no. 1, pp. 11–25.

61. Han, L. H., Li, W. and Bajorhovde, R. (2014). 'Development and advances applications of concrete filled steel tubular (CFST) Structures: Members', *Journal of Constructional Steel Research,* vol. 100, pp. 211-228.

62. Hassan, M. K., Tao, Z., Mirza, O., Song, T.Y. and Han, L.H. (2014). 'Finite element analysis of steel beam-CFST column joints with blind bolts', *The Australasian Structural Engineering 2014 Conference (ASEC 2014),* 9-11 July 2014, Auckland, New Zealand, Paper No 56.

63. He, C., Van Velsor, J.K., Lee, C.M. and Rose, J.L. (2006). 'Health monitoring of rock bolts using ultrasonic guided waves', *Quantitative nondestructive evaluation, In: Thompson, D.O. and Chimenti, D.E.(eds), AIP Conference Proceedings,* Aarhus, Denmark, pp.195–201.

64. Herrera, R. (2005). 'Seismic behaviour of concrete filled tube column-wide flange beam frames'. Ph.D. dissertation. Bethlehem (PA, USA): Department of Civil and Environmental Engineering, Lehigh University.

65. Huang, C. (2002). 'Axial load behaviour of Stiffened concrete-filled Steel columns', *Journal of Structural Engineering,* ASCE, vol.128, no. 9, pp. 1222-1230.

66. Hu, H.T., Huang, C.S., Wu, M.H. and Wu, Y.M. (2003). 'Nonlinear Analysis of Axially Loaded Concrete-Filled Tube Columns with Confinement Effect', *Journal of Structural Engineering,* ASCE, vol. 129, no. 10, pp. 1322-1329.

67. Hu, H.T., Huang, C. S. and Chen, Z. L. (2005). 'Finite element analysis of CFT columns subjected to an axial compressive force and bending moment in combination', *Journal of Constructional Steel Research*. vol. 62, pp. 1692–712.

68. Hu, J.W., Choi, E. and Leon, R.T., (2011). 'Design, Analysis and Application of Innovative Composite PR Connections between Steel Beams and CFT Columns', Smart Materials and Structures, 2011, vol. 20, No. 2, pp. 0964-1726.

69. IS: 1608-1972, *Indian standard for Method for Tensile testing of Steel products,* Bureau of Indian Standards, New Delhi.

70. IS: 4923-1997, *Indian standard hollow steel sections for structural use-specifications,* Bureau of Indian Standards, New Delhi.

71. IS: 1161-1998, *Product Manual for Certification of Steel Tubes for Structural Purposes,* Bureau of Indian Standards, New Delhi.

72. IS: 456-2000, *Indian standard for plain and reinforced concrete code of practice,* Bureau of Indian Standards, New Delhi.

73. IS: 1364-2003, *Hexagon Head Bolts, Screws and Nuts of Product Grades A and B*, Bureau of Indian Standards, New Delhi.

74. Jayaganesh, S., Raja Murugadoss, J. Ganesh Prabhu, G., and Jegan, J. (2015), 'Effects of concentrical partial (local) compression on the structural behavior of concrete filled steel tubular column', *Advances in Materials Science and Engineering*, vol. 2015, Article ID 491038, 9 pages.

75. Kang, J.Y., Choi, E.S., Chin, W.J. and Lee, J.W. (2007). 'Flexural behavior of concrete-filled steel tube members and its application', *International Journal of Steel Structures*, vol. 7, pp. 319-324.

76. Kaushik, K., Sharma, A.K. and Kumar, R. (2013). 'A Review on Finite Element analysis of beam to column endplate bolted connection', *IOSR Journal of Mechanical and Civil Engineering*, volume 8, no. 1, pp, 97-103.

77. Kaushik, K., Sharma, A.K. and Kumar, R. (2013). 'Modeling and FE analysis of column to beam end-plate bolted connection', *Engineering Solid Mechanics*, vol. 2, pp. 51-66

78. Kawaguchi, J., Morino, S. and Sugimoto, T. (1997). 'Elasto-plastic behaviour of concrete-filled steel tubular frames', *In: Composite construction in steel and concrete III, Proceedings of an engineering foundation conference*, pp. 272–281.

79. Kilpatrick, A.E. and Rangan, B.V. (1997). '*Deformation - Control analysis of composite concrete columns'*, Research report No 3/97, July 1997, School of Civil Engineering, Curtin University of Technology, Perth, Western Australia.

80. Kim, J. O., Wang, Y. and Bau, H. H. (1991) 'The effect of an adjacent viscous fluid on the transmission of torsional stress waves in a submerged waveguide', *Journal of Acoustical Society of America*, vol. 89, pp. 1414–1422.

81. Kim, J., Yoon, J. C. and Kang, B. S. (2007). 'Finite element analysis and modeling of structure with bolted joints', *Applied Mathematical Modelling*, vol. 31, no. 5, pp. 895-911.

82. Knowles, R.B. and Park, R. (1969). 'Strength of concrete filled steel tubular columns'. *Journal of the Structural Division*, ASCE, vol. 105, no.12, pp. 2565–2587.

83. Knowles, R.B. and Park, R. (1969). 'Strength of concrete filled steel tubular columns'. *Journal of the Structural Division,* ASCE, vol. 105, no.12, pp. 2565–2587.

84. Kosteski, N. and Packer, J.A. (2003). 'Welded Tee-to-HSS Connections', *Journal of Structural Engineering,* vol. 129, no. 2, pp. 151-159.

85. Leon, R.T., Hajjar, J.F. and Gustafson, M.A. (1998). 'Seismic response of composite moment-resisting connections. I: Performance', *Journal of Structural Engineering,* vol. 124, no. 8, pp. 868-76.

86. Liang, Q.Q., Uy, B., Bradford, M.A. and Ronagh, R.H. (2005). 'Strength analysis of steel-concrete composite beams in combined bending and shear*',* *Journal of Structural Engineering,* ASCE, vol. 131, no.10, pp. 1593-1600.

87. Liang, Q. Q. (2008). 'Nonlinear analysis of short concrete-filled steel tubular beam columns under axial load and biaxial bending', *Journal of Constructional Steel Research,* vol. 64, pp. 295-304.

88. Liew, J.Y.R., and Uy, B. (2001). 'Advanced analysis of composite frames', *Prog. Structural Engineering Materials,* vol. 3, pp. 159-169.

89. Liew, J.Y.R., Chen, H. and Shanmugam, N.E. (2001). 'Nonlinear analysis of steel frames with composite beams', *Journal of structural Engineering (ASCE),* vol. 127, no. 2, pp. 361-370.

90. Lin, M.L. and Tsai, K.C. (2001). 'Behavior of double-skinned composite steel tubular columns subjected to combined axial and flexural loads', *Proceedings of the first international conference on steel & composite structures,* Pusan, Korea, June14-16 2001, pp. 1145-52.

91. Liu, D., Gho, W.M. and Yuan, J. (2003). 'Ultimate capacity of high-strength rectangular concrete-filled steel hollow section stub columns', *Journal of Constructional Steel Research,* vol. 59, no.12, pp. 1499-1515.

92. Liu, D. (2004). 'Behaviour of high strength rectangular concrete-filled steel hollow section columns under eccentric loading', *Thin-Walled Structures*. vol. 42, pp. 1631–1644.

93. Lu, L.H., Puthli, R.S. and Wardenier, J. (1993). 'Semi-Rigid Connections Between Plates and Rectangular Hollow Section Columns', '*In: Proceedings of*

the Fifth International Symposium on Tubular Connections, Nottingham, UK, E & FN Spon, London, pp. 723-731.

94. Lu, L.H. and Wardenier, J. (1998). 'The ultimate strength of I-beam to RHS column connections', *Journal of Constructional Steel Research*, vol. 46, no. 1-3, pp. 139.

95. Mander, J. B., Priestley, M. J. N., and Park, R. (1998). 'Theoretical stress-strain model for confined concrete', *Journal of Structural Engineering*, vol. 114, no.8, pp. 1804–1826.

96. Matsui, C. (1995). 'Strength and behaviour of frames with concrete filled square steel tubular columns under earthquake loading', *In: Proceeding of 1st international specialty conference on concrete filled steel tubular structures*, pp. 104–111.

97. Menetrey, Ph. and Willam, K. J. (1995). 'Triaxial Failure Criterion for Concrete and its Generalization', *ACI Structural Journal*, vol. 92, no.3, pp. 311–318.

98. Mourad, S., Korol, R.M. and Ghobarah, A. (1996). 'Design of extended end-plate connections for hollow section columns', *Canadian Journal of Civil Engineering*, vol. 23, pp. 277-286.

99. Na, W., Kundu, T. and Ehsani, M.R. (2002). 'Ultrasonic guided waves for steel bar concrete interface testing', *Materials Evaluation*, vol. 60, pp. 437–444.

100. Na, W.B. and Kundu, T. (2002). 'Underwater Pipeline Inspection Using Guided Waves', *Journal of Pressure Vessel Technology*, vol. 124, No. 2, pp. 196-200.

101. Na, W.B., Kundu, T. and Ryu, Y.S. (2002). 'Underwater Inspection of Concrete-Filled Steel Pipes Using Guided Waves', *KSCE Journal of Civil Engine*ering, vol. 6 no.1, pp. 25–31.

102. Na, W. B. and Kundu, T. (2002). 'EMAT-Based Inspection of Concrete Filled Steel Pipes for Internal Voids and Inclusions', *ASME Journal of Pressure Vessel Technology*, vol. 124, pp. 265-272.

103. Na, W., Kundu, T. and Ehsani, M.R. (2003). 'Lamb waves for detecting delamination between steel bars and concrete', *Computer-Aided Civil and Infrastructure Engineering*, vol. 18, pp. 57–62.

104. Neogi, P.K., Sen, H.K. and Chapman, J.C. (1969). 'Concrete-filled tubular steel columns under eccentric loading', *The Structural Engineer*, vol. 47, no. 5, pp. 187–195.

105. Neves, L.F.C., Silva, L.A.P.S. and Vellasco, P.C.G.S. (2002). 'Experimental behaviour of end plate I-beam to concrete-filled rectangular hollow section column joint', *Proc. of the Third International Conf. on Advances in Steel Structures* (ICASS '02), Hong Kong, 9-11 December 2002, pp. 253-260.

106. Neves, L.F.C., Silva, L.A.P.S. and Vellasco, P.C.G.S. (2003). 'Experimental behaviour of end plate I-beam to concrete-filled rectangular hollow section column joints under cyclic loadings', *In Proc. of the Fourth International Conf. on the Behaviour of Steel Structures in Seismic Areas* (STESSA '03), Naples Italy 9-12 June 2003, pp. 277-283.

107. Nishiyama, I., Morino, S., Sakino, K., Nakahara, H. and Fujimoto, T. and Mukai, A. (2002). 'Summary of research on concrete-filled structural steel tube column system', carried out under *the US–Japan cooperative research program on composite and hybrid structures*. BRI Research Paper No.147. Japan: Building Research Institute.

108. Oliveira, W.L.A., Hardin, S.D., Ana Lucia, H.C. and J.L., El Debs, M.K., (2009). 'Influence of concrete strength and length/diameter on the axial capacity of CFT columns', *Journal of Constructional Steel Research,* vol. 65, no. 12, pp. 2103-2121.

109. O'Shea, M.D. and Bridge, R.Q. (1997). 'Local buckling of thin-Walled circular steel sections with or without internal restraint', *Journal of Constructional Steel Research*, vol. 41, no. 2-3, Feb-March 1997, pp. 137-157.

110. O'Shea, M.D. and Bridge, R.Q. (2000). 'Design of circular thin-walled concrete filled steel tubes', *Journal of Structural Engineering*, ASCE, vol. 126, no. 11, pp. 1295–1303.

111. Park, H.C. and Kim, D.S. (2001). 'Evaluation of dispersive phase and group velocities using harmonic wavelet transform', *NDT and E International*, vol. 34, no. 7, pp. 457-467.

112. Patel, V.K.I., Liang, Q.Q. and Muhammad, N.S. Hadi. (2012). 'High Strength thin-walled rectangular concrete-filled steel tubular slender beam-columns, Part II: Behavior', *Journal of Constructional Steel Research,* vol. 70, pp. 368-376.

113. Pavlakovic, B. N. and Cawley, P., (2000). *DISPERSE User's Manual Version 2.0.1.1*. Imperial College,715 University of London, London.

114. Pirmoz, A. (2006). 'Evaluation of nonlinear behavior of bolted, connections under dynamic loads', MS thesis. Tehran (Iran): K.N. Toosi University.

115. Pirmoz, A., Daryan, A. S., Mazaheri, A. and Darbandi, H. E. (2008*).* 'Behavior of bolted angle connections subjected to combined shear force and moment', *Journal of Constructional Steel Research*. vol. 64, pp. 436-446.

116. Prabhavathy, A.R. and Samuel Knight, G.M. (2006). 'Behaviour of Cold-Formed Steel Concrete Infilled RH Connections and Frames', *Steel and Composite Structures,* vol. 6, no. 1, pp. 71-85.

117. Redwood, M. (1960). *Mechanical Waveguides*. Bristol: Pergamon Press.

118. Reis, H., Ervin, B.L., Kuchma, D.A. and Bernhar, J.T. (2005). 'Estimation of corrosion damage in steel reinforced mortar using guided waves', *Journal of Pressure Vessel Technology,* vol.127, pp. 255–261.

119. Rose, J. L. (2003). 'Back to Basics – Dispersion Curves in Guided Wave Testing', *Material Evaluation*. vol. 61, no. 1, pp. 20-22.

120. Rose, J.L., Avioli, M.J., Mudge, P. and Sanderson, R., (2004). 'Guided wave inspection potential of defects in rails', *NDT & E International*. vol. 37, pp. 153-161.

121. Rose, J.L., Cho, Y. and Avioli, M.J. (2009). 'Next generation guided wave health monitoring for long range inspection of pipes', *Journal of loss prevention in the process industries,* vol.22.

122. Sakino, K., Nakahara, H., Morino, S. and Nishiyama, I. (2004). 'Behaviour of centrally loaded concrete-filled steel-tube short columns', *Journal of Structural Engineering (ASCE),* vol. 130, no. 2, pp. 180–188.

123. Satyarnarayan, L., Chandrasekaran, J., Bruce Maxfield and Balasubramaniam, K. (2008). 'Circumferential higher order guided wave modes for the detection

and sizing of cracks and pinholes in pipe support regions', *NDT&E International*, vol.41, pp. 32–43.

124. Schneider, S.P. (1998*). '*Axially loaded concrete-filled steel tubes', *Journal of Structural Engineering (ASCE)*, vol. 124, no.10, pp. 1125-1138.

125. Schneider, S.P. and Alostaz, Y.M. (1998). 'Experimental behaviour of connections to concrete-filled steel tubes', *Journal of Constructional Steel Research*, vol. 453, pp. 321-52.

126. Schneider, S.P., Kramer, D.R. and Sarkkinen, D.L. (2004). 'The design and construction of concrete-filled steel tube column frames', *13th World Conference on Earthquake Engineering,* Vancouver, B.C., Canada August 1-6, 2004 Paper No. 252.

127. Serras, D.N., Skalomenos, K.A., Hatzigeorgiou,G. D. and Beskos, D.E. (2015).'On the Nonlinear Cyclic Behavior of Circular Concrete-Filled Steel Tubes', *8th GRACM International Congress on Computational Mechanics Volos,* 12 July – 15 July 2015.

128. Shakir-Khalil, H. and Zeghiche, J. (1989). 'Experimental behaviour of concrete-filled rolled rectangular hollow section columns', *The Structural Engineer*, vol. 67, no. 19, pp. 346–353.

129. Shakir, K.H. and Mahmoud, M.A. (1995). 'Steel beam connections to concrete-filled tubular columns', *Sweden: Nordic steel construction conference*; June 1995.

130. Shams, M. and Saadeghvaziri, M.A. (1997). 'State of the art of concrete-filled steel tubular columns', *ACI Structural Journal*, vol. 94, no. 5, pp. 558–371.

131. Shanmugam, N.E. and Lakshmi, B. (2001). 'State of the art report on steel-concrete composite columns', *Journal of Constructional Steel Research*, vol. 57, no.10, pp. 1041–1080.

132. Sharma, S. and Mukherjee, A. (2009). 'Damage detection in reinforcing bars in concrete using ultrasonic waves', *Journal of Pure Applied Ultrasonic,* vol.31, pp. 85-93.

133. Sharma, S. and Mukherjee, A. (2010 a). 'Propagating ultrasonic guided waves through concrete reinforcements with simulated and actual corrosion', *CINDE Journal,* vol. 31, no. 2.

134. Sharma, S. and Mukherjee, A., (2010 b). 'Monitoring Corrosion in Oxide and Chloride Environments', *Journal of Materials in Civil Engineering,* vol. 23, no. 2, pp. 207-211.

135. Sharma, S. and Mukherjee, A. (2010 c). 'Longitudinal guided waves for monitoring chloride corrosion in reinforcing bars in concrete', *Structural Health Monitoring,* vol. 9, no. 6, pp. 555–567.

136. Sharma, S., Bhise, P.C., and Mukherjee, A. (2011). 'Damage detection in steel bars using ultrasonic guided waves: An Experimental & Analytical Study', *Journal of Structural Engineering,* vol. 37, no. 6, pp. 408-420.

137. Sharma, S. and Mukherjee, A. (2013). 'Non-Destructive Evaluation of Corrosion in varying Environments using guided waves', *Research in Non-Destructive Evaluation,* vol. 24, pp.1–26.

138. Sharma, S. and Mukherjee, A. (2014). 'Ultrasonic guided waves for monitoring corrosion in submerged plates', *Structural Control and Health Monitoring,* vol. 22, no.1, pp. 19-35.DOI: http://dx.doi.org/10.1002/stc.1657.

139. Sharma, S. and Mukherjee, A. (2015a). 'Monitoring freshly poured concrete using ultrasonic waves guided through reinforcing bars', *Cement Concrete and Composites,* vol. 55, pp. 337-347.

140. Sharma, S. and Mukherjee, A. (2015b). 'A Non-Contact Technique for Damage Monitoring in Submerged Plates Using Guided Waves', *Journal of Testing and evaluation-ASTM,* vol. 39, no.5, pp. 1009-1034.

141. Sharma, A., Sharma, S., Sharma, S. and Mukherjee, A. (2015). 'Ultrasonic guided waves for monitoring corrosion of FRP wrapped concrete structures,' *Construction and Building Materials,* vol. 96, pp. 690-702.

142. Sheet, S., Gunasekaran, U. and Gregory, A. MacRae (2013). 'Experimental investigation of CFT column to steel beam connections under cyclic loading', *Journal of Constructional Steel Research,* vol. 86, pp. 167–182.

143. Silva, L.A.P.S., Neves, L.F.C. and Gomes, F.C.T. (2003). 'Rotational Stiffness of Rectangular Hollow Sections Composite Joints', *Journal of Structural Engineering*, vol. 129, no. 4, pp. 487-494.

144. Singh, H. and Gupta, P.K. (2014). 'Numerical Modeling of Rectangular Concrete-Filled Steel Tubular Short Columns', *Latin American Journal of Solids and Structures*, vol. 11, pp. 1445-1462.

145. Tan, K. (2003). 'Mechanical properties of High Strength Concrete Filled Steel Tubular Columns Part-I Concentrically loaded', *ACI Journal*. April 2003.

146. Tizani, W., Ali, A.M. and John, S. O. and Pitrakkos, T. (2013). 'Rotational stiffness of a blind-bolted connection to concrete filled tubes using modified hollo-bolts', *Journal of Constructional Steel Research*, vol. 80, pp. 317–333.

147. Tomii, M. (1991). 'Ductile and Strong Columns Composed of Steel Tube, Infilled Concrete, and Longitudinal Steel Bars', *Proceedings of the Third International Conference on Steel-Concrete Composite Structures*, Special Volume, Wakabayashi, M. (ed.), Fukuoka, Japan, September 26-29, 1991, Association for International Cooperation and Research in Steel-Concrete Composite Structures, pp. 39-66.

148. Tomii, M., Yoshimura, K. and Morishita, Y. (1977). 'Experimental studies on concrete filled steel tubular stub columns under concentric loading', *In: Proc. of the International Colloquium on Stability of Structures under Static & Dynamic Loads*. Washington, SSRC/ASCE, pp. 718–41.

149. Tort, C. and Hajjar, J.F. (2010). 'Mixed finite-element modeling of rectangular concrete-filled steel tube members and frames under static and dynamic loads', *Journal of Structural Engineering*, ASCE, vol. 136, no. 6, pp. 654–64.

150. Tsai, K.C., Weng, Y.T. and Lin, M.L. (2003). 'Pseudo dynamic tests of a full-scale CFT/BRB composite frame: Displacement based seismic design and response evaluations', *In: Proceeding of the international workshop on steel and concrete composite constructions*.

151. Uy, B. (1998). 'Local and post-local buckling of concrete filled steel welded box columns', *Journal of Constructional Steel Research*, vol. 47, no. 1-2, pp. 47-72.

152. Uy, B. (2001a), 'Strength of short concrete filled high strength steel box columns', *Journal of Constructional Steel Research*, vol. 57, pp. 113–34.

153. Uy, B. (2001b). 'Local and post-local buckling of fabricated thin-walled steel and steel-concrete composite sections', *Journal of Structural Engineering*, vol. 127, no. 6, pp. 666–77.

154. Vesiljevic, M. and Kundu, T. (2008), 'Pipe wall damage detection by electro-magnetic acoustic transducer generated guided waves in absence of defect signals', *Journal of Acoustical Society of America*, vol. 123, no. 5, pp. 2591-2597.

155. Wang, J.F., Chen, X. and Shen, J. (2012). 'Performance of CFTST column to steel beam joints with blind bolts under cyclic loading', *Thin Walled Structures*, vol. 60, no. 12, pp. 69-84,

156. Wang, J.F. and Guo, S. (2012). 'Structural performance of blind bolted end plate joints to concrete-filled thin-walled steel tubular columns', *Journal of Thin-Walled Structures,* vol. 60, pp. 54–68.

157. Wang, JF., Han, LH. and Uy, B. (2009). 'Behaviour of flush end plate joints to concrete-filled steel tubular columns', *Journal of Constructional Steel Research*, vol. 65, pp. 925-939.

158. Wang, J.F. and Spencer, B.F. (2013). 'Experimental and analytical behavior of blind bolted moment connections', *Journal of Constructional Steel Research*, vol. 82, pp. 33–47.

159. Wang, J.F., Xing W.B., Gong, X.D. (2012). 'Experiment, analysis and design of semi-rigid joints to concrete filled steel tubular columns', *In: Proceedings of the 12th international symposium on structural engineering*. Wuhan China, December 17–19; 2012. pp. 414–19.

160. Wang, J.F., Zhang, L. and Spencer Jr., B.F. (2013). 'Seismic response of extended end plate joints to concrete-filled steel tubular columns', *Engineering Structures,* vol. 49, pp. 876–89.

161. Wang, N., and Lee, M. J. (2015). 'Structural behavior of beam-to-column connections of circular CFST columns by using mixed diaphragms', *International Journal of Steel Structures,* vol. 15, no. 2, pp. 347–364.

162. Wang, N., Kim, K.H. and Lee, M.J. (2017). 'Structural behavior of beam-to-column connections of rectangular CFST columns using mixed diaphragms', *International Journal of Steel structures,* vol. 17, no.1, pp 351–365.

163. Wang, W.D., Han, L.H. and Uy, B. (2008). 'Experimental behaviour of steel reduced beam section to concrete-filled circular hollow section column connections', *Journal of Constructional Steel Research,* vol. 64, no. 5, pp. 493–504.

164. Xiamuxi, A. and Hasegava, A. (2012). 'A study on axial compressive behaviors of reinforced concrete filled tubular steel columns', *Journal of Constructional Steel Research,* vol. 76, pp. 144 –154.

165. Xu, B., Zhang, T., Song, G. and Gu, H. (2013). 'Active interface debonding detection of a concrete-filled steel tube with piezoelectric technologies using wavelet', *Journal of Mechanical Systems and Signal Processing,* vol. 36, pp. 7 - 17.

166. Xue, JQ., Briseghella, B. and Chen, BC. (2012). 'Effects of debonding on circular CFST stub columns', *Journal of Constructional Steel Research,* vol. 69, pp. 64–76.

167. Yang, Y.F. and Han, L.H. (2009) 'Experiments on rectangular concrete-filled steel tubes loaded axially on a partially stressed cross-sectional area', *Journal of Constructional Steel Research,* vol. 65, no. 8-9, pp. 1617–1630.

168. Yang, Y.F. and Han, L.H., (2012) 'Concrete filled steel tube (CFST) columns subjected to concentrically partial compression', *Thin-Walled Structures,* vol. 50, no. 1, pp. 147–156.

169. Yu, H., Qian, J., Feng, Y., Hai, D., Jianhua, L. and Yueming, L. (2006). 'Experimental study on full-scale steel beam-to-column moment connections', *Earthquake Engineering Vibrations,* vol.4, no. 2, pp. 311–23.

170. Zeghiche, J. & Chaoui, K. (2005). 'An experimental behaviour of concrete-filled steel tubular columns', *Journal of Constructional Steel Research,* vol. 61, no.1, pp. 53-66.

171. Zhang, J.Q. and Brahmachari, K. (1994). 'Flexural Behavior of Rectangular Tubular Sections Filled with Fibrous High Strength Concrete', *Tubular Structures VI,* Rotterdam, Holland, pp. 247-254.

172. Zhang, F.G., Wu, C.Q. and Wang, H.W. (2015). 'Numerical simulation of concrete filled steel tube columns against blast loads', *Thin-Walled Structures,* vol. 92, no. 1, pp. 82–92.

173. Zhao, H. (2016). 'Analysis of seismic behavior of composite frame structures', *Steel and Composite Structures, An International Journal,* vol. 20, no. 3, pp. 719-729.

174. Zhao, J.H., Wei X.Y. and Ma, S.F. (2008). 'The Finite Element Analysis for Concrete Filled Steel Tubular Columns under Blast Load'. *Analysis of Discontinuous Deformation: New Developments and Applications.* pp. 669-674.

175. Zhao, X.L. (2002). 'Void-Filled Rectangular Hollow Section Braces Subjected to Large Deformation Cyclic Axial Loading', *Journal of Structural Engineering*, vol.128, no. 6, pp. 746-753.

176. Zhao, X.L. and Grzebieta, R.H. (1999). 'Void-Filled SHS Beams Subjected to Large Deformation Cyclic Bending', *Journal of Structural Engineering*, vol. 128, no. 9, pp. 1020-1027.

177. Zhao, H.L., Kunnath, S.K. and Yuan, Y. (2010). 'Simplified Nonlinear Response Simulation of Composite Steel-concrete Beams and CFST Columns', Engineering Structures, vol. 32, no. 9, pp. 2825-2831.

178. Zhou, T., Chen, Z. and Liu, H. (2012) 'Seismic behavior of special shaped column composed of concrete filled steel tubes', *Journal of Constructional Steel Research*, Vol. 75, pp. 131–141.